

# The effect of *APOE* genotype on astrocytic phenotypes in sporadic Alzheimer's disease

Adele Pryce Roberts

A thesis submitted to Cardiff University for the degree of Doctor of Philosophy

September 2020



This thesis is dedicated to the memory of my grandmothers,  
Marion Pyburn and Marian Roberts, who inspired me to begin  
this work.

And to my children, Alys and Idris, who gave me the motivation to  
finish it.

## Acknowledgements

I would first like to thank my supervisors, Professors Julie Williams, Adrian Harwood and Jeremy Hall, whose doors have always been open for help, support and excellent advice. Major thanks also to Alzheimer's Research UK (ARUK) who funded this work via a Clinical Research Fellowship with a particular mention to Katy Stubbs and Sara Imarisio.

Thanks to the numerous people at the Hadyn Ellis Building who have helped me in all manner of ways: members of the AD lab team, past and present, Mel, Taniesha, Jodie, Rhodri, Rachel, Beccy, Helen, Aurelian, Gareth, Salha and the Field Team (in particular Nicola, Alun, Rachel and Amy). Special mention to the Annas who guided me through my first year and to Emily who has always been on hand to offer statistics advice.

Thanks to all in the Core Team, in particular Alex for help with the SNP arrays and Jo for the RNASeq work and to Mark Bishop and Jo Twomey for their help with FACS. Also to those in the NMHRI who answered my various pleas for help: Will, Mouhamed, Tanya, Gareth and Bret.

In the HD team, thanks to Lyn for being so helpful and knowledgeable, Branduff for his expertise screening for off-target effects, Tom for ongoing chats and to Jasmine who has accompanied me on the CRISPR roller-coaster ride and become a good friend. Special mention to Professor Lesley Jones who has offered sage guidance at every stage of the project.

Thanks to Professor Meng Li who introduced me to Zoe Noakes who taught me everything I know about neuronal differentiation in the most patient and cheerful manner imaginable. Thanks also to Professor Val O'Donnell and Dr Vikki Tyrrell for access to your lab and expertise for the lipid work which is so central to this thesis.

Outside of Cardiff University, thanks to Andrew Bassett at the Sanger Institute, Cambridge for all your advice about CRISPR. Also to Anne Hedegaard and Jackie

Robbins at Oxford University and Lucy Crompton at Bristol University for ongoing discussions about astrocyte culture.

Finally, I owe a huge debt to Karolina Dec who taught me a wide range of lab techniques and helped with so many aspects of the project; I couldn't have done this without you.

On a personal note, thanks to my parents, Bryan, Meirion and Norma for your support throughout my various career changes and, in particular, for giving me the confidence to make them.

Thanks most of all to my long-suffering partner, Mary, who has been remarkably understanding about the weekends and holidays spent in the lab and, without whom, I would never have completed this thesis.

“Genes count.” – Marion Pyburn, 1993

## Abstract

Alzheimer's disease is the most common form of dementia worldwide accounting for between 60 and 70% of cases. For many years, Alzheimer's disease has been considered a disease driven by beta-amyloid, however this has been increasingly questioned, largely due to the poor correlation between amyloid deposition and the cognitive deficits seen in the disease plus the failure of a multitude of anti-amyloid drugs. A better understanding of the pathogenesis of the disease, especially the first cellular events, is vital in the development of disease modifying treatments that could address this global health issue.

The best neuropathological correlate of the cognitive deficits seen in Alzheimer's disease is synaptic loss and the most significant genetic risk factor is variation of the Apolipoprotein E (APOE) protein sequence, particularly the *APOE3* and *APOE4* alleles. The objective of this thesis was to use CRISPR-Cas9 technology to create isogenic *APOE* cell lines differing by only their *APOE 3* and *4* genotypes.

As ApoE is largely produced by astrocytes within the central nervous system, the effects of these genetic variations on astrocyte cell biology was investigated, in particular effects on ApoE expression, glutamate uptake, phagocytosis, cholesterol homeostasis and the expression profile of pro-inflammatory cytokines. All of these characteristics were changed in cells carrying the E4 genotype. I describe how these may be connected by a common pathway and outline future directions for further development of the cell model.

Overall, this thesis describes a model system which has elucidated a number of astrocytic phenotypes associated with the *APOE* genotype highlighting areas of enquiry that are most likely to be fruitful.

## List of Abbreviations

A $\beta$	beta amyloid
ABCA1	ATP Binding Cassette Subfamily A Member 1
ABCG1	ATP Binding Cassette Subfamily G Member 1
ACAT1	Acetyl-CoA Acetyltransferase 1
ACh	Acetylcholine
AChE	Acetylcholinesterase
AD	Alzheimer's Disease
AMPA	$\alpha$ -amino-3-hydroxy-5-methyl-4-isoxazolepropionic acid
AMPA	AMPA receptor
AP	Action potential
APOE	apolipoprotein (gene)
ApoE	apolipoprotein (protein)
ApoER2	apolipoprotein E receptor 2
APP	amyloid precursor protein
AQP4	aquaporin 4
BBB	blood brain barrier
BDNF	brain derived neurotrophic factor
bFGF	basic fibro-blast growth factor
BMP4	bone morphogenic protein 4
BSA	bovine serum albumin
CA1	cornus ammonis 1
cDNA	complementary DNA
CDR	Clinical Dementia Rating

CEs	cholesteryl esters
CETP	cholesteryl ester transfer protein
CNA	copy number alteration
CNS	central nervous system
CNTF	ciliary neurotrophic factor
CRISPR	Clustered Regularly Interspaced Short Palindromic Repeats
CSF	cerebrospinal fluid
CYP46A1	cytochrome P450 Family 46 Subfamily A Member 1
DNA	deoxyribonucleic acid
DMEM	Dulbecco's Modified Eagle Medium
DMSO	dimethyl sulfoxide
dNTP	deoxyribonucleotide triphosphates
dsDNA	double stranded DNA
DSB	double strand break
EC	entorhinal cortex
EAAT 1&2	excitatory amino acid transporters 1& 2
EGF	epidermal growth factor
ER	endoplasmic reticulum
ELISA	Enzyme-Linked Immunosorbent Assay
ENA-78	epithelial-derived neutrophil-activating peptide 78
FACS	fluorescence assisted cell sorting
fAD	familial Alzheimer's disease
FBS	fetal bovine serum
FDA	Food and Drug Administration
FDG	fluorodeoxyglucose

GABA	gamma-Aminobutyric acid
GABAAR	GABA-A receptor
GDNF	glial cell line-derived neurotrophic factor
GFAP	glial fibrillary acidic protein
GFP	green fluorescent protein
GRO/GRO- $\alpha$	growth-regulated oncogene/growth-regulated oncogene alpha
GWAS	Genome Wide Association Study
HDL	high density lipoprotein
HDR	homology directed repair
hESC	human embryonic stem cells
HMGCR	HMG-CoA reductase
hPSC	human pluripotent stem cells
IFN $\gamma$	interferon-gamma
IGAP	International Genomics of Alzheimer's Project
IGF-1	insulin-like growth factor 1
I $\kappa$ B	inhibitor of nuclear factor kappa-B
IKK	I $\kappa$ B kinase
IL	interleukin
iPSC	Induced Pluripotent Stem Cells
JAK-STAT	Janus kinase-signal transducer and activator of transcription
LCAT	lecithin-cholesterol acyltransferase
LC-MS	Liquid Chromatography-Mass Spectrometry
LD	linkage disequilibrium
LDL	low-density lipoprotein
LDLR	low-density lipoprotein receptor

LIF	leukaemic inhibitory factor
LIPE	lipase E, Hormone Sensitive Type
LOAD	late onset Alzheimer's disease
LPL	lipoprotein lipase
LTD	long-term depression
LTP	long-term potentiation
LRP1	low density lipoprotein receptor-related protein 1
LXR	liver X receptor
MAPT	microtubule-associated protein tau
MCP1&2	monocyte chemoattractant protein 1 & 2
MCSF	macrophage colony-stimulating factor
MMSE	Mini Mental State Examination
MRI	magnetic resonance imaging
mRNA	messenger RNA
NFKB	nuclear factor-kappa-beta
NFT	neurofibrillary tangles
NGS	next generation sequencing
NHEJ	non-homology end joining
NMDA	N-methyl-D-aspartate
NMDAR	NMDA receptor
NPC	neuronal progenitor cells
NT	nucleotide
OR	odds ratio
PAM	protospacer adjacent motif
PBS	phosphate buffered saline

PCR	polymerase chain reaction
PDGF	platelet-derived growth factor
PET	positron emission tomography
PiB	Pittsburgh Compound B (PiB)
PLTP	plasma phospholipid transfer protein
PRS	polygenic risk score
PSEN1	presenilin 1
PSEN2	presenilin 2
PSD	post-synaptic density
ptau	phosphorylated tau
RANTES	regulated on activation, normal T cell expressed and secreted
RelA	v-rel avian reticuloendotheliosis viral oncogene homolog A
RNA	ribonucleic Acid
RNP	ribonucleoprotein
RT	room temperature
sAPP	soluble APP
SD	standard deviation
SDF1	stromal cell-derived factor 1
SEM	standard error of the mean
sgRNA	short guide RNA
SNP	single nucleotide polymorphism
SNV	single nucleotide variant
SREBP	sterol regulatory element-binding proteins
ssODN	single-stranded DNA oligonucleotides
sAD	sporadic Alzheimer's Disease

TARC	thymus and activation regulated chemokine
TGF $\beta$	transforming growth factor beta
TNF $\alpha$ & $\beta$	tumour necrosis factor alpha & beta
VEGF	vascular endothelial growth factor
VLDL	very low density lipoprotein

# Table of contents

<b>1</b>	<b>INTRODUCTION</b>	<b>1</b>
<b>1.1</b>	<b>CLINICAL ALZHEIMER'S DISEASE</b>	<b>1</b>
1.1.1	CLINICAL FEATURES	1
1.1.2	CURRENT TREATMENTS AND DRUGS IN DEVELOPMENT	2
<b>1.2</b>	<b>NEUROPATHOLOGY OF ALZHEIMER'S DISEASE</b>	<b>5</b>
1.2.1	NEUROFIBRILLARY TANGLES (NFTs) AND BRAAK STAGING	5
1.2.2	SENILE (AMYLOID) PLAQUES	6
1.2.3	SCORING SYSTEMS FOR AMYLOID DEPOSITION	7
1.2.4	'ABC' SCORING OF AD PATHOLOGY	8
1.2.5	THE AMYLOID HYPOTHESIS	8
1.2.6	CLINICOPATHOLOGICAL CORRELATION STUDIES	9
1.2.7	THE TEMPORAL RELATIONSHIP OF AMYLOID AND TAU	10
1.2.8	ABERRANT PROTEIN AGGREGATIONS: CAUSE OR EFFECT?	12
1.2.9	THE ROLE OF THE SYNAPSE IN AD	14
<b>1.3</b>	<b>GENETICS OF ALZHEIMER'S DISEASE</b>	<b>18</b>
1.3.1	FAMILIAL ALZHEIMER'S DISEASE (FAD)	18
1.3.2	SPORADIC ALZHEIMER'S DISEASE	20
<b>1.4</b>	<b>THE APOE GENE</b>	<b>24</b>
1.4.1	BASIC GENETICS AND EXPRESSION	24
1.4.2	APOE STRUCTURE	25
1.4.3	FUNCTIONS OF APOE IN HEALTH AND DISEASE	27
<b>1.5</b>	<b>ASTROCYTES IN HEALTH AND DISEASE</b>	<b>34</b>
1.5.1	HISTOPATHOLOGICAL ASTROCYTIC CHANGES IN NEURODEGENERATIVE DISEASES	35
1.5.2	SUBTYPES OF ASTROCYTES	36
1.5.3	FUNCTIONS OF ASTROCYTES	36
1.5.4	EFFECTS OF APOE GENOTYPE ON ASTROCYTIC PHENOTYPE	43
<b>1.6</b>	<b>STEM CELLS FOR MODELLING NEURODEGENERATIVE DISEASES</b>	<b>48</b>
1.6.1	EMBRYONIC STEM CELLS (ESC)	48
1.6.2	INDUCED PLURIPOTENT STEM CELLS (IPSC)	48
1.6.3	ADULT STEM CELLS	49
1.6.4	DIFFERENTIATION OF STEM CELLS	49
1.6.5	ADVANTAGES AND CHALLENGES OF USING STEM CELL MODELS	50

<b>1.7</b>	<b>GENE EDITING</b> .....	<b>52</b>
1.7.1	REPAIR MECHANISMS: NONHOMOLOGOUS END JOINING (NHEJ) AND HOMOLGY-DIRECTED REPAIR (HDR)	52
1.7.2	ZINC-FINGER NUCLEASES (ZFNs) AND TRANSCRIPTOR ACTIVATOR-LIKE EFFECTOR NUCLEASES (TALENS)	52
1.7.3	CRISPR-CAS9 .....	53
<b>1.8</b>	<b>AIMS</b> .....	<b>55</b>
<b>2</b>	<b>MATERIALS AND METHODS</b> .....	<b>56</b>
<b>2.1</b>	<b>CELL CULTURE</b> .....	<b>56</b>
2.1.1	HPSC CULTURE .....	56
2.1.2	HPSC FREEZING AND THAWING.....	56
2.1.3	HPSC DIFFERENTIATION TO NEURONAL PRECURSOR CELLS (NPC) .....	57
2.1.4	FREEZING AND THAWING OF NPCs.....	58
2.1.5	DIFFERENTIATION OF NEURONS.....	59
2.1.6	DIFFERENTIATION OF ASTROCYTES.....	59
2.1.7	PRODUCTION OF ASTROCYTE CONDITION MEDIA (ACM) .....	59
<b>2.2</b>	<b>CELL TECHNIQUES</b> .....	<b>60</b>
2.2.1	SAMPLE PREPARATION FOR IMMUNOCYTOCHEMISTRY .....	60
2.2.2	CALCULATION OF CORRECTED TOTAL CELL FLUORESCENCE .....	62
2.2.3	CHOLESTEROL STAINING ASSAYS.....	62
2.2.4	INDUCTION OF ASTROGLIOSIS .....	63
2.2.5	GLUTAMATE UPTAKE ASSAY.....	63
2.2.6	PHAGOCYTOSIS ASSAY .....	65
2.2.7	CYTOKINE ARRAY .....	66
2.2.8	QUANTITATION OF CHOLESTEROL, CHOLESTERYL ESTERS AND OXYLIPINS .....	67
<b>2.3</b>	<b>PROTEIN TECHNIQUES</b> .....	<b>70</b>
2.3.1	BCA (BICINCHONINIC ACID) ASSAY.....	70
2.3.2	ELISA .....	71
<b>2.4</b>	<b>NUCLEIC ACID TECHNIQUES</b> .....	<b>73</b>
2.4.1	ISOLATION OF PLASMIDS .....	73
2.4.2	DNA EXTRACTION, PURIFICATION AND QUANTITATION .....	73
2.4.3	POLYMERASE CHAIN REACTION (PCR) INCLUDING PRIMER DESIGN .....	75
2.4.4	GEL ELECTROPHORESIS .....	76

2.4.5	DNA EXTRACTION FROM AGAROSE GEL.....	76
2.4.6	SANGER SEQUENCING .....	77
<b>2.5</b>	<b>GENE EXPRESSION ANALYSIS .....</b>	<b>78</b>
2.5.1	RNA EXTRACTION.....	78
2.5.2	REVERSE TRANSCRIPTION .....	79
2.5.3	QUANTITATIVE REAL-TIME PCR (QRT-PCR) .....	79
<b>2.6</b>	<b>GENOME EDITING TECHNIQUES.....</b>	<b>82</b>
2.6.1	GENOTYPING WILD-TYPE CELL LINES.....	82
2.6.2	PLASMID-BASED APPROACH .....	83
2.6.3	GENOME EDITING USING THE INTEGRATED DNA TECHNOLOGIES (IDT) ALT-R SYSTEM .....	88
2.6.4	QUALITY CONTROL MEASURES ON ISOGENIC LINES .....	91
<b>2.7</b>	<b>STATISTICAL ANALYSIS .....</b>	<b>92</b>
<b>3</b>	<b><u>CREATION AND VALIDATION OF ISOGENIC APOE LINES.....</u></b>	<b>93</b>
<b>3.1</b>	<b>CREATION OF ISOGENIC LINES.....</b>	<b>94</b>
3.1.1	CREATION OF THE CRISPR/Cas9 TARGETING PLASMID.....	94
3.1.2	GUIDE RNA SELECTION AND TESTING.....	94
3.1.3	RESULTS OF PLASMID TRANSFECTIONS.....	95
3.1.4	RESULTS OF TRANSFECTIONS WITH RNP USING THE IDT ALT-R SYSTEM.....	95
3.1.5	CREATION AND TESTING OF REPAIR TEMPLATES .....	96
3.1.6	ENRICHMENT OF THE EDITED POPULATION WITH FACS SORTING .....	98
3.1.7	RESULTS OF SANGER SEQUENCING OF CLONES .....	99
<b>3.2</b>	<b>VALIDATION OF ISOGENIC LINES .....</b>	<b>101</b>
3.2.1	KARYOTYPING .....	101
3.2.2	EXOME SEQUENCING.....	101
<b>3.3</b>	<b>BASIC CHARACTERISATION OF ISOGENIC LINES .....</b>	<b>103</b>
3.3.1	ASSESSMENT OF PLURIPOTENCY OF STEM CELLS .....	103
3.3.2	DIFFERENTIATION TO NEURAL PROGENITOR CELLS (NPCs).....	105
<b>3.4</b>	<b>DISCUSSION.....</b>	<b>107</b>
3.4.1	GENE EDITING CONSTRUCTS .....	107
3.4.2	VERIFICATION OF KARYOTYPE AND OFF-TARGET EFFECTS .....	109
3.4.3	PLURIPOTENCY AND DIFFERENTIATION .....	111
3.4.4	SUMMARY.....	112

<b>4</b>	<b><u>ASTROCYTIC DIFFERENTIATION AND VALIDATION</u></b>	<b>113</b>
<b>4.1</b>	<b>ASTROCYTE DIFFERENTIATION</b>	<b>113</b>
4.1.1	SIGNALLING PATHWAYS AND CYTOKINES INVOLVED IN ASTROGENESIS	114
4.1.2	PROTOCOLS FOR CREATING ASTROCYTES FROM HUMAN STEM CELLS	115
4.1.3	RESULTS OF INITIAL DIFFERENTIATION	117
<b>4.2</b>	<b>FURTHER DIFFERENTIATION AND CHARACTERISATION</b>	<b>119</b>
4.2.1	PROLONGED DIFFERENTIATION	121
<b>4.3</b>	<b>APOE PRODUCTION</b>	<b>123</b>
<b>4.4</b>	<b>DISCUSSION</b>	<b>124</b>
4.4.1	MARKERS IN 12-WEEK ASTROCYTES	124
4.4.2	MARKERS AND MORPHOLOGY IN 26-WEEK ASTROCYTES	126
4.4.3	APOE LEVELS	127
<b>4.5</b>	<b>CONCLUSIONS</b>	<b>129</b>
<b>5</b>	<b><u>ASTROCYTIC PHENOTYPES: GLUTAMATE UPTAKE AND PHAGOCYTOSIS</u></b>	<b>130</b>
<b>5.1</b>	<b>INDUCTION OF ASTROGLIOSIS</b>	<b>130</b>
5.1.1	RESULTS OF INDUCING ASTROGLIOSIS	132
<b>5.2</b>	<b>GLUTAMATE UPTAKE</b>	<b>133</b>
5.2.1	MECHANISMS OF REDUCED GLUTAMATE UPTAKE	134
<b>5.3</b>	<b>PHAGOCYTOSIS</b>	<b>140</b>
5.3.1	POSSIBLE MECHANISMS OF REDUCED PHAGOCYTOSIS IN <i>APOE44</i> ASTROCYTES	141
<b>5.4</b>	<b>DISCUSSION</b>	<b>145</b>
5.4.1	GLUTAMATE UPTAKE	145
5.4.2	PHAGOCYTOSIS	148
<b>5.5</b>	<b>CONCLUSIONS</b>	<b>151</b>
<b>6</b>	<b><u>EFFECT OF APOE GENOTYPE ON MICROGLIAL TO ASTROCYTE SIGNALLING</u></b>	<b>152</b>
<b>6.1</b>	<b>RESULTS</b>	<b>152</b>
6.1.1	RESULTS IN QUIESCENT ASTROCYTES	152
6.1.2	RESULTS IN ACTIVATED 'A1' ASTROCYTES	153
<b>6.2</b>	<b>DISCUSSION</b>	<b>155</b>
6.2.1	CYTOKINE EXPRESSION IN QUIESCENT ASTROCYTES	155

6.2.2	<i>APOE</i> DEPENDENT DIFFERENCES IN QUIESCENT ASTROCYTES.....	156
6.2.3	ACTIVATED 'A1' ASTROCYTES .....	156
6.2.4	DIFFERENCES BETWEEN <i>APOE</i> GENOTYPES IN 'A1' ASTROCYTES.....	157
<b>6.3</b>	<b>CONCLUSIONS .....</b>	<b>168</b>
<b>7</b>	<b><u>THE EFFECT OF <i>APOE</i> GENOTYPE ON CHOLESTEROL METABOLISM .....</u></b>	<b><u>170</u></b>
<b>7.1</b>	<b>CHOLESTEROL HOMEOSTASIS IN THE CNS.....</b>	<b>170</b>
7.1.1	CHOLESTEROL SYNTHESIS .....	171
7.1.2	CHOLESTEROL EFFLUX AND TRANSPORT .....	173
7.1.3	CHOLESTEROL ENDOCYTOSIS.....	175
7.1.4	CHOLESTEROL STORAGE.....	176
<b>7.2</b>	<b>RESULTS .....</b>	<b>178</b>
7.2.1	CHOLESTEROL LEVELS .....	178
7.2.2	CHOLESTERYL ESTER LEVELS.....	180
7.2.3	GENE EXPRESSION IN CHOLESTEROL METABOLISM PATHWAYS .....	180
<b>7.3</b>	<b>DISCUSSION.....</b>	<b>183</b>
7.3.1	<i>APOE</i> LEVELS .....	183
7.3.2	CHOLESTEROL LEVELS .....	183
7.3.3	CHANGES IN CHOLESTERYL ESTER LEVELS (CEs).....	186
7.3.4	EXTRACELLULAR ESTERIFICATION MECHANISMS .....	188
<b>7.4</b>	<b>CONCLUSIONS .....</b>	<b>190</b>
<b>8</b>	<b><u>GENERAL DISCUSSION.....</u></b>	<b><u>192</u></b>
<b>8.1</b>	<b>SUMMARY OF KEY FINDINGS .....</b>	<b>192</b>
<b>8.2</b>	<b>CENTRAL ROLE OF ASTROCYTES IN SYNAPTIC FUNCTION IN ALZHEIMER'S DISEASE .....</b>	<b>194</b>
<b>8.3</b>	<b>ASTROGLIOSIS: A POTENTIAL THERAPEUTIC TARGET .....</b>	<b>195</b>
<b>8.4</b>	<b>A UNIFYING THEME? NUCLEAR FACTOR-KAPPA B (NF-<math>\kappa</math>B) SIGNALLING .....</b>	<b>196</b>
<b>8.5</b>	<b>THE PLACE OF THE ASTRO-CENTRIC VIEW ALONGSIDE TRADITIONAL NEUROPATHOLOGICAL MODELS .</b>	<b>198</b>
<b>8.6</b>	<b>FUTURE WORK .....</b>	<b>200</b>

## List of figures

- Figure 1.1A Alzheimer's Drug Development Pipeline 2018.
- Figure 1.1B Alzheimer's Drug Development Pipeline 2020.
- Figure 1.2 The amyloidogenic & non-amyloidogenic pathways.
- Figure 1.3 Time course of pathological changes in AD.
- Figure 1.4 Structure of the  $\epsilon 3$  and  $\epsilon 4$  isoforms of ApoE.
- Figure 1.6 Summary of APOE4 astrocytic phenotypes.
- 
- Figure 2.1 Results of PX458sgRNA Sanger sequencing.
- 
- Figure 3.1 sgRNAs used with the px458 plasmid.
- Figure 3.2 FACS of control and sgRNA 44908683 transfected cells.
- Figure 3.3 six ssODN repair templates tested.
- Figure 3.4 Results of transfections with six different ssODNs.
- Figure 3.5 Number of edited clones in sorted and unsorted samples.
- Figure 3.6 Sanger sequencing of edited clones.
- Figure 3.7 Immunofluorescence in edited stem cells and wild-type (WT) controls.
- Figure 3.8 qPCR of stem cell markers in wild-type (WT) cells and isogenic lines.
- Figure 3.9 Expression of nestin and PAX6 in Day 24 NPCs.
- Figure 3.10 Expression of FOXG1 and OTX2 in Day 24 NPCs.
- Figure 3.11 Cells positive for NPC markers as a % of DAPI.
- 
- Figure 4.1 Astrocytes derived using FBS and CNTF/BMP4.
- Figure 4.2 Expression of astrocytic genes using different growth factors.
- Figure 4.3A Expression of astrocytic markers in E3/E3 and E4/E4 cells at 12 weeks.
- Figure 4.3B Astrocytic markers in E3/E3 and E4/E4 astrocytes at 12 weeks.
- Figure 4.4A Expression of astrocytic markers in E3/E3 astrocytes at 12 & 26 weeks.
- Figure 4.4B Expression of astrocytic markers in E4/E4 astrocytes at 12 & 26 weeks.
- Figure 4.4C Astrocytic markers in E3/E3 astrocytes at 12 and 26 weeks.
- Figure 4.5A *APOE* gene expression.

- Figure 4.5B ApoE protein expression.
- Figure 5.1 Induction of astrogliosis: A) *C3* and B) *APOE* expression.
- Figure 5.2A-E Results of glutamate experiments.
- Figure 5.3A-E Results of phagocytosis experiments.
- Figure 6.1A Highly expressed cytokines in Quiescent & 'A1' astrocytes by genotype.
- Figure 6.1B Other cytokines expressed in Quiescent & 'A1' astrocytes by genotype.
- Figure 7.1 Cholesterol metabolism in the CNS.
- Figure 7.2 Cholesterol levels in A) astrocyte lysates and B) astrocyte media.
- Figure 7.3 Filipin fluorescence in untreated and cholesterol treated astrocytes.
- Figure 7.4 Cholesteryl ester levels in astrocyte lysates.
- Figure 7.5 Cholesteryl ester levels in astrocyte media.
- Figure 7.6 Ratio of CE in media:lysate in E3/E3 and E4/E4 samples.
- Figure 7.7 Expression of cholesterol metabolism genes in E3/E3 and E4/E4 astrocytes.
- Figure 7.8: Expression of cholesterol metabolism genes in E4/E4 astrocytes.

## List of tables

Table 1.1	<i>APOE</i> SNPs and alleles.
Table 1.2	SAD risk genes expressed on astrocytes.
Table 2.1	Antibodies used for immunofluorescence.
Table 2.2	Parent to daughter ion transitions for MRM monitoring.
Table 2.3	Primers used for RT-qPCR.
Table 3.1	On and off target scores for selected sgRNAs.
Table 3.2	FACS results using different sgRNAs.
Table 3.3	Silent mutation sites with codon adaptation indices (CAI).
Table 3.4	Sequences of the 6 ssODN repair templates tested.
Table 3.5	Changes at off-target sites identified by exome sequencing.
Table 6.1	Summary of significant cytokine array results.
Table 7.1	Function and expression of cholesterol metabolism genes in E4/E4 astrocytes.

# 1 Introduction

First described by Alois Alzheimer in 1906, Alzheimer's disease (AD) is characterised by a clinical triad of amnesia, agnosia and apraxia. Globally, the numbers of people living with Alzheimer's disease will increase from an estimated 40 million in 2020 to around 105 million in 2050. In addition to the devastation experienced by patients and their carers, the economic costs of Alzheimer's disease are huge; according to Alzheimer's Research UK, in the UK alone, expenditure is expected to more than double in the next 25 years from its current level of £26 billion to £55 billion in 2040.

This social and economic time bomb makes a treatment imperative; a modest 1-year delay in onset by 2020 would result in there being 9.2 million fewer cases in 2050<sup>1</sup>. Although there are a small number of drugs available which can help the symptoms of SAD there are, to date, no disease modifying treatments (DMTs) despite a significant number of clinical trials.

## 1.1 Clinical Alzheimer's disease

### 1.1.1 Clinical features

Impairment of memory is the most common presenting symptom of AD. The pattern is relatively distinct with declarative episodic memory (events which occur at a particular time and place) most profoundly affected<sup>2</sup>. The pattern of cognitive defects reflects the areas of the brain most affected. Declarative episodic memory relies heavily on medial temporal lobe structures including the hippocampus and entorhinal cortex which tend to be affected early in the disease course. By contrast, immediate memory, which is encoded by the sensory association and pre-frontal cortex, and remote memory (which does not rely on the hippocampus) tend to be affected much later in the disease<sup>3</sup>. Other cognitive deficits may appear with or after the development of memory impairment; executive dysfunction and visuospatial impairment often present

relatively early, while deficits in language and behavioural symptoms tend to manifest later.

### 1.1.2 Current treatments and drugs in development

There are currently only four drugs licensed for use in AD in the UK. None of these are disease modifying treatments but allow patients to function at a cognitively higher level than they would without them. Three of the drugs are cholinesterase inhibitors (donepezil, rivastigmine and galantamine) which work by inhibiting the breakdown of the neurotransmitter acetylcholine thus increasing its availability at synapses.

Cholinesterase inhibitors are available in the UK for mild to moderate Alzheimer's disease.

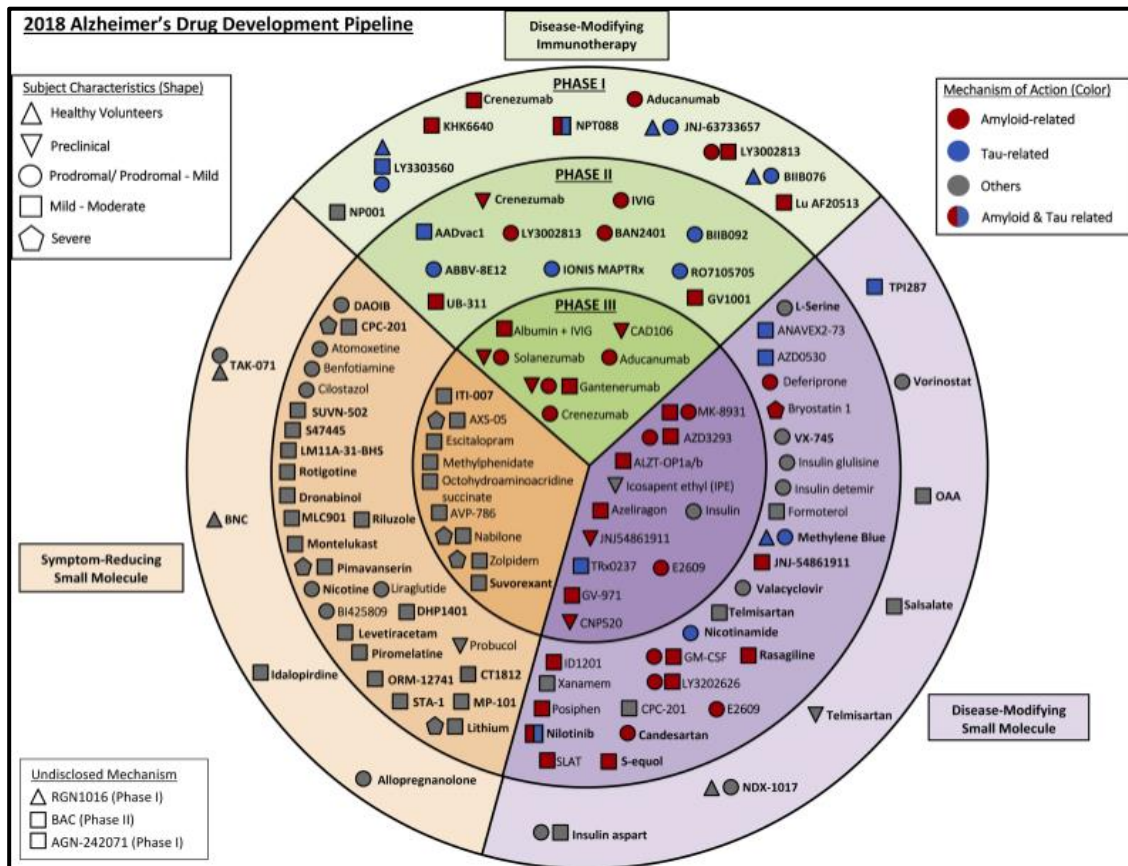
The fourth drug is memantine. It is available for use in people with more severe AD and for those with moderate AD if cholinesterase inhibitors are not tolerated. The precise mechanism of action of memantine is elusive but is believed to be the blockade of N-methyl-d-aspartate (NMDA) glutamate receptors reducing neuronal excitability and excess stimulation; it is also an antagonist of the type 3 serotonergic (5-HT<sub>3</sub>) receptor, and a low-affinity antagonist of the nicotinic acetylcholine receptor<sup>4</sup>.

Over the past 20 years, hundreds of agents have failed in clinical trials costing billions of pounds. Due to the primacy of the amyloid hypothesis – that is the assertion that accumulation of beta-amyloid protein is the causative agent of AD by destroying synapses and ultimately inducing neuronal loss<sup>5</sup> - the majority of drugs have been anti-amyloid therapies. As of 2018, there were 112 agents in the AD treatment pipeline. Of these, 26 were in Phase 3 trials: 17 DMTs, one cognitive-enhancing agent, and 8 drugs for behavioural symptoms. Among the DMTs, 14 targeted amyloid, one a tau-related target, one was a neuroprotective agent, and one had a metabolic mode of action<sup>6</sup> – see Figure 1.1A.

Since publication, several of these drugs have failed including solanezumab and crenezumab. While trials of aducanumab were initially halted because they were

unlikely to meet their primary objective a later analysis based on additional follow-up data in patients receiving the highest doses of the drug showed that it did meet its primary goal. On this basis, aducanumab has recently been granted a priority review by the Food and Drug Administration (FDA), meaning that the agency plans to expedite the review process to determine whether they will approve the medication.

**Figure 1.1A: Alzheimer’s Drug Development Pipeline 2018, Cummings et al, 2018<sup>6</sup>.**



Alzheimer’s Drug Development Pipeline 2018: demonstrating the dominance of amyloid related therapies. Of the 17 disease modifying treatments in phase III trials, 14 were anti-amyloid treatments. Figure reproduced with kind permission of the authors and publisher.

Although trial data showed these agents were highly effective at removing amyloid from the brain, their effects on cognitive function were very modest. While proponents of the amyloid hypothesis suggest that the reason for failure of these drugs is that trial participants’ disease is already too advanced, it has led many others to question the validity of the amyloid hypothesis itself leading to a change in the landscape of drug trials. In 2020, there are 121 drugs in clinical trials. In Phase 3 there are 29 agents in 36 trials, 17 of which are disease-modifying agents; 5 biological



## 1.2 Neuropathology of Alzheimer's disease

Alois Alzheimer first described Alzheimer's disease in his patient, Auguste Deter, at a meeting in Munich in 1906. She died 4 years after initial hospitalisation and post mortem examination, using the newly available Bielschowsky's silver stain, revealed degenerating neurons with senile plaques, neurofibrillary tangles (NFT) and glial changes<sup>8</sup>. In his second patient, Johann F. Credit, Alzheimer specifically noted hypertrophied glial cells surrounding the plaque which now we refer to reactive astrocytes<sup>9</sup>. Over 100 years later, senile plaques and NFTs are still considered the neuropathological hallmarks of AD but Alzheimer's observation of reactive glial cells has been largely neglected until recent years.

### 1.2.1 Neurofibrillary tangles (NFTs) and Braak Staging

Tau is a microtubule associated protein (MAP) whose most well established role is the stabilisation of axonal microtubules<sup>10</sup>. However, tau is not just restricted to the axons and may be found in multiple neuronal compartments, extracellular spaces as well as in glial cells<sup>11</sup>. It is also becoming clear that tau has a multitude of roles other than axonal stabilisation including maintaining structural integrity, axonal transport and signalling within and between neurons<sup>12</sup>. If tau is aberrantly modified, it forms insoluble aggregates which are accompanied by synaptic dysfunction and neural cell death in a range of neurodegenerative disorders, collectively referred to as tauopathies. Abnormally phosphorylated and aggregated tau, in the form of paired helical and straight filaments, is the major constituent of the NFTs found in AD<sup>13</sup>.

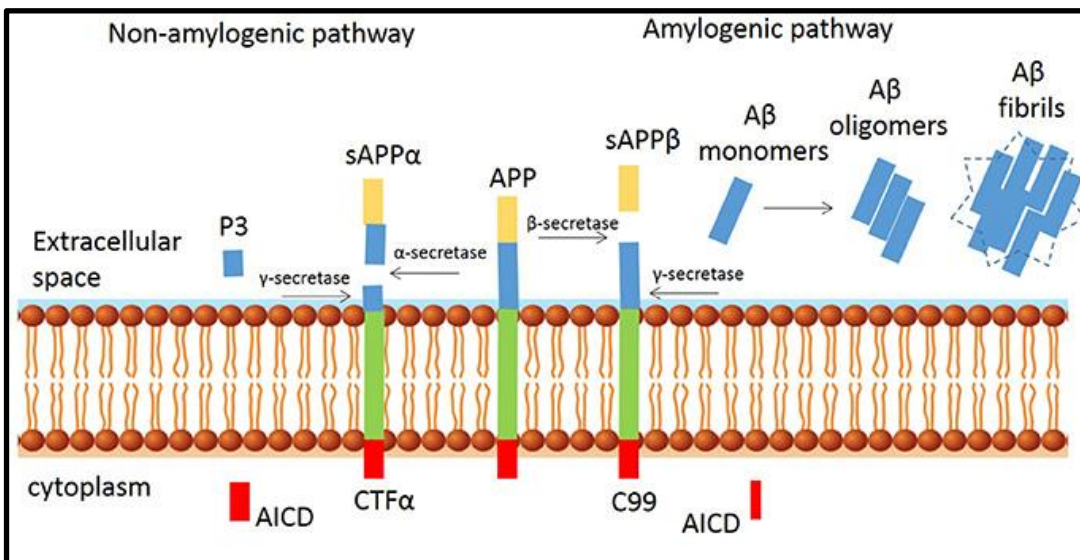
Braak staging characterises progressive neuropathological stages of AD which relate to increasing severity of NFTs in different brain regions<sup>14-16</sup>. The appearance of NFTs is predictable; they occur sequentially in the transentorhinal/peripheral cortex (stage I), the CA1 region of the hippocampus (stage II), limbic structures (stage III), amygdala, thalamus and claustrum (Stage IV), isocortical areas (stage V), and finally, primary sensory, motor and visual regions (stage VI)<sup>16</sup>. This predictability suggests that affected brain regions may be anatomically connected.

### 1.2.2 Senile (amyloid) plaques

Beta-amyloid ( $A\beta$ ) is a 36 to 43 amino acid peptide which is part of the larger, transmembrane, Amyloid Precursor Protein (APP). The precise physiological functions of APP are not well elucidated but both *in vitro* and *in vivo* studies have shown important roles in various neuronal and synaptic processes<sup>17</sup>.

APP may be cleaved initially by either  $\alpha$ -secretase or  $\beta$ -secretase to proceed, respectively, down the non-amyloidogenic or amyloidogenic pathways (Figure 1.2). In the amyloidogenic pathway,  $A\beta$  monomers are derived from the sequential cleavage of APP by the enzymes  $\beta$ - and  $\gamma$ -secretase.  $A\beta$  monomers polymerise into soluble oligomers and then into larger insoluble fragments such as  $A\beta_{38}$ ,  $A\beta_{40}$ ,  $A\beta_{42}$  and  $A\beta_{43}$  (designated by their amino acid length) which precipitate as amyloid fibrils<sup>18</sup>.  $A\beta_{40}$  is the most abundant  $A\beta$  species however  $A\beta_{42}$  and  $A\beta_{43}$  are hydrophobic and therefore more prone to aggregating into senile plaques<sup>19</sup>.

**Figure 1.2: amyloidogenic & non-amyloidogenic pathways from Sumner, 2018<sup>20</sup>.**



In the non-amyloidogenic pathway,  $\alpha$ -secretase cleaves APP within the  $A\beta$  region, forming sAPP $\alpha$  and CTF $\alpha$  which is subsequently cleaved into P3 and the membrane-bound AICD. In the amyloidogenic pathway,  $\beta$ -secretase cleavage results in the production of sAPP $\beta$  and generation of a carboxy-terminal fragment (C99), which is cleaved by  $\gamma$ -secretase and generates monomeric  $A\beta$  species including  $A\beta_{38}$ ,  $A\beta_{40}$ ,  $A\beta_{42}$  and  $A\beta_{43}$ ; the latter fragments are prone to aggregate and forms oligomers and fibrils. Figure reproduced with kind permission from the authors and publishers.

Senile plaques are spherical lesions found in the cerebral cortex and there are two main types: diffuse plaques and neuritic plaques. Both contain A $\beta$  but the latter also contain dystrophic neurites, tau paired helical filaments, reactive astrocytes and microglia<sup>21</sup>. Whereas diffuse plaques are observed in the healthy individuals, so may be a consequence of normal ageing, neuritic plaques are predominantly found in AD patients<sup>22</sup>.

### 1.2.3 Scoring systems for amyloid deposition

The first amyloid scoring system to be established was the Khachaturian criteria in 1985<sup>23</sup> which was based on the density of total amyloid plaques (both diffuse and neuritic). Subsequent to that, the Consortium to Establish a Registry for Alzheimer's disease (CERAD) published a protocol in which a semiquantitative assessment of neuritic plaques was combined with clinical data to produce a diagnostic scoring system<sup>24</sup>. This was the same year in which Braak & Braak distinguished three stages of amyloid deposition<sup>16</sup>. In stage one, plaques are found in the basal portions of the frontal, temporal and occipital lobes. In stage two isocortical areas are affected with some plaque formation in the hippocampus but a lack of plaques in the primary sensory, motor and visual cortices. In the final stage amyloid plaques may be found in primary isocortical areas in addition to the cerebellum and subcortical nuclei.

In 1997, the National Institute on Aging (NIA) suggested new guidelines combining the CERAD score for neuritic plaques with the topographic staging of NFTs proposed by Braak and Braak<sup>25</sup>.

Since then, advances in knowledge have led to various updates and iterations of these scoring systems. Thal phase<sup>26</sup> provides a more granular assessment of A $\beta$ -deposition, based on a proposed hierarchical progression of A $\beta$  through neuroanatomical areas (similar to the Braak staging of NFTs). Thal phase distinguishes 5 phases based on progressive deposition of amyloid in neocortex (1), allocortex/limbic (2),

diencephalon/basal ganglia (3), brainstem/midbrain (4), cerebellum (5). However, the assessment does not distinguish between compact and diffuse amyloid deposits.

#### 1.2.4 'ABC' scoring of AD pathology

Since 2012, an 'ABC' score, published by the National Institute on Aging–Alzheimer's Association (NI-AAA), has been widely used for the neuropathologic assessment of AD<sup>27,28</sup>.

This approach was based on an analysis of the National Alzheimer's Coordinating Center (NACC) database. An accumulation of data demonstrated that some older individuals who were cognitively intact proximate to death had significant AD neuropathologic change and that the pathophysiologic processes were present well in advance of subjective or objective cognitive deficits. This led to a consensus to disentangle the clinicopathologic term 'Alzheimer's disease' from AD neuropathologic change.

The 'ABC' score of AD pathology incorporates histologic assessments of A $\beta$  plaques (A) based on the Thal score, staging of NFTs (B) based on the Braak staging system and scoring of neuritic plaques (C), based on CERAD criteria. Each of the A (amyloid), B (Braak), and C (CERAD) scores are then transformed to state the level of AD neuropathologic change on a four tiered scale (non, low, intermediate and high).

#### 1.2.5 The amyloid hypothesis

The amyloid hypothesis postulates that AD is caused by a cascade whose initiating event is A $\beta$  deposition which leads linearly to tau pathology, synaptic dysfunction, inflammation, neuronal loss and then cognitive deficits<sup>29</sup>. The hypothesis has its origins in Alzheimer's original finding that senile plaques were present in the brain of his patients. It gained traction in the 1990s with the discovery of causative mutations for familial AD (FAD) in three genes which are all involved in the production of beta-amyloid (discussed in section 1.3.1). In recent years, the validity of the hypothesis has

been questioned, in particular as a result of the failure of anti-amyloid therapies. Some of the key problems with the amyloid hypothesis are discussed in the forthcoming sections.

#### 1.2.6 Clinicopathological correlation studies

Despite being considered the key pathological substrate, numerous studies have found that overall amyloid plaque burden does not correlate well with the severity of AD<sup>30,31</sup> and that senile plaques may be present in cognitively normal individuals, some of whom have a disease burden equivalent to those with AD<sup>32</sup>.

The presence of neuritic, rather than diffuse, plaques, is a better predictor of the extent of cognitive decline<sup>22</sup> but the density of neocortical NFTs correlates better with ante-mortem cognitive status better than both types of plaque<sup>33</sup>. As previously noted, however, NFTs are not specific to AD and are present in a large number of neurodegenerative disorders; they are also found in cognitively normal aged subjects<sup>34–36</sup>.

Although the presence of senile plaques and NFTs in cognitively normal individuals suggests that they are not the cause of symptomology in AD an extensive review of the literature conducted in 2012 questions some of the findings above<sup>33</sup>. The authors note that it is extraordinarily rare for a case with widespread, dense AD-type neocortical lesions to lack documented antemortem cognitive decline. Similarly, they found that no significant subset of patients with severe age-associated cognitive decline exists that lacks any pathologic substrate when modern methods (i.e. immunohistochemistry) are used in the neuropathologic examination.

Overall, the relationship between the presence of the pathological substrates of AD and the clinical presentation is not straightforward but most would agree that overall amyloid plaque burden is a poor predictor of the cognitive deficits seen in the disease.

## 1.2.7 The temporal relationship of amyloid and tau

### 1.2.7.1 *Chicken or egg?*

Another source of conjecture is the temporal relationship of amyloid and tau. Some autopsy data of cognitively unimpaired elderly subjects show that NFTs are predominantly confined to the entorhinal and adjacent temporal isocortices and not often seen in temporal neocortex or extra-temporal regions<sup>16,30,34</sup>. This finding has been replicated in tau-PET studies where, in normal aging, signal has been described to occur in the medial temporal lobe, but only in other regions when amyloid is present<sup>37</sup>.

The observation that tau is found in the medial temporal lobe in normal aging and only in other regions when amyloid is present, has led many to conclude that amyloid is necessary for the spread of pathological tau species. This hypothesis is supported by data from rat models where treatment of cultured neurons with soluble A $\beta$  oligomers isolated from the AD cortex causes neuritic dystrophy and tau hyperphosphorylation, however no dystrophy ensues if tau is first knocked down<sup>38</sup>. Similar studies in humans suggest that A $\beta$ , particularly soluble oligomers of A $\beta$ 42, may trigger AD-type tau alterations<sup>39</sup>.

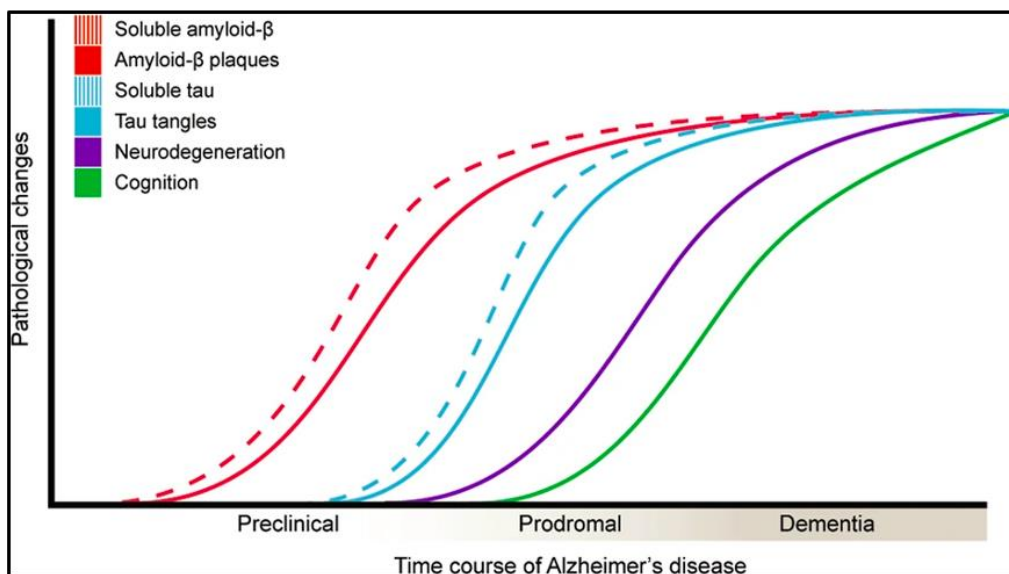
An intriguing possibility, which applies not only to AD but across the neurodegenerative spectrum, is that tau is the key pathogenic element but that other protein aggregates, be they amyloid, alpha-synuclein or Huntingtin, precipitate the damaging non-physiological distortions such as hyperphosphorylation<sup>12</sup>.

### 1.2.7.2 *Evidence from biomarker studies*

The current consensus on the cellular and temporal relationship of amyloid and tau is of a modified A $\beta$  cascade, where amyloidosis precedes the spread of pathologic tau, which in turn causes neurodegeneration and cognitive decline<sup>40</sup>. The increasing availability and sophistication of biomarkers has shed further light on the relationship.

A study of dominantly inherited AD by Bateman and colleagues<sup>41</sup> found a sequence of changes which was also replicated in sporadic AD<sup>42</sup>. The first biomarker change was decreased A $\beta$ 42 levels in CSF (known to correlate with amyloid plaque burden) which began to decline as early as 25 years before the onset of symptoms. Fibrillar A $\beta$  deposition, as detected by PiB-PET, was detected 15 years before expected symptom onset. Increased concentrations of CSF tau and brain atrophy were detected 15 years before expected symptom onset and cerebral hypometabolism and impaired episodic memory were observed 10 years before expected symptom onset. Global cognitive impairment, measured by the Mini-Mental State Examination (MMSE) and the Clinical Dementia Rating (CDR) scale, was detected 5 years before expected symptom onset, and patients met diagnostic criteria for dementia at an average of 3 years after expected symptom onset.

**Figure 1.3: time course of pathological changes in AD ( Leuzy *et al.*, 2019).**



The temporal relationship of the pathological changes seen in AD showing that deposition of amyloid appears to pre-date tau deposition both of which appear many years before cognitive symptoms are apparent. Figure reproduced with kind permission from the authors and publishers.

An addendum to Bateman et al's schema was made possible with the advent of tau-PET technology. In line with the relationship between CSF A $\beta$ 42 and amyloid-PET imaging, studies demonstrated a similar temporal delay between CSF and PET

measures of tau with changes in soluble levels of tau preceding changes in PET markers; the schema incorporating tau-PET is shown above in Figure 1.3<sup>37</sup>.

In light of recent advances such as improved PET imaging, a new, biomarker-driven framework has been proposed to update the 2011 National Institute on Aging and Alzheimer's Association (NIA-AA) diagnostic criteria for AD<sup>43</sup>. The research framework focuses on the diagnosis of AD with biomarkers in living persons with biomarkers grouped into those of A $\beta$  deposition, pathologic tau and neurodegeneration (the AT(N) system).

It also outlines two different categorical cognitive schemes for staging the severity of cognitive impairment: a scheme using three traditional syndromal categories (cognitively unimpaired, mild cognitive impairment (MCI) and dementia) and a six-stage numeric scheme based on cognitive testing, neurobehavioral assessments and functional impairments.

Overall, the framework acknowledges the prevailing conviction that A $\beta$  drives the pathogenesis of AD, with pathological tau occurring as a secondary event, but also accepts that this view may be too simplistic. It notes that other pathological sequences may be possible and further improvements in biomarkers are necessary to shed light on this complicated relationship.

#### 1.2.8 Aberrant protein aggregations: cause or effect?

While there is little doubt that senile plaques and NFTs are the neuropathological hallmarks of AD, there is substantial debate about whether they are a cause or consequence of the disease. Although there are few clear answers from clinico-pathological correlative studies, functional studies do seem to suggest that amyloid and tau species have deleterious effects within the central nervous system (CNS).

### 1.2.8.1 *Oligomers: the key amyloid species?*

The toxicity of administering A $\beta$  to cultured primary neurons was first demonstrated in 1989 and provided a mechanism for the role of A $\beta$  in the pathogenesis of AD<sup>44</sup>. The dominant theory for many years was that secreted, fibrillar A $\beta$  found in extracellular plaques was the key pathogenic substrate. However, as noted above, amyloid plaque burden does not correlate well with cognitive decline, and removal of amyloid plaques from the CNS has little effect on cognitive status. As such, the pathogenicity of plaques themselves has been increasingly questioned. More recently lower molecular weight protofibrils, and particularly prefibrillar soluble A $\beta$  oligomers, have been shown to be the most toxic species<sup>45</sup> and to correlate more robustly with both synaptic loss and severity of cognitive impairment than other forms of amyloid<sup>46</sup>.

Soluble A $\beta$  oligomers are a key constituent of plaques and may be sequestered within them as a neuroprotective mechanism<sup>5</sup>. The quantity of A $\beta$  oligomers in neuritic plaques was compared in subjects who were classified as either clinically normal (CDR of 0) or mildly demented (CDR of 1) shortly before death; subjects were chosen to have similar plaque densities. Oligomer-to-plaque ratios were significantly higher in the mildly demented, plaque-rich patients and completely distinguished (without overlap) the cases from controls<sup>47</sup>.

A $\beta$  oligomers have also been shown to produce cognitive deficits in the absence of plaques<sup>48</sup>. When various constituents of amyloid plaques from AD patients were isolated, it was found that soluble oligomers of A $\beta$ 42 (but not amyloid plaque cores or A $\beta$  monomers) dose-dependently impaired synaptic function in healthy adult rats<sup>39</sup>.

Soluble A $\beta$  oligomers bind to post-synaptic excitatory sites<sup>49</sup> and affect many critical neuronal activities, including attenuating long-term potentiation (LTP) and enhancement of long-term synaptic depression<sup>50</sup>. Oligomers also affect synaptic structures such as dendritic spines and have been shown to interfere with calcium homeostasis in neurons, inducing oxidative stress and tau hyperphosphorylation<sup>51</sup>.

#### 1.2.8.2 *NFTs and tau oligomers*

Although NFTs correlate better than amyloid species with cognitive decline and neuronal loss, cell death in AD occurs prior to the formation of NFTs<sup>52</sup>. Analogous to the role of amyloid, NFTs are not the most toxic tau aggregates, with numerous studies suggesting that soluble oligomers drive tau toxicity<sup>53,54</sup>.

The concentration of tau oligomers is four times higher in AD brains than in healthy controls<sup>55</sup> and, like A $\beta$  oligomers, tau oligomers have a variety of deleterious effects within the CNS. When recombinant tau oligomers are administered to healthy mice they display synaptic dysfunction and memory impairment<sup>56</sup>. Hyperphosphorylation of tau causes its redistribution from axon to the cell body causing decreased dendritic length, arborisation, and spine density<sup>57</sup> and also promotes an increase in long term depression (LTD)<sup>58</sup>.

#### 1.2.9 The role of the synapse in AD

Decreased synapse number has long been recognised as the strongest quantitative neuropathological correlate of the cognitive changes seen in AD<sup>59,60</sup>. These findings are, perhaps, unsurprising as synaptic function, in particular synaptic plasticity, is at the very heart of cognition. Synaptic dysfunction may precede some of the other pathological events in AD and, as such, it is an attractive interventional target<sup>61</sup>.

##### 1.2.9.1 *Synaptic architecture and formation*

Synapses act as the point of contact between neurons and may be either electrical or chemical. In chemical synapses communication occurs via the movement of neurotransmitters from the pre-synaptic bouton, across the synaptic cleft to the post-synaptic region. The pre-synaptic bouton contains the complex machinery required for synthesis, storage and release of neurotransmitters<sup>62</sup>. The architecture of the synaptic cleft is reliant on adhesion proteins that hold the synapse in place; mutations in genes coding these proteins have been implicated in psychiatric and cognitive disorders<sup>63</sup>.

The post-synaptic region contains neurotransmitter receptors and may be found on the neuronal cell body or on dendrites which are branched protoplasmic extensions of the neuron. Immediately behind the postsynaptic membrane is an elaborate complex of interlinked proteins called the postsynaptic density (PSD). Proteins in the PSD are involved in anchoring and trafficking neurotransmitter receptors and modulating the activity of these receptors. Some key components of the post-synaptic density include scaffolding proteins (such as postsynaptic density 95 (PSD-95), shank and homer) neuroligin (a cellular adhesion molecule), NMDA and AMPA receptors, several protein kinases and actin<sup>64</sup>.

#### 1.2.9.2 *Synaptic plasticity: Long-term potentiation (LTP) and Long-term depression (LTD)*

The average human brain contains around 86 billion neurons and more than 100 trillion synapses<sup>65,66</sup>. Ramon y Cajal, noted that the number of neurons does not appear to change over the course of the lifetime suggesting that memories were unlikely to be due to their production. Instead he suggested that changes in the strength of connections between existing neurons could be the mechanism for memory formation (reviewed in Spires-Jones, 2014<sup>67</sup>). In 1949, the Canadian psychologist Donald Hebb suggested connections between neurons were dynamic and that they would be strengthened if they activate simultaneously (now termed long term potentiation - LTP) and weaken if they activate separately (now termed long term depression – LTD). First described in rabbit hippocampal slices, LTP is a long-lasting increase in synaptic strength of synaptic transmission when the pre- and postsynaptic neurons are activated simultaneously<sup>68</sup>. LTP can be pre- or postsynaptic, but postsynaptic mechanisms seem most affected in AD models<sup>69</sup>. There are also early and late phases of LTP, with the early phase dependent upon protein kinase activation causing several changes to synaptic AMPA receptors (AMPA). In late-phase LTP, increased levels of calcium and persistent activation of kinases lead to activation of transcription factors which, in turn, causes production of proteins which are involved in new dendritic spine formation<sup>70</sup>.

LTD is a weakening of synaptic strength following a stimulus. LTD can occur via several mechanisms, which, unsurprisingly, have effects opposite to those seen in LTP, including internalisation of AMPA receptors<sup>71</sup>. LTD is thought to be important for clearing old memory traces and in situations requiring behavioural flexibility.

#### 1.2.9.3 *Dendritic activity*

Dendrites are the neuronal compartment primarily devoted to collecting and collating input from other neurons and provide an enlarged surface area to receive signals. They are highly dynamic structures capable of plastic changes during adult life<sup>72</sup>. Their morphology, such as branch density and grouping patterns, is closely associated with the function of the neuron; malformation of dendrites is also tightly correlated to impaired nervous system function<sup>72</sup>.

Dendritic spines are small membranous protrusions from the dendrite that typically receive input from a single axon at the synapse<sup>73</sup>. The dendrites of a single neuron can contain thousands of spines which serve as an anatomical substrate for synaptic strength<sup>74</sup>. Post-synaptic receptors and post-synaptic densities (PSDs) are found in dendritic spines thus increasing the receptive properties of dendrites. Spines are motile and plastic structures whose morphology and lifespan are influenced by changes in sensory input. Patterns of neuronal activity known to induce synaptic plasticity effect changes in spine morphology suggesting that morphology reflects the dynamic state of the associated synapse and are therefore a morphological measure of plasticity<sup>74</sup>. Specifically, LTP has been associated with the formation of new dendritic spines and with the enlargement of spine heads; conversely, LTD has been associated with spine shrinkage and loss<sup>75</sup>.

Dendritic arborisation is the process by which neurons form new dendritic trees and branches to create new synapses. Branching may be extensive with as many as 100,000 inputs to a single neuron. The pattern of dendritic branching along with the receptor and channel composition and density of synapses regulate the electrical

properties of neurons. Abnormalities in dendritic tree development lead to serious dysfunction of neuronal circuits and, consequently, the whole nervous system<sup>76</sup>.

#### 1.2.9.4 *Synaptic dysfunction in AD*

Abnormalities in synapses from AD brain tissue were first described more than 50 years ago<sup>77</sup>. Quantitative ultrastructural and immunohistochemical histopathological studies have since confirmed that synapse reduction, including the loss of synaptic elements such as synaptophysin, SV2 and p65, is an early structural correlate of the cognitive changes seen in AD<sup>59,60,78,79</sup>.

Studies using hippocampal tissue from AD patients have shown morphological abnormalities in dendrites, as well as a significant reduction in the number of dendritic spines<sup>80</sup>. These findings have been recapitulated in numerous transgenic mouse models which have found reduced spine density<sup>81-83</sup>. Several studies noted a spatial correlation between amyloid plaques and dendritic abnormalities however other reports suggested that abnormalities also occur in areas devoid of amyloid plaques suggesting that soluble A $\beta$  species are not the cause<sup>84</sup>. Several reports have demonstrated that synthetic A $\beta$  oligomers can disrupt the molecular processes involved in LTP, leading to a significant reduction of the latter in hippocampal slices<sup>85</sup>. Oligomeric A $\beta$  extracted from the cerebral cortex of humans with AD has also been shown to inhibit LTP, while enhancing long-term depression (LTD) in rat organotypic hippocampal slices<sup>39,85,86</sup>.

Interestingly, similar changes are also seen in transgenic tau mice which show a decrease in the spine density of pyramidal neurons<sup>87</sup> as well as a marked reduction in the complexity of dendritic arborisation<sup>87,88</sup>. The prevailing wisdom is that oligomers of both A $\beta$  and tau, are the most likely cause of the dendritic changes seen.

### 1.3 Genetics of Alzheimer's disease

Alzheimer's disease can be defined in two main ways, by age of onset or heritability giving rise to four categories:

	Genetic	Sporadic
Early-onset	Early onset Familial AD	Early onset sporadic
Late-onset	Late onset Familial AD	Late onset sporadic

Early onset Alzheimer's disease (EOAD) is generally characterised by disease onset before the age of 65 (although some researchers advocate different cut-offs<sup>89,90</sup>) and accounts for 10% of all AD cases<sup>91</sup>; the more common late-onset Alzheimer's disease (LOAD) is generally accepted to have an onset after the age of 65.

Both early and late onset AD can be further categorised into familial and sporadic (also known as non-familial) forms. The majority of EOAD cases are genetically unexplained<sup>92</sup> with sporadic AD thought to account for approximately 90% of cases<sup>93</sup>. Familial AD (FAD) has Mendelian inheritance and accounts for approximately 5-10% of EOAD cases<sup>94</sup>; it may also occur after the age of 65 (and therefore be classified as late-onset) in approximately 5% of cases<sup>95</sup>.

#### 1.3.1 Familial Alzheimer's disease (FAD)

Familial AD is dominantly inherited and caused by three genes; the first found in the *APP* gene and the other two presenilin 1 (*PSEN1*) and presenilin 2 (*PSEN2*). 10-15% of FAD cases are estimated to have *APP* mutations, 50-70% of cases *PSEN1* mutations and 5% of cases are due to rare *PSEN2* mutations; the remaining familial AD patients are thought have *de novo* mutations<sup>96,97</sup>. All three genes are involved in the production of A $\beta$  which is one of the key reasons for the primacy of the amyloid hypothesis.

#### 1.3.1.1 *APP*

The observation that those with Down syndrome (DS) – trisomy of Chromosome 21 - exhibited comparable CNS pathology to patients with AD was key to the discovery of *APP*. Linkage studies and the discovery that amyloid plaques peptides were cleaved from *APP*, identified *APP* located on chromosome 21q21<sup>98,99</sup>. The discovery explained why those with DS, who have three copies of the *APP* gene, develop clinical features of AD in their fourth decade. Individuals who have trisomy 21 but, due to a translocation, only have two copies of *APP* have DS features but do not develop AD<sup>100</sup>. Furthermore, individuals with the *APP* gene micro-duplicated but not the rest of the chromosome do not have DS but develop AD during their fifth decade<sup>101</sup>. Over 50 pathogenic mutations in *APP* have been reported in 119 probands of autosomal dominant families<sup>92</sup>. *APP* mutation carriers have an average age of onset of 45-65<sup>102</sup>.

#### 1.3.1.2 *PSEN 1 & PSEN2*

*PSEN1* (Presenelin 1) located on chromosome 14q24.2, was identified as a pathogenic gene for fAD in 1995<sup>103</sup>. Mis-sense mutations in *PSEN1* have complete penetrance and are the most common cause of fAD<sup>104</sup>. *PSEN2* (Presenilin 2), located on chromosome 1q42.13, has high homology to *PSEN1* and was identified as a candidate gene in familial AD in 1995<sup>105</sup>. *PSEN2* mutations have a lower penetrance than *PSEN1* mutations suggesting that environmental or other genetic factors may influence disease<sup>106</sup>.

Those with the *PSEN1* gene mutations have the earliest ages of onset, which falls largely within the range 35-55 years, although one such family member has recently been recorded with onset at 24 years. Families carrying mutations in the *PSEN2* gene have ages of onset largely within the range 40-70 years and thus show some overlap with late-onset Alzheimer's disease<sup>102</sup>. The products of *PSEN1* and *PSEN2* are essential components of a protein complex that is responsible for  $\gamma$ -secretase activity<sup>107</sup>.

### 1.3.2 Sporadic Alzheimer's disease

While most sources consider early and late onset sporadic AD to be the same clinical entity there are reasons to suppose they might be different. Clinically, patients with early-onset SAD are more likely to present with atypical syndromes and a more aggressive disease course<sup>108</sup>. Neuropathological studies have reported a higher burden of neuritic plaques and neurofibrillary tangles, as well as greater synapse loss than in those with early-onset sporadic AD<sup>109</sup>.

A relatively small number of studies have investigated the genetic basis of early-onset sporadic AD. Thus far, research has implicated both late-onset sporadic AD risk genes, such as *SORL1*<sup>110</sup> and *TREM2*<sup>111,112</sup> as well as some novel genes residing in endolysosomal transport pathways<sup>94</sup>. The vast majority of studies over the past 20 years, however, have concentrated on the genetic associations of late-onset sporadic AD.

#### 1.3.2.1 *Genome wide association studies*

Although age is the strongest risk factor, late-onset SAD is highly heritable with estimates varying between 58 and 79%<sup>113</sup>. First degree relatives of patients with late-onset SAD have a lifetime risk of 20-25%, compared to the general population who have a 10.4% risk<sup>114</sup>.

Genome Wide Association Studies (GWAS) are the most successful approaches to disease gene detection, made possible by advances in chip-based assay technology capable of genotyping millions of single nucleotide polymorphisms (SNPs) and powerful datasets. GWAS utilise a case-control method to determine differences in allele frequency between control subjects and those with a particular disease status to identify genetic variations. The technique has revolutionised the approach to complex diseases, such as psychiatric conditions and AD, where the aetiology is linked to multiple small, genetic 'hits' rather a single causative gene.

In the AD field, two major GWAS were published in 2009. The first published by Harold et al<sup>115</sup>, showed highly significant associations for *CLU* and *PICALM* loci and suggestive evidence for an association with *BIN1*. These findings were replicated by Lambert et al<sup>116</sup> in a separate cohort who identified two further genome wide significant markers at the *CLU* locus and another locus of interest at *CR1*. Further GWAS over the next two years<sup>117–119</sup> meant that by 2011 ten susceptibility loci had been identified: *APOE*, *CR1*, *CLU*, *PICALM*, *BIN1*, *EPHA1*, *MS4A*, *CD33*, *CD2AP* and *ABCA7*.

In 2013 the largest GWAS meta-analysis took place. The International Genomics of Alzheimer's Project (IGAP) conducted a two-stage meta-analysis using four GWAS samples with European ancestry<sup>120</sup>. Overall, the meta-analysis identified 11 new susceptibility loci (*HLA-DRB5-HLA-DRB1*, *PTK2B*, *SORL1*, *SLC24A4-RIN3*, *DSG2*, *CELF1*, *NME8*, *FERMT2*, *CASS4*, *INPP5D* and *MEF2C*) and confirmed the association of ten previously identified loci. Since then, further single-nucleotide, genome-wide, transethnic and proxy design studies (based on reports of parental history) have identified a further 30 novel GWS loci bringing the current total to over 50<sup>121</sup>.

Interestingly, one important finding that arises from the various GWAS is that the genes that cause autosomal dominant forms of AD do not have a signal of a size that would implicate their involvement in most sporadic AD.

#### 1.3.2.2 Identification of rare variants

In spite of the burgeoning numbers of common variants associated with SAD, it is estimated that 60% of the genetic component remains unaccounted<sup>122</sup>. The missing heritability is likely attributable to rare variants with large effect sizes that are not represented on GWAS platforms and common variants with small effect sizes that GWAS do not have sufficient power to detect.

Next Generation Sequencing (NGS) has been used to good effect to identify rare variants with substantial effect sizes. NGS has uncovered *TREM2* as an AD risk gene, with associated odds ratios similar to that of a single *APOE* E4 allele<sup>123,124</sup>. Additionally,

a significant single nucleotide variant (SNV) (a variation in a single nucleotide without any limitations of frequency) in *TREM2* was found plus two novel susceptibility loci, *PLCG2* and *ABI3*<sup>125</sup> using an exome-chip design.

#### 1.3.2.3 *Pathway analysis*

An additional use for GWAS data is pathway analysis which permits a more detailed understanding of the biological processes at play in SAD. Pathway analyses combine associations across multiple variants from GWAS data at a pathway-level by examining variants in all genes clustered in defined biological pathways. Pathway gene-sets are derived from a variety of sources such as curated, publicly-available databases such as the KEGG (Kyoto Encyclopedia of Genes and Genomes) and GO (Gene Ontology). The analysis aims to identify gene-sets with stronger associations that would be expected by chance.

One of the earliest examples of this analysis using the GERAD data-set found a significant overrepresentation of association signals in pathways related to cholesterol metabolism and the immune response<sup>126</sup>; this replicated earlier findings from Lambert et al where the innate immune response was strongly implicated<sup>127</sup>. A subsequent study in 2014, using the larger IGAP dataset, reinforced the role of the immune system and cholesterol metabolism in conferring AD susceptibility and also implicated the regulation of endocytosis and protein ubiquitination<sup>128</sup>. A more recent GWAS of almost 100,000 individuals implicated similar pathways with immunity, lipid metabolism again prominent but tau binding proteins and amyloid precursor protein (APP) metabolism also noted<sup>129</sup>.

#### 1.3.2.4 *Polygenic risk scores*

The polygenic risk score (PRS) assesses aggregate genetic effects, notably including those loci that have not reached the genome wide significance threshold. The PRS has been shown to predict case-control status with approaching 75% accuracy when *APOE* genotype and SNPs with association p values <0.5 were included (Escott-Price et al.,

2015). However, if one considers individuals at the extremes of polygenic risk score (the highest and lowest 2%) the PRS can give prediction accuracy of over 90% (Escott-Price et al., 2015). Such tools permit the identification of asymptomatic populations at greatest and lowest risk of AD which could prove useful in the selection of participants for longitudinal studies and clinical trials.

## 1.4 The *APOE* gene

As discussed above, there are now over 50 known risk genes for SAD. However, despite the success of GWAS and NGS, the *APOE* E4 allele remains the strongest genetic risk factor. Apolipoprotein-E (*APOE*) was the first loci to be robustly associated with LOAD via linkage analysis and association analysis<sup>130,131</sup>. Located on chromosome 19 (19q13.2), *APOE* encodes apolipoprotein E (ApoE), a protein with a large number of functions both within and outside the CNS.

### 1.4.1 Basic genetics and expression

In humans, *APOE* has three major allelic variants which give rise to six different genotypes. Alleles are distinguished by two non-synonymous SNPs in exon 4 of chromosome 19, rs429358 and rs7412. A thymine (T) to cytosine (C) change at rs429358 encodes arginine rather than cysteine at aa112; the same change at occurs at rs7412. The effects of these changes on the resultant alleles are shown in Table 1.1.

**Table 1.1: *APOE* SNPs and alleles.**

rs429358 (44908684)	rs7412 (44908822)	Allele
T	T	ε2
T	C	ε3
C	C	ε4

The most common allele is E3 (79%) and E2 the least common (7%) allele. The E4 allele frequency is approximately 14% in the general population but is around 40% in patients with AD<sup>132</sup>. E4 heterozygotes are three to four times as likely, and E4 homozygotes over nineteen times as likely, to develop SAD than those without E4 alleles<sup>133</sup>. This compares to odds ratios for alleles at other loci where risk is typically less than 1.5<sup>134</sup>. E4 alleles increase the lifetime risk of developing AD and reduce the age of onset in a dose-dependent manner; the frequency of AD and mean age at clinical onset are 91% and 68 years in E4 homozygotes, 47% and 76 years in E4 heterozygotes, and 20% and 84 years in E4 noncarriers<sup>135</sup>.

The E2 allele reduces AD risk and delays age of onset<sup>133</sup>, however it has been linked to cardiovascular disease<sup>136</sup>. The E4 allele is also a risk factor for a variety of other conditions including atherosclerosis, HIV disease progression plus other neurological disorders, including cerebral amyloid angiopathy (CAA) and CAA-associated cerebral haemorrhages, tauopathies, dementia with Lewy bodies (DLB), Parkinson's disease and multiple sclerosis<sup>137</sup>.

#### 1.4.2 ApoE structure

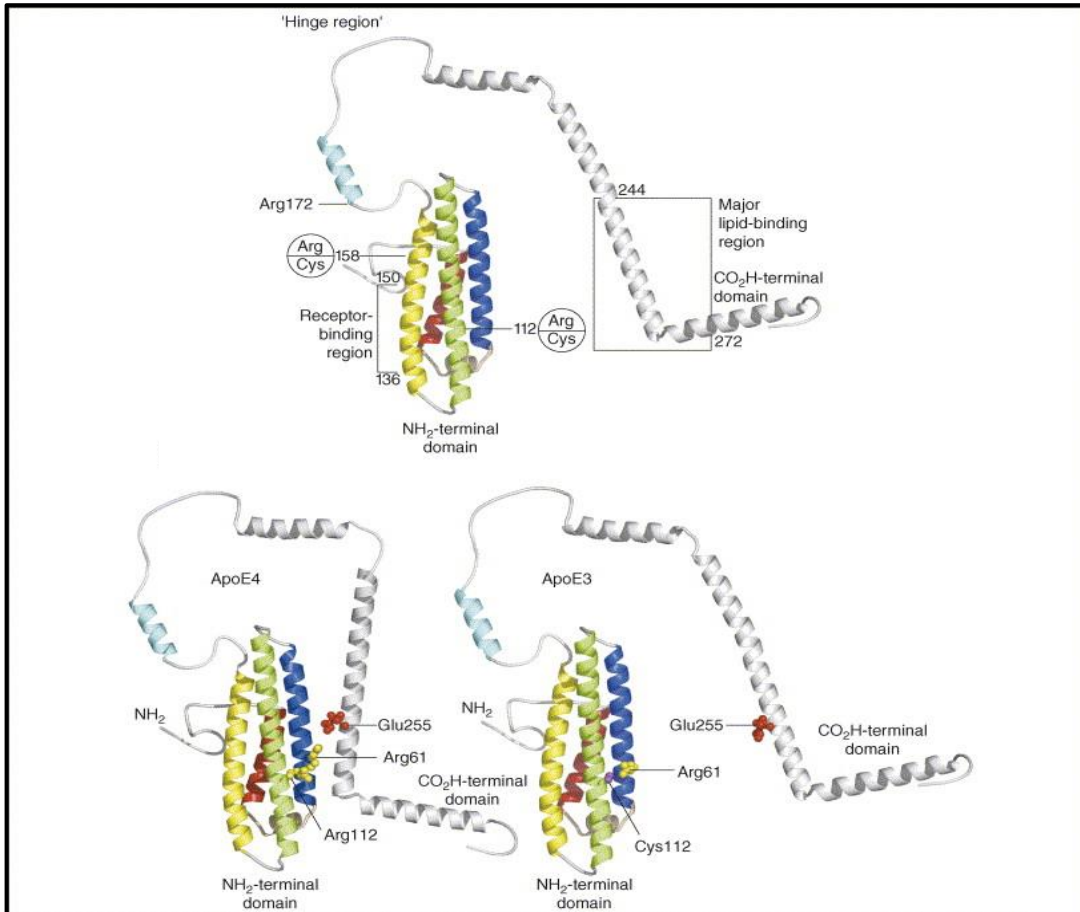
ApoE is a 34-kDa protein comprising 299 amino acids. Like other apolipoproteins, ApoE contains amphipathic  $\alpha$ -helical lipid-binding domains that enable it to switch reversibly between a lipoprotein-bound and a lipid-free state<sup>138</sup>. In the lipid-free state, ApoE contains two independently folded structural domains; the N-terminal domain (amino acids 1-191) and the C-terminal domain (amino acids 223-299) linked by a hinge region (amino acids 192-222). The N-terminal domain is an elongated four-helix bundle and the C-terminal domain is highly  $\alpha$ -helical but its precise structure is unknown.

Each structural domain is responsible for different functions; broadly speaking the N-terminal domain is the receptor binding region while the C-terminal binds lipids<sup>139</sup>. The LDL-receptor-binding region (amino acids 136–150) is located in helix 4. High-affinity binding to LDL receptors requires ApoE to be associated with lipid. The principal lipid-binding region is found in the C-terminal domain (amino acids 241–272) although the N-terminal domain also binds lipid to a lesser extent<sup>140</sup>. Full receptor-binding activity also requires an arginine at position 172, located in the 'hinge region' connecting the two domains<sup>141</sup>.

As noted above, the three common allelic isoforms ( $\epsilon$ 2,  $\epsilon$ 3 &  $\epsilon$ 4) differ at positions 112 and 158. ApoE3, the most common isoform, contains cysteine and arginine, respectively, whereas ApoE2 has two cysteines and ApoE4 has two arginines at these positions. In ApoE4, domain interaction occurs as a result of a salt bridge between Arg61 and Glu255 that stabilises closer contact between the N- and C-terminal domains. This interaction does not occur to the same extent in ApoE2 and ApoE3

because the side chain of Arg61 adopts a different conformation (in which it is buried between helices 2 and 3) owing to Cys112, resulting in a less accessible side chain conformation for salt-bridge formation with Glu255<sup>138</sup>.

**Figure 1.5: Structure of the  $\epsilon 3$  and  $\epsilon 4$  isoforms of ApoE from Hatters et al, 2006<sup>138</sup>.**



The structure of the  $\epsilon 3$  and  $\epsilon 4$  isoforms of ApoE demonstrating the N-terminal domain (receptor binding region) and the C-terminal domain (principal lipid-binding region) linked by a hinge region. In the  $\epsilon 4$  isoform, a salt bridge forms between the Arg61 and Glu255 allowing closer contact between the N- and C-terminal domains thus affecting its receptor and lipid binding capacity. Figure reproduced with kind permission from the authors and publishers.

The main functional consequences of this conformational change are differences in domain interaction and stability. The ApoE isoforms differ considerably in the conformational stability of their N-terminal domains: ApoE4 is the least resistant to thermal and chemical denaturation<sup>142</sup>. In the peripheral circulation, ApoE4 has also been found to preferentially bind to large lower-density lipoproteins, namely VLDLs and LDLs, whereas ApoE3 and ApoE2 prefer smaller, cholesterol-rich high-density lipoproteins such as HDLs<sup>143</sup>. These two major structural differences are thought to underlie the association of ApoE4 with disease.

### 1.4.3 Functions of ApoE in health and disease

Outside of the CNS, ApoE is mainly produced by the liver and macrophages and its primary role is in cholesterol metabolism<sup>144</sup>. Within the CNS, ApoE is mainly produced by astrocytes but to a lesser extent by microglia<sup>145</sup>. Neurons are also able to synthesise ApoE albeit at lower levels than astrocytes, a function that is upregulated with aging and stress conditions<sup>146–148</sup>. Interestingly, ApoE derived from different cellular sources exhibit different properties; ApoE4 produced by astrocytes has neuroprotective effects when exposed to excitotoxic challenge, whereas neuronal expression of ApoE4 promotes excitotoxic cell death<sup>149</sup>.

Although its relationship with AD was identified over 20 years ago, the role of ApoE within the CNS, and contribution towards the aetiology of AD, is still not well understood. The best-known physiological role of ApoE is in lipid metabolism, as it shuttles cholesterol produced by astrocytes to neurons where it is utilised in a variety of key physiological functions. Much of the work on ApoE in AD has concentrated on its roles in the clearance and deposition of A $\beta$  and the prevailing view that its key role in SAD is the modulation of A $\beta$  metabolism remains<sup>5</sup>. However, there is increasing recognition from both genetic and functional studies that ApoE has other important roles within the CNS.

Studies of AD using mouse models expressing humanised ApoE isoforms, human and animal cell lines, and post-mortem human samples have revealed multiple pathological phenotypes impacted by ApoE, including A $\beta$  metabolism, tau phosphorylation and neurotoxicity, lipid metabolism, synaptic function and neuroinflammation. Each of these, and in particular the differential effects of the E4 isoform, are discussed below.

#### 1.4.3.1 A $\beta$ metabolism

Both human and murine studies have consistently shown that brain A $\beta$  levels and amyloid plaque loads are ApoE isoform dependent (E4 > E3 > E2) suggesting an

important role for ApoE in A $\beta$  metabolism<sup>150,151</sup>. Increased A $\beta$  levels are thought to be attributable to both increased production and decreased clearance although most agree that the latter is the more dominant mechanism<sup>152</sup>.

Upregulation of A $\beta$  by ApoE4 is supported by several findings. Exogenously applied ApoE4 increases A $\beta$  accumulation by stimulation of APP endocytosis and processing, via the LDL-receptors ApoER2 and LRP1<sup>153,154</sup>. Additionally, ApoE isoforms differentially regulate cholesterol levels, which have been shown to modulate  $\gamma$ -secretase activity and therefore A $\beta$  production<sup>155</sup>.

ApoE4 has been shown to be less efficient in A $\beta$  clearance than ApoE3 in mouse models that express human ApoE isoforms; this observation was noted even in young mice well before any amyloid deposition occurred<sup>156</sup>. ApoE4 binds secreted A $\beta$  less efficiently than other isoforms compromising its uptake and lysosomal degradation<sup>157,158</sup>. ApoE4 may also be less efficient at clearing A $\beta$  at the blood-brain barrier<sup>159</sup>. Furthermore, ApoE4 competes with A $\beta$  for the same degradation pathways<sup>160</sup>. Finally, microglial studies have demonstrated that ApoE3 promotes degradation of A $\beta$  more efficiently than ApoE4<sup>161</sup>.

#### 1.4.3.2 *ApoE proteolysis, neurotoxicity and tau phosphorylation*

As discussed above, abnormally phosphorylated tau is one of the key components of NFTs. In *APOE* knock-in mice, tau phosphorylation is higher in ApoE4 animals than in those with ApoE3<sup>162</sup>. Furthermore, tau hyperphosphorylation increases in transgenic mice expressing human ApoE4 in neurons but not in those expressing ApoE4 in astrocytes suggesting a neuron specific effect of ApoE4<sup>163,164</sup>. A recent isogenic ApoE model in human iPSCs found, that independent of its effect on A $\beta$ , ApoE4 triggered phosphorylation and mislocalisation of tau<sup>165</sup>.

Various mechanisms by which ApoE4 induces tau hyperphosphorylation and aggregation have been described. Neuronal ApoE4 is more susceptible to proteolytic cleavage than ApoE3 and fragments are present at higher levels in the brains of AD

patients compared with healthy controls<sup>164,166</sup>. Cleavage of ApoE4 following stress or injury produces a C-terminal truncated fragment<sup>164</sup> which increases tau hyperphosphorylation with attendant cytoskeletal disruption and the formation of intraneuronal NFT-like inclusions<sup>166</sup>. It is also associated with AD-like neurodegeneration and behavioural deficits in transgenic mouse models<sup>167</sup>.

Another possible mechanism is interaction with reelin. Activation of this pathway via the binding of reelin to ApoER2 and VLDL receptors reduces tau phosphorylation. ApoE competitively inhibits reelin binding to these receptors with ApoE3 and ApoE4 reducing reelin binding to VLDLR by approximately 60%, compared to just 10% in ApoE2<sup>168</sup>. Once bound to these receptors, there is also an isoform specific signalling effect (ApoE2 > ApoE3 > ApoE4) with attenuated ApoE4 signalling resulting in increased tau hyperphosphorylation<sup>169</sup>.

#### 1.4.3.3 Lipid metabolism

One of the best known physiological functions of ApoE is its role in lipid metabolism, transporting cholesterol, mainly from astrocytes to neurons, where it is an essential component in axonal growth, synaptic formation and remodelling - events crucial for maintaining cognitive integrity<sup>170,171</sup>.

Lipid and cholesterol processing mechanisms have been consistently implicated in the pathogenesis of AD by pathway analyses. In addition, a number of genes, other than APOE, are implicated: clusterin (CLU, also known as ApoJ) like ApoE acts as a cholesterol transporter; *PICALM* and *BIN1* are both implicated in receptor mediated endocytosis (RME) which is involved in the internalisation and transport of lipids; *ABCA7* which promotes phospholipid (but not cholesterol) efflux; and *SORL1* which is a member of the LDL receptor family<sup>172</sup>.

There are a number of isoform dependent effects of ApoE within lipid metabolism. Brain cholesterol levels are substantially reduced in the hippocampus and cortical areas in AD brains compared to controls<sup>173,174</sup> and ApoE4 knock-in mice have been

shown to have lower brain cholesterol concentrations than their ApoE3 counterparts<sup>175</sup>. The effect of ApoE genotype on astrocytic production of cholesterol is discussed in the next section but ApoE4 is thought to be less efficient than ApoE3 at promoting cholesterol efflux from both neurons and astrocytes<sup>176</sup>. Transport of brain cholesterol to neurons is also affected which may be due to insufficient levels of ApoE and/or impaired ApoE function: lower levels of CNS ApoE are found in ApoE4 carriers which is speculated to be caused by preferential degradation of ApoE4 in astrocytes<sup>177</sup>; impaired neuronal delivery of cholesterol may also contribute, with ApoE4 operating less efficiently than ApoE3<sup>178,179</sup>.

Finally, neuronal endocytosis of cholesterol requires functional ApoE receptors of the LDL family especially LRP1, LDL, VLDL and ApoER2. Some of ApoE's isoform specific effects pertaining to the reelin pathway have been discussed in the previous section, beyond this the literature is limited. Different receptor affinities of the three ApoE isoforms with respect to LDL-receptors has been described outside of the CNS where ApoE2 is known to be defective (<2% LDL receptor binding activity compared with ApoE3 and ApoE3) resulting in the cardiovascular condition type III hyperlipoproteinemia (HLP)<sup>180</sup>. However, the effects of ApoE4 isoform on LDL receptor binding in the CNS remain enigmatic.

#### *1.4.3.4 APOE's role in synaptic function and dysfunction*

As discussed above, reduced synaptic density is one of the best correlates of the cognitive changes seen in AD. There is a significant body of work that implicates ApoE in AD-associated plasticity<sup>181</sup> possibly through its isoform-specific functions in cholesterol and phospholipid metabolism and trafficking<sup>144</sup>.

Complete genetic deficiency of ApoE, or deficiency limited to the CNS, results in a reduction of synapse number that is at least partially due to loss of astrocyte-derived factors. Changes in dendritic spine density and morphology with accompanying changes in LTP are well-described in AD. There is evidence to suggest that all of these effects are impacted by ApoE in an isoform-dependent manner.

#### 1.4.3.4.1 Neuritic & dendritic and effects

Neurites are projections from the cell body of a neuron and can be either axonal or dendritic; they are typically called dendrites at an early stage of neurogenesis when it is difficult to distinguish between axons and dendrites. Both neurites and dendrites are affected by ApoE in an isoform dependent manner.

In cell culture models using cultured dorsal root ganglion neurons and Neuro-2a cells, treatment with ApoE3 plus  $\beta$ -VLDL significantly stimulates neurite extension, whereas ApoE4 plus  $\beta$ -VLDL markedly inhibits neurite extension and branching and disrupts the cytoskeleton<sup>182,183</sup>. Similar effects are found in rat hippocampal neurons where astrocyte-derived ApoE3, but not ApoE4, stimulates neurite outgrowth<sup>184</sup>.

ApoE4-associated inhibition of neurite extension is thought to be due to its effect on microtubule stability<sup>182</sup> and is likely mediated by cell-surface lipoprotein receptors. In a study by Holtzman and colleagues, the addition of anti-LRP antibody completely abolished the neurite-promoting effect of ApoE3 suggesting the mechanism of neurite extension is via interaction with the LRP receptor family. A similar conclusion was reached by Sun and colleagues, who noted that effects on neurite outgrowth were not dependent on direct astrocyte–neuron contact but required the low-density lipoprotein receptor-related protein<sup>184</sup>.

Isoform specific effects on dendritic spines, which are often considered the physical manifestation of synaptic plasticity, have also been observed consistently. ApoE4 impairs synaptogenesis *in vivo* in various rodent models. The density of dendritic spines is decreased by ApoE4, relative to ApoE3, in rat primary cortical neuronal cultures<sup>185</sup>. In several transgenic and gene-targeted murine models ApoE4 animals were found to have reduced spine density, length, arborisation and impaired morphology<sup>186–189</sup>.

Interestingly, Jain and colleagues, found that glial fibrillary acidic protein (GFAP)-apoE4 mice, which express ApoE4 solely in astrocytes, do not have impairments in their

dendritic arborisation, spine density or morphology compared to GFAP-ApoE3 mice indicating that the effects of ApoE4 may be influenced by its cellular source<sup>187</sup>.

#### 1.4.3.4.2 Impaired response to neuronal injury

Neuronal injuries are known to induce ApoE expression. Such an increase in ApoE level may help to repair neurons by delivering cholesterol and lipids to neurons<sup>190</sup>.

Chronic neuronal degeneration is accompanied by growth and reorganisation of the dendritic tree which is regarded as an attempt by the nervous system to counteract the functional impairments resulting from degenerative events. A histopathological study of brains from 64 AD patients and 20 age-matched controls showed an inverse relationship between the number of *APOE4* alleles and the extent of this plastic neuronal remodelling. The authors suggest that, in ageing, reparative capacity is progressively exhausted so although dendritic elements continue to grow during the progression of AD, the reparative capacity is reduced in those with *APOE4* alleles<sup>191</sup>.

These findings are replicated in a murine model which shows adult neurogenesis is reduced in both ApoE knockout and ApoE4 mice<sup>192</sup>. In another transgenic mouse model, environmental stimulation, which increases neurogenesis in the dentate gyrus of ApoE3-transgenic and wild-type mice, has the opposite effect on the ApoE4 mice, where it triggers apoptosis while decreasing hippocampal neurogenesis suggesting that the pathological effects of ApoE4 may be accentuated upon exposure to stress<sup>193</sup>.

#### 1.4.3.4.3 Long term potentiation (LTP) & Long-term depression (LTD)

Electrophysiological studies demonstrate the impairment of LTP in aged ApoE4 mice using *in vitro* hippocampal slices<sup>194</sup> and in wild-type mice with local injection of ApoE4<sup>195</sup>. Using hippocampal slices from wild-type, *APOE* knockout and mice expressing human ApoE2, E3, or E4 the authors who found that although all strains show comparable basal synaptic transmission, LTP was significantly greater in wild-type and ApoE3 mice than in ApoE-KO, ApoE4<sup>196</sup>.

Alterations of synaptic functions in young ApoE mice remain unclear with conflicting results: both enhancements<sup>189,197</sup> and no change<sup>198</sup> of hippocampal synaptic LTP have been reported in young ApoE4 mice compared to ApoE3 mice. The effects of ApoE genotype on LTD have not been well-described.

#### 1.4.3.5 Innate immunity: effects on microglial phenotype

Neuroinflammation, in particular the innate immune system, is strongly implicated in the pathogenesis of AD by various pathway analyses<sup>126,128,129</sup>. The main cell type traditionally implicated in the immune response within the CNS is microglia although there is increasing evidence that astrocytes also have key functions (discussed in the next section). ApoE has multiple effects on microglial phenotype in AD.

The role of microglia in AD is a burgeoning field after it was established that a number of risk genes are expressed predominantly by them including *TREM2*, *BIN1*, *CASS4*, *CD33*, *INPP5D*, *MEF2C*, *MS4A* and *PLCG2*. ApoE is expressed at very low levels by adult microglia in the healthy brain<sup>199</sup> but is upregulated in the diseased brain<sup>200</sup>. The transcriptional profile of microglia is altered in AD, switching from a protective, homeostatic phenotype to a disease-associated microglial (DAM) phenotype<sup>201</sup>. ApoE is a key regulator of the microglial transcriptional profile<sup>200</sup> and isogenic conversion of human iPSC-derived microglia from *APOE33* AD patients to *APOE44* transforms the microglia transcriptome to a DAM-like phenotype<sup>202</sup>.

One of the roles of microglia is phagocytosis. Morphology of *APOE4* microglia-like cells is different to their *APOE3* counterparts with fewer and shorter processes, a reduced capacity to phagocytose A $\beta$  and are deficient in lipid debris clearance<sup>202</sup>. This finding is replicated in murine models, where *APOE4* microglia are less efficient at plaque engulfment compared to *APOE4* microglia<sup>203</sup>. However, in murine N9 microglia cells expressing human ApoE isoforms, although expression of ApoE4 led to significantly reduced uptake of A $\beta$  in contrast to the other isoforms, it actually increased phagocytosis of apoptotic neuronal cells<sup>204</sup>.

ApoE isoforms may also affect microglial migration although the results are equivocal. Studies using primary microglia from mice with human ApoE isoforms found that microglia expressing ApoE4 or ApoE2 have significantly reduced C5a- and ATP-stimulated migration compared with microglia expressing human ApoE3<sup>205</sup>. However, in another study, ApoE4 significantly promoted microglial motility<sup>200</sup>. Numerous studies suggest that the presence of ApoE4, either exogenously applied or endogenously expressed, results in an increase in pro-inflammatory cytokine production in microglia with TNF $\alpha$ , IL-1 $\beta$ , IL-6, IFN $\gamma$  and nitric oxide (NO) consistently reported<sup>206,207</sup> although the specific cytokines identified are not universal<sup>200</sup>.

Overall, although the findings are quite equivocal, data suggest that ApoE4 negatively affects several aspects of microglial function that may hinder their ability clear extracellular debris from AD brains and may also influence the inflammatory profile of the CNS.

#### 1.4.3.5.1 Astrocytes

Work on the effect of ApoE genotype on the inflammatory phenotype of astrocytes is far less extensive than the work on microglia but there is increasing interest in the subject which is discussed in the next section.

### 1.5 Astrocytes in health and disease

Estimates suggest that astrocytes make up around 20–40% of the total number of cells in the brain<sup>208</sup>. The astrocytes/neuron ratio varies in different parts of the brain; they tend to be sparse in areas with a high density of neuronal cell bodies whereas they are replete in areas with dendrites and axons<sup>209</sup>. Astrocytes are intimately involved with neurons and a single astrocyte may be in contact with thousands of synapses via its processes; in the adult hippocampus a single astrocyte can contact up to 140,000 synapses<sup>210</sup>. The ratio of astrocytes to neurons also increases with the increasing complexity of the organism<sup>211</sup>.

Astrocytes were traditionally thought of as simple, homogenous cells whose primary function was to provide the architecture of the CNS. Over the past 25 years, however, it has become clear that astrocytes are responsible for a wide variety of complex and essential functions in the healthy CNS. Genetic data show that the majority of risk for developing Alzheimer's disease is associated with genes mainly expressed in glial cells. Among these, Clusterin (ApoJ), Sortilin-related receptor 1, Fermitin family member 2 and ApoE are mainly expressed by astrocytes suggesting a key role of astrocytes in the pathogenesis of AD<sup>212</sup>.

#### 1.5.1 Histopathological astrocytic changes in neurodegenerative diseases

It has been posited that astrocyte dysfunction can cause disturbances in homeostasis which could potentiate neurodegenerative disease including AD<sup>213</sup>. Astrocytic changes are the pathological hallmarks of several neurodegenerative diseases and show changes in others. Under pathological conditions, human astrocytes undergo changes that can be classified into three morphologically defined categories: atrophy, pathological remodelling and astrogliosis<sup>211,214</sup>.

Although there are no pathognomonic astrocytic lesions found in AD, atrophic and reactive astrocytes are found in post-mortem tissue of patients with Alzheimer's disease and were first described by Alois Alzheimer himself<sup>215</sup>. Astroglial atrophy occurs in AD as well as many other CNS disorders including frontotemporal dementia, amyotrophic lateral sclerosis, epilepsy and schizophrenia<sup>211</sup>. There are a number of examples of astroglial pathological remodelling including Rosenthal fibres, tufted astrocytes and astrocytic plaques. Rosenthal fibres, which accompany chronic reactive astrogliosis, are eosinophilic, elongated structures that appear as amorphous masses surrounded by dense bundles of intermediate filaments. Rosenthal fibres are found in leukodystrophies, for instance Alexander disease, a genetic disorder caused by mutant GFAP leading to severe leukomalacia<sup>211</sup>. Tufted astrocytes and astrocytic plaques are considered the pathological hallmarks of sporadic 4-repeat tauopathies. Tufted astrocytes, which are caused by accumulations of tau protein from the cytoplasm to

the proximal processes, are found in progressive supranuclear palsy (PSP). Astrocytic plaques found in corticobasal degeneration (CBD) show arrangement of tau aggregates in the distal portions of astrocytic processes; they often located in the immediate vicinity of the synaptic structures<sup>216</sup>.

#### 1.5.2 Subtypes of astrocytes

Since the late nineteenth century, astrocytes have been divided into two main subtypes, protoplasmic or fibrous on the basis of differences in their cellular morphologies and anatomical locations. Protoplasmic astrocytes are found throughout the cortex and have several stems that give rise to finely branching processes in a uniform distribution that tend not to overlap with other astrocytes. Fibrous astrocytes are found throughout the white matter and exhibit a morphology of many long fibre-like processes. They have fewer GFAP expressing processes than protoplasmic astrocytes and their main function is likely to be metabolic support of neurons given the absence of synapses in white matter<sup>217</sup>.

In addition, there is recognition of a whole family of astroglial cells that share similarities with, but also exhibit differences to, protoplasmic and fibrous astrocytes. These include Muller glia in the retina, Bergmann glia of the cerebellum, tanycytes at the base of the third ventricle, pituicytes in the neurohypophysis, cribrocytes at the optic nerve head and others<sup>218</sup>.

#### 1.5.3 Functions of astrocytes

Historically, it was thought that brain function resulted exclusively from neuronal activity. This has been challenged as evidence has accumulated of the importance of neuronal-glia interactions and, in particular, the role of astrocytes. Astrocytes have a large number of vital roles within the CNS including ion and fluid homeostasis, regulation of neurotransmitters, cholesterol and lipoprotein production, modulation of synaptic function and maintenance of the blood-brain barrier. A description of these functions plus any known effects of *APOE* genotype are discussed below.

### 1.5.3.1 *Calcium signalling*

Astrocytes express both sodium and potassium channels and can exhibit evoked inward currents, but unlike neurons, do not produce action potentials<sup>219</sup>. They do, however, exhibit increases in extracellular calcium concentration that are a form of excitability which allow astrocytes to communicate between themselves and with neurons<sup>220</sup>.

Calcium elevations in astrocytes may be triggered intrinsically by release from intracellular stores or by neurotransmitters released during neuronal activity<sup>219</sup>. In response to calcium elevations, astrocytes may themselves release neurotransmitters, such as glutamate, which propagates to neighbouring astrocytes or triggers receptor mediated currents in neurons<sup>221,222</sup>. Calcium signalling provides a mechanism by which astrocytes can monitor and respond to ongoing synaptic transmission<sup>223</sup>.

### 1.5.3.2 *Regulation of neurotransmitters, pH, fluid and ions*

Astrocytic processes envelop nearly all synapses and maintain pH, fluid, ion and neurotransmitter homeostasis of the synaptic interstitial fluid which is critical for healthy synaptic transmission<sup>223</sup>.

Astrocyte membranes have various mechanisms that control the pH of interstitial fluid including the Na<sup>+</sup>/H<sup>+</sup> exchanger, bicarbonate transporters, monocarboxylic acid transporters, and the vacuolar-type proton ATPase<sup>224</sup>. Astrocyte processes are rich in the aquaporin 4 (AQP4) water channel especially where they are in contact with the vasculature. These channels play a critical role in regulating fluid homeostasis in the healthy CNS and are instrumental in the vasogenic and cytotoxic oedema associated with CNS disturbance<sup>225</sup>. Astrocyte processes also have abundant potassium transporters, in particular the Kir4.1 potassium channels, which regulate extracellular K<sup>+</sup> levels and are expressed in the CNS primarily by astrocytes<sup>226</sup> with particularly high levels in the hippocampus<sup>227</sup>.

Astrocytes express high levels of receptors for many different neurotransmitters including glutamate, GABA, and glycine. One of their key roles is to mediate removal of neurotransmitter from the extracellular space to maintain effective synaptic transmission and to avoid excitotoxicity<sup>228</sup>. Ablation of astrocytes in murine models leads to neuronal degeneration and death as a result of excitotoxicity caused by a failure to remove glutamate which leads to excessive activation of glutamate receptors<sup>229</sup>. Uptake of glutamate is accomplished by two glia-specific transporters — excitatory amino acid transporter 1 (EAAT1) and EAAT2 and glutamate transporter 1 (GLT1), respectively; it is speculated that dysfunction of glial glutamate transporters may represent a phenomenon common to many neurodegenerative conditions<sup>225</sup>. After uptake into astrocytes, the transmitters are converted by enzymes such as glutamine synthetase into precursors such as glutamine and recycled back to synapses for reconversion into active transmitters.

#### 1.5.3.3 Cholesterol and lipoprotein production

The neuronal plasma membrane is comprised mainly of cholesterol. Maintenance of the neuron's large surface area plus the formation of new dendrites requires the continuous addition of new membrane including cholesterol<sup>230</sup>. When the blood-brain barrier (BBB) is intact, dietary and hepatic cholesterol cannot cross it therefore the brain requires *de novo* cholesterol synthesis which occurs primarily in astrocytes<sup>137,170</sup>. Although neurons are capable of producing cholesterol, this tends to be confined to early development; when synaptogenesis accelerates the production is 'outsourced' to astrocytes<sup>171,231</sup> which are far more efficient<sup>231,232</sup>.

As well as being the main source of cholesterol, astrocytes are also the main source of apolipoproteins in the CNS, including ApoE and ApoJ (also known as clusterin, *CLU*), both of which are strongly implicated in the pathogenesis of AD. ApoE (and perhaps also ApoJ) ferry cholesterol and phospholipids in the form of small, high-density lipoprotein (HDL)-like particles from glia to neurons where it is utilised<sup>233,234</sup>. The key role of cholesterol in synaptic function is discussed below.

#### 1.5.3.4 *Synaptogenesis and modulation of synaptic function*

Astrocytes have been consistently shown to have effects on synapse formation, maturation, function and elimination<sup>79,221</sup>.

The observation that synapse formation correlates with the appearance of astrocytes led to the hypothesis that astrocytes are intimately involved in the process of synaptogenesis<sup>235</sup> and *in vitro* cellular models have consistently shown that synaptogenesis is enhanced when neurons are co-cultured with astrocytes<sup>236,237</sup>. In the early part of the century, several studies aimed to define the role of glial cells in synaptic development. In 1997, Pfrieger and Barres showed that a soluble factor secreted by astrocytes increased the level of spontaneous synaptic activity in purified retinal ganglion cells (RGCs) from postnatal rats<sup>238</sup>. Subsequent studies showed that this was due to a strong increase in the number and the efficacy of synapses but the causative agent was unknown<sup>239,240</sup>. In 2001, Mauch and colleagues identified the synaptogenic factor as cholesterol and found that the ability of CNS neurons to form synapses was limited by its availability<sup>170</sup>. The contribution of cholesterol is particularly important during synaptic development, when it contributes to presynaptic maturation and enhances release of neurotransmitter from presynaptic terminals, thus strengthening the synaptic connection<sup>170</sup>.

However, cholesterol is not the only astrocyte-derived substance to contribute to synaptogenesis with several factors regulating specific steps of synapse formation including thrombospondins and hevin, which induce structural synapse formation; glypicans, Wnts, chondroitin sulphate proteoglycans (CSPGs), and tumour necrosis factor  $\alpha$  (TNF $\alpha$ ) which recruit AMPA glutamate receptors (AMPARs); secreted protein acidic and rich in cysteine (SPARC) which inhibits synapse formation and decreases synaptic AMPARs; and activity-dependent neurotrophic factor, which increases levels of NMDA glutamate receptors (reviewed in Allen, 2014). Each of these factors acts on a subpart of synapse formation, and no factor has been identified that can induce the formation of a fully functional synapse by itself.

Once synaptogenesis is established, astrocytes continue to monitor and respond to synaptic transmission. The calcium signalling described above, provides a way in which astrocytes can dynamically modulate information processing, signal transmission and regulation of neural and synaptic plasticity by regulating neurotransmitter trafficking and recycling, nutrient and ion metabolism, trophic support and releasing neuro-modulatory factors<sup>209</sup>.

Astrocytes play direct roles in synaptic transmission through the regulated release of synaptically active molecules including glutamate, GABA and ATP and adenosine as well as a huge variety of neurotransmitter precursors, neuromodulators and hormones. In addition to direct effects on synaptic activity via the release of gliotransmitters, astrocytes also exert longer-term influences on synaptic function through the release of growth factors including BDNF, neurotrophin-3 (NT3) and nerve growth factor (NGF) which have multiple trophic effects including regulation of neuronal survival, growth and regeneration<sup>217</sup>. Astrocyte-derived factors also regulate synaptic balance by increasing and decreasing expression of excitatory and inhibitory receptors; for example TNF- $\alpha$  increases synaptic AMPAR levels and decreases synaptic GABAAR levels, leading to an overall increase in neuronal excitability<sup>241</sup> whereas thrombospondin decreases synaptic AMPAR levels and increases synaptic glycine receptors, leading to an overall decrease in neuronal excitability<sup>242</sup>. These effects are vital in homeostatic synaptic scaling, a type of plasticity that occurs when the activity of a whole neuronal network is altered, ensuring that the relative strengths of synapses are maintained<sup>241</sup>.

#### 1.5.3.5 *Blood–brain barrier function*

The blood–brain barrier (BBB) is a semipermeable membrane that separates blood from the CNS. It regulates the movement of oxygen, nutrients and toxins from the periphery to the brain and also clears carbon dioxide and toxic metabolites from the CNS. The brains of AD patients are characterised by impairment of the BBB<sup>243</sup>.

The most abundant and important cellular component of the BBB is endothelial cells but astrocytes also play a major role through their interaction with endothelial cells and pericytes<sup>244</sup> with data supporting the importance of vascular astrocytes in AD pathology<sup>245</sup>. The end-feet of BBB astrocytes are a vital link between endothelial cells and neurons, surrounding approximately 98% of the basal membrane of brain microvessels and expressing molecules which regulate ionic concentrations and protein transporters in the BBB, including aquaporin 4 which is used as an astrocytic marker<sup>246</sup>. Astrocytes also support the BBB via the release of several growth factors, including vascular endothelial growth factor (VEGF), glial cell line-derived neurotrophic factor (GDNF), basic fibro-blast growth factor (bFGF), and angiopoietin 1 (ANG-1)<sup>247</sup>. Astrocytes regulate the blood flow to the brain in response to neuronal synaptic activity by elevating calcium levels in the endfeet<sup>248</sup>.

#### 1.5.3.6 *CNS Homeostasis*

The final role of astrocytes within the CNS, and one which has probably gained the most attention in recent years, is their functions within the immune system.

Alongside microglia, astrocytes are one of the two key immune cells within the CNS. As described above, under physiological conditions astrocytes are vital for the maintenance of homeostasis, however in the pathological state they may exacerbate the process of neurodegeneration<sup>228</sup>. Although it now seems certain that neuroinflammation contributes to the pathogenic process in Alzheimer's disease whether it is an initiating event or one that exacerbates or accelerates the disease process is subject to debate<sup>249</sup>.

Astrocytes promptly react to CNS insults by undergoing a process of hypertrophy, termed reactive astrogliosis, and forming scar tissue<sup>218</sup>. There is greater astrogliosis in AD patients than in age-matched controls<sup>250</sup> with hypertrophic astrocytes accumulating around A $\beta$  plaques<sup>213</sup>.

Cytokines are proteins that function as signalling molecules and have key roles in regulating inflammation and the immune response. Astrocytes express cell surface receptors for many cytokines, growth factors and other proteins involved in inflammatory signalling such as interleukin-1 $\beta$  (IL1 $\beta$ ), IL6, interferon- $\gamma$  (IFN $\gamma$ ), TNF $\alpha$ , TGF $\beta$ , CCL12 (SDF-1), thrombin and endothelin-1<sup>251</sup>. These cytokines and related molecules are produced and released in autocrine, paracrine and endocrine fashions, and astrocytes can thus be influenced by distant cells, local non-homologous cells, other nearby astrocytes or even autocrine release<sup>252</sup>.

There has been substantial debate about whether astrogliosis is detrimental or beneficial and there is no simple answer. Numerous analyses of transcriptomic profile have been conducted in recent years using astrocytes isolated from a variety of murine sources including healthy young adults, normally aged individuals and a variety of induced disease states<sup>251,253,254</sup>. These studies demonstrate that astrocytes exhibit diverse changes in transcriptome profiles suggesting that the outcome of astrogliosis is not straightforward and is regulated by the type of environmental stimulation and where in the life-cycle these insults occur.

By using two injury models, a middle cerebral artery occlusion to induce ischaemia and an LPS injection, Zamanian and colleagues found that reactive astrogliosis caused a rapid change in gene expression, but astrocytic phenotype varied according to the type of insult<sup>253</sup>. They found that LPS stimulation induced neurotoxic 'A1' astrocytes which induce fewer, weaker synapses and which have impaired phagocytosis; however ischaemia induced "A2" astrocytes which express growth factors that promote neuronal survival and synapse formation.

Numerous studies in both human and mouse models consistently show that the loss of reactive astrocytes during the early phases of injury results in exacerbation of clinical signs, scar disorganisation, persistence of inflammatory cells, BBB alterations, and, and neuronal death. By contrast, astrocyte depletion during the chronic phase of disease ameliorates disease expression and reduces leukocyte infiltration into the CNS (reviewed in Colombo and Farina 2016<sup>255</sup>).

In summary, the role of astrocytes in the regulation of CNS inflammation is highly complex, context dependent and regulated by multiple extracellular signalling events that may change at different time points after CNS injury.

#### 1.5.4 Effects of ApoE genotype on astrocytic phenotype

The section above describes the key roles of astrocytes within the CNS; this section examines what is currently known about how *APOE* genotype affects these functions. There are a whole range of astrocytic phenotypes associated with *APOE* status including changes in astrocyte morphology, the blood-brain barrier, phagocytosis and autophagy, lipid metabolism, synaptogenesis and neurotrophic functions, synaptic pruning and inflammatory profile. Many of these differences have been elucidated in three recent publications, two of which have used isogenic *APOE* lines as a cellular model.

##### 1.5.4.1 *Morphological changes in astrocytes*

Although not strictly comparing *APOE* associated phenotypes, a paper by Jones and colleagues showed that astrocytes generated from patients carrying both a FAD-linked presenilin mutation and *SAD APOE4* homozygote exhibited reduced morphological complexity and altered localisation of key astrocyte markers, indicating both a sub-functional astrocytic phenotype and, interestingly, similar effects of FAD and *SAD* variants<sup>256</sup>.

##### 1.5.4.2 *Blood-brain barrier changes*

Astrocytic ApoE4 appears to promote BBB disruption in AD. Whereas ApoE3 and ApoE2 mediate physiological BBB tightness, ApoE4 promotes BBB disruption, as observed in mutant mice with human ApoE isoforms<sup>257</sup>. ApoE4 also accelerates

pericyte loss and microvascular reduction by enhancing pro-inflammatory pathway both in pericytes and endothelial cells<sup>258</sup>

#### 1.5.4.3 *Phagocytosis and autophagy*

Although there is some evidence that *APOE4* status may enhance A $\beta$  production<sup>153</sup>, most agree that it confers at least some of its AD risk through deficient A $\beta$  clearance. Reactive astrocytes can take up and degrade extracellular deposits of A $\beta$ 42 and that this function is attenuated in ApoE<sup>-/-</sup> astrocytes<sup>259</sup> (although this particularly study did not look at differences between particular ApoE isoforms). Two recent studies using iPSC-derived astrocytes from isogenic ApoE lines demonstrated that *APOE4* astrocytes show impaired A $\beta$  uptake compared with *APOE3* astrocytes<sup>202,260</sup>. Autophagy, which plays an important role in degradation pathways of proteins, organelles and protein aggregates, may also be impaired in AD. In a study of mouse-derived astrocytes those expressing ApoE4 exhibit lower autophagic flux compared to astrocytes expressing ApoE3 and that *APOE4* astrocytes eliminate A $\beta$  plaques less effectively than the corresponding *APOE3* astrocytes<sup>261</sup>.

#### 1.5.4.4 *Lipid metabolism*

As described above, astrocytes are the main source of cholesterol and ApoE in the CNS and are important for normal brain function. Ageing leads to decreased cholesterol synthesis in astrocytes which may contribute to the associated cognitive decline<sup>262</sup>. The three recent studies of astrocytes derived from isogenic *APOE* lines found that levels of cellular cholesterol measured by gas chromatography/mass spectrometry and filipin staining were significantly higher in *APOE4* astrocytes than their *APOE3* counterparts. This might be expected given that ApoE4 from primary astrocytes is poorly lipidated compared to ApoE3<sup>179</sup> however a similar increase was noted in free (or unesterified) extracellular cholesterol (although not cholesteryl ester levels). However, these findings contrast with results in mouse models which suggest that astrocytes from targeted-replacement *APOE4* mice secrete less cholesterol than astrocytes from *APOE3* mice<sup>179</sup>. The same isogenic *APOE* studies also found that E4/E4

astrocytes have much lower levels of both intracellular (80% reduction) and secreted (63% reduction) ApoE compared to E3/E3 astrocytes<sup>202,260,263</sup>.

Transcriptomic analysis of isogenic *APOE* lines identified pathways consistent with lipid accumulation which led the authors investigate sterol metabolism *in vitro*<sup>263</sup>. They found elevated levels of HMG-CoA reductase (HMGCR), the enzyme responsible for the rate limiting step in cholesterol biosynthesis, in E4/E4 compared to E3/E3 astrocytes. Furthermore, ATP-binding cassette transporter ABCA1, a major regulator of cellular cholesterol homeostasis through the transport of lipids via ApoE, was also significantly decreased in E4/E4 compared to E3/E3 astrocytes which would explain the increased levels of intracellular cholesterol but not the concomitant increase in secreted cholesterol. One possible explanation for the increased free, extracellular cholesterol is that less is bound to ApoE in E4/E4 models due to there being less ApoE4 and its tendency to be poorly lipidated.

Normally, negative feedback loops ensure that cells laden with lipids reduce synthesis and uptake while increasing efflux. It may be that these cells are unable to properly sense that intracellular cholesterol levels are high; consistent with this signalling mechanism, *SREBP2* was in fact downregulated in *APOE4* iPSC-derived astrocytes<sup>202</sup>. Overall, these results suggest that *APOE4* is associated with increased lysosomal cholesterol levels and decreased cholesterol efflux, demonstrating decoupled lipid metabolism<sup>264</sup>.

#### 1.5.4.5 *Synaptogenesis, neurotrophic function and synaptic pruning*

iPSC-derived astrocytes have also been shown to promote the survival, maturation and function of co-cultured human neurons, effects that can be impaired by *APOE4* mutations<sup>202,260</sup>. *APOE4* astrocytes were found to be less capable of promoting synapse formation than *APOE3* astrocytes and the expression of synaptic proteins was also decreased. Furthermore, *APOE4* astrocytes reduced the survival of neurons and eventually led to neurodegeneration<sup>260</sup>.

In mouse studies, *APOE4* astrocytes were less phagocytic towards pHrodo-labelled synaptosomes than *APOE3* and *APOE2* astrocytes leading to a decreased rate of synaptic pruning and turnover in the brain, causing the accumulation of senescent, C1q-tagged non-functional synapses which are more vulnerable to AD<sup>265</sup>. It has also been proposed that *APOE4* may be deficient in lipid debris clearance<sup>202</sup>.

#### 1.5.4.6 *Inflammatory profile*

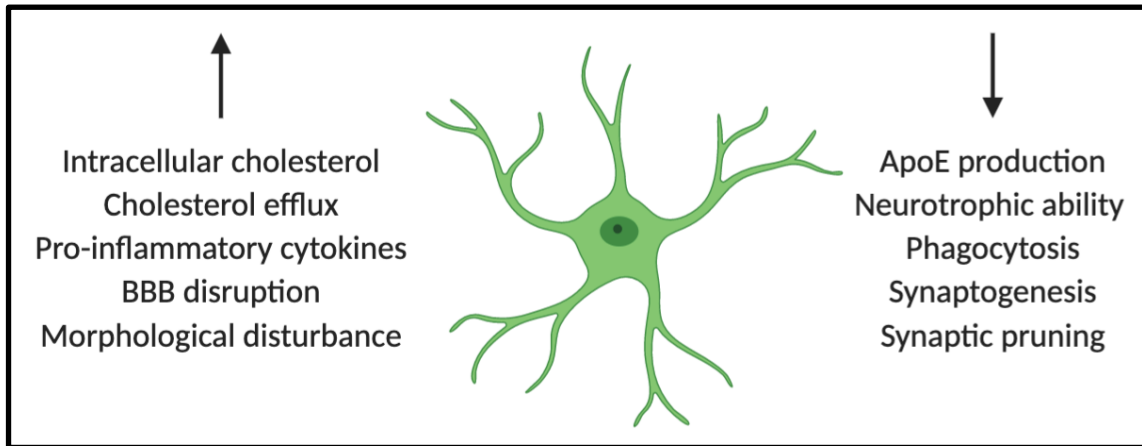
Finally, *APOE* genotype has significant effects on astrocytes' inflammatory profile. A recent review found that the process of cytokine release by glia to maintain homeostasis and respond to damage is dysfunctional in the ageing and AD brain, with substantial evidence suggesting that the *APOE4* allele plays a crucial role in this<sup>266</sup>.

In a murine model, expression of inflammation-related genes including IL-1 $\beta$ , IL-6 and TNF- $\alpha$  was greater in *APOE4* mice. The findings were corroborated by immunofluorescence which showed that the number of IL-1 $\beta$ , IL-6 and TNF- $\alpha$  stained cells was also markedly higher in hippocampi of *APOE4* mice<sup>267</sup>. Similar findings were reported in another targeted-replacement mouse model which found that after intravenous administration of LPS, *APOE4* animals had significantly greater systemic and brain elevations of TNF- $\alpha$  and IL-6 as compared with their *APOE3* counterparts<sup>268</sup>. However, contradictory results were found in primary cultures of astrocytes from targeted replacement *APOE* mice which were stimulated with LPS and cytokine secretion measured. Only IL-6, IL-1 $\beta$  and TNF- $\alpha$  changed significantly with concentrations of all higher in *APOE2* than *APOE3* which in turn was higher than *APOE4*<sup>269</sup>. The authors also note the perhaps contradictory finding that while *APOE4* and *APOE3* genotypes were mildly damaging to neurons, the *APOE2* genotype showed no neurotoxic effect despite exhibiting a more pro-inflammatory phenotype.

In a recent isogenic human model, a panel of secreted proteins including chemokines, cytokines and growth factors was measured. When absolute protein levels were compared between *APOE3/3* and *APOE4/4* astrocytes, 10 proteins showed significantly higher levels in the media from *APOE4/4* glia, supporting elevated chemotactic

molecules and cytokines in *APOE4/4* astrocyte transcriptomes<sup>263</sup>. The figure below summarises the key effects of astrocyte genotype on key phenotypes.

**Figure 1.6: Summary of APOE4 astrocytic phenotypes.**



The APOE4 genotype is associated with several key astrocytic phenotypes which are summarised in the diagram above.

## 1.6 Stem cells for modelling neurodegenerative diseases

Pluripotent stem cells are cells that have the capacity to self-renew and, when exposed to the right signals, to become any type of specialised cell. There are three main types: embryonic stem cells (ESC), adult stem cells and induced pluripotent stem cells (iPSC).

### 1.6.1 Embryonic stem cells (ESC)

Stem cells were first discovered in blood from the human umbilical cord in 1978<sup>270</sup>. This was followed by the isolation and establishment of embryonic stem cells (ESCs) in vitro from mouse blastocysts in 1981<sup>271</sup>. Human embryonic stem cells (hESCs) were first derived from the inner cell mass of a human blastocyst in 1998<sup>272</sup>. They were found to proliferate in an undifferentiated state for 4-5 months, owing to their high telomerase activity, and maintained the potential to differentiate into all three embryonic germ layers; endoderm, mesoderm and ectoderm. Ethical issues surrounding the use of embryonic stem cells led to the development of techniques for creating induced pluripotent stem cells.

### 1.6.2 Induced pluripotent stem cells (iPSC)

In 2007, Yamanaka and colleagues induced pluripotency in adult human fibroblasts by forcing the expression of four key transcription factors (OCT3/4, SOX2, KLF4 and c-Myc) by viral transduction<sup>273</sup>. The reprogramming factors then initiate a self-regulatory loop that initiates and maintains pluripotency<sup>274</sup>. Although first undertaken in fibroblasts many different cell types are now used including keratinocytes<sup>275</sup>, blood cells<sup>276</sup>, renal tubular cells<sup>277</sup> and dental pulp<sup>278</sup>. Furthermore, techniques entailing a more streamlined and efficient approach with fewer transcription factors are now in use. The key advantages of iPSC over human embryonic stem cells is that there are fewer ethical concerns surrounding their usage and they permit patient-derived cell lines so that disease-associated phenotypes can be readily explored.

### 1.6.3 Adult stem cells

Adult stem cells, in common with other types, share a capacity for self-renewal and the ability to give rise to mature cell types with specialised functions. Adult stem cell populations have been found in tissues that develop from all three embryonic germ layers: haematopoietic, muscle, intestinal, neural and skin<sup>279</sup>. Despite being found in variety of tissues, adult stem cells are rare. For example, only an estimated 1 in 10,000 to 15,000 cells in the bone marrow is a hematopoietic stem cell<sup>280</sup>.

Within the CNS there are two key populations of adult stem cells. Over 50 years ago, Altman and Das showed that two regions of the postnatal rat brain, the hippocampus and the olfactory bulb, contain dividing cells that become neurons<sup>281</sup>. Within the past 25 years, a number of studies have showed that stem cells occur in the adult mammalian brain and that these cells can generate its three major cell lineages: neurons, astrocytes and oligodendrocytes<sup>282</sup>. Normally, adult neurogenesis is restricted to two areas of the brain the subventricular zone, which lines the lateral ventricles, and the dentate gyrus of the hippocampal formation<sup>283</sup>. Declining hippocampal neurogenesis has been speculated to play a part in ageing and cognitive dysfunction<sup>284</sup>.

### 1.6.4 Differentiation of stem cells

By definition, human pluripotent stem cells (hPSCs), have the ability to produce any cell of the human body. This was demonstrated for the first time in 2000 when somatic differentiation of hESCs to an early neuroectoderm stage was undertaken. Cells were then isolated and went on to demonstrate morphology and expression of markers characteristic of mature neuronal differentiation<sup>285</sup>. The possibility of creating hESC-derived cells was a hugely exciting prospect as it could offer a potentially limitless source of specific cell types for cell biology models, regenerative medicine and drug discovery.

### 1.6.5 Advantages and challenges of using stem cell models

Apart from the availability of hPSC and the relative cost-effectiveness of stem cell models they have other advantages, particularly when investigating the role of ApoE.

Murine models have formed the backbone of AD research over the last 25 years and have made significant contributions to our understanding of the disease. The mostly neuronally expressed FAD proteins are nearly identical between human and mouse, exhibiting greater than 90% amino acid identity (97.3%, 92.7% and 96.0% respectively for the key FAD genes APP, PSEN1 and PSEN2). In stark contrast, the proteins encoded by a number of SAD risk genes, including the microglial cell surface proteins TREM2, CD33, CR1 and MS4A6A, are only about 50% identical between human and mouse; this is comparable to the difference between human and insect presenilin proteins. ApoE shares a 71.7% amino acid identity with its mouse orthologue<sup>286</sup>. Comparison of murine and human transcriptomes has also demonstrated that examination of mouse ApoE44 glia only partially capture the defects observed in human ApoE44 glia: although matrisome associated, extra-cellular matrix (ECM) and inflammatory pathways were enriched in ApoE44 mouse glial cells, dysfunction of the crucial lipid metabolism pathways was not found to be significant<sup>263</sup> thus stressing the importance of studying ApoE genotype-dependent effects in human model systems.

Although an enormously useful research tool, hPSC models have several shortcomings that can be summarised as lack of functional maturity, insufficient complexity and variability. The majority of hPSC differentiations produce populations that most closely resemble fetal or neonatal cells. To effectively model adult, or even aged, physiological responses cells may need to be matured, artificially or otherwise. Stem cell models are capable of exhibiting similar connectivity to primary cells in culture however most consider the defining property of electrically-active cells as their ability produce action potentials (APs). Although neurons derived from human iPSCs have been shown to fire APs after just 3 weeks of differentiation<sup>287</sup>, synchronised burst firing (simultaneous AP bursts) increases steadily from 16 to 30 weeks in culture<sup>288</sup>. The most obvious way of maturing neurons is long-term culture although there are significant resource

implications of doing so. Another method, and one utilised in recent studies, is the addition of neurotrophins to accelerate the process of synaptogenesis<sup>202,289</sup>.

Although invaluable for studying specific cellular mechanisms, cultures of individual cell types do not recapitulate the complexity of the human CNS. In recent years there has been a movement away from models using single cell types to various two-dimensional co-cultures and increasingly 3-dimensional brain organoids. The development of more complex multiorgan models is hampered by the different culture conditions required for their constituent cells however significant progress is being made. Single cell RNA sequencing comparing cells derived from organoid and non-organoid cultures has found that those from organoids display genetic profiles more akin to those of the fetal cerebral cortex<sup>290</sup>.

Arguably the key challenge in using either embryonic or patient derived stem cell lines is their diversity, both genetic and otherwise, which can make detection of phenotypic differences difficult. Variability arising during the course of differentiation can be addressed to a certain extent by using standardised protocols and multiple differentiations. Another source of difference is clonal variability; studies investigating mutational load in iPSC lines have demonstrated a significant risk of new mutations as a result of reprogramming<sup>291</sup>. Copy number alterations (CNA), including duplications and deletions, between iPSC and their donor cells which appear to arise from genetic mosaicism in cultures established from nonclonal colonies<sup>292</sup> have also been reported; this suggests that genotyping arrays to detect CNAs should be undertaken to ensure consistency of karyotype between clones and during the differentiation process.

However, although CNAs were a common finding, donor effects (that is, between individual differences) explained the largest proportion of variation (46.4%) substantially more than any other factor, including copy-number status (23.4%), culture conditions (26.2%), passage (2%) and gender (1.9%)<sup>292</sup>. Tools for genome editing which allow for the introduction or correction of specific mutations without altering the genetic background have been revolutionary. Their use is discussed in the next section.

## 1.7 Gene editing

Over the last 15 years, a number of technologies have emerged with the aim of direct genome editing. These technologies have enabled researchers to introduce a variety of genetic alterations into cells, including insertion of genes, deletions of chromosomal regions and the knock-in of single nucleotide variants in order to create isogenic cell lines that provide powerful models for elucidating the biological effects of specific genetic variants.

### 1.7.1 Repair mechanisms: Nonhomologous end joining (NHEJ) and homology-directed repair (HDR)

When double-stranded breaks (DSBs) occur in DNA, cells may repair them using either nonhomologous end joining (NHEJ) or homology-directed repair (HDR). NHEJ can occur at any phase of the cell cycle but can result in erroneous repair which can be exploited to introduce frameshifts into the coding sequences of genes which can knock out the gene by two mechanisms: truncation of the protein and nonsense-mediated decay of the mRNA transcript<sup>293</sup>. HDR typically occurs in during late S phase or G<sub>2</sub> phase when a sister chromatid is available to serve as a repair template. HDR can be utilised to insert specific mutations into the DNA sequence using a repair template containing the desired mutation flanked by homology arms. Traditionally, exogenous double-stranded DNA vectors were used as repair templates<sup>294</sup>. More recently, however, exogenous single-stranded DNA oligonucleotide (ssODN) with much shorter homology arms have been used<sup>295</sup>.

### 1.7.2 Zinc-finger nucleases (ZFNs) and Transcriptor Activator-like effector nucleases (TALENs)

Zinc Finger Nucleases (ZFN) comprise two functional domains: 1) A DNA-binding domain with a chain of two-finger modules, each recognising a unique hexamer (6 bp) sequence of DNA. Two-finger modules combine to form a Zinc Finger Protein, each

with specificity of  $\geq 24$  bp 2) a DNA-cleaving domain containing the endonuclease domain of the bacterial FokI restriction enzyme. To create a DSB at a specific site in the genome, ZFNs are designed as a pair that recognises two sequences flanking the site, one on the forward strand and the other on the reverse. Upon binding of the ZFNs on either side of the site, the FokI enzyme creates a DSB<sup>293</sup>.

Transcription activator-like effectors (TALEs) are found in particular species of plant pathogens. They first infect their targets by injecting a TAL protein which recognises specific DNA sequences. The naturally occurring TALE repeats comprise tandem arrays with 10 to 30 repeats, each 33 to 35 amino acids in length, with two adjacent amino acids (termed the repeat-variable di-residue [RVD]) conferring specificity for one of the four DNA base pairs<sup>296,297</sup>. This gives a one-to-one correspondence between the repeats and the base pairs in the target DNA sequences. Elucidation of the RVD code permitted the creation of engineered site-specific nuclease that fuses a domain of TALE repeats to the FokI endonuclease domain (TALENs)<sup>298</sup>.

### 1.7.3 CRISPR-Cas9

Clustered regularly interspaced short palindromic repeats (CRISPR)-Cas9 technology is based on the adaptive immune system of bacteria and archaea which use it to defend against invading viruses<sup>299,300</sup>. Upon encountering an invading virus, the prokaryotic cell uses a CRISPR-associate nuclease (Cas) to 'snip' viral DNA by creating a double stranded break. Cleaving the DNA destroys the viral invader and also creates a fragment of viral DNA (a spacer) which may be incorporated into the bacterial host genome at specific locations to provide a genetic memory. Thus, if the virus re-invades it can be rapidly targeted and destroyed<sup>300</sup>.

The discovery of CRISPR-Cas9 has led to the development of the newest set of genome-editing tools. In the last 5 years, CRISPR-Cas9 has become the method of choice for gene editing over previous technologies due to its efficiency, relative ease, high specificity and cost-effectiveness<sup>301</sup> and it has already been used to correct the genetic basis of many diseases in isolated cells or animal models<sup>302-306</sup>.

The CRISPR-Cas9 system comprises two key components: CRISPR associated endonuclease – Cas9 – and the guide RNA (gRNA) which allows the endonuclease to be targeted to a specific place in the genome. The gRNA and Cas9 combine to form a ribonucleoprotein (RNP) complex. Like ZFNs and TALENs, Cas9 acts as a pair of molecular scissors to make a DSB in DNA. The gRNA itself also consists of two elements: the CRISPR RNA (crRNA) and transactivating CRISPR RNA (tracrRNA). The crRNA is the 18-20bp sequence that binds to the genomic target while the tracrRNA acts as a scaffold for the crRNA-Cas9 interaction. In many systems, the gRNA and the tracrRNA are annealed to form a duplex molecule however they may also be produced synthetically with crRNA and tracrRNA connected by a linker loop; these are known as single guide RNAs (sgRNAs)<sup>301,307</sup>.

Binding of the gRNA to the target DNA is dependent on the presence of a short protospacer adjacent motif (PAM) located directly downstream of the target. Cas proteins from different bacterial species recognise different PAM sequences. The most commonly used Cas9 protein is derived from *Streptococcus pyogenes* for which the PAM is 5'-NGG-3'. If a PAM match is made and the gRNA binds successfully, then Cas9 cleaves both DNA strands approximately 3 nucleotides upstream of the PAM site. Once a DSB is made, the nature of the ensuing repair mechanism (either NHEJ or HDR if a donor construct is present) will determine the editing outcome<sup>307</sup>.

In contrast to ZFNs and TALENs, which require recoding of proteins using large DNA segments (500–1500 bp) for each new target site, CRISPR-Cas9 can be easily adapted to target any genomic sequence simply designing appropriate gRNAs. Genome editing technologies are evolving rapidly; the use of CRISPR-Cas9 to create isogenic lines reduces the variability associated with the use of patient-derived iPSC cells. It may also be used to correct specific genetic mutations in patient-derived cells allowing powerful phenotype-genotype observations to be made with minimum (perhaps even no) background noise.

## 1.8 Aims

The aim of this thesis is identify ways in which the *APOE* genotype contributes to the pathogenesis of sporadic Alzheimer's disease.

- The first aim is to create isogenic cell lines which provide powerful models for elucidating the biological effects of specific genetic variants.
- Once created and validated, the second aim is to take isogenic stem cells and differentiate them into astrocytes.
- The third aim is to identify phenotypic differences between astrocytes with E3/E3 and E4/E4 genotypes by investigating the effects on some of their key physiological functions.
- Finally, astrocytes will be exposed to stressors to induce astrogliosis to examine whether this potentiates or attenuates physiological functions.

An isogenic *APOE* cell line and a robust method for differentiating astrocytes will provide a valuable model to achieve the aims of this thesis and for future work. In due course, this will be made available to the scientific community.

## 2 Materials and methods

### 2.1 Cell culture

All cell cultures were maintained at 37°C and 5% CO<sub>2</sub> (Galaxy 170 R, New Brunswick). Cell work was carried out under a laminar flow hood (Maxisafe 2020, Thermo Scientific) under sterile conditions. Cells were grown on cell culture-treated plastic multi-well plates (Thermo Scientific) or glass coverslips (VWR).

#### 2.1.1 hPSC culture

All experiments were carried out using the H7 hESC line (WiCell). Multi-well plates were coated with hESC-qualified Matrigel (Corning) diluted in knockout DMEM (Gibco) for at least 1 hour at 37°C. H7 were maintained in Essential 8 (E8) medium (Life Technologies) with media changed at least every other day. Cells were passaged when they reached 80% confluency as follows; all media was aspirated and cells washed once with PBS (Life Technologies) once, then Versene (Thermo Fisher Scientific) was added and the cells incubated at 37°C for 2-4 mins. The Versene was aspirated and medium added. A serological pipette was used to gently dissociate the cells into small clusters. The cell suspension was centrifuged at 140g for 3 minutes (5810 R, Eppendorf) to create a cell pellet that was gently resuspended in fresh medium and seeded at 1:3 (for standard passaging) onto fresh hESC-qualified Matrigel coated plates.

#### 2.1.2 hPSC freezing and thawing

Cells were stored in liquid nitrogen tanks at low passage numbers for future use. Cells were passaged as described above (2.1.1) but kept in large clusters and resuspended in Cryostor CS10® (STEMCELL Technologies). Cell suspension from one well of 80% confluency was transferred into a cryogenic vial and placed inside a cell freezing container to slow the rate of freezing once placed at -80°C. Cells were kept at -80°C for

up to 2 weeks before being placed in liquid nitrogen storage tanks. Cell thawing was carried out as quickly as possible by placing cryogenic vials straight from liquid nitrogen into a bead bath at 37°C. 1ml of E8 media containing Revitacell (1:100; Gibco) was added dropwise to the cryogenic vial, the contents transferred to a 15ml centrifuge tube (Falcon) containing pre-warmed medium and Revitacell and centrifuged at 140g for 3 minutes. The cell pellet was gently resuspended in fresh medium also containing Revitacell and plated into a single well. Media was changed the next day to E8 without Revitacell.

### 2.1.3 hPSC differentiation to neuronal precursor cells (NPC)

Cells were passaged as above (2.1.1) when almost completely confluent at a ratio of 2:3. Cells were plated on Growth Factor Reduced Matrigel (Corning) (diluted 1:15 in KO DMEM and coated for 1 hour at 37°C) and E8. After 24 hours, when cells were 100% confluent, medium was changed to N2B27-defined medium (see below) which was changed at least every other day. This was designated as day 0 of differentiation. For cortical neuron differentiation, the ALK4/5/7 inhibitor SB431542 (10 µM; Tocris) and the ALK2/3/6 inhibitor dorsomorphin (1µM; Tocris) were added to the medium from days 0-9. Cells were passaged at day 9 when a uniform neuroepithelial sheet had formed. Manual dissociation was carried out with Versene as above (2.1.1) but cells were kept in large clusters and triturated very gently without the centrifugation step. Cells were split at a 2:3 ratio onto fibronectin-coated plates (15 µg/ml, 1 hour at 37°C; Millipore). After the first passage, cells continued to be cultured with N2B27 media (changed every day) with the addition of FGF2 20ng/ml (R&D Systems); this was withdrawn after 4 days. The second passage took place on day 17 using Versene as above but with more vigorous trituration to make smaller clusters of cells, which were plated onto poly-D-lysine and laminin-coated plates. Poly-D-lysine (10 µg/ml in ddH<sub>2</sub>O; Sigma-Aldrich) was added for 30 minutes at room temperature, washed and dried under UV. Laminin (10 µg/ml; Sigma-Aldrich) was then added and incubated overnight at 37°C. Media was changed daily until day 24 when NPCs were cryopreserved.

Constituents of N2B27 Medium	Supplier	Volume
DMEM/F-12	Life Technologies	250ml
Neurobasal	Life Technologies	250ml
N2	Life Technologies	2.5ml
Insulin (10mg/ml)	Sigma	125uL
L-Glutamine (200mM)	Life Technologies	2.5ml
Non-essential amino acids NEAA (100x)	Life Technologies	2.5ml
B27 (without retinoic acid)	Life Technologies	5ml
B-mercaptoethanol (50mM)	Life Technologies	1ml
Primocin	Invivogen	0.5ml

#### 2.1.4 Freezing and thawing of NPCs

On day 24, cells were washed once with MgCl<sub>2</sub> and CaCl<sub>2</sub> free DPBS (Thermofisher) and 0.5ml Accutase (Life Technologies) added to the well. Cells were incubated with Accutase at 37°C for 3-5mins then triturated to form a single-cell suspension. This was diluted with 10mls of neural maintenance medium and centrifuged at 140g for 5 minutes. The wash and spin was repeated then the cells resuspended in 1ml of Cryostor CS10<sup>®</sup> supplemented with 20ng/ml of FGF2. The cell suspension was transferred into each a cryovial and frozen in a cell freezing container at – 80 °C overnight. Cryovials were then transferred to liquid nitrogen for long-term storage.

Cell thawing was carried out as quickly as possible by placing cryogenic vials straight from liquid nitrogen into a bead bath at 37°C. 1ml of neural maintenance medium containing 20ng/ml of FGF2 was added dropwise to the cryogenic vial and the contents transferred to a 15ml centrifuge tube (Falcon) containing pre-warmed medium (including FGF2) and centrifuged at 140g for 3 minutes. The medium was aspirated and the cell pellet gently resuspended in fresh medium also containing FGF2 and plated into poly-D-lysine/laminin-coated dishes. FGF2 was withdrawn the next day and culturing continued as per protocol.

### 2.1.5 Differentiation of neurons

NPCs were thawed and plated as described in 2.1.4. at an optimised density of 50,000 cells/cm<sup>2</sup>. On day 1, N2B27 media was replaced by with BrainPhys (Stemcell TECHNOLOGIES) with growth factors BDNF (10 ng/ml; Peprotech), NT3 (10ng/ml; Peprotech) and laminin (0.2 mg/ml; Sigma-Aldrich) added to promote neuronal survival. On days 5-7, 1 mM of the anti-mitotic cytosine arabinoside (Ara-C) (Sigma-Aldrich) was added to cultured media. From day 8, Ara-C was removed from the media and differentiation continued until neurons were ready for experimental assays.

### 2.1.6 Differentiation of astrocytes

Protocols for the differentiation of astrocytes are not so well-established as those for neuronal differentiation so there is not the same degree of uniformity in published methods. In order to establish the best approach to astrocyte production, a variety of methods were used and their efficacy established by measuring prototypical markers with qPCR. The results of this work are discussed in Chapter 4.

### 2.1.7 Production of astrocyte condition media (ACM)

Once the astrocytes had matured (from around Day 60) they were transitioned over the course of three days to B27 medium (Neurobasal medium supplemented with 1x B27 and 1 x GlutaMAX™ (Thermofisher) for maintenance. After 72h ACM was collected, filtered and stored at 4°C. The protein and ApoE concentrations were determined by BCA assay and ApoE ELISA respectively. The amount of ACM added to cultures was determined by each individual experiment.

## 2.2 Cell techniques

### 2.2.1 Sample preparation for immunocytochemistry

Cultured cells were washed twice with DPBS and then fixed with cold 3.7% paraformaldehyde (PFA) for 15 mins. PFA incubation was followed by three DPBS washes before proceeding with staining. For surface markers, cells were blocked in 2% BSA, 5% serum (Gentaur) in PBS for 1-2 hours at RT then incubated with primary antibodies in PBS+5% serum overnight at 4°C. They were then washed with DPBS (3x 20 minutes) and fixed in cold 3.7% PFA for 15 min before further PBS washes (3x20 minutes).

Where nuclear stains were used, methanol washing was undertaken; 3 mins incubation at RT in 33% methanol, 3 mins at RT in 50% methanol, 3 mins at RT in 66% methanol, 20 min incubation in the freezer in 100% methanol, 3 mins incubation at RT in 66% methanol, 3 mins at RT in 50% methanol, 3 mins at RT in 33% methanol, then 3 mins incubation at RT in DPBS.

Cells were then washed twice with PBS + 0.3% Triton X-100 (PBST), 5 min each; PBS only was used for surface antigens. Cells were then blocked with 2% BSA, 5% serum (Gentaur) in PBST for 10-20 min. Cells were incubated with primary Ab in PBST + 3% serum overnight at 4°C. They were then washed with PBST at RT (3 x 20 min). Cells were then incubated with AlexaFluor secondary antibodies (1:1000; Thermofisher) at RT for 1-2 hr in PBST in the dark. They were then counterstained with DAPI (1:3000 in PBS) for 5 min. After a final set of DPBS washes (3 x 10 mins) cells were mounted with fluorescent mounting medium (Dako) and kept in the dark at 4°C until use.

**Table 2.1: antibodies used for immunofluorescence.**

Target	Marker of	Species	Dilution	Supplier	Cat no
OCT3/4	pluripotent stem cells	Goat	1:500	Santa Cruz	SC-8628
Tra-1-60	pluripotent stem cells	Mouse	1:100	Santa Cruz	SC-21705
SOX2	pluripotent stem cells	Rabbit	1:200	Abcam	Ab97959
Nestin	neuroectodermal stem cells	Mouse	1:300	BD Pharmigen	BD 611659
FOXP1	NPC	Rabbit	1:250	Abcam	ab18259
PAX6	NPC	Mouse	1:1000	DSHB	PAX6
PAX6	NPC	Rabbit	1:500	Abcam	ab195045
OTX2	NPC	Goat	1:500	R&D	
MAP2	neurons	Mouse	1:500	Sigma	
S100B	astrocytes	Mouse	1:1000	Sigma	S2532
GFAP	astrocytes	Chicken	1:1000	Abcam	ab4674
CD44	astrocytes	Rat anti-mouse	1:100	BD	5550538
EAAT1	astrocytes	Rabbit	1:200	Abcam	ab416
EAAT2	astrocytes	Guinea Pig	1:100	Millipore	1783
Glutamine synthetase	astrocytes	Mouse	1:500	BD Biosciences	610517
ApoE		Mouse	1:100	Abcam	ab1906

Stained cells were imaged using a Leica DM6000B inverted microscope. For quantification, random fields were acquired for each well at a 20x magnification. Cell counting of DAPI and most nuclear markers was performed using the ITCN (Image-based tool for counting nuclei) Plugin for ImageJ developed by Thomas Kuo and Jiyoung Byun<sup>308</sup>. Images were converted to eight-bit greyscale and inverted before using ITCN. Cell detection was performed by detecting dark peaks with parameters optimised to ensure accurate cell capture.

Other measurements, such as number and morphology of neural rosettes and astrocytes, were performed manually, using the ImageJ software. Data analysis and representation was carried out using Microsoft Excel. Unless otherwise stated, all the

immunohistochemistry quantifications were collected from at least two independent experiments, with at least three biological replicates for each marker counted.

#### 2.2.2 Calculation of Corrected Total Cell Fluorescence

Images were taken using a Leica DM6000B inverted microscope (Leica Microsystems, Germany). Care was taken to ensure that microscope settings for images were identical. Analysis of images was performed using Image J; individual cells were identified as regions of interest and then measurements of mean grey values and cell area obtained. For each field, two background readings were taken.

Corrected total cell fluorescence (CTCF) was calculated for each cell using the formula  $CTCF = \text{Integrated Density} - (\text{Area of selected cell} \times \text{Mean fluorescence of background readings})$ .

#### 2.2.3 Cholesterol staining assays

Free cholesterol levels in astrocytes were measured with filipin (Peprotech) a naturally fluorescent polyene antibiotic that binds to cholesterol but not to esterified sterols (ie free cholesterol). Astrocytes were washed three times with DPBS and fixed with 4% paraformaldehyde in PBS for 15min, washed a further three times with DPBS then incubated with filipin III (50 µg/ml in PBS for 45-60 mins at room temperature). Cells were washed a further three times with DPBS before detection.

Fluorescence from cholesterol-bound filipin III was detected with two methods: first, by microplate reader (BMG Clariostar) with UV excitation at 360nm and emission at 480nm (media from each well was retained in order to perform BCA assays for normalisation).

Cells were also viewed in PBS by fluorescence microscopy. Images (5 images per experiment, an average of 18 cells per image) were acquired with an inverted fluorescence microscope (Leica Microsystems, Germany) using a 20x objective with UV

filter, 360 nm excitation and 460nm emission and ensuring the same settings were used for each image. Random fields were selected and, as filipin fluorescence photobleaches very quickly, images were taken as rapidly as possible as soon as the microscope alighted upon a field. Corrected total cell fluorescence (CTCF) was calculated as described in 2.2.2.

#### 2.2.4 Induction of astrogliosis

Induction of astrogliosis was undertaken using the combination of cytokines set out in Liddelow and colleagues' 2017 publication<sup>309</sup>. Cells were first plated at the appropriate density 3-5 days prior to the particular experiment. 24 hours prior to the experiment, media was aspirated from the wells and cells were washed twice with warmed DPBS. Media containing Il-1 $\alpha$  (3ng/ml; Sigma-Aldrich, I13901), TNF $\alpha$  (30ng/ml; NEB 8902SF) and C1q (400ng/ml; MyBioSource, MBS143105) was then added to each well. After 24 hours, media was aspirated, cells washed twice with DPBS and cells harvested as appropriate.

#### 2.2.5 Glutamate uptake assay

Removal of glutamate from the extracellular space is one of the key functions of astrocytes. This was assessed using a glutamate uptake assay (Sigma Cat no: MAK004). Astrocytes were plated in 48-well plates at least 24 hours prior to testing. Cells were starved in HBSS media (Thermofisher) for 10 minutes before HBSS containing L-glutamate (50 $\mu$ M: Sigma) was added to each well. At 60 minutes, 100uL samples of the medium at were taken and cells harvested for BCA protein normalisation (see 2.3.1). Reaction mixes were set up according to the table below.

Reagent	Blank Sample	Samples and standards
Glutamate assay buffer	92 $\mu$ L	90 $\mu$ L
Glutamate developer	8 $\mu$ L	8 $\mu$ L
Glutamate enzyme mix	-	2 $\mu$ L

To prepare glutamate standards for colorimetric detection, 10  $\mu\text{L}$  of the 0.1 M glutamate standard was added to 990  $\mu\text{L}$  of the Glutamate Assay Buffer to prepare a 1 mM standard solution. Different standards were then produced according to the table below with Glutamate Assay Buffer as diluent and added into a 96-well plate.

Glutamate standard	Diluent ( $\mu\text{l}$ )	Glutamate ( $\mu\text{l}$ )	Final concentration ( $\mu\text{M}$ )
A	320	80 of 1mM stock	200
B	200	200 of A	100
C	370	30 of 1mM stock	75
D	200	200 of B	50
E	200	200 of D	25
F	200	200 of E	12.5
G	200	200 of F	6.25
H	200	0	0

50 $\mu\text{L}$  of all samples and standards were added to a 96-well flat-bottomed plate. 100 $\mu\text{L}$  of the reaction mix was added to each well and mixed well by pipetting. The reaction was protected from light and incubated for 30 minutes at 37°C. The absorbance of the product was measured at 450 nm using a microplate reader.

The concentration of extracellular glutamate in the samples was estimated from the standard curve. As a control, serum-free medium containing 50 $\mu\text{M}$  glutamate was added to empty wells (free of astrocytes) and processed together with those containing astrocytes.

The background for the assays was the value obtained for the HBSS without glutamate; this was subtracted from all readings to obtain a corrected measurement for each sample. Using the corrected measurement, the molar concentration of glutamate was determined from the standard curve. amount of glutamate present in the sample,

Glutamate uptake was calculated by subtracting the concentration of glutamate in the sample after 60 minutes from the starting concentration.

The concentration of glutamate (C) =  $S_a/S_v$  where  $S_a$  is the amount of glutamate in the unknown sample (nmol) from the standard curve and  $S_v$  is the sample volume (mL) added into the wells. The Glutamate Uptake was calculated as glutamate uptake/ $\mu$ g protein in the sample.

#### 2.2.6 Phagocytosis assay

Phagocytosis is another key function of astrocytes within the CNS; assessment of this was undertaken with the Vybrant Phagocytosis Assay kit (Thermofisher cat: V6694).

Astrocytes were plated in 96-well plates at a density of 30,000 cells/cm<sup>2</sup> at least 24 hours prior to testing. As a negative control, 3 wells of wild-type (E3/E3) astrocytes were treated with the cell-cycle inhibitor Cytochalasin D (5 $\mu$ g/ml for 30 min at 37°C; Thermofisher) which inhibits phagocytosis<sup>310</sup>.

The fluorescent E. coli BioParticle suspension was prepared by pipetting concentrated HBSS into the fluorescent particle vial, vortexing and passing through a syringe and needle several times before transferring to a centrifuge tube containing 4.5 mL of deionised water. This was vortexed until the fluorescent particles were homogeneously dispersed.

Cells were incubated for 2 hours with 100  $\mu$ l of fluorescein-labelled E. coli Bioparticles. The E. coli suspension was aspirated, and 100  $\mu$ l of Trypan Blue was added for 1 minute at RT to quench extracellular fluorescence. Following Trypan Blue aspiration, fluorescence was measured (480 nm excitation/520 nm emission) using a microplate reader.

To minimise experimental errors, average fluorescence intensity values from groups of 3 replicates of negative control, positive control and experimental samples were used.

Results were normalised to protein levels in the cell media assessed using a BCA assay to give fluorescent intensity per microgram of protein.

To calculate the net phagocytosis, the average of values of the negative-control wells was subtracted from the positive-control wells (quiescent E3/E3 astrocytes) to yield the Net Positive Reading. The Net Experimental Reading was obtained by subtracting the average fluorescence intensity of the negative-control wells from the experimental wells. The phagocytosis response was expressed as follows:

$$\% \text{ Effect} = (\text{Net Experimental Reading} / \text{Net Positive reading}) \times 100\%$$

#### 2.2.7 Cytokine array

A Human Cytokine Antibody Array (Abcam #ab133997) was used to test for differences in the production of 42 cytokines in quiescent astrocytes and 'A1' astrocytes of E3/E3 and E4/E4 genotypes. One week prior to induction, astrocytes were transitioned to a serum free media; 'A1' astrocytes were induced as described in Chapter 2 using a cocktail of C1q, TNF- $\alpha$  and IL-1 $\alpha$  for a period of 24 hours. Two separate differentiations were used with media from three separate technical replicates pooled for each sample. Each antigen-specific antibody spot is duplicated so results represent the mean of these two values.

The array was undertaken according to the manufacturer's instructions. Briefly, membranes were first blocked by incubating with 2 mL 1X Blocking Buffer at room temperature (RT) for 30 min. Parallel samples (n = 3 or 4) from each treatment were pooled and added to each membrane of the array kit and left overnight at 4°C; the result from each membrane therefore represents the mean value of this pool. Samples of media were used as blanks. Each membrane was then washed with 20mls of Wash Buffer I at RT with gentle shaking or rocking for 30-45 min. Membranes were then washed a further 2 times with 2 ml of 1X Wash Buffer I, for 5 minutes at RT. Then 2 further washes with 1X Wash Buffer II for 5 minutes at RT.

1 ml of 1X Biotin-Conjugated Anti-Cytokines was pipetted into each well and incubated overnight at 4°C. Membranes were again washed 3 times with 2 ml of 1X Wash Buffer I, for 5 minutes at RT then 2 further washes with 1X Wash Buffer II for 5 minutes at RT.

Chemiluminescent detection was achieved by pipetting 500µl of the Detection Buffers mixture onto each membrane (250 µl of Detection Buffer C and 250 µl of Detection Buffer D) and incubating for 2 minutes. A CCD camera was then used to detect chemiluminescence. Images were taken using the same exposure times to allow for comparison of temporally distinct samples. The array contains two parallel antibody spots for each cytokine to ensure that all of the steps in the array are performed technically correctly and no unspecific reactions occur.

The signal intensity of each antigen-specific antibody spot is proportional to the relative concentration of the antigen. Expression levels of each cytokine were quantified using densitometry and background readings from negative-control spots were subtracted. Values were then normalised to the positive-control levels for each membrane which provide an internal control for the total amount of protein in the sample.

#### 2.2.8 Quantitation of cholesterol, cholesteryl esters and oxylipins

Cholesterol, cholesteryl esters and oxylipins were extracted under the guidance of Dr Victoria Tyrrell in Professor Val O'Donnell's laboratory.

All extractions took place in single use all-glass tubes (Chromacol). Lipids were extracted by adding a solvent mixture of 1M acetic acid/isopropanol/hexane (2:20:30, v/v/v) to the sample at a ratio of 2.5ml solvent mixture: 1ml sample. For each 1 ml of sample, 10ng of CE(18:1)D7 and 1µg Chol-D7 internal standards plus a stable isotope-labelled standard for each oxylipin class was added and vortexed for 60 seconds. 2.5ml of hexane was added and vortexed for a further 60 seconds ensuring that both phases mixed thoroughly. The samples were then centrifuged at 280g in the Thermo Fisher Heraeus Megafuge 40R table-top centrifuge for 5 min at 4°C . The lipids in the hexane

layer (the upper layer) were removed, taking care not to remove the interface or aqueous layer, using a glass pipette and bulb and transferred to a new Chromacol tube. The samples were then re-extracted by addition of another 2.5ml of hexane then vortexed and centrifuged as before. Hexane layers were then placed in the RapidVap to commence drying (settings were Vacuum: 200, Heat: 30, Shaking:30).

The Bligh and Dyer method was then used to extract the organic bottom layer. For 1ml of sample, 3.75ml of 1:2 (v/v) CHCl<sub>3</sub>:MeOH was added to the Chromacol tube and vortexed for 60 seconds. 1.25 ml dH<sub>2</sub>O was then added and vortexed. The tube was then centrifuged at 280g in the Thermo Fisher Heraeus Megafuge 40R for 5 minutes at 4°C to give a two-phase system (aqueous on the top, organic on the bottom). The organic bottom phase was recovered by inserting a glass Pasteur pipette through the upper phase with gentle positive-pressure to avoid contamination with the upper phase. The bottom phase was then carefully withdrawn through the pipette, recovering approximately 90% of bottom phase to avoid contamination by the upper phase. The bottom organic layer was then pooled with the hexane layers already placed in the RapidVap to continue drying. Once dry, samples were resuspended in 200µl methanol and transferred to a HPLC vial with a 300µl insert, flushed with nitrogen and capped and kept at -80°C ready for MS analysis.

Cholesterol and cholesteryl esters were separated by liquid chromatography using a gradient of 90-100% B over 20 minutes (Mob A: 4mM Am Acetate + 5%B; Mob B: ACN/IPA 60/40 + 4mM Am Acetate) on a Hypersil Gold C18 100X2.1MM 1.9µm Column (ThermoFisher), and analysed on a Sciex QTRAP® 6500 LC-MS/MS system. Source conditions: TEM 150°C, IS -5000, GS1 25, GS2 50, CUR 35. Oxylipins were separated by liquid chromatography (LC) using a gradient of 30-100% B over 20 minutes (A: Water:Mob B 95:5 + 0.1% Acetic Acid, B: Acetonitrile: Methanol 80:15 + 0.1% Acetic Acid) on an Eclipse Plus C18 Column (Agilent), and analysed on a Sciex QTRAP® 6500 LC-MS/MS system. Source conditions: TEM 475°C, IS -4500, GS1 60, GS2 60, CUR 35. Lipids and their deuterated standards were detected using MRM monitoring with defined parent to daughter ion transitions (see Table 2.2 below).

Chromatographic peaks were integrated using Multiquant 3.0.2 software (Sciex). The criteria for assigning a peak was signal:noise ratio of at least 3:1 and with at least 7 points across a peak. The ratio of analyte peak areas to internal standard was taken and lipids quantified using a standard curve made up and run at the same time as the samples.

**Table 2.2: parent to daughter ion transitions for MRM monitoring**

Q1 MASS	Q3 MASS	DWELL TIME	ID	DP	CE	CXP
404.389	369.1	100	CHOLESTEROL	70	20	25
614.587	369.1	100	CE(14:0)	70	20	25
642.618	369.1	100	CE(16:0)	70	20	25
640.603	369.1	100	CE(16:1)	70	20	25
638.587	369.1	100	CE(16:2)	70	20	25
670.650	369.1	100	CE(18:0)	70	20	25
668.634	369.1	100	CE(18:1)	70	20	25
666.618	369.1	100	CE(18:2)	70	20	25
664.603	369.1	100	CE(18:3)	70	20	25
692.634	369.1	100	CE(20:3)	70	20	25
690.618	369.1	100	CE(20:4)	70	20	25
688.603	369.1	100	CE(20:5)	70	20	25
714.618	369.1	100	CE(22:6)	70	20	25
675.600	376.3	100	CE(18:1)D7	70	20	25
411.300	376.1	100	CHOL-D7	70	20	25

## 2.3 Protein techniques

### 2.3.1 BCA (Bicinchoninic Acid) assay

BCA assays were used to measure the protein concentration of samples in order to normalise results of other assays. Ready-made BCA standards were used (Thermofisher, Cat no 23208).

Samples were taken from the freezer and kept on ice until ready to use. Lysate samples were diluted 1:10 and media samples 1:2 by adding the appropriate quantity of lysis buffer. 10  $\mu$ L of each standard was added to a well of a clear flat bottomed 96 well plate. 10 $\mu$ L of samples were added to the plate. 10 $\mu$ L of lysis buffer was used as a blank for the protein lysates and standards. Each well was duplicated to ensure accurate results.

The Pierce™ BCA Protein Assay Kit (Thermo Fisher Scientific) was used to determine protein concentration. Reagent B was added to Reagent A at a ratio of 1:50. 200 $\mu$ L of the mixture was added to the wells containing standards, blank and samples and mixed with a pipette. The plate was incubated at 37°C for 30 minutes. Following incubation, optical density was measured using a  $\mu$ Quant™ Microplate Spectrophotometer at 562nm wavelength.

Duplicate measurements were averaged and the appropriate blank measurement subtracted. To analyse the results, a graph of the protein standards concentration against their optical reading was plotted. A line of best fit was created and the  $y=mx+c$  equation was used to calculate the concentration of the protein lysate measured.

### 2.3.2 ELISA

Enzyme-linked immunosorbent assay (ELISA) is a technique designed for quantification of peptides, proteins, antibodies and hormones. Human ApoE protein was quantified using the Invitrogen Human ApoE ELISA following the manufacturers guidelines (Invitrogen. Cat no. EHAPOE).

#### 2.3.2.1 Reagent and sample preparation

All reagents and samples were brought to RT before use. Assay Diluent was diluted 5-fold with deionised water. Biotinylated antibody was prepared by adding of 100 µL of Assay Diluent to produce an antibody concentrate which was then diluted 80-fold with 1X Assay Diluent for use. Streptavidin-HRP Reagent was diluted 1500-fold with 1X Assay Diluent. All standards and samples were run in duplicate. For extracellular ApoE samples, the appropriate medium was used as a blank.

#### 2.3.2.2 Standard preparation

400µL 1X Assay Diluent was added to the vial of lyophilized standard and mixed to prepare a 400 ng/mL standard solution. 300 µL 1X Assay Diluent into each tube. The 400 ng/mL standard solution was used to produce a dilution series (shown below). 1X Assay Diluent served as the zero standard (0ng/mL).

	400ng/ml	160ng/ml	64ng/ml	25.6ng/ml	10.24ng/ml	4.10ng/ml	1.64ng/ml
Assay diluent (uL)	300	300	300	300	300	300	300
Standard vol (uL)		200@ 400ng/ml	200@ 160ng/ml	200@ 64ng/ml	200@ 25.6ng/ml	200@ 10.24ng/ml	200@ 4.10ng/ml

#### 2.3.2.3 Procedure

100µL of diluted samples, standards and appropriate blanks were added to the wells, covered and incubated at RT for 2.5 hours with gentle shaking. Following incubation, the samples, standards and blanks were removed and the wells washed with 300µL of TX Wash buffer four times. 100µL of 1X prepared biotinylated antibody was added to the wells and incubated at RT for 1 hour with gentle shaking. Following incubation, the detection antibody was removed and the wells washed four times with wash buffer. 100µL of prepared Streptavidin-HRP solution was added to each well and incubated at 45 minutes at RT with gentle shaking. The solution was discarded and the wells again washed four times. 100µL of TMB Substrate was then added to each well and incubated at RT in the dark with gentle shaking. After 30 minutes, 50 µl of Stop Solution to each well.

The plate was evaluated within 30 minutes of stopping the reaction. The absorbance of each well was measured on a µQuant™ Microplate Spectrophotometer using 450nm wavelength.

#### 2.3.2.4 Calculation of results

A standard curve was generated by plotting the standard protein concentration against optical density and a line of best fit found. The average optical density of the blanks was subtracted from the optical density of each sample its replicates. Blanked technical replicates were then averaged. The formula for the line of best fit ( $y=mx + c$ ) was applied to calculate the protein concentrations of the samples from the optical density recorded. This value was multiplied by the dilution factor and then divided by the total protein concentration of the sample lysate (ApoE ng/mg).

## 2.4 Nucleic acid techniques

### 2.4.1 Isolation of plasmids

Plasmids were isolated from transformed E.coli using the QIAprep® Spin Miniprep Kit (Qiagen Cat no: 27104); all centrifugation steps took place at 17900g for 1 minute unless otherwise stated. Transformed cultures were incubated ON and collected in a microcentrifuge tube. Bacterial cells were harvested by centrifuging for 3 minutes at RT at 6800g. The supernatant was discarded and the cell pellet resuspended in 250µL of buffer P1. 250 µL of cell lysis buffer P2 was added and the tubes inverted to mix; the tubes were left for 5 minutes. To neutralise the reaction, 350 µL of Qiagen buffer N3 was added and mixed and the tube centrifuged for 10 minutes. The supernatant was added to a QIAprep spin column and then centrifuged. The filtrate was discarded, 500 µL of Qiagen buffer PB was added to the column and then centrifuged. The filtrate was discarded, 750 µL of Qiagen buffer PE was added to the column and centrifuged. The filtrate was discarded and the column was centrifuged again to remove any residual buffer. The column was placed in a clean microcentrifuge tube. The DNA was eluted by adding of 30µL of elution buffer to the column, incubated for 1 minute then centrifuged.

### 2.4.2 DNA extraction, purification and quantitation

Two methods of DNA extraction were used depending on the final use of the DNA.

#### 2.4.2.1 *General DNA extraction methods*

When DNA was being extracted from a small number of samples the QIAamp® DNA Mini Kit (Qiagen, Cat no: 51304) was used. Cells were removed from culture plates (see 2.1.1) and a maximum of  $5 \times 10^6$  cells added to a microcentrifuge tube and centrifuged for 5 minutes at 300g. The supernatant was aspirated and the cell pellet resuspended in 200 µL of DPBS. 20µL of proteinase K then 200µL of Qiagen Buffer AL was added to

the cell suspension, mixed and incubated at 56°C for 10 minutes. 200 µL of 100% ethanol was added to the sample, mixed and then added to the QIAamp Mini spin column. The column was centrifuged for 1 minute at 6000g. The filtrate was discarded and 500 µL of Qiagen Buffer AW1 added to the spin column which was then centrifuged for 1 minute at 6000g. The filtrate was discarded and 500 µL of Qiagen Buffer AW2 was added to the column. The column was centrifuged for 3 minutes at 20,000g. The filtrate was discarded and the column was centrifuged for a further minute. The column was placed into a clean microcentrifuge tube and 20µL of warmed elution buffer added to the column incubated for 1 minute at RT. The DNA was eluted by centrifuging the column at 6000g for 1 minute; the process was repeated with a further 20µL of elution buffer.

#### 2.4.2.2 *DNA extraction from clones post transfection*

For screening of clones post transfection, a cheaper and more crude method of DNA extraction was used. Cells were washed twice with DPBS then 150uL of lysis buffer and 1uL of proteinase K (PK) (see tables below) added to each well of a 24-well plate. Plates were then sealed with Parafilm (Sigma-Aldrich) and placed in a plastic container with damp tissue paper for humidification. The container was sealed and placed in an oven at 56°C and left overnight. The next day, 10uL of the lysis mix was removed from each well and added to 90uL of 10mM Tris ph8.0; it was then heated at 95°C for 30 mins to inactivate the PK. When cooled, 1uL was used in PCR reactions. PCR products using DNA extracted using this method underwent gel electrophoresis and gel extraction (see below) before being sent for Sanger sequencing.

Reagents for lysis buffer	Supplier	Volume
Nuclease free H <sub>2</sub> O		46ml
1M Tris pH 8.0	Thermofisher	2.5ml
0.5M EDTA	Thermofisher	1ml
10% SDS	Sigma Aldrich	155uL
5M NaCl	Sigma Aldrich	200uL

Reagents for Proteinase K	Supplier	Volume
Protein kinase	Promega	100mg
Nuclease free H <sub>2</sub> O		4.7ml
1M Tris pH8.0	Thermofisher	250uL
1M CaCl	Sigma Aldrich	100uL

#### 2.4.2.3 Quantitation of DNA

DNA levels were quantified using the NanoDrop™ 2000 Spectrophotometer and then stored at -20°C until required.

#### 2.4.3 Polymerase chain reaction (PCR) including primer design

PCR is a technique that amplifies a particular region of DNA. The DNA region of interest is bounded by primers designed to complement DNA flanking the region of interest. Primers bind to their complementary sequence to form double stranded DNA, then a thermostable Taq polymerase synthesises a complementary DNA strand using excess deoxyribonucleotide triphosphates (dNTPs) in the reaction mixture. The product is then exponentially replicated in order that it can be detected; this takes place in three steps. The first step is denaturing which causes the template DNA to become single stranded. Next, primers anneal to their complementary sequence within the template DNA. Finally, the elongation step in which the new DNA strands are synthesised. A typical PCR will have around 30 cycles of these steps carried out at specific temperatures. All PCRs were carried out using C1000/S1000 Thermal Cyclers (Bio-Rad).

PCR primers were designed using the Primer3 web resources (<http://bioinfo.ut.ee/primer3-0.4.0/>). Primers were designed to be approximately 20bp in length and have an annealing temperatures of around 60°C. Primers were verified for specificity with the UCSC In-Silico PCR website (<https://genome.ucsc.edu/cgi-bin/hgPcr>).

Screening for clones was assisted by Karolina Dec while working as an Erasmus student and by two medical students, John Lynch and Christopher Bailey as part of their Year 4 Student Selected Component (SSC).

#### 2.4.4 Gel electrophoresis

When a potential difference is applied to an agarose gel loaded with DNA, fragments of different size migrate toward the anode at different speeds thus allowing separation. 0.6-2% agarose gels were used depending on the DNA fragment size or the resolution required; 0.6% gels were used for DNA extractions to maximise yield. Standardly, a 1.2% agarose gel was made by dissolving 1.2 g of high-resolution agarose (Sigma) per 100 mL of 0.5X Tris-Borate-EDTA (TBE) buffer (Thermofisher). 1 $\mu$ L of ethidium bromide (10 mg/mL; Thermofisher) was then added per 100 mL of agarose solution. The solution was poured into a cast with the appropriate comb to form the number of wells desired and left to set. Once set, the gel was placed in an electrophoresis tank containing 0.5X TBE. PCR product was mixed with 6X loading dye (NEB) and loaded into the formed gel. An appropriate DNA ladder (Thermofisher/NEB) was run alongside the PCR product to estimate the size of the fragment. Gels were typically electrophoresed at 80V. Gels were imaged using Image Lab software (Bio-Rad).

#### 2.4.5 DNA extraction from agarose gel

DNA fragments were visualised in the gel using a UV Transilluminator (UVP) and excised with a scalpel. DNA was extracted from agarose gels using QIAquick Gel Extraction Kit (Qiagen; Cat no 28706) and then purified using QIAquick PCR purification Kit (Qiagen; Cat no 28104). All centrifugation steps were carried out for 1 minute at RT at 17,900g. Three volumes of Qiagen Buffer GQ were added to 1 volume of the gel then incubated at 50°C until the gel dissolved. One volume of 100% isopropanol (Thermofisher) was added to the sample and mixed. The sample was then applied to a QIAquickspin column and centrifuged. The filtrate was discarded and 500  $\mu$ L of Qiagen buffer QG added. The filtrate was discarded, 750 $\mu$ L of Qiagen buffer PE added and the

column centrifuged. The filtrate was discarded and the column centrifuged again. The column was then placed into a clean microcentrifuge tube and 20 $\mu$ L of warmed elution buffer added to elute DNA. The column was incubated for 1 minute then centrifuged; this process was repeated with a further 20 $\mu$ L of elution buffer to maximise yield. To purify the DNA, 5 volumes of Qiagen buffer PB was added to 1 volume of sample and mixed. The sample was added to a QIAquick spin column and centrifuged. The filtrate was discarded and 750 $\mu$ L of Qiagen buffer PE was added to the column and centrifuged. The column was placed into a clean microcentrifuge tube elution carried out as above.

#### 2.4.6 Sanger sequencing

Sanger sequencing was undertaken by GATC Biotech's LIGHTrun™ Sequencing service. 5 $\mu$ L of cleaned product was combined with 5 $\mu$ L of forward or reverse primer (5 pmol/ $\mu$ L). Results were analysed using SnapGene software.

## 2.5 Gene expression analysis

Gene expression analysis work was assisted by Karolina Dec, funded as a research assistant by my Alzheimer's Research UK (ARUK) Clinical Fellowship.

### 2.5.1 RNA extraction

Cells for RNA extraction were first washed once with DPBS. Cells were removed from culture plates using a cell scraper. They were then washed in PBS and centrifuged at 2000g for 5 minutes and the supernatant removed. In order to analyse results simultaneously, cell pellets were re-suspended in 10 volumes of RNALater<sup>TM</sup> (Invitrogen) solution and transferred to -80°C for storage until all samples from multiple cell lines and/or multiple time points were collected. Biological triplicates for each sample of each experiment were taken.

RNA was isolated using the Invitrogen PureLink RNA Mini Kit [cat. no. 12183018A] according to the manufacturer's instructions. Frozen cell pellets in RNALater, were left at RT for 2-3 minutes to defrost. Samples were then centrifuged at 2000g for 5 minutes. RNALater was aspirated from the cell pellet, lysis buffer added (0.3ml for <math><1 \times 10^6</math> cells) and the sample vortexed until the cells were dispersed.

The lysate was passed 5-10 times through an 18 gauge syringe needle. One volume of 70% ethanol was added to each volume of cell homogenate and vortexed to disperse any visible precipitate. Up to 700uL of the sample was transferred to the spin cartridge with collection tube and centrifuged at 12,000g for 30 seconds. The flow-through was discarded and the process repeated until the entire sample had been processed.

700uL of Wash Buffer I was added, centrifuged at 12,000g for 30 seconds and flow-through discarded. 500uL of Wash Buffer II was then added, centrifuge at 12,000g for 30 seconds and flow-through discarded. This step was then repeated. The spin cartridge was then centrifuged at 12,000g for a further 1-2 minutes to dry the membrane with bound RNA. The spin cartridge was then placed into a collection

Eppendorf and 40uL of RNase-free water (Thermofisher) added to the centre of the cartridge. It was incubated at RT for 1 minute then centrifuged for 2 minutes at 12,000g, at RT. RNA was then transferred to long-term storage at -80°C

### 2.5.2 Reverse transcription

The High Capacity cDNA Reverse Transcription Kit (Applied Biosystems Cat no. 4368814) was used for reverse transcription according to the manufacturer's instructions. 10µl of mastermix was made up on ice for each reaction according to the table below.

Component	Volume (µl)
10xRT Buffer	2.0
25x dNTP Mix (100mM)	0.8
10x Random Primers	2.0
Multiscribe reverse transcriptase	1.0
Nuclease free H <sub>2</sub> O	4.2
TOTAL	10

RNA samples were diluted in DEPC-treated ddH<sub>2</sub>O to a volume of 10 µl such that each contained 0.75µg of RNA. This was combined with 10µl of Mastermix. Samples were placed in a T100 Thermal Cycler (Biorad) and the recommended program was run (25°C for 10 minutes, 37°C for 120 minutes and 85°C for 5 minutes). The resulting cDNA was diluted 1:3 with ddH<sub>2</sub>O and stored at -20°C.

### 2.5.3 Quantitative real-time PCR (qRT-PCR)

Quantitative PCR was used to quantify transcripts of interest using fluorescent dsDNA binding dye and primers designed to amplify the sequence of interest. Primers were designed to be intron-spanning in order to avoid amplification of DNA (see table below). Where possible, primers from published papers were used; where this was not possible, they were designed using PrimerBlast.

The reaction was undertaken using SyGreen Blue Mix Hi Rox kit (PCRBiosystems Cat no PB20.15-20). Each sample was run in triplicate. For each reaction, 10 µl of 2X qPCR SyGreen Blue Mix, 0.8µl of both primers (from 10µM stock) for the gene of interest and 75ng of cDNA were combined and made up to 20µl with ddH<sub>2</sub>O. The qPCR reaction was run on a Bio-Rad CFX Connect Real-Time System. The program used included an initial incubation at 95°C for 2 mins, followed by 40 cycles of 95°C for 30 secs and 60°C for 15 secs. For every primer, a melt curve was generated to check for the specificity of the product; any primers that generated more than one peak were discarded.

**Table 2.3: Primers used for RT-qPCR**

Gene	Marker	Forward Sequence	Reverse Sequence
B-actin	Reference gene	TCACCACCACGGCCGAGCG	TCTCCTTCTGCATCCTGTCTG
OCT3/4	Stem cell	TTCTGGCGCCGGTTACAGAACCA	GACAACAATGAAAATCTTCAGGAG A
Nanog	Stem cell	GCTTGCCTTGCTTTGAAGCA	TTCTTGACCGGGACCTTGTC
SOX2	Stem cell/NPC	ACTTTTGTCTGGAGACGGAGA	GTTTCATGTGCGCGTAACTGT
PAX6	NPC	GTGTCCAACGGATGTGTGAG	CTAGCCAGGTTGCGAAGAAC
FOXG1	NPC	AGGAGGGCGAGAAGAAGAAC	TCACGAAGCACTTGTGAGG
TUBB3	Neurons	CATGGACAGTGTCCGCTCAG	CAGGCAGTCGCAGTTTTTAC
MAP2	Neurons	AACCGAGGAAGCATTGATTG	TTCGTTGTGTCGTGTTCTCA
Vimentin	Astrocyte	TGGACCAGCTAACCAACGAC	GCCAGAGACGCATTGTCAAC
GFAP	Astrocyte	GAGCAGGAGGAGCGGCAC	TAGTCGTTGGCTTCGTGCTT
S100b	Astrocyte	ATGTCTGAGCTGGAGAAGGC	TTCAAAGAACTCGTGGCAGG
SLC1A3 (EAAT1)	Astrocyte	CGAAGCCATCATGAGACTGGTA	TCCCAGCAATCAGGAAGAGAA
SLC1A3 (EAAT2)	Astrocyte	TAACTCTGGCGGCCAATGGAAAGT	ACGCTGGGGAGTTTATTCAAGAAT
AQP4	Astrocyte	GGCCGTAATCTGACTCCCAG	TGTGGGTCTGCACTCATGC
APOE	Astrocyte	GAGCAGGCCAGCAGATAC	CTGCATGTCTCCACCAGGG
GLUL (GS)	Astrocyte	CCTGCTTGATGCTGGAGTC	GATCTCCCATGCTGATTCCT
CD44	Astrocyte precursor	AGCATCGGATTTGAGACCTG	GTTGTTTGTGCACAGATGG
LRP1	Cholesterol	GATCCCAATGACAAGTCAGATGC	ATGCCATTGGTCACCACGTCTTC
LDLR	Cholesterol	GCGAAGATGCGAAGATATCGATG	CCGGTTGGTGAAGAAGAGGTAG
CYP46A	Cholesterol	CCTGAGTCGGTTAAGAAGTTC	GGTCTATGACTCTCCGCTGC
ACAT	Cholesterol	GGAGGCTGGTGCAGGAAATAA	ACCCAATACTGCCTGCCTTG

NR1H3	Cholesterol	CCTTCAGAACCCACAGAGATCC	ACGCTGCATAGCTCGTTCC
PLTP	Cholesterol	GGCGCACATGCAGAGTTCC	CCTTCACCTCAGAGATGTTGTAGT
CETP	Cholesterol	CCCGCATGCTGTACTIONCTGG	AGCACTGCCTTGAACCTCGTC
LIPE	Cholesterol	ACAGCGATCAGCCCTAGAGT	CTTGAGGCTGTATCCTGGTAGT
LPL	Cholesterol	CCGCCGACCAAGAAGAGAT	TAGCCACGGACTCTGCTACT
ABCG1	Cholesterol	TCGACCAGCTTTACGTCCTG	GTGGTAGGTTGGGCAGTTCA
NR1H2	Cholesterol	ATCGTGGACTTCGCTAAGCAA	GATCTCGATAGTGGATGCCTTCA
SREBP2	Cholesterol	TAACCCCTTGACTTCCTTGC	CACACCATTTACCAGCCACA
C3	Complement	AAAAGGGGCGCAACAAGTTC	GATGCCTCCGGGTTCTCAA
MEGF10	Phagocytosis	AGCGGATTCAGAGAGGTTGT	GGTGATGCTGTCCAATCCA
MERTK	Phagocytosis	TGGACAACCTTTCACAGCGG	GCAGAGGAATATGCTTTGGTCC

Data were analysed with Microsoft Excel using the  $\Delta\Delta CT$  method for relative quantification<sup>311,312</sup>. Data are based on three biological replicates with each sample run in triplicate; experiments represent the results from three separate differentiations unless otherwise stated. Expression levels of each gene were first normalised to levels of  $\beta$ -actin and then, for the majority of experiments, levels in each isogenic line were normalised to levels in quiescent *E3/E3* samples.

## 2.6 Genome editing techniques

During the course of this research, the sophistication of CRISPR-Cas9 technology changed considerably. The initial method used was a plasmid-based approach which enabled identification of suitable short guide RNAs (sgRNAs) but had poor editing efficiency. It was superseded by a ribonucleoprotein (RNP) based system which had much higher editing efficiency and cell survival. Both techniques are described below.

### 2.6.1 Genotyping wild-type cell lines

Prior to genetic modification, it is necessary to determine the genotype of the wild-type cell lines. A 250bp region containing the entirety of Exon 4 and thus the rs429358 and rs7412 SNPs was sequenced. DNA was extracted from unmodified cell lines with the QIAamp DNA mini kit (Qiagen) (see Section 2.4.2.1). The region surrounding rs429358 and rs7412 was amplified via PCR using the primer sequences below to give a 585bp product.

<b>Forward sequencing primer 5'-3'</b>	CTCTTGGGTCTCTCTGGCTCA
<b>Reverse Sequencing Primer 5'-3'</b>	CTGCCCATCTCCTCCATCCG

Thermocycler conditions and reagents are shown in the tables below.

Reagents	Supplier	Volume ( $\mu$ L)
Qiagen buffer x10	Qiagen	1.2
ddH <sub>2</sub> O		4.24
dNTPs (2 $\mu$ M)	NEB	0.48
Primers (5pmol/ $\mu$ L) x 2	Eurofins Genomics	0.56
Hot Start Taq	NEB	0.06
DMSO	Sigma Aldrich	0.9
DNA (5ng/ $\mu$ L)		4
<b>TOTAL</b>		<b>12</b>

Step	Temperature (°C)	Time (s)
Initial Denaturation	95	60
34 Cycles	95	30
	58	60
	72	60
Final Extension	72	300
Hold	4-10	

The PCR product size was confirmed with gel electrophoresis. 10 µL of PCR product was purified using the AMPure PCR purification system (Agencourt®) using Biomek® NXP Laboratory Automation Workstation (Beckman Coulter). 5 µL of AMPure cleaned product was combined with 5µl of forward primer (5 pmol/µL) and then sequenced by GATC Biotech's LIGHTrun™ Sequencing service.

#### 2.6.2 Plasmid-based approach

Plasmids are small, circular, double-stranded DNA molecules that are distinct from a cell's chromosomal DNA. Plasmids have been used for many years to clone, transfer, and manipulate genes. DNA fragments or genes can be inserted into a plasmid vectors, creating a recombinant plasmid. This plasmid can then be introduced into a bacterium (transformation) which are used as factories to copy DNA fragments in large quantities.

##### 2.6.2.1 *Creation of the CRISPR/Cas9 targeting plasmid*

The gene editing approach used followed the protocol by Ran et al, 2013<sup>313</sup>. The chosen plasmid (single wild-type nickase pSpCas9n(BB)-2A-GFP (PX458) Addgene.org #48138) was isolated from *E.coli* using the QIAprep Spin Miniprep Kit (Qiagen) (described in section 2.4.1). Restriction enzyme digests were used to validate the plasmid obtained.

Guide RNAs were selected using Benchling.com (described in Chapter 3). Sense and anti-sense sgRNA oligonucleotides were annealed and phosphorylated in a single reaction forming a DNA duplex with overhanging sticky ends for cloning into PX458. The reaction was incubated at: 37°C for 30 minutes; 95°C for 5 minutes for denaturation of the oligonucleotides; 95°C decreasing 5°C per minute until 25°C to allow accurate annealing. Phosphorylated and annealed oligonucleotides were diluted 1:200 in nuclease free water.

Reagents for annealing & phosphorylation of sgRNAs	Per reaction (μL)
forward sgRNA (100μM; Eurofins Genomics)	1
reverse sgRNA (100μM; Eurofins Genomics)	1
T4 ligation buffer 10X (NEB, cat. no. B0202S)	1
T4 PNK (NEB, cat. no. M0201S)	1
ddH2O	6
<b>Total</b>	<b>10</b>

To clone sgRNA duplexes into PX458, PX458 was first digested by the enzyme BbsI to create the cloning site and sgRNA duplexes ligated into the cloning site; this was performed in one reaction. A no-insert, PX458 only negative control ligation reaction was also carried out. This digestion and subsequent ligation reaction was incubated at 37°C for 5 minutes, 21°C for 5 minutes, repeated 6 times (see table below).

Reagents for ligation of sgRNA duplex into PX458	Per reaction (μL)
PX458 (200ng/μL)	0.5
Oligonucleotide duplex (diluted 1:200)	2
Tango Buffer x10 (Thermo Fisher Scientific)	2
DTT, 10mM (Thermo Fisher Scientific)	1
ATP, 10mM (NEB)	1
FastDigest BbsI (Thermo Fisher Scientific)	1
T7 Ligase (Enzymatics, MA, US)	0.5
ddH2O	to 20
<b>Total</b>	<b>20</b>

Once the reaction was complete, the product was treated with PlasmidSafe™ DNase (Epicentre Biotechnologies, MI, USA) to digest any residual linearised DNA (reagents in table below). The PlasmidSafe™ DNase reaction was incubated at 37°C for 30 minutes to degrade any contaminating chromosomal dsDNA into deoxynucleotides. The final step was incubation at 70°C for 30 minutes to deactivate the enzyme.

Reagents for PlasmidSafe™ DNase reaction	Per reaction (µL)
Digestion and ligation reaction product	11
PlasmidSafe Buffer (Epicentre Biotechnologies)	1.5
PlasmidSafe ATP-Dependent DNase (Epicentre Biotech)	1
ATP, 10mM (NEB)	1.5
<b>Total</b>	<b>15</b>

#### 2.6.2.2 Transformation of PX458sgRNA into chemically competent cells

Both subcloning Efficiency™ DH5α™ Competent cells (Thermo Fisher Scientific) and Stbl3™ E.coli strain (Thermo Fisher Scientific) and were used for transformations and culture. For each transformation, one vial of chemically competent cells was thawed on ice for 10 minutes. 3µL of plasmid DNA from the PlasmidSafe DNA purification reaction was added into the vial of cells and gently mixed by flicking the tube 3-5 times. pUC19 control DNA (NEB; 10 pg/µL) was used as a positive control for transformation. A negative control was performed using the no-insert PX458 negative ligation reaction. The vials were incubated on ice for 30 minutes then underwent heat-shock by incubating at 42°C for exactly 30 seconds then placed on ice for a further five minutes. 475µL of pre-warmed SOC media (Thermo Fisher Scientific) was added to each vial. For the pUC19 control, the transformation mix was diluted 1:10 with Luria-Bertani (LB) broth (Thermo Fisher Scientific). The vials were incubated horizontally at 37°C for one hour in a shaking incubator. 20-100µL of each transformation reaction was then spread onto a pre-warmed selective LB agar plate (containing ampicillin 100 µg/mL) and incubated for 24-36 hours at 37°C. Plasmids that successfully incorporated the duplex DNA are termed PX458sgRNA.

### 2.6.2.3 Confirming the creation of PX458sgRNAs

After incubation, 10-20 colonies per plate were picked, placed in 1.5ml of LB broth containing ampicillin 100µg/mL and incubated overnight. Plasmids were then isolated from transformed minicultures by miniprep (QIAprep Spin Miniprep Kit, Qiagen; section 2.4.1). To identify cultures with successfully incorporated sgRNAs, a restriction enzyme digest was performed and the DNA products run on a 1% agarose gel for analysis. Plasmids thought to contain the sgRNA duplexes were purified and Sanger sequenced to confirm the presence of the sgRNA sequence at the desired location; 10 µL of each plasmid sample was purified for sequencing using AMPure PCR purification system (Agencourt®) using Biomek® NXP Laboratory Automation Workstation (Beckman Coulter). The products were sequenced by GATC Biotech’s LIGHTrun™ Sequencing service. Primers are shown below together with the sequences showing successful incorporation of the 4 guide RNAs into the px458 plasmid (PX458sgRNAs).

Primer sequences for the PX458 plasmid	
Forward sequencing PX458-sgRNA Primer	GAGGGCCTATTTCCCATGATTCC
Reverse sequencing PX458-sgRNA Primer	TTTGTCTGCAGAATTGGCGC

**Figure 2.1: Results of PX458sgRNA Sanger sequencing.**

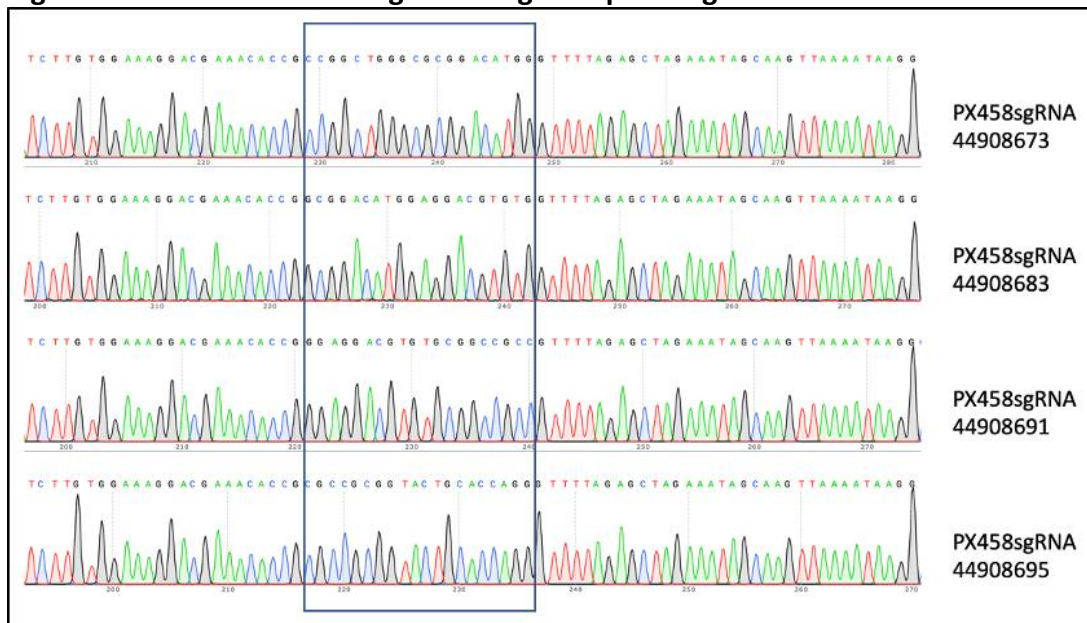


Figure shows the sequencing of the PX458 plasmid for each of the selected sgRNAs with the sgRNA insertion site highlighted.

#### 2.6.2.4 *Transfection of PX458 into the hESC7 cell line*

Transfections were undertaken using the Amaxa 4-D electroporation system. To establish optimum transfection efficiency, initial experiments used PX458 without cloning modifications and a GFP-expressing control plasmid. The experimental factors optimised were the concentration of plasmid DNA (found to be 0.75ug of plasmid) and electroporation parameters (CB150 programme found to be most effective). GFP expression was used as a marker of transfection efficiency.

Pre nucleofection, cells were cultured on Matrigel (Corning) and E8 medium (Life Technologies). Cells were passaged at 70-80% confluence for at least 2-3 passages with a passage undertaken 2-3 days before nucleofection at a 1:4 split. On the day of transfection cells were fed with their usual E8 media with the addition of Revitacell (1:100: Thermofisher). Matrigel coated plates were prepared for cells post-transfection.

To prepare cells for nucleofection, medium was aspirated and added to the prepared Matrigel plates ready for cells post-transfection. Cells were washed once with PBS, Accutase at 37°C added and left for 5 minutes. Accutase was aspirated and cells scraped cells into 5mls of E8 and Revitacell. Cells were pipetted up and down to achieve a single cell suspension and strained through a 40uM cell strainer (Sigma Aldrich) into a 50ml centrifuge tube (Falcon). Cells were counted twice using a Cell Scepter (Millipore) and counts averaged. 200,000 cells per reaction were then placed in a 15 ml centrifuge tube and topped up with 10mL E8 and Revitacell. Cells were centrifuged at 140g for 5 minutes.

P3 buffer from the P3 Primary Cell 4D-Nucleofector Kit (Lonza) was prepared by adding 3.6uL of the supplement provided to the 16.6uL of Nucleofector™ Solution (20uL per experiment). Cells were resuspended in the P3 buffer (200,000 cells per 20uL of buffer) and 0.75ug of plasmid DNA added and cells gently swirled with a pipette tip to ensure mixing and added to the nucleofection cuvette avoiding bubbles and ensuring the solution was positioned between the electrodes. Cells were then electroporated using

the Amaxa-4D CB150 programme. After transfection, 100uL of conditioned medium was added to each cuvette, cells gently aspirated and added to warmed plates. Cells were incubated for 24 hours then media exchanged for E8 without Revitacell. Results are shown in Chapter 3.

### 2.6.3 Genome editing using the Integrated DNA Technologies (IDT) Alt-R system

Cas9 protein can be produced in cells by delivering the corresponding coding sequences as purified DNA (e.g. in a plasmid), as mRNA, or as part of a viral genome however these methods have high levels of cell toxicity and stimulate cells' innate immune response. The Integrated DNA Technologies (IDT) Alt-R system is also based on the *S. pyogenes* CRISPR-Cas9 system but Cas9 is delivered as a preformed sgRNA ribonucleoprotein (RNP) complex comprising a shortened target-specific crRNA (crRNA) bound to a trans-activating crRNA (tracrRNA) which, in turn, binds high-fidelity Cas 9<sup>314</sup>. The shortened sequences of crRNA and tracrRNAs (36 and 67 nucleotides respectively) are purported to increase on target efficiency and elicit less innate immune activation thereby increasing post-transfection cell survival.

Transfections were undertaken in two stages. First, four different guide RNAs were used in order to establish which was the most efficient. Once the most efficient guide was identified, single-stranded oligo DNA nucleotides (ssODNs) were designed around the guide and tested. The most efficacious guide RNA and ssODN were then combined to create the isogenic lines.

#### 2.6.3.1 *Transfection*

Passaging and pre-nucleofection treatment was identical to the method used for plasmid transfections outlined above.

The crRNA:tracrRNA complex was prepared by mixing 1uL of 200uM crRNA and 1uL of 200uM tracrRNA (containing an Atto 550 fluorophore) with 2.5uL IDTE duplex buffer to give a volume of 4.5uL; each reaction required 1uL (all from IDT). The mix was

annealed at 95°C for 2 minutes then allowed to cool. The ribonucleoprotein (RNP) complex was formed by diluting Cas9 protein (stock concentration of 10 µg/µl; IDT) in IDTE duplex buffer to a concentration of 4ug/uL. In 8 well PCR strips 1uL of Cas9 protein (4ug/uL) and 1uL of RNA complex were gently mixed by swirling a pipette tip incubated at RT for 10-20 minutes.

Cells were prepared as for the plasmid transfections but after centrifugation cells were instead resuspended in P3 buffer (IDT); 20uL per 200,000 cells. 20uL of P3 buffer containing 20,000 cells was added to each well of a PCR plate and 1uL each of RNA complex, Cas9 protein and, when used, 1uL of ssoDN (100uM stock) added. The mix was gently stirred and quickly added to the nucleofection cuvette as described above. Again, cells were transfected using programme CB150 of the Amaxa-4D electroporation system. Post-transfection steps were identical to those outlined above for plasmid transfections.

#### 2.6.3.2 *Cell selection with flow cytometry*

The day after transfection, flow cytometry was used to select transfected cells in order to increase screening efficiency. On the morning of analysis, cells were fed with E8 media containing Revitacell (1:100). After a minimum of 2-3 hours the media was aspirated and retained for post-FACS re-plating. Cells were washed once with DPBS and warmed Accutase added. This was incubated at 37°C for 3-5 minutes after which time the Accutase was removed. Cells were resuspended in cold DPBS, gently triturated then passed through a 40µm cell strainer to achieve a single cell suspension; they were then kept on ice until analysis with a BD LSR Fortessa cytometer (BD Biosciences). The instrument was set up by Mark Bishop, lab manager for the European Cancer Stem Cells Research Institute of Cardiff University. Lasers of appropriate wavelength to detect the Atto550 fluorophore were used and gates set using unstained samples as negative controls. Data were analysed with FlowJo V10 software; results are shown in Chapter 3.

### 2.6.3.3 Isolation of clones

FACS-selected cells transfected with the ssODN repair template were re-plated on warmed 10cm plates at clonal density (500-1000 cells per plate) using the retained E8 media and left to grow until small colonies emerged. After 5-10 days, colonies were manually picked and plated into 48-well plates; in total approximately 150 colonies were expanded as single clones. When sufficiently expanded, cells from each well were split in half; half of the cells were used for DNA extraction and the other re-plated for continued growth. DNA was extracted using the technique detailed in Section 2.4.2.2 and screened for cells containing the ssODN template.

### 2.6.3.4 Identification of edited clones

Edited clones were identified using PCR. Considerations around the design of the repair template are discussed in Chapter 3 but one of its key features is the introduction of silent mutations. These are recommended within the PAM sequence to minimise re-cutting but were also used to aid screening using PCR.

Primers were created to recognise when the HDR template had been incorporated by designing a reverse primer which lay over the edit site and included the three silent mutations (shown in red) and the intended mutation (shown in blue). Through trial and error, the primers below were found to identify edited cells but not unedited ones by creating a 193bp product; the key design feature appeared to be having a different nucleotide to the wild-type at the 3' end of the primer.

Primers to identify wild-type and edited cells	Sequence 5' to 3'
Forward primer	CACTGTGCGACACCTCC
Reverse primer for wild-type	GGCCGCaCACGTCTCCATG
Reverse primer for edited cells (silent mutations & E3)	GGCCACaCACGTCTTCCATA
Reverse primer for edited cells (silent mutations & E4)	GGCCACgCACGTCTTCCATA

DNA from clones that were positive for edited product underwent a further PCR, this time using primers flanking the edit site and creating a 250bp product (primers below). PCR products were purified for sequencing using AMPure PCR purification system (Agencourt®) using Biomek® NXP Laboratory Automation Workstation (Beckman Coulter). Sanger sequencing to verify the results of the PCR screening and to determine the exact nucleotide sequence of the targeted locus was the undertaken by GATC Biotech’s LIGHTrun™ Sequencing service; results are shown in Chapter 3.

Primers for sequencing the <i>APOE</i> region	Sequence 5' to 3'
<b>Forward primer</b>	ACAAATCGGAACTGGAGGAACAA
<b>Reverse primer for wild-type</b>	TTCTGCAGGTCATCGGCAT

#### 2.6.4 Quality control measures on isogenic lines

Once clones had been identified they underwent exome sequencing to identify off-target effects and SNP arrays to verify that karyotype remained constant. The results of this analysis are shown in Chapter 3 but the methods are outlined below.

##### 2.6.4.1 Exome Sequencing

Exome sequencing was kindly carried out by Branduff McAllister in Cardiff University. Exome libraries were produced from 75 ng (10 µL at 7.5 ng/ µL) of genomic DNA using the TruSeq Rapid Exome Library Prep Kit (Illumina), according to manufacturer’s instructions. DNA clean-up was performed using SPRI beads (Beckman Coulter). Exomes were sequenced in-house using the HiSeq 4000 to produce raw FASTQ files. To call and annotate the variants, three pipelines were used: a standard GATK pipeline, quality control (QC) pipeline and an annotation pipeline. Sequenced reads were aligned to the human reference genome [Human GRCh37 (hg19) build] using Burrows-Wheeler Aligner (BWA). Base recalibration and de-duping were performed as standard QC measures, followed by quality control following the Picard pipeline ([www.gatk.co.uk](http://www.gatk.co.uk)) to produce variant-ready BAM files. Variants were called using the

Genome Analysis Toolkit (GATK) ([www.gatk.co.uk](http://www.gatk.co.uk)), creating variant calling files (VCFs). Additional QC measures were employed, considering variants  $\geq 10$  reads and genotyping quality  $\geq 30$ . Variant annotation used a custom hail pipeline and annotated variants with gnomad and dbNSFP.

#### 2.6.4.2 SNP Arrays

SNP array genotyping was kindly carried out by Alexandra Evans in Cardiff University's Medical Research Centre (MRC), Hadyr Ellis Building. Genomic DNA was extracted using QIAamp DNA Mini Kit (see section 2.4.2.1) and 20 $\mu$ L at 80ng/ $\mu$ L provided for genotyping. Samples were genotyped on the Infinium PsychArray-24 Kit (Illumina) or the Infinium Global Screening Array-24 (Illumina) and scanned using the iScan System (Illumina). Data were exported from Genome Studio and analysed using PennCNV.

#### 2.7 Statistical analysis

All statistical analysis was carried out using SPSS versions 25 and 26. All data are expressed as mean  $\pm$  standard deviation. Multiple groups were analysed using one-way ANOVAs with post-hoc Tukey tests. Comparisons between two or more groups with more than one condition were analysed by using two-way ANOVAs with post-hoc Tukey tests. For screening assays such as the cytokine arrays and for multiple qPCR measures, statistical significance was determined using an error probability level of  $p < 0.05$  corrected by a false discovery rate (FDR) analysis (Benjamini Hochberg method).

### 3 Creation and validation of isogenic *APOE* lines

Sporadic Alzheimer's disease (SAD) is caused by a complex interaction of environmental and genetic factors. Around 50 genetic variants have been demonstrated to increase the risk of developing SAD. Of these, *APOE*, the gene first associated with the condition, remains the strongest genetic risk factor.

A perennial problem with understanding diseases of the CNS is the availability of suitable cellular models. Although transgenic animal models have provided invaluable insights into the pathophysiology of SAD, many of the findings have failed to translate into human systems. The use of human embryonic stem cells (hESC) or patient-derived induced pluripotent stem cells (iPSCs) has become an attractive alternative to the generation of animal models. However, because of the genetic variability between individuals, experiments need to include several clonal lines from different patients in order to produce reliable results. A potential solution to this problem is to work with genetically modified cells (either iPSCs or hESCs) and their parental isogenic line. This means, theoretically, that the genetic background of the cell lines is identical save for the edited gene and thus any observed differences in cellular phenotype are attributable to the gene of interest.

This chapter describes the creation of a cellular model using the CRISPR-Cas9 system to edit the human embryonic stem cell line (hESC7) at the *APOE* locus to create and validate isogenic stem cells with E3/E4 and E4/E4 genotypes.

### 3.1 Creation of isogenic lines

#### 3.1.1 Creation of the CRISPR/Cas9 targeting plasmid

Initially, a single, wild-type nickase plasmid (pSpCas9n(BB)-2A-GFP (PX458) Addgene.org (Addgene plasmids #48138) which makes a double-stranded DNA cut was used for transfections (full methods described in Chapter 2.6.2). The px458 plasmid contained a 2A-GFP fused to Cas9 to allow screening of transfected cells.

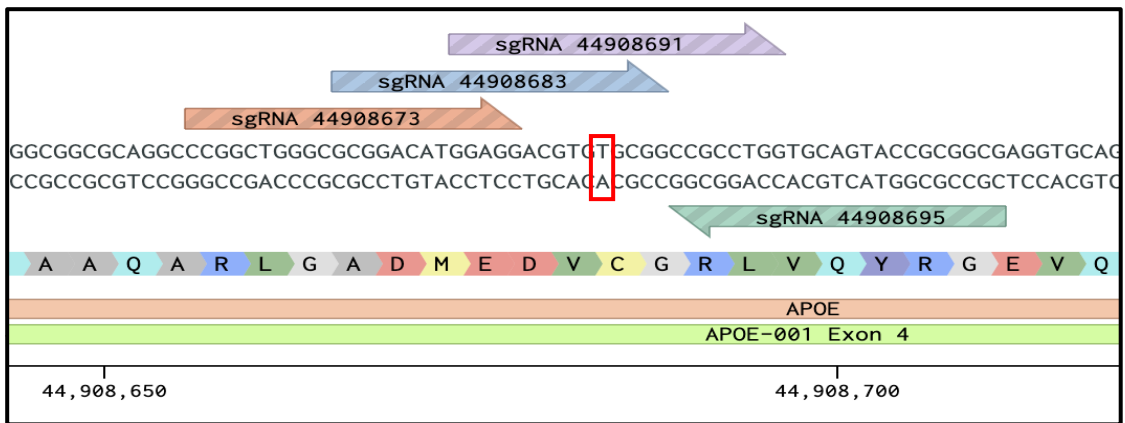
#### 3.1.2 Guide RNA selection and testing

There are several websites for generating sgRNAs for gene editing experiments. The algorithms used vary but are based on maximising on-target efficiency while minimising off-target effects. Benchling.com was used to generate sgRNAs for use with the px458 plasmid as it was one of the few sites at the time to give both on and off target scores based on their sensitivity<sup>315</sup> and specificity<sup>313</sup>. The selected sgRNAs with on and off target scores are shown in Table 3.1; Figure 3.1 shows their position in relation to the rs429358 SNP of *APOE*.

**Table 3.1: on and off target scores for selected sgRNAs.**

Guide	Sequence	On-target score % (Doench 2016)	Off-target score % (Hsu 2013)
sgRNA114 (44908673)	CCGGCTGGGCGCGGACATGG <b>AGG</b>	60.2	69.9
sgRNA124 (44908683)	GCGGACATGGAGGACGTGtG <b>CGG</b>	62.0	81.4
sgRNA132 (44908691)	GGAGGACGTGtGCGGCCGCC <b>TGG</b>	40.8	69.4
sgRNA-136 (44908695)	<b>GGC</b> CGCCGCGGTACTGCACCAGG	69.4	83.8

**Figure 3.1: sgRNAs used with the px458 plasmid.**



Positions of the sgRNAs used for editing at the APOE locus; the rs429358 SNP is denoted by the red box.

Experiments to optimise transfection conditions with the Amaxa 4D nucleofactor were undertaken. Results demonstrated two efficacious sgRNAs (sgRNA 44908683 and sgRNA 44908695) evidenced by the presence of GFP positive cells. However, transfection efficiency and cell survival were low so a new system was adopted.

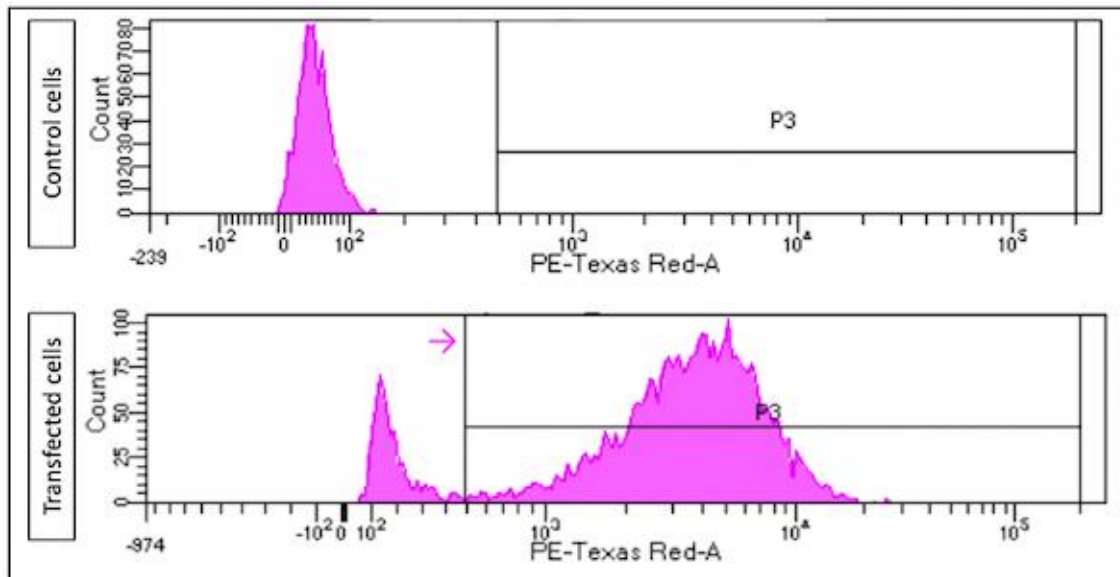
### 3.1.4 Results of transfections with RNP using the IDT Alt-R system

As described in Chapter 2, the initial stage of transfections with RNP using the Integrated DNA technologies (IDT) Alt-R system the four guide RNAs described above (without a repair template) in order to test their relative efficiencies. At the point at which transfections were undertaken, IDT had recently introduced a tracrRNA with an Atto550 fluorophore; use of this product was adopted in order to help with screening. Cells were transfected and after 24 hours underwent selection with FACS (methods described in Chapter 2.6.3). The results are shown in table 3.2 and figure 3.2.

**Table 3.2: FACS results using different sgRNAs.**

Guide	% single cells	% single cells positive for Atto550	Mean fluorescence	Median fluorescence
sgRNA 44908673	77.9	75.3	6.203	4.290
sgRNA 44908683	82.4	99.4	9.240	6.237
sgRNA 44908691	65.3	85.5	7.795	6.082
sgRNA 44908695	75.0	84.9	9.900	5.047

**Figure 3.2: FACS of control & sgRNA 44908683 transfected cells.**

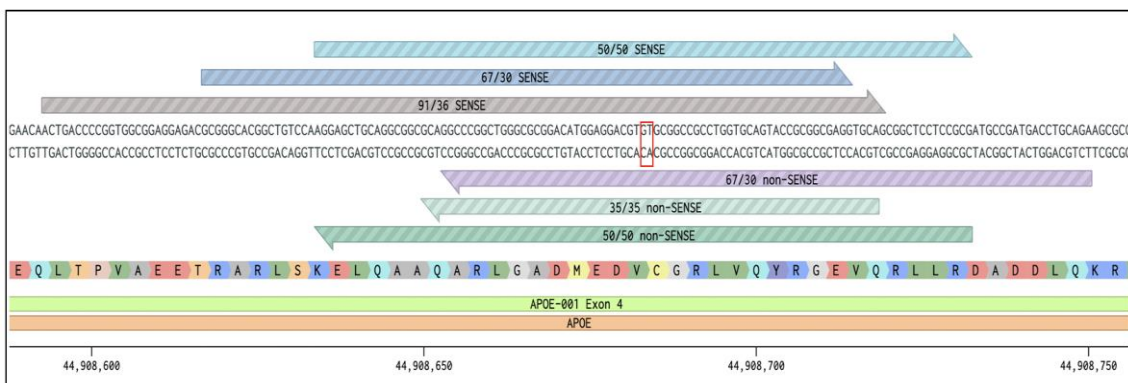


The figure shows the levels of fluorescence in un-transfected control cells (top) and cells transfected with a tracrRNA with an Atto550 fluorophore (bottom). The arrow shows the 'gate' ie. only cells exceeding this level of fluorescence were selected for onward plating.

### 3.1.5 Creation and testing of repair templates

On the basis of the results of FACS sorting, sgRNA 44908683 was selected. Single stranded DNA oligonucleotides (ssODNs) to facilitate homology directed repair (HDR) were designed around this guide using paradigms set out in recently published papers<sup>316–318</sup>; the characteristics of these can be summarised as size, strand and symmetry. The distribution of the six different oligonucleotides tested are summarised in Figure 3.3.

**Figure 3.3: six ssODN repair templates tested.**



The location of each of the six ssODN repair templates tested in relation to the rs429358 edit site denoted by the red box.

### 3.1.5.1 Silent mutations

As part of the editing process, it is recommended that silent mutations are introduced into the repair template to minimise post-edit re-cutting<sup>319</sup>. Four mutations were introduced: one within the protospacer adjacent motif (PAM) and three elsewhere in the guide RNA. Silent mutations were chosen to maintain a codon adaptation index (CAI) as close to the original value as possible (see Table 3.3). As described in Chapter 2.6.3, three silent mutations in addition to the intended mutation allowed a novel method for detection of edited cells. The final sequences of the six templates used including mutations (shown in red) are shown in Table 3.3.

**Table 3.3: silent mutation sites with their attendant codon adaptation indices (CAI).**

Amino acid coded	A	D	M	E	D	V	C/R	G
Wildtype	GCG 0.11	GAC 0.54	ATG 1.00	GAG 0.58	GAC 0.54	GTG 0.46	tGC	GGC 0.34
Silent mutations	GCA 0.23	GAT 0.46		GAA 0.42	GAT 0.46	GTC 0.24	tGT 0.08	GGA 0.25
Final (E3→E4)	GCG	GAT	ATG	GAA	GAC	GTG	cGT	GGC
Final (E4→E3)	GCG	GAT	ATG	GAA	GAC	GTG	tGT	GGC

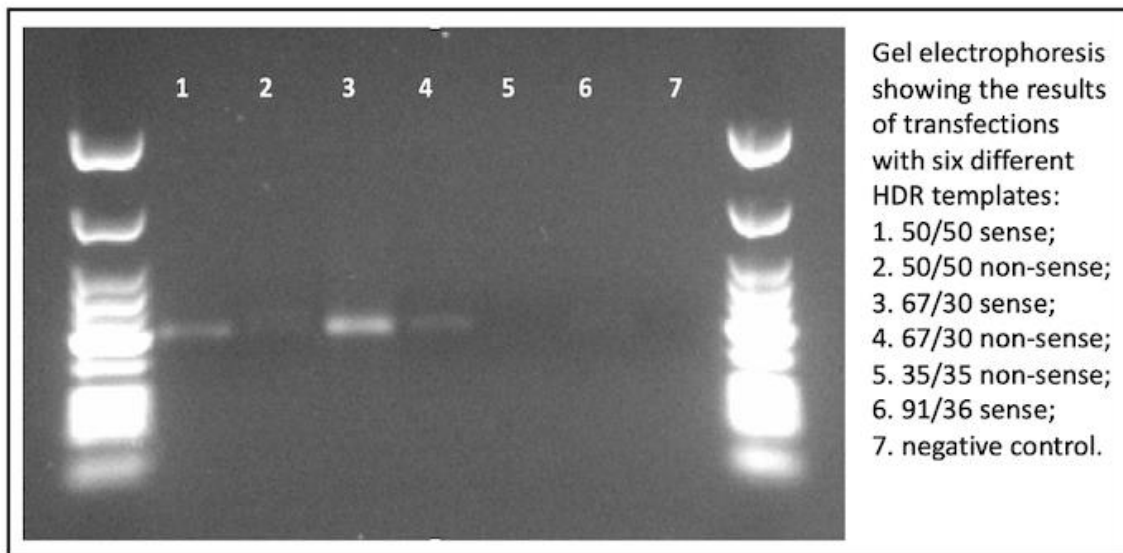
**Table 3.4: sequences of the 6 ssODN repair templates tested.**

Name	Sequence 5' to 3'
50/50 sense	AGGAGCTGCAGGCGGCGCAGGCCCGGCTGGGC <b>GCGGATATGGAAGACGTGcGTGG</b> CCGCCTGGT GCAGTACCGCGGCGAGGTGCAGGCCATGCTCGGCC
50/50 non-sense	GGCCGAGCATGGCCTGCACCTCGCCGCGGTA <b>CTGCACCAGGCGGCCACgCACGTCTCCATATCCGC</b> GCCAGCCGGGCTGCGCCGCTGCAGCTCCT
67/30 sense	GCGGGCACGGCTGTCCAAGGAGCTGCAGGCGGCGCAGGCCCGGCTGGGC <b>GCGGATATG</b> <b>GAAGACGTGcGTGG</b> CCGCCTGGTGCAGTACCGCGGCGAGG
67/30 non-sense	TCTGCAGGTCATCGGCATCGCGGAGGAGCCGCTGCACCTCGCCGCGGTA <b>CTGCACCAGGCGGCCAC</b> <b>gCACGTCTCCATATCCGC</b> GCCCAGCCGGGCC
35/35 non-sense	TGCACCTCGCCGCGGTA <b>CTGCACCAGGCGGCCACgCACGTCTCCATATCCGC</b> GCCCAGCCGGGCT GC
91/36 sense	ACTGACCCCGGTGGCGGAGGAGACGCGGGCACGGCTGTCCAAGGAGCTGCAGGCGGCGCAGGCC CGGCTGGGC <b>GCGGATATGGAAGACGTGcGTGG</b> CCGCCTGGTGCAGTACCGCGGCGAGGTGCAG

### 3.1.5.2 Results demonstrating the efficacy of different repair template designs.

After transfection and FACS sorting, cells were plated. They were harvested on day 3 and DNA extracted. PCR primers were designed to amplify DNA with the edited sequence; the reverse primer contained the edited nucleotide plus the 3 silent mutations noted above. Figure 3.6 shows a gel electrophoresis representing each of the six different ssODN templates plus a negative control in lane 7 using unedited DNA. As demonstrated by the band intensity, the efficacy of templates 1 and 3 were demonstrated; these were 50/50 sense and 67/30 sense (ie 67 nucleotides on the 5' side of the PAM sequence and 30 nucleotides on the 3' side of the PAM sequence) .

**Figure 3.4: results of transfections with six different ssODNs.**

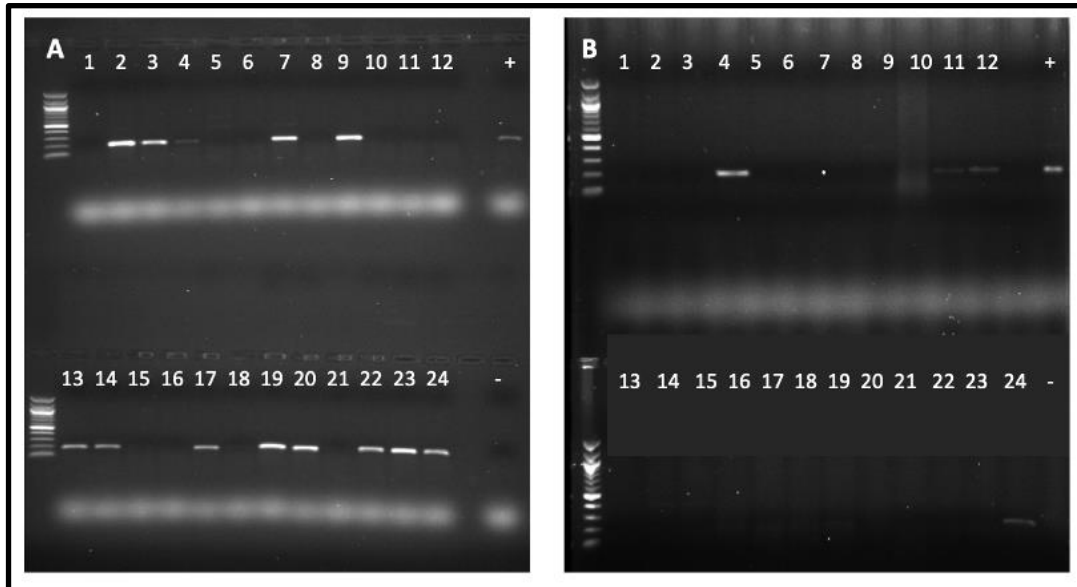


### 3.1.6 Enrichment of the edited population with FACS sorting

As table 3.2 shows, successful uptake of the various sgRNAs without the use of ssODNs was high. The electrophoresis gels in Figure 3.5 show the proportion of clones including the HDR repair ssODN in sorted and unsorted samples. In unsorted cells, the number of clones including the HDR repair was approximately 15% whereas in sorted cells the figure was approximately 55%; results which were replicated in subsequent transfections. This suggests unedited cells proliferate at a higher rate than edited cells

thus decreasing the proportion of edited cells over time and demonstrates the utility of FACS for enriching edited populations.

**Figure 3.5: number of edited clones in sorted and unsorted samples**



Results of gel electrophoresis from DNA extracted from clones (lanes 1-24) from FACS sorted samples (A) & unsorted (B) with 100bp DNA ladder. Positive & negative control lanes are also shown. A 193NT band is seen in DNA samples which had incorporated the HDR template. 13 of 24 clones picked from sorted cells contained the HDR template (54%). For unsorted samples, 4/24 contained the HDR template (17%).

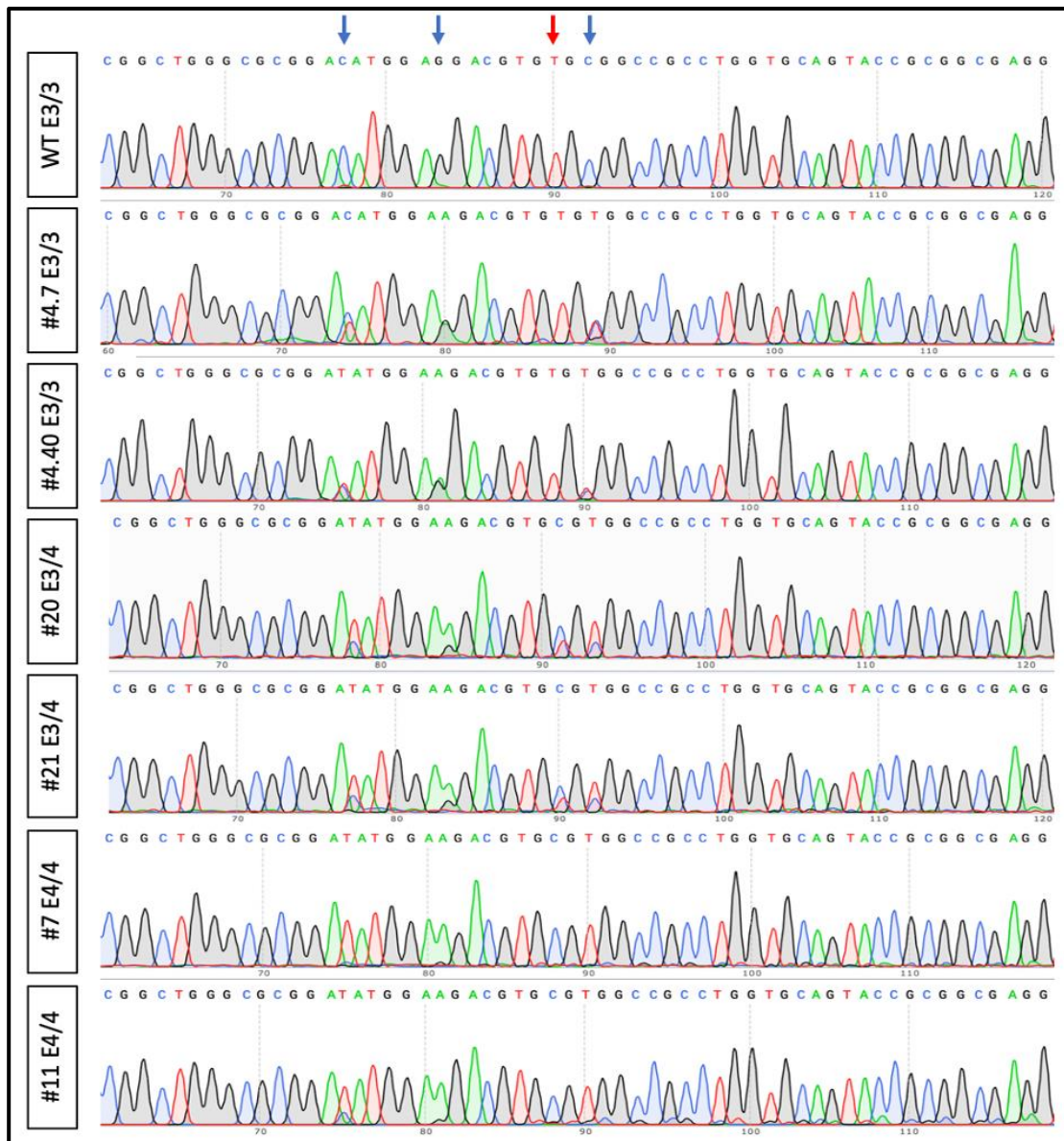
### 3.1.7 Results of Sanger sequencing of clones

Sanger sequencing to verify the results of the PCR screening and to determine the exact nucleotide sequence of the targeted locus was undertaken by GATC Biotech's LIGHTrun™ Sequencing service as described in Chapter 2.4.6. Although incorporation of the HDR template occurred on one allele in around 50% of clones, this was often accompanied by a single nucleotide insertion. A single nucleotide insertion at the site of the DNA break was also the most common overall editing event. So, despite a high editing efficiency, the majority of clones were unusable as they contained the edited sequence on one allele with an insertion on the other. After screening approximately 100 clones two heterozygotes were found with the HDR template on one allele and which remained unedited (wild-type) on the other allele. No homozygote clones were found which necessitated a further round of transfection. After this, two homozygote

clones were identified after screening of a further 48 clones. This gave two heterozygote (E3/E4) and two homozygote (E4/E4) clones.

In addition to the E3/E4 (#20 E3/E4 and #21 E3/E4) and E4/E4 lines (#7 E4/E4 and #11 E4/E4), a control line was created with the three silent mutations but without the T to C change at the *APOE* locus (#A4.7 E3/E3 and #A4.40 E3/E3) to ensure that silent mutations were truly silent and did not affect the phenotype of isogenic lines. Transfected WT cells unedited at the *APOE* locus were also retained as controls.

**Figure 3.6 Sanger sequencing of edited clones.**



The T→C edit at rs429358 is denoted by the red arrow; this causes a change at aa112 from cysteine to arginine (E3→E4). Silent mutations are denoted by the blue arrows.

## 3.2 Validation of isogenic lines

Once clones had been isolated they underwent SNP arrays to verify that karyotype remained constant and exome sequencing to identify off-target effects. Detailed methods are described in Chapter 2.6.4.

### 3.2.1 Karyotyping

Karyotyping was carried out using the Illumina Global Screening Array v2.0 and data analysed alongside approximately 500 additional samples using PennCNV with GRCh38/hg38 as reference genome. CNVs >100kb and spanning >10 SNPs met criteria for inclusion; they were subsequently confirmed by visual inspection of the LRR/BAF traces.

All isogenic and wild-type lines were karyotypically normal. There were, however, three CNVs identified which met standards for inclusion however these were present in both WT and isogenic lines. Wild-type lines also underwent karyotyping as stem cells, once differentiated to neural progenitor cells and once differentiated to astrocytes; a total differentiation period of 12 weeks. Karyotype and CNVs remained constant over this period.

### 3.2.2 Exome sequencing

Exome sequencing of the wild-type and isogenic lines was undertaken using the methods outlined in Chapter 2.6.4. As noted in Chapter 1, the current orthodoxy for identifying off-targets is to perform exome sequencing on isogenic clones produced by CRISPR then to interrogate the off-target sites predicted by computational design tools. Exomic off-targets were generated using Benchling.com, the website used to identify suitable sgRNAs. It identified five genes (SLC45A1, MUM1, LIMCH1, SMPD1 and an un-named genetic region) which would be susceptible to off-target effects;

upon interrogation of the exome sequencing no changes were identified at any of these sites.

More recently, machine-learning-based predictive modelling approaches have been used to identify potential off-targets and have outperformed competing methods by a substantial margin<sup>320</sup>. Using the search engine described in that paper ([www.crispr.ml](http://www.crispr.ml)), a list of 1,236 potential off-targets in genetic regions was generated. Interrogation of this list found changes at 8 sites in isogenic lines when compared to the hg19/GRCh37 reference genome (Table 3.5). Of these, four were intron variants, one an inframe deletion, one a non-coding transcript exon variant and one a synonymous variant so would be unlikely to have effects on the phenotype of the isogenic lines. The remaining edit was frameshift variant in GOLGA6L2, a gene whose expression is restricted to the testis so it is unlikely that this would have an effect on the phenotype of neuronal or glial cells. Furthermore, this edit was present on both WT and isogenic lines so is more likely to be a an-built mutation rather than one that can be attributed to the gene editing process.

**Table 3.5 changes at off-target sites identified by exome sequencing.**

Gene	Identifier	Chromosome	Nature of edit
CBLB	ENSG00000114423	3	intron variant
FMN2	ENSG00000155816	1	inframe deletion
GOLGA6L2	ENSG00000174450	15	frameshift variant
PARK2	ENSG00000185345	6	intron variant
SLC14A2	ENSG00000132874	18	intron variant
TTC38	ENSG00000075234	22	intron variant
WDR61	ENSG00000140395	15	non-coding transcript exon variant
WIPF3	ENSG00000122574	7	synonymous variant

### 3.3 Basic characterisation of isogenic lines

Characterisation of isogenic lines for pluripotency is essential to ensure a uniform starting point before differentiation is undertaken. Assays were guided by the StemBANCC workflow ([www.stembancc.org](http://www.stembancc.org)) and included immunocytochemical staining for hPSC markers and gene expression profiling.

In order to ensure that the transfection process did not affect the pluripotency of the isogenic lines and their ability to differentiate, the WT E3/3 line, one of the E3/3 lines containing silent mutations (#4.7), one of the E3/4 heterozygote lines (#21) and one of the homozygote lines (#7) were differentiated into neuronal progenitor cells (NPCs).

#### 3.3.1 Assessment of pluripotency of stem cells

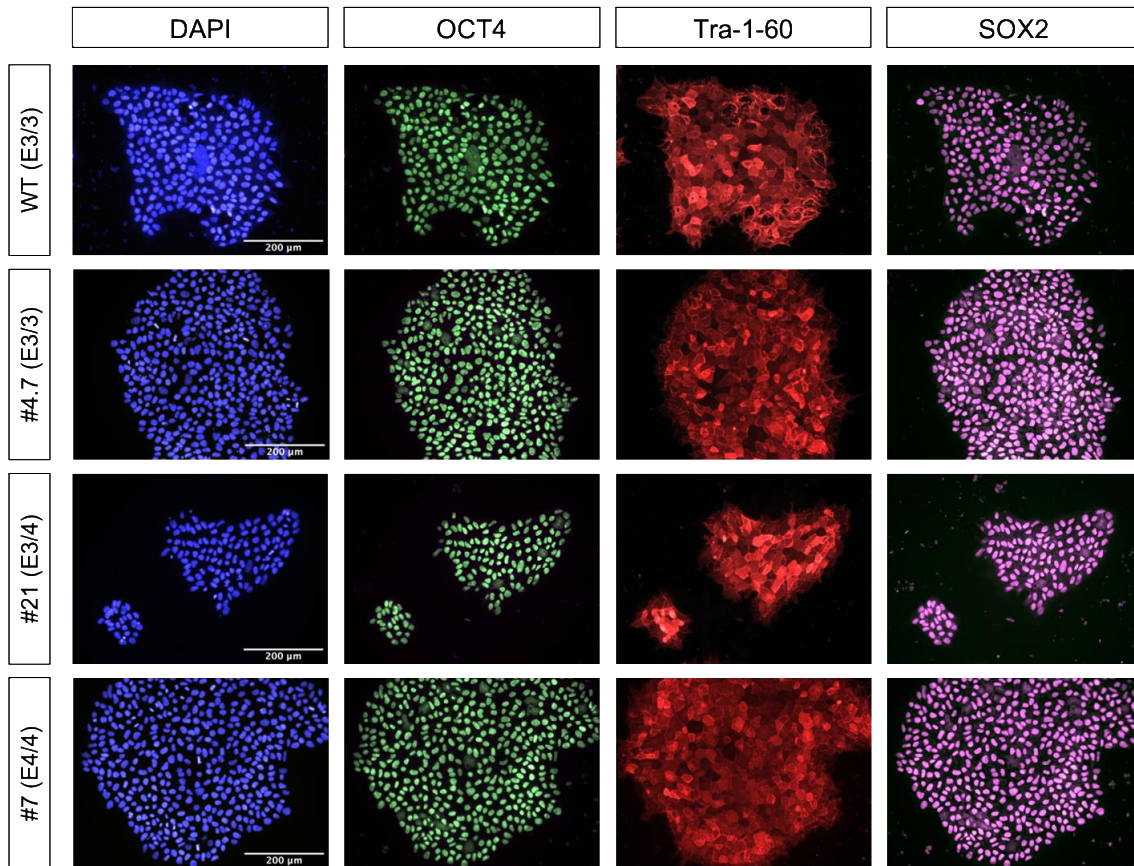
Prior to the start of differentiation, RNA was collected and stem cells were fixed and stained for pluripotency markers. Gross morphology of hESC colonies showed a characteristic high nuclear to cytoplasmic ratio and smooth borders with no obvious differences between parent and isogenic lines.

Standard markers to confirm pluripotency include intracellular transcription factors OCT4, SOX2 and Nanog plus the extracellular membrane glycosphingolipid stage specific embryonic antigen 4 (SSEA-4) and the cell-surface Tra-1-60 antigen. All of these markers are known to be expressed in hPSCs but are lost upon differentiation<sup>321-323</sup>. Owing to the availability of antibodies, OCT4, SOX2 and Tra-1-60 were selected for immunocytochemistry while OCT4, SOX2 and Nanog were measured with qPCR.

Figure 3.7 shows the results of stem cell staining with OCT4, SOX2 and Tra-1-60. Quantification of cells expressing OCT4 and SOX2 (as a percentage of those stained for DAPI) was undertaken using Image J with data obtained from two separate platings. Expression of both OCT4 and SOX2 was >99% for all lines and showed uniform expression within colonies. As a membranous marker, it was not possible to quantify

Tra-1-60 however it demonstrated widespread cell surface expression in all colonies with some typical cell-to-cell variation.

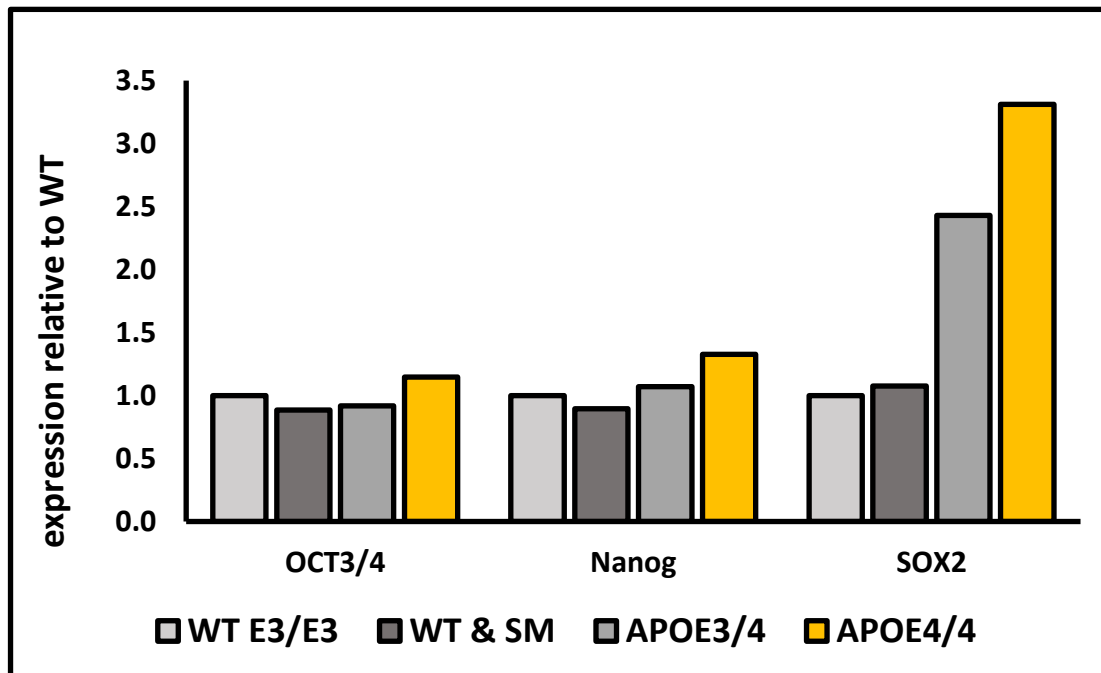
**Figure 3.7: immunofluorescence in edited stem cells and wild-type (WT) controls.**



Immunofluorescence for OCT4 (green), Tra-1-60 (red) and SOX2 (magenta) in wild-type (WT) and edited cell lines: #4.7 (E3/3 but containing silent mutations); Clone 21 (E3/4); and Clone 3.7 (E4/4) . All nuclei were counterstained with DAPI (blue).

Quantitative qPCR for measurement of gene expression in stem cells was undertaken for the markers OCT4, Nanog and SOX2; see Figure 3.10. Although the expression of OCT4 and nanog was similar between wild-type and isogenic lines, the expression of SOX2 was increased in isogenic cell lines in a dose-dependent manner; there was not, however, any difference between the wild-type cell line and the line containing silent mutations. When this was checked in the other isogenic clones, similar results were found.

**Figure 3.8: qPCR of stem cell markers in wild-type (WT) cells and isogenic lines.**



Quantitative qPCR for measurement of gene expression in stem cells was undertaken for the key pluripotency markers OCT4, Nanog and SOX2. Results are normalised to those in WT E3/E3 cells. Error bars are not shown as data were obtained from a single qPCR experiment.

Collectively, the positive expression of these proteins confirmed the pluripotent state of the wild-type and isogenic stem cells. Possible reasons for, and consequences of, the differential expression of SOX2 are discussed below.

### 3.3.2 Differentiation to neural progenitor cells (NPCs)

Having established the pluripotency of isogenic lines, cells were differentiated to NPCs using the method described in Chapter 2. During the process of differentiation, cells were fixed for staining and RNA extracted on Day 24, the day on which they were frozen as NPCs. All wild-type and isogenic lines showed expression of the NPC markers nestin, PAX6, OTX2 and FOXG1. Quantification of cells expressing the nuclear stains PAX6, FOXG1 and OTX2 as a percentage of the total expressing DAPI was undertaken to ensure that progression to the NPC stage was comparable in WT and isogenic lines. Immunofluorescent images are shown in figures 3.9 and 3.10 and the percentage of positive cells of each genotype in figure 3.11.

**Fig 3.9: nestin & PAX6 in Day 24 NPCs.**

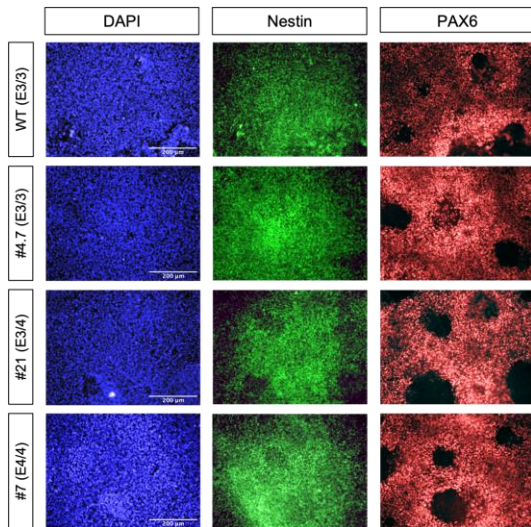


**Fig 3.10: FOXG1 & OTX2 in Day 24 NPCs.**

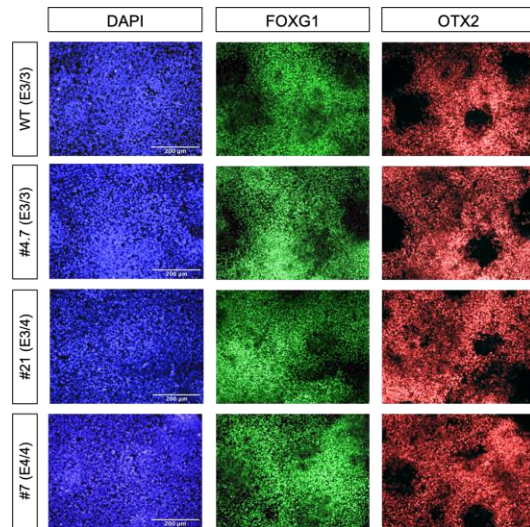
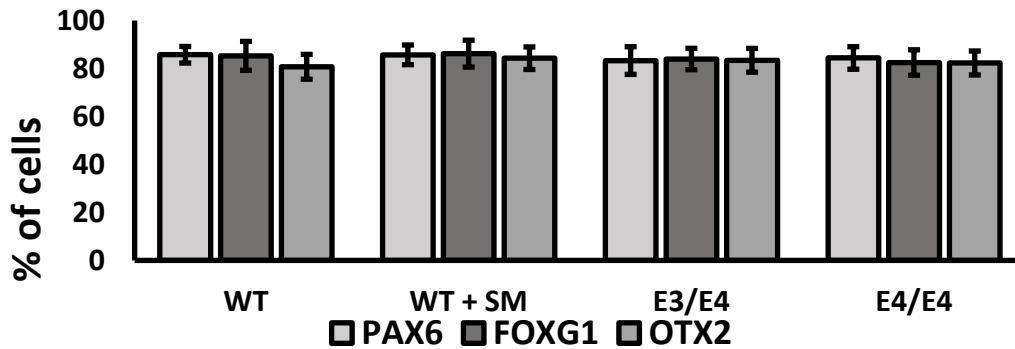


**Figure 3.11: cells positive for NPC markers as a % of DAPI.**



Quantification of cells expressing the nuclear NPC markers PAX6, FOXG1 and OTX2 (as a percentage of those stained for DAPI). Data were obtained from two distinct differentiations (starting stem cells from two different vials and differentiated on separate culture plates). For each differentiation, at least 3 images were obtained from a minimum of three separate wells

Virtually all cells in WT and edited isogenic lines were positive for nestin, an intermediate filament widely expressed by proliferating cells of the developing CNS<sup>324</sup>. Approximately 80% of cells were also positive for three key transcription factors; PAX6 expressed by dorsal forebrain progenitors and OTX2 and FOXG1 expressed by all forebrain cells<sup>325</sup> with no significant differences between WT and edited isogenic lines. Although there were no significant differences in the number of cells expressing each of the NPC markers, RT-qPCR data showed expression levels of some markers did vary across lines however the differences were in line with typical variations<sup>326</sup>. Fold increases of approximately 200 in PAX6 and of 4-5 in nestin when compared to stem cells were observed which is in line with published data on the hESC7 cell line<sup>327</sup>.

OCT3/4 levels reduced approximately 200-fold from stem cells to D24 NPCs which again is in line with published data.

### 3.4 Discussion

The human embryonic stem cell line (hESC7) underwent gene editing at the *APOE* locus using CRISPR-Cas9 to create stem cells with E3/E4 and E4/E4 genotypes.

#### 3.4.1 Gene editing constructs

While a traditional plasmid-based approach was used initially, and enabled the identification of two efficacious sgRNAs, this was superseded by a ribonucleoprotein based system which demonstrated greater editing efficiency and reduced cell toxicity promoting improved cell survival post-transfection.

The two effective guide RNAs were those with the highest on-target scores with cut-sites very close to the edit sites (1 and 3 bp). The key factor for on-target scores is proximity of the double-stranded break to the desired edit site; efficiency decreases dramatically when the cut site is >30bp from the proximal ends of the repair template<sup>316</sup>. Other features which improve editing efficiency are a cytosine at the variable nucleotide of the PAM, having moderate GC frequency with 10-12 bases optimum and sequence features including guanine at position 20 and cytosine at position 7<sup>315,320</sup>. Despite these algorithms, one of the largest studies of sgRNA efficacy undertaken by the Sanger Institute found that there was only a weak correlation of such predictions to the actual activity of a guide and that around 20–25% of guides generated were unusable due to low activity<sup>319</sup>.

With respect to the repair oligonucleotides used to facilitate HDR, by far the most effective guides were a symmetrical 100bp template with 50bp either side of the cut-site and an asymmetric 97bp template with 67bp on the 3' side and 30bp on the 5'

side. Both of these shared homology with the sense strand which was the one targeted by the sgRNA.

The Zhang laboratory, who pioneered gene editing using the CRISPR-Cas9 system, have typically recommended around 100-150bp total homology using ssODNs; they also suggested that the mutation is introduced in the middle, giving 50-75bp homology arms<sup>301</sup>. A number of papers have suggested other designs; in one paper optimal HDR efficiency of 1.5% was achieved using a 70bp ssODN complementary to the gRNA<sup>316</sup>. Others have suggested an asymmetric donor DNA optimised for annealing by overlapping the Cas9 cut site with 36bp on the PAM-distal side, and with a 91bp extension on the PAM-proximal side of the break; they observed that this supported a vastly superior HDR frequency of 57%<sup>317</sup>. Another paper suggest asymmetric ssODNs with 67bp on the 3' side and 30bp on the 5' side<sup>318</sup>.

Richardson and colleagues found that dissociation of Cas9 from double-stranded DNA (dsDNA) substrates is slow (lifetime ~6 h) and that before complete dissociation occurs, Cas9 asymmetrically releases the 3' end of the cleaved DNA strand that is 'not complementary to the sgRNA (nontarget strand)'<sup>317</sup>. They suggested that by using ssODNs 'complementary to the strand that is released first' (i.e. complementary to the nontarget strand) the rate of HDR in human cells was 2.6-fold greater. This finding contradicted work previously done by Ran and colleagues who found that efficiency was improved with 'oligonucleotides which were complementary to the sgRNA'<sup>316</sup>. Liang and colleagues, however, did not find any differences in varying the strand<sup>318</sup>. Again, one of the largest studies conducted by the Sanger Institute found that the design of the most efficient HDR templates was target dependent and appeared to be idiosyncratic with no rules to determine the best design; given this their recommendation was to revert to the original design of the Zhang laboratory, that is a 100bp oligos with 50bp of homology either side of the desired change<sup>319</sup>.

The same authors at the Sanger Institute also found that for point mutations that are very close (+/-5 bp) to the CRISPR cut site, the strand of the ssODN HDR template is immaterial. However, for mutations that are further away (5–20bp), there is a

significant difference between the two strands of ssODN. A simple rule is that if the mutation to be introduced is downstream of the CRISPR cut site, the antisense template ssODN (i.e. the one that binds to the top strand) should be used. Similarly, if the mutation is upstream of the CRISPR cut site, the sense ssODN should be used. This is irrespective of the strand to which the guide binds<sup>319</sup>.

#### 3.4.2 Verification of karyotype and off-target effects

Off-target effects are induced mutations at sites other than the intended genomic target site. There is no consensus on the extent to which off-target effects are a significant problem. Some argue that the mutation frequency for CRISPR using a well-designed guide RNA and nuclease falls below the background mutation frequency that occurs spontaneously. Others, however, contest that it is a significant issue and that current methods for identifying off-target changes are inadequate and more rigorous approaches should be utilised especially given new clinical applications of the technology.

The current orthodoxy for identifying off-targets is to perform whole-genome or exome sequencing on clones produced by CRISPR then to interrogate the off-target sites predicted using computational design tools such as MIT CRISPR and E-Crisp. These tools identify potential off-target sites based on 'rules' about mismatch number and position however it has been shown that unintended indels can occur at off-target cleavage sites that differ by as many as five positions within the protospacer or and even where sequences harbour alternative PAM sequences<sup>328</sup>.

Several techniques have been developed to quantify off-target effects, such as GUIDE-seq<sup>328</sup>, CIRCLE-Seq<sup>329</sup> and BLISS<sup>330</sup> however scaling these assays to all gRNAs genome wide is not feasible for most laboratories owing to prohibitive monetary and time costs. The GUIDE-Seq method identifies DSBs by integration of a blunt, double-stranded oligodeoxynucleotide (dsODN) at the break site. Integration sites are then precisely mapped at the nucleotide level using unbiased amplification and next-

generation sequencing thus identifying the actual positions of DSB rather than those predicted.

Direct physical detection of off-target sites through techniques like GUIDE-Seq have demonstrated the limitations of prediction algorithms. In a direct comparison of computational design tools and the GUIDE-Seq method, using nine RNA-guided nucleases (RGNs) the authors discovered that neither program identified the vast majority of off-target sites found by GUIDE-seq. Both programs substantially overestimated the number of off-target sites but also failed to identify actual off-target sites: MIT identified 41.9% of sites correctly and E-Crisp 25.8% correctly<sup>328</sup>.

As noted above, new machine-learning-based predictive modelling approaches have outperformed competing methods by a substantial margin and do not require the significant resource requirements of physical approaches such as GUIDE-Seq<sup>320</sup>. Utilising this method generated over 1200 potential off-targets in genetic regions whereas conventional methods tended to generate between 5 and 10. Analysis of these sites showed only one potential off-site target in a coding region. This was a frameshift variant in *GOLGA6L2*, a gene whose expression is restricted to the testis so it is unlikely that this would have an effect on the phenotype of neuronal or glial cells. Furthermore, this edit was present on both WT and isogenic lines so is more likely to be an in-built mutation rather than one that can be attributed to the gene editing process.

Karyotyping was also undertaken to ensure that no abnormalities emerged during the editing and differentiation processes. Although no new karyotypic abnormalities or CNVs emerged, wild-type cells did contain three CNVs which are likely to have occurred from repeated passages of these lines. As these were present across isogenic lines they are unlikely to have any effects on the phenotypes seen but do highlight the need to regularly assess cell lines for the accumulation of mutations and to, wherever possible, start with a 'clean' cell line of low passage number.

### 3.4.3 Pluripotency and differentiation

Assessment of the pluripotent state of cells was undertaken with immunofluorescent staining and RT-qPCR for pluripotency markers. Using immunocytochemistry, over 99% of cells were shown to express the stem cell markers OCT4 and SOX2. Expression of pluripotency markers was confirmed with qPCR which showed levels of OCT4 and nanog were equivalent across wild-type and isogenic lines however SOX2 expression was increased in APOE isogenic lines in a dose-dependent manner; two-fold in E3/E4 cells and threefold in E4/E4. When differentiated to NPCs, over 80% of cells expressed the pluripotency markers PAX6, FOXG1 and OTX2 while the increases in PAX6 and nestin and decreases in OCT3/4 were across wild-type and isogenic lines were in line with expectations.

In addition to being a marker of stem cell pluripotency, SOX2 is also proposed to be a neuroectodermal lineage specifier; knockdown of SOX2 has been shown to induce differentiation to endoderm-like cells, whereas overexpression of SOX2 promotes neural differentiation<sup>331</sup>. As such, it could be argued that the higher expression of SOX2 in APOE4 isogenic lines simply demonstrates that they are more differentiated than their APOE3 counterparts. However the gross morphology of the stem cells of isogenic lines was identical to wild-type lines, maintaining the high nuclear to cytoplasm ratio and smooth edges characteristic of stem cell colonies. Furthermore, the expression of other NPC markers including PAX6 and nestin was not increased suggesting that the effect was peculiar to SOX2. Interestingly, SOX2 is a marker of endogenous NPCs in the adult nervous system which are self-renewing multipotent progenitors that give rise to neurons, astrocytes and oligodendrocytes<sup>332,333</sup>. They are restricted to only a few sites within the CNS notably including the dentate gyrus of the hippocampus. The precise role of these cells is unknown but declining hippocampal neurogenesis has been speculated to play a part in ageing and cognitive dysfunction<sup>284</sup>. Given this role of SOX2, and its possible link to cognitive status, further exploration of this possible *APOE*-related phenotype may warrant further exploration.

#### 3.4.4 Summary

This chapter describes the creation of a cellular model by using the CRISPR-Cas9 system to edit the human embryonic stem cell line (hESC7) at the *APOE* locus using to create isogenic stem cells with E3/E4 and E4/E4 genotypes. Subsequent chapters describe the use of this model to investigate astrocytic phenotypes associated with the different *APOE* genotypes.

## 4 Astrocytic differentiation and validation

Interest in the role of astrocytes in Alzheimer's disease has increased in recent years with GWAS identifying several risk genes that are expressed mainly, or exclusively, on astrocytes.

Methodological limitations have made the study of human astrocytes challenging; most of our knowledge of astrocyte physiology in health and disease is extrapolated from experiments in rodents. However, human astrocytes are far more complex and diverse, and their morphology is drastically different to murine and primate astrocytes<sup>334</sup>. They are also around 20 times larger than rodent astrocytes and contact up to 10-times the number of synapses<sup>335</sup>.

In Chapter 1, the various types of astrocytes found within the CNS were described including their morphological and functional heterogeneity. Thanks to RNA-sequencing studies, evidence now exists of human-specific morphological, transcriptional and functional profiles<sup>253,336</sup> highlighting the need for a robust and reproducible method for differentiating astrocytes from human stem cells.

### 4.1 Astrocyte differentiation

The first task was to establish such a method. Several protocols for the differentiation of hPSCs into astrocytes have been developed over the past 10 years, however, while the production of glutamatergic cortical neurons has become fairly standardised, the differentiation of astrocytes differs from protocol to protocol. Importantly, the precise cocktails of growth factors used to induce astrocytes can profoundly change their morphology, function and transcriptional profiles. Finding a combination that consistently produces prototypic astrocytes is therefore challenging but of great value.

#### 4.1.1 Signalling pathways and cytokines involved in astrogenesis

*In vivo*, neurogenesis precedes astrogenesis. The production of astrocytes relies on the inhibition of neurogenesis and the activation of astrogenesis which is known as the gliogenic switch<sup>337,338</sup>. A key element of this is Notch signalling which both inhibits neurogenesis and promotes astrogenesis by activating the JAK-STAT pathway, a key regulator of astrocytic development<sup>339</sup>.

Together with Notch, several cytokines secreted by differentiating neurons also converge on the JAK-STAT pathway including members of the IL-6 family, ciliary neurotrophic factor (CNTF) and leukaemia inhibitory factor (LIF)<sup>340</sup>. These molecules act through the heterodimerisation of the signal-transducing co-receptors LIFRb and gp130, which act upstream of the JAK-STAT pathway. Downstream, STAT3 is a direct transcriptional activator of the astrocytic genes, GFAP and S100 $\beta$ <sup>341</sup>. However, this is not the only mechanism by which STAT3 effects astrogenesis, it also interacts with the p300/CBP co-activator complex to initiate astrocyte gene expression<sup>342</sup>.

This latter effect is the same mechanism by which bone morphogenic proteins (BMP) cause astrogenesis. BMP signalling via downstream SMAD effector proteins synergises with the STAT3:p300/CBP pathway to activate gliogenesis through the formation of a larger Smad1:p300/CBP:STAT3 complex with the same effect of initiating astrocyte gene expression<sup>343</sup>. While both BMP and CNTF/LIF may activate astrogliogenesis through STAT3 synergistically, they are also capable of acting independently<sup>343</sup>.

However, STAT3 activation alone is not sufficient to induce astrogenesis. During early embryogenesis, chromatin modifications at gliogenic promoters prevent extrinsic signals from triggering astrocyte fate specification<sup>342</sup>. One of the key chromatin modifications is found at the GFAP promoter where methylation prevents its expression even when STAT3 is activated<sup>344</sup>. However, this is a transient methylation state; as development continues the Notch effector protein, NFIA, binds to the GFAP promoter and induces the dissociation of the DNA methylating enzyme, DNA

methyltransferase 1 (DNMT1)<sup>345</sup>. The lack of methylation then relaxes the chromatin state and allows the STAT3:p300/CBP complex to initiate transcription.

Although both BMPs and CNTF/LIF appear to exert their astrogenic effects via a common STAT3 pathway, they may produce phenotypically different astrocytes. When astrocytes differentiated with either BMPs or CNTF/LIF were compared, GFAP+ cells generated with LIF had a bipolar/tripolar morphology, remained in cell cycle, contained progenitor cell markers and demonstrated self-renewal with enhanced neurogenesis - characteristics typical of adult stem cells/astrocytes. By contrast, BMP-induced GFAP+ cells were stellate, exited the cell cycle, and lacked progenitor traits and self-renewal - characteristics typical of astrocytes in the non-neurogenic adult cortex<sup>346</sup>.

#### 4.1.2 Protocols for creating astrocytes from human stem cells

Knowledge of these pathways has informed the cocktail of growth factors and cytokines used to differentiate astrocytes from NPCs. While BMPs (typically BMP4 or BMP2), plus CNTF/LIF are the mainstays of most astrocyte differentiation protocols, other growth factors including epidermal growth factor (EGF), fibroblast growth factor 2 (FGF2), insulin plus varying quantities of FBS (from 2-10%) have all been used in recent publications<sup>256,347-353</sup>.

While early protocols tended to rely on the generation of astrocytes via embryoid bodies, the majority of newer protocols use monolayer methods. Most utilise the SMAD inhibition method described in Chapter 2 to produce neuronal progenitor cells (NPCs) however instead of inducing a neuronal fate, they are instead directed to produce astrocytes.

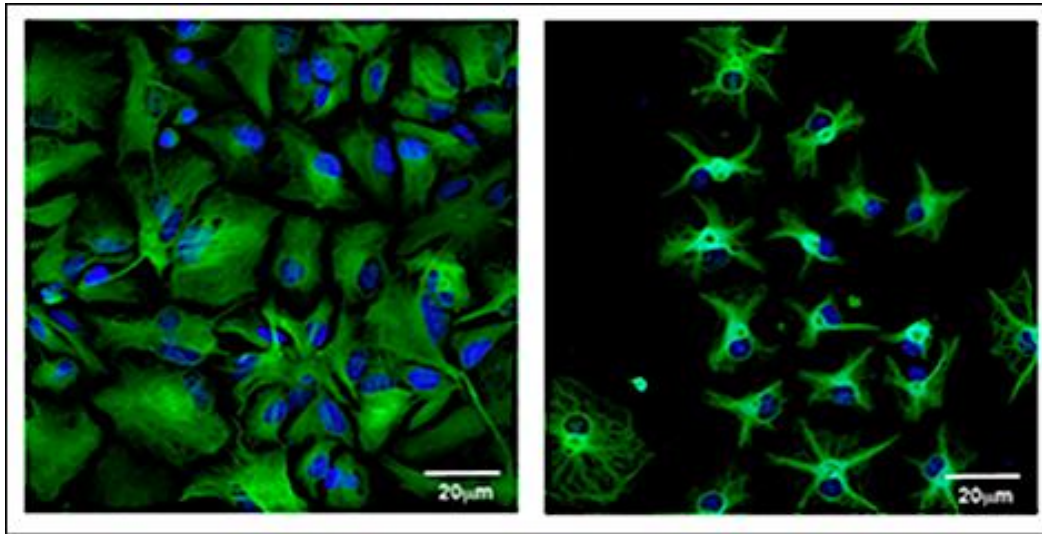
TCW and colleagues compared the efficiency of a number of different methods for astrocyte differentiation<sup>350</sup> using various combinations of growth factors. They found that the best results were obtained using two commercial astrocyte differentiation medias, ScienCell and Lonza, which yielded S100b and GFAP positive astrocyte-like

cells, with astrocyte morphology, within 10 days and stellate astrocyte morphologies within 30 days. Key features of this method are a low initial seeding density (nearly single cells: 15,000 cells/cm<sup>2</sup>) and minimal serum exposure (1%–2%).

The gene expression pattern in differentiated astrocytes was compared to the RNA-seq dataset of “proinflammatory” A1-type and “immunoregulatory” A2-type murine astrocytes induced, respectively, by treatment with LPS and middle cerebral artery occlusion, plus their saline and sham treated control<sup>253</sup>; due to the methods of induction, no comparable dataset exists for human astrocytes. They found that the gene expression of differentiated astrocytes best clustered with the control conditions suggesting that they are closer to quiescent rather than reactive astrocytes.

The results of TCW and colleagues echoed earlier findings which used transcriptomic analysis to characterise the gene expression activated during the differentiation of NPCs into astrocytes using FBS or a combination of CNTF and BMP4<sup>354</sup>. RT-qPCR carried out on astrocytes differentiated with FBS versus CNTF/BMP4 revealed differences in gene expression. Gene ontology analysis of FBS-astrocytes enriched genes showed a clear overrepresentation of genes involved in neurogenesis, neuronal differentiation and synapse formation suggesting the presence of neuronal cells among the differentiated cells. Expression profiles of FBS and CNTF/BMP4 differentiated astrocytes were also compared to those upregulated in reactive gliosis<sup>253</sup>; the authors found a statistically significant enrichment for reactive-astrocytes genes in FBS-astrocytes that was not present in CNTF/BMP4-astrocytes<sup>354</sup>. They also noted stark differences in the morphology of astrocytes treated with either FBS or CNTF/BMP4 with the latter exhibiting the more prototypic stellate morphology (see Figure 4.1). In summary, Magistri and colleagues<sup>354</sup> found that the combination of CNTF and BMP4 activates the JAK/STAT and SMAD signalling cascades, leading to the inhibition of oligodendrocytes lineage commitment and activation of astrocyte differentiation whereas FBS-derived astrocytes have properties of reactive astrocytes.

**Figure 4.1: morphological differences in astrocytes; Magistri 2016.**



Astrocytes derived using FBS (L) and CNTF/BMP4 (R) demonstrate very different morphologies with those differentiated using CNTF/BMP4 (with low concentrations of FBS) demonstrating the more typical stellate morphology shown by astrocytes *in vivo*. Figure reproduced with the kind permission of the authors and publishers.

#### 4.1.3 Results of initial differentiation

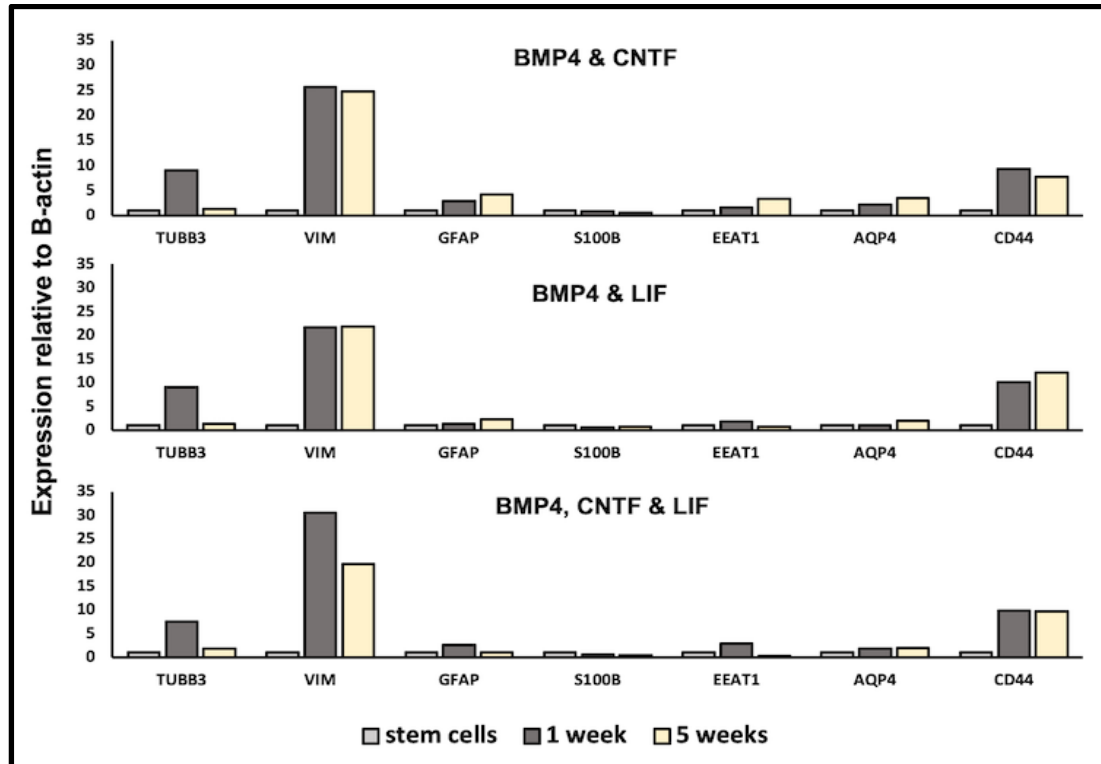
As the experimental plan was to stress astrocytes and induce astrogliosis it was important to produce a baseline phenotype which represented quiescent cells. For this reason, a low FBS (2%) medium was used to avoid the production of reactive astrocytes; NPCs were grown for 3 weeks in commercial astrocyte medium from Sciencell (used in preference to medium from Lonza on the basis of cost). It was also desirable to produce functionally mature astrocytes without the need for long-term differentiations. To achieve this, the isogenic E4/E4 line was differentiated using three different cocktails of growth factors (BMP4 & CNTF; BMP4 & LIF; BMP, CNTF & LIF) for 5 weeks after the initial 3-week differentiation in Sciencell astrocyte media.

Morphological heterogeneity of astrocytes coincides with a substantial diversity in expression of different molecules and hence antibodies against them only label subpopulations of astroglial cells<sup>217</sup>. Screening of astrocytes usually includes immunoreactivity or qPCR markers; although Aldh1L1 is a pan-astrocyte marker which labels all astrocytes independent of activation state<sup>251</sup> it has also been shown to be expressed in oligodendrocytes<sup>355</sup>. Identification of astrocytes thus requires

combinations of markers however there is no consensus about the precise combination that should be used nor the sequence of their appearance.

RNA was extracted one week and five weeks into differentiation from NPCs (total differentiation times of 5 weeks and 8 weeks respectively). RT-qPCR was performed using a variety of astrocytic markers including CD44, vimentin, glial fibrillary acidic protein (GFAP), excitatory amino acid transporters 1 (EAAT1), aquaporin 4 (AQP4) S100 calcium-binding protein beta (S100 $\beta$ ) plus the neuronal marker TUBB3 ( $\beta$ -III tubulin). Results were first normalised to the housekeeping gene  $\beta$ -actin and then normalised to levels of the same markers in undifferentiated stem cells (shown in Figure 4.2). On the basis of these results, the combination of BMP4 and CNTF was selected as it yielded the expected profile of a gradual increase in GFAP, vimentin, EAAT1, AQP4 plus the downregulation of the neuronal marker TUBB3 and the astrocyte precursor marker CD44 (although levels of S100B remained lower than anticipated in all groups).

**Figure 4.2 Expression of astrocytic genes using different growth factors.**



Expression of key astrocytic genes in stem cells and immature astrocytes derived using different combinations of growth factors to accelerate maturity. Data are derived from a single differentiation so no error bars are shown.

## 4.2 Further differentiation and characterisation

After the initial round of differentiations using different combinations of growth factors, all isogenic lines were differentiated and experiments carried out after a total differentiation period of 12 weeks; 4 weeks from stem cells to NPCs (as described in Chapter 2), 3 weeks with Lonza astrocyte medium then a further 5 weeks with medium containing the growth factors BMP4 and CNTF each at a concentration of 20ng/ml. A differentiation period of 12 weeks was decided upon to attempt to mature the astrocytes as far as possible within the constraints of time and resources.

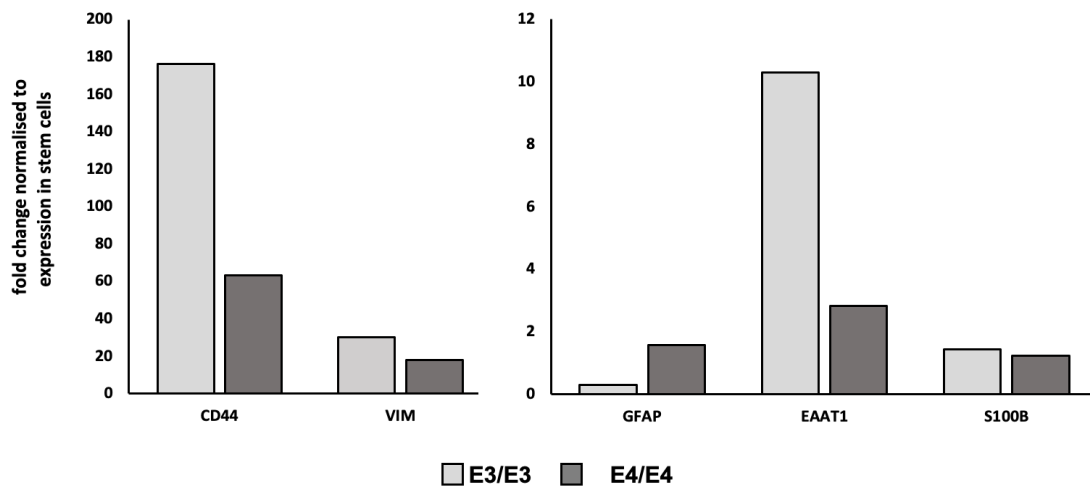
To encourage pure astrocyte cultures, cells were passaged at least weekly during the initial 3-week differentiation and further 3 times during the next five weeks. For the first differentiation, cells were passaged onto plates coated with poly-d-lysine and laminin (as they were still at the relatively fragile NPC stage). The next two passages were carried out onto Geltrex (Fisher Scientific; 15180617). The fourth and subsequent passages were onto uncoated plates which served to remove any residual neuronal cells. In addition, robust trituration of cells at each passage helped select for the hardy astrocytic population by removal of the more delicate neuronal cells.

HeSC-derived astrocytes from the E3/E3 and E4/E4 isogenic lines were then characterised for the expression of astrocyte-specific markers at the gene and protein levels. Gene expression analysis with RT-qPCR revealed expression of transcripts typical for developing astrocytes, including CD44 and vimentin plus smaller quantities of other astrocytic markers including the excitatory amino acid transporters 1 (EAAT1), the S100 calcium-binding protein beta (S100 $\beta$ ) and glial fibrillary acidic protein (GFAP); the neuronal marker MAP2 was also assessed using RT-qPCR but was found to be undetectable in all samples. Figure 4.3A shows the expression of all of these markers in 12-week old astrocytes derived from the wild-type E3/E3 cells and the isogenic E4/E4 lines, first normalised to  $\beta$ -actin then compared to levels in their respective stem cells; this was done to ensure that the fold changes in key markers were broadly in line with published data and that there were no unexpected differences between genotypes. The expression profiles were similar to those found when comparing the effects of

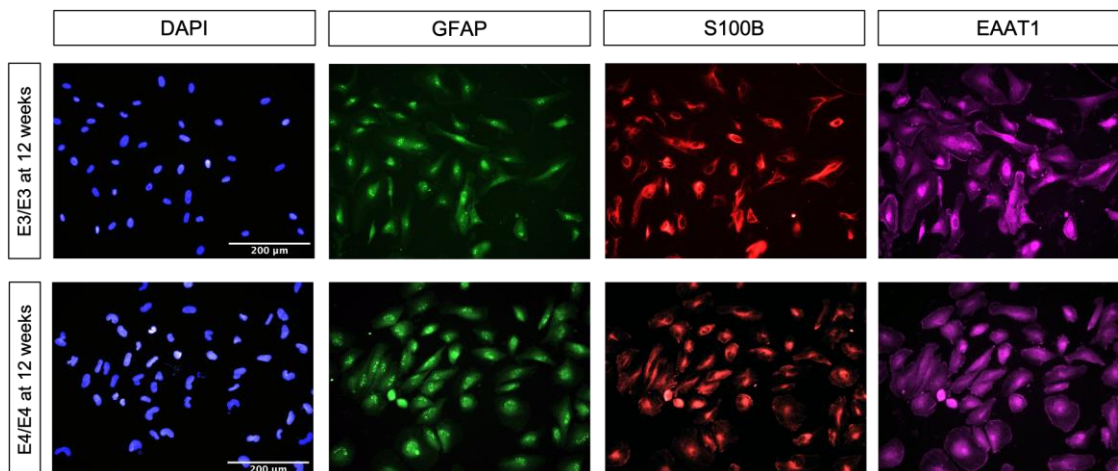
various growth factors (Figure 4.2 above) with CD44 and vimentin the most highly expressed markers. Some of the differences in expression between E3/E3 and E4/E4 astrocytes are explored in the next chapter.

Major astrocyte-specific markers were also confirmed by immunocytochemical staining of GFAP, S100 $\beta$  and EAAT1 (methods described in 2.2.1). To confirm that cultures were negative for neuronal markers, the cells were also stained for microtubule-associated protein 2 (MAP2) which, like gene expression, was undetectable.

#### 4.3A Gene expression of markers in E3/E3 and E4/E4 astrocytes at 12 weeks.



#### 4.3B Astrocytic markers in E3/E3 and E4/E4 astrocytes at 12 weeks.

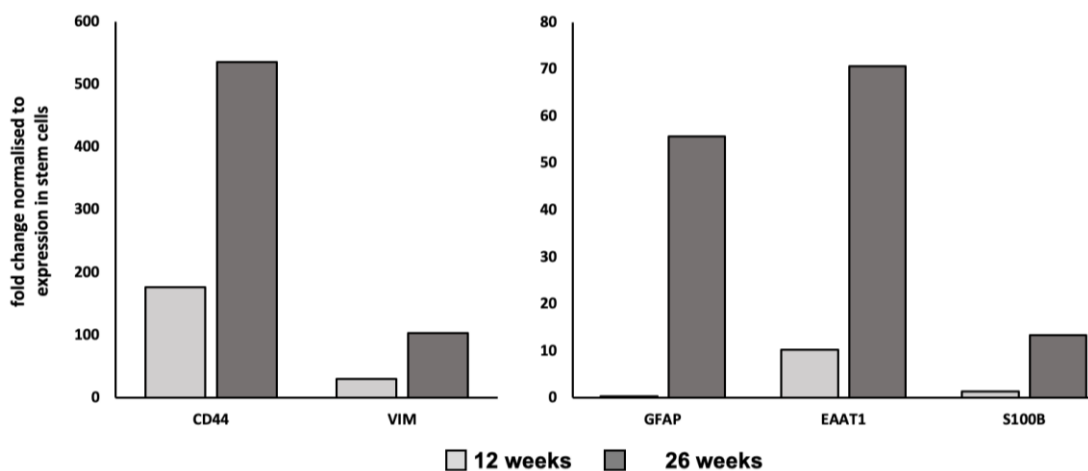


#### 4.2.1 Prolonged differentiation

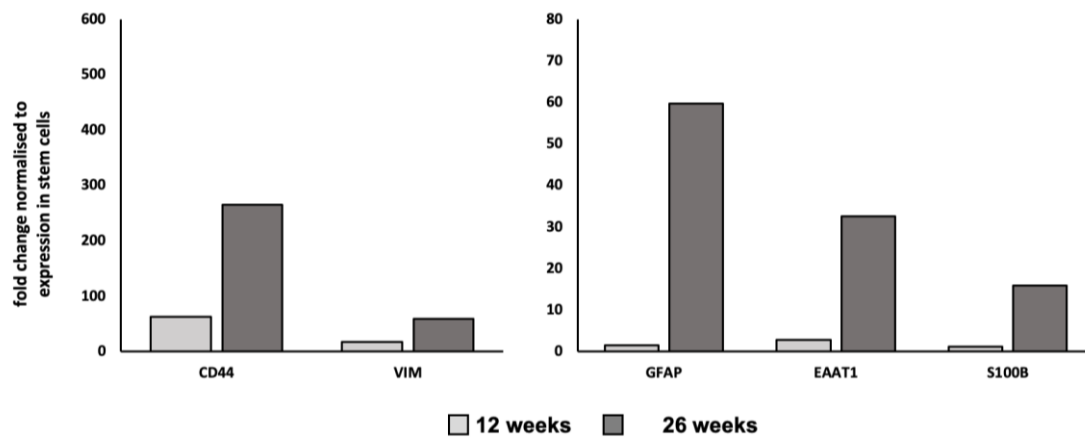
Towards the end of the project, some astrocytes were grown beyond the period of 12 weeks where the majority of experimentation took place. At the end of the 12-week period, astrocytes were transitioned to serum free media over the course of 1 week; CNTF and BMP4 were also withdrawn over the same period. At a total differentiation time of 26 weeks, cells were fixed and stained as described in 2.2.1 and RT-qPCR was also performed to compare levels of key astrocytic markers to their levels in stem cells and at 12 weeks; Figures 4.4A and 4.4B show levels in E3/E3 and E4/E4 astrocytes respectively.

Morphologically, the astrocytes started to exhibit a more typical stellate appearance and, although markers of immature astrocytes (CD44 and vimentin) remained, other key markers were also upregulated including GFAP, EAAT1 and S100B. These features suggest that prolonged differentiation produces more prototypic astrocytes and that experimentation at this point, given further time and resources, would have been desirable.

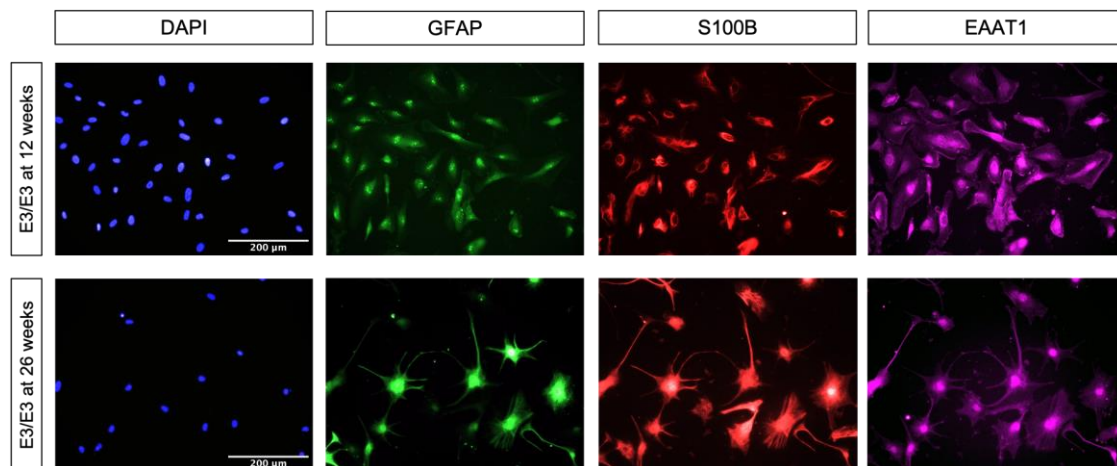
#### 4.4A Expression of astrocytic markers in E3/E3 astrocytes at 12 and 26 weeks.



#### 4.4B Gene expression of markers in E4/E4 astrocytes at 12 and 26 weeks.



#### 4.4C Astrocytic markers in E3/E3 astrocytes at 12 and 26 weeks.



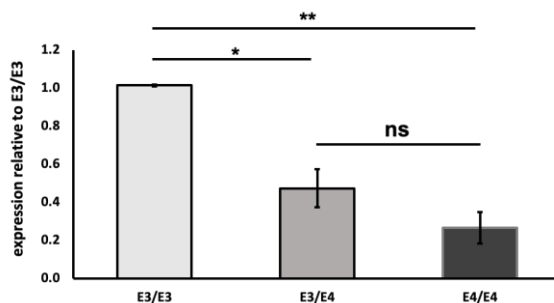
Figures 4.4A-C show the results of the prolonged differentiation of astrocytes. While most of the experiments described in this thesis were undertaken with 12-week astrocytes, the final differentiation of E3/E3 and E4/E4 astrocytes was prolonged to 26 weeks in order to investigate whether transcriptional and morphological changes emerged. Figure 4.4A&B shows that gene expression (measured with qPCR) of key astrocytic markers was substantially upregulated in 26-week old astrocytes of both genotypes. Figure 4.4C shows that morphological differences also emerged after prolonged differentiation; initial plating density was the same.

### 4.3 ApoE production

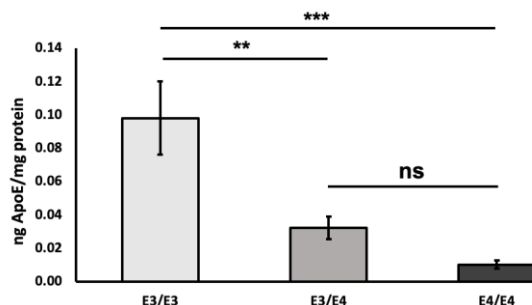
ApoE levels were measured with RT-qPCR (Figure 4.5A) and ELISA (Figure 4.5B). Data were obtained from two separate differentiations for qPCR and three differentiations for the ELISA; data were analysed using a one-way ANOVA with Tukey's multiple comparison test.

RT-qPCR showed a dose dependent reduction in the expression of *APOE* according to genotype; there was an overall difference between the groups ( $F=53.826$ ,  $p=0.004$ ) with significant differences between E3/E3 and E3/E4 ( $p=0.011$ ), E3/E3 and E4/E4 ( $p=0.004$ ) but not E3/E4 and E4/E4 ( $p=0.132$ ). Levels of ApoE in astrocyte supernatant were measured with ELISA (described in section 2.3.2). There was an overall difference between the groups ( $F=35.130$ ,  $p<0.001$ ) with significant differences between E3/E3 and E3/E4 genotypes ( $p = 0.002$ ), E3/E3 and E4/E4 ( $p<0.001$ ) but not between E3/E4 and E4/E4 ( $p= 0.186$ ).

**4.5A *APOE* gene expression (qPCR)**



**4.5B ApoE protein expression (ELISA)**



Figures 4.5A&B show *APOE* expression according to genotype. Figure 4.5A shows qPCR data obtained from two separate differentiations; data are normalised to levels in WT E3/E3 astrocytes. Figure 4.5B shows ApoE protein expression by genotype measured with ELISA using data from 3 separate differentiations.

#### 4.4 Discussion

This chapter has described a monolayer method which consistently produces astrocytes in a 12-week period which display a range of typical markers using both gene expression and immunocytochemistry. The method used was selected to produce astrocytes with a quiescent phenotype in order that stressing the cells might highlight differences in phenotype; these experiments are discussed in the next chapter.

It was also shown that the differentiated astrocytes produce ApoE and levels of production are genotype dependent, an effect which has previously been described in the literature. However, a prolonged differentiation showed that astrocytes at 26-weeks display a more mature genetic profile and are morphologically more similar to astrocytes *in vivo* than their 12-week old counterparts.

##### 4.4.1 Markers in 12-week astrocytes

Screening of astrocytes usually includes immunoreactivity or qPCR markers which may include GFAP, S100b, EAAT1, vimentin and AQ4 but there is no universal marker that stains all astrocytes in the CNS. Morphological heterogeneity of astrocytes coincides with a substantial diversity in expression of different molecules and hence anti-bodies against them only label subpopulations of astroglial cells<sup>217</sup>. Identification of astrocytes requires co-staining with a number of different antibodies however there is no consensus about the precise combination that should be used nor in the sequence of their appearance.

Genetic profiling of the 12-week astrocytes showed that CD44 and vimentin were the most abundant markers with fold-changes from stem cells of approximately 100 and 20 respectively demonstrating the relative immaturity of the cultured astrocytes. CD44 is known to be a marker of astrocyte precursor cells and early astrocytes being expressed in culture from Day 12 from NPCs; however it is also quite specific as cells expressing CD44 are restricted to maturing into astrocytes<sup>356</sup>.

Vimentin is expressed in immature astrocytes, in subpopulations of protoplasmic and fibrous astrocytes, in Bergmann glia, and in tanycytes<sup>217</sup>. Along with glial fibrillary acidic protein (GFAP), vimentin is one of the intermediate filament proteins that serve a largely cyto-architectural function<sup>211</sup>, modulating astrocyte motility and shape by providing structural stability to astrocytic processes<sup>357</sup>.

GFAP was the first molecular marker to be robustly associated with astrocytes and is still considered to be prototypical<sup>357</sup>. It was perhaps, unexpected, therefore to see such low expression levels in our 12-week astrocytes (levels were very similar to those seen in stem cells). However, one of the key aims of our induction protocol was to produce quiescent astrocytes. GFAP is a reliable marker of astrogliosis which is characterised by a change in morphology and rapid synthesis of GFAP intermediate filaments. So although GFAP is a reliable marker of CNS trauma and astrogliosis, it not be detectable in healthy tissue, even in mature astrocytes<sup>209</sup>.

The other key markers in our samples were S100B and EAAT1. S100B is one of a family of calcium binding glycoproteins, which act as both calcium buffers and sensors<sup>217</sup>. S100B is more broadly expressed than GFAP in both grey and white matter<sup>358</sup> and substantially changes in CNS injury; it has been suggested that increased levels in serum and CSF fluids may have diagnostic relevance<sup>359</sup>; in fact, elevated CSF S100B is key to the diagnosis of prion disease. In our 12-week samples, the expression of S100B was approximately twice that of stem cells and was very similar in E3/E3 and E4/E4 cells.

The final marker we examined in 12-week astrocytes was EAAT1. Rapid removal of glutamate from the extracellular space is required for the survival and normal function of neurons. EAAT1, along with EAAT2, is one of two major glutamate transporters which remove glutamate from the synaptic cleft after it is released from the pre-synaptic bouton. In our sample, the fold change in EAAT1 at 12-weeks in E3/E3 astrocytes was three times that of E4/E4 cells (10 and 3 respectively); phenotypes pertaining to glutamate uptake are explored further in the next chapter.

#### 4.4.2 Markers and morphology in 26-week astrocytes

After the third 12-week astrocytic differentiation, cells were allowed to continue growing until 26 weeks. The most stark change between 12 weeks and 26 weeks was morphologically with the 26-week astrocytes exhibiting a more prototypic stellate morphology with an increased number of processes.

All of the markers demonstrated at 12 weeks were greatly upregulated at 26 weeks. It might have been anticipated that CD44 and vimentin would have decreased over this period as they are generally considered to be markers of immature astrocytes however both CD44 and vimentin increased approximately 4-fold between 12 and 26 weeks.

The fold-change in CD44 and vimentin was, however, more modest than the increases seen in S100B and EAAT1 which both increased approximately 10-fold between 12 and 26 weeks (with consistent results in E3/E3 and E4/E4 cells). The *in vitro* data regarding the temporal detection of S100b are not conclusive; some suggest that the onset of S100b expression coincides with the onset of astrogenesis<sup>353</sup> while others have reported a high level of S100b in undifferentiated astrocytes<sup>360</sup>. There is very little published on the temporal appearance of EAAT1 but although it tends to be prominent in the developmental period of the CNS *in vivo*<sup>361</sup> it is generally considered to be a marker of maturity in differentiated astrocytes<sup>256,350</sup> which would accord with these findings.

Surprisingly, the largest increase between 12 and 26 weeks was in GFAP which increased on average approximately 100-fold. The low levels of GFAP at 12 weeks suggested that the astrocytes produced were of a quiescent phenotype however this increase suggests that GFAP may simply be expressed in more mature astrocytes. Another possibility is that the astrocytes were somehow activated over their prolonged differentiation period although they were transitioned to a fully serum-free media which should, theoretically, have allowed them to maintain their quiescent state. It should be noted, however, that these data were obtained from a single

differentiation, to give an indication of how astrocytes change over time, so results need to be viewed in this context.

#### 4.4.3 ApoE levels

The results above confirmed that all isogenic lines produce ApoE and found that gene expression and protein levels were significantly lower in E4/E4 than in E3/E3 cells.

Much debate about the role of ApoE in the pathogenesis of SAD has centred on whether the ApoE4 isoform is toxic or simply less effective at carrying out its physiological roles. A key feature in support of the latter is that ApoE levels in blood, tissues (including the brain) and CSF tend to be genotype dependent with E2/2 > E3/3 > E4/4.

The effect was first shown in a 2005 when an ApoE4-like, Arg-61 domain interaction was engineered into a mice leading to low levels of ApoE in various brain regions and the CSF, although not of mRNA<sup>362</sup>. These findings were consolidated in *APOE22*, *APOE33*, and *APOE44* targeted replacement mice where there was a genotype-dependent decrease in ApoE levels; in *APOE22* > *APOE33* > *APOE44*<sup>177</sup>. In humans, the protein level of ApoE in blood showed a similar genotype-dependent relationship<sup>363</sup>. In CSF, findings are mixed with some studies showing no clear relationship<sup>364,365</sup> while others demonstrate an *APOE2* > *APOE3* > *APOE4* effect on CSF ApoE levels<sup>366,367</sup>. The results are similarly mixed in histopathological studies of various brain regions; some have found the pattern of *APOE2* > *APOE3* > *APOE4*<sup>368,369</sup> while others have not<sup>370,371</sup>.

The two recent studies in isogenic APOE models have found reduced levels of ApoE protein and mRNA in APOE4 astrocytes<sup>202,263</sup>. It should be noted that this contrasts another recent study of iPSC-derived astrocytes which showed similar ApoE levels in *APOE3* versus *APOE4* cells, however, a isogenic model was not used<sup>372</sup>. Interestingly, the study by Lin and colleagues found that the reduced ApoE4 mRNA and protein levels was specific to astrocytes (and not found in neurons) indicating the effect may be cell-type specific.

The reduced levels of ApoE in E4/E4 cells could be due to lower production, increased degradation or increased binding (to either receptors or to cholesterol). It is difficult to ascertain whether synthesis of ApoE is decreased as controlling the other two mechanisms is near impossible. However, it is interesting to note that both protein and mRNA levels of ApoE were decreased suggesting that ApoE4 can negatively impact its own transcription.

It has been suggested that the lower levels of ApoE4 in the CNS are likely to represent increased degradation caused by its unique structural features; ApoE4 is known to form a molten globule intermediate that makes it less stable than ApoE3<sup>138</sup>.

Experimentally, however, while neuronally derived ApoE4 has been reported to be more prone to proteolysis than neuronally derived ApoE3, there was no similar effect in astrocyte derived ApoE<sup>164</sup>. This could be investigated further by looking for evidence of increased levels of ApoE degradation products in the media from E4/E4 cells.

There is some evidence to suggest that lower levels of ApoE4 may be due to increased binding which, in turn, is due to interaction of the amino-terminal and carboxyl-terminal domains. The low density lipoprotein receptor (LDLR) has a high affinity for ApoE and demonstrates an ApoE isoform specific binding affinity (E4 >E3 >E2) which, in plasma, is the cause of familial hypertriglyceridaemia<sup>373,374</sup>. There is also preferential binding of ApoE4 to the very low density lipoprotein receptor (VLDLR) in plasma<sup>143</sup>.

ApoE may also bind to lipids in an isoform dependent manner. Investigation of lipid particles generated by ApoE3 and ApoE4 expressing astrocytes has shown that ApoE3 has the ability to generate similarly sized ApoE lipid particles with fewer ApoE molecules than ApoE4. In fact, ApoE4-containing lipid particles may contain 2-fold numbers of ApoE molecules compared with an ApoE3- containing lipid particle<sup>179</sup> thus lowering free ApoE levels. This hypolipidation effect is explored in more detail in Chapter 7.

In conclusion, it appears that a combination of lower production, increased degradation and increased binding may be responsible for the lower level of ApoE associated with the E4/E4 genotype.

#### 4.5 Conclusions

In this chapter a protocol has been described for the production of quiescent astrocytes which have been shown to express typical markers both genetically and with immunocytochemistry. The levels of the neuronal marker TUBB3 (which encodes  $\beta$ III-tubulin) was found to increase in NPC cells but return to stem cell levels in astrocytes. In addition, expression of the neuronal marker MAP2 was found to be undetectable via both qPCR and immunocytochemistry indicating the purity of the astrocyte samples.

The method used was selected to produce astrocytes with a quiescent phenotype in order that stressing the cells might highlight differences in phenotype; these experiments are discussed in the next chapter. It was also shown that the differentiated astrocytes produce ApoE and levels of production are genotype dependent, an effect which is consistent with published literature giving an early indication that the isogenic model created is robust.

The key limitation of this method is that, despite efforts to mature astrocytes with the growth factors BMP4 and CNTF, they still display a relatively immature genetic signature with the expression of vimentin and CD44 higher than those of other astrocytic markers such as EAAT1 and S100B. As is shown from the astrocytes which were matured for 26 weeks (rather than the standard 12 weeks when most experiments were undertaken) a more mature transcriptional profile and typical stellate morphology more akin to *in vivo* astrocytes was observed. If this work were to be continued, it would be useful to conduct experiments with more mature astrocytes to see if the phenotypes observed in subsequent chapters remain or are indeed accentuated.

## 5 Astrocytic phenotypes: glutamate uptake and phagocytosis

As discussed in Chapter 1, astrocytes fulfil a vast range of physiological functions within the CNS and, while once considered to have a purely structural role, it is becoming increasingly apparent they are key to the maintenance of CNS homeostasis. This chapter explores the effect of *APOE* genotype on two key astrocytic roles; glutamate homeostasis and phagocytosis in both quiescent cells and those that have been stressed to undergo astrogliosis.

### 5.1 Induction of astrogliosis

In addition to their many physiological functions within the healthy CNS, astrocytes respond to damage and disease through the process of astrogliosis whereby they undergo a variety of changes in gene expression, cellular structure and function<sup>375</sup>.

Astrogliosis is associated with essential beneficial functions but may also lead to harmful effects. Although the trophic factors released by astrocytes during astrogliosis are of benefit to tissue repair, they also amplify the inflammatory response, augment vascular permeability and result in increased microglial activation and potentiate release of cytokines and chemokines<sup>376</sup>. Numerous studies in both human and mouse models consistently show that the loss of reactive astrocytes during the early phases of injury results in exacerbation of clinical signs, scar disorganisation, persistence of inflammatory cells, BBB alterations and neuronal death. By contrast, astrocyte depletion during the chronic phase of disease ameliorates disease expression and reduces leukocyte infiltration into the CNS (reviewed in Colombo and Farina, 2016).

Astrogliosis is a prominent neuropathological feature of AD with greater astrogliosis in patients than in age-matched controls<sup>250</sup>. Hypertrophic astrocytes, together with activated microglia, tend to accumulate around A $\beta$  plaques<sup>213</sup> but the extent of astrogliosis also correlates with the burden of neurofibrillary tangles<sup>250</sup>.

Astrogliosis is not, however, a simple stereotypic response but is rather a finely tuned spectrum of potential changes that range from reversible alterations in gene expression and cellular hypertrophy to pronounced cell proliferation with compact scar formation and permanent tissue rearrangement<sup>375</sup>. Much work has been undertaken in recent years to better understand the process of astrogliosis; analyses using astrocytes isolated from a variety of murine sources including healthy young adults, normally aged individuals and a variety of induced disease states have demonstrated that astrocytes exhibit diverse changes in transcriptome profiles suggesting that the outcome of astrogliosis is not straightforward and is regulated by the type of environmental stimulation and where in the life-cycle these insults occur<sup>251,253,254</sup>.

By using two injury models, a middle cerebral artery occlusion to induce ischaemia and an LPS injection, Zamanian and colleagues found that reactive astrogliosis caused a rapid change in gene expression, but astrocytic phenotype varied according to the type of insult<sup>253</sup>. They found that LPS stimulation produced neurotoxic 'A1' astrocytes which induce fewer, weaker synapses and which have impaired phagocytosis. Building on this work, Liddelw and colleagues<sup>309</sup> found production of 'A1' astrocytes is mediated by microglia which, in response to LPS, secrete various mediators that convert quiescent astrocytes into neurotoxic 'A1' cells. They identified three mediators, the cytokines Il-1 $\alpha$  and TNF- $\alpha$  and complement protein C1q, that were necessary and sufficient to induce 'A1' reactive astrocytes whose gene profiles closely mirrored that of 'A1' reactive astrocytes *in vivo*.

For our experiments, we replicated Liddelw and colleagues' method (described in Chapter 2.2.4) to induce astrogliosis although it has been suggested that short and long TNF- $\alpha$  exposure in isolation is sufficient to recapitulate canonical astrogliosis events in human-induced pluripotent stem cells-derived astrocytes<sup>377</sup> or that a combination of TNF- $\alpha$  and Il-1 $\beta$  could achieve the same effect<sup>378</sup>.

### 5.1.1 Results of inducing astrogliosis

The key marker of reactive astrocytes is the complement component C3 which is specifically upregulated in 'A1' astrocytes but not in quiescent or 'A2' reactive astrocytes<sup>309</sup>. Gene expression of *C3* (Figure 5.1A) and *APOE* (figure 5.1B) were measured in quiescent and 'A1' astrocytes of E3/E3 and E4/E4 genotypes to ensure that the induction process was effective.

**Figure 5.1: induction of astrogliosis, A) *C3* and B) *APOE* expression**

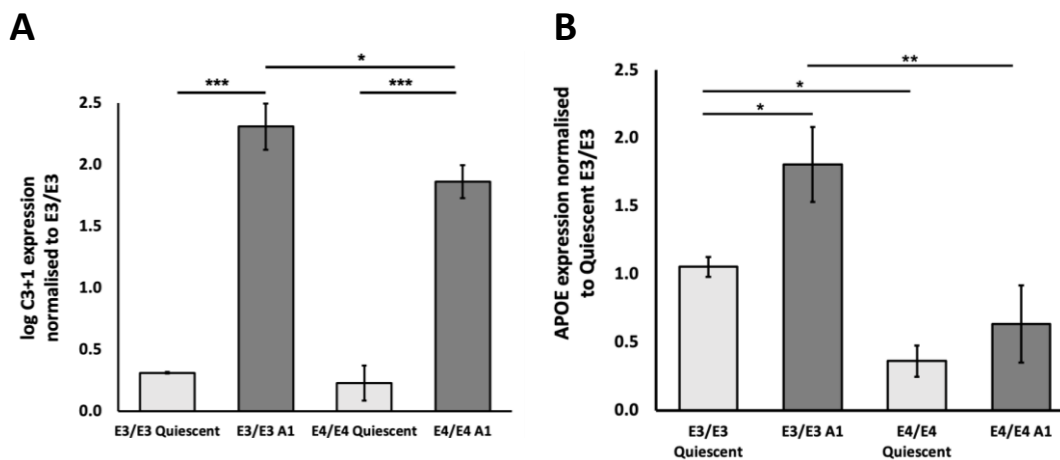


Figure 5.1 shows the gene expression using RT-qPCR of A) *C3* and B) *APOE* in quiescent and 'A1' astrocytes according to *APOE*3/3 and *APOE*4/4 genotypes. Results represent 3 separate differentiations each using 3 biological replicates performed in triplicate; values were first normalised to the house-keeping gene  $\beta$ -actin then to Quiescent E3/E3 cells. Analysis of *C3* gene expression shows an expected increase in *C3* in activated 'A1' astrocytes (Fig. 5.1A, two-way ANOVA effect of treatment  $F(1, 8) = 9.903$ ,  $P < 0.001$ , effect of *APOE* genotype  $F(1, 8) = 11.505$ ,  $P = 0.009$ , but interaction between just failed to reach significance  $F(1, 8) = 5.336$ ,  $P = 0.05$ ). Tukey's post hoc tests between quiescent E3/E3 and quiescent E4/E4  $P = 0.868$ , activated 'A1' E3/E3 and activated 'A1' E4/E4  $P = 0.016$ , quiescent E3/E3 and activated E3/E3  $P < 0.001$  and quiescent E4/E4 and activated 'A1' E4/E4  $P < 0.001$ . Analysis of *APOE* gene expression shows an increase in *APOE* according to genotype and treatment (Fig. 5.1B, two-way ANOVA effect of genotype  $F(1, 8) = 59.530$ ,  $P < 0.001$ , effect of treatment  $F(1, 8) = 17.991$ ,  $P = 0.003$ , but no significant interaction  $F(1, 8) = 3.935$ ,  $P = 0.083$ ). Tukey's post hoc tests between quiescent E3/E3 and quiescent E4/E4  $P = 0.016$ , activated 'A1' E3/E3 and activated 'A1' E4/E4  $P = 0.001$ , quiescent E3/E3 and activated 'A1' E3/E3  $P = 0.010$  and quiescent E4/E4 and activated 'A1' E4/E4  $P = 0.432$ .

As anticipated, *C3* expression was significantly higher in activated 'A1' cells when compared to their quiescent counterparts for both E3/E3 and E4/E4 cells; figure 5.1A shows log *C3*+1 gene expression. Analysis of log *C3*+1 with a two-way ANOVA shows an expected increase in *C3* in activated 'A1' astrocytes (Fig. 5.1A, two-way ANOVA effect of treatment  $F(1, 8) = 9.903$ ,  $P < 0.001$ , effect of *APOE* genotype  $F(1, 8)$

=11.505,  $P=0.009$ , but interaction between genotype and treatment just failed to reach significance ( $F(1, 8) = 5.336$ ,  $P=0.05$ ). Tukey's post hoc tests between quiescent E3/E3 and quiescent E4/E4  $P=0.868$ , activated 'A1' E3/E3 and activated 'A1' E4/E4  $P=0.016$ , quiescent E3/E3 and activated E3/E3  $P < 0.001$  and quiescent E4/E4 and activated E4/E4  $P < 0.001$ . The non-logarithmic values showed in activated 'A1' cells showed a fold changes from baseline (quiescent APOE33 cells) of 215.8 in E3/E3 cells and 74.3 in E4/E4 cells.

Results in the previous chapter demonstrated *APOE* expression was significantly higher in E3/E3 cells; this result was replicated in these further differentiations and also in activated 'A1' cells. Analysis of *APOE* gene expression shows an increase in *APOE* according to genotype and treatment (Fig. 5.1B, two-way ANOVA effect of genotype  $F(1, 8) = 59.530$ ,  $P < 0.001$ , effect of treatment  $F(1, 8) = 17.991$ ,  $P=0.003$ , but no significant interaction between genotype and treatment  $F(1, 8) = 3.935$ ,  $P=0.083$ . Tukey's post hoc tests between quiescent E3/E3 and quiescent E4/E4  $P=0.016$ , activated 'A1' E3/E3 and activated 'A1' E4/E4  $P=0.001$ , quiescent E3/E3 and activated E3/E3  $P=0.010$  and quiescent E4/E4 and activated E4/E4  $P=0.432$ .

## 5.2 Glutamate uptake

Glutamate is the major excitatory neurotransmitter in the CNS. Clearance of glutamate from the synaptic cleft is ensured by a high affinity glutamate uptake system<sup>379,380</sup>. Although glutamate transporters are expressed by all CNS cell types, astrocytes are primarily responsible for glutamate uptake and ablation of astrocytes in murine models leads to a failure to remove glutamate<sup>229</sup>. The resulting excess of glutamate is involved in the pathogenesis of several neurological disorders, when its extracellular concentration rises to toxic levels, a process termed excitotoxicity<sup>381,382</sup>. Interestingly, the action of memantine, the only non anti-cholinesterase drug currently licensed for use in AD, is believed to be the blockade of NMDA glutamate receptors thus reducing neuronal excitability and excess stimulation<sup>4</sup>.

Astrocytes were differentiated from NPCs derived from lines with each of the three *APOE* genotypes over a period of 8 weeks (a total differentiation time from stem cells of almost 12 weeks). There were 2 separate differentiations and 3 biological replicates for each genotype and condition. Using the assay described in section 2.2.5, the levels of glutamate uptake in each isogenic line under quiescent and activated conditions was tested.

A two-way ANOVA was carried out on glutamate uptake by *APOE* genotypes and astrocyte treatments (quiescent vs activated 'A1'). There were statistically significant main effects of both genotype [ $F(2, 6)=5.324, P=0.047$ ] and treatment [ $F(1, 6)=12.598, P=0.012$ ] but no statistically significant interaction [ $F(1, 6)=3.081, P=0.123$ ]. Tukey's post hoc tests showed no significant difference in glutamate uptake in quiescent astrocytes according to *APOE* genotype with all genotypes having values of approximately 3ng glutamate/ug protein. In activated 'A1' astrocytes however there was a significant difference ( $P=0.048$ ) between activated 'A1' E3/E3 (3.04ng/ug) and activated 'A1' E4/E4 (1.36ng/ug) but not between any other groups.

### 5.2.1 Mechanisms of reduced glutamate uptake

Glutamate uptake is undertaken by two glia-specific transporters — excitatory amino acid transporter 1 and 2 (EAAT1 and EAAT2, also known, respectively, as GLAST-1 and GLT1). After uptake, glutamate is either converted to glutamine by the glia-specific glutamine synthetase (GS encoded by the *GLUL* gene) and recycled back to synapses<sup>383</sup> or converted to  $\alpha$ -ketoglutarate ( $\alpha$ -KG) through oxidation by glutamate dehydrogenase (GLDH) or transamination by aspartate aminotransferase<sup>384</sup>.

The levels of the two main glutamate transporters (EAAT1 and EAAT2) plus GS were measured using immunocytochemistry and RT-qPCR. For qPCR experiments, quiescent and 'A1' astrocytes were differentiated for a total of 12 weeks using the methods previously outlined. Three separate differentiations were used with three biological replicates and three technical replicates for each condition. Expression was first

normalised to  $\beta$ -actin then normalised to expression levels in quiescent E3/E3 astrocytes; results are shown in Figure 5.2B.

Two-way ANOVAs were carried out for expression of EAAT1, EAAT2 and GS. For EAAT2 and GS there were no statistically significant main effects for genotype, treatment or interaction. For EAAT1, there were statistically significant effects for all three: genotype  $F(1, 8)=24.506$   $p = 0.001$ , treatment  $F(1, 8)=37.119$ ,  $P<0.001$ , interaction  $F(1, 8)=6.086$ ,  $p = 0.039$ . Tukey's post hoc tests between groups for EAAT1 showed some significant differences: quiescent E3/E3 and activated 'A1' E3/E3  $P= 0.001$ , activated 'A1' E3/E3 and activated 'A1' E4/E4  $P=0.003$  but none between quiescent E3/E3 and quiescent E4/E4  $P=0.358$  or quiescent E4/E4 and activated 'A1' E4/E4  $P=0.123$ ).

For immunocytochemistry experiments, astrocytes were differentiated for a period of 12 weeks as outlined previously. Data represent two separate differentiations with three separate conditions for each; quiescent, 'A1' (treated with cytokines as described above) and glutamate treated (cells were starved in HBSS media for 10 minutes before HBSS containing 50 $\mu$ M L-glutamate was added to each well for 60 minutes before washing and fixing). Images were taken as described in Chapter 2 (see Figure 5.2C) and corrected total cell fluorescence (CTCF) was then calculated for each antibody (see Chapter 2.2.2 for full methods) using 5 separate fields for each differentiation; a total of 10 fields for each condition. Each field contained an average of 40 astrocytes.

Two-way ANOVAs were carried out on CTCF levels of EAAT1, EAAT2 and GS. For all three markers, there were statistically significant main effects for genotype but none for treatment or interaction effects. Results showing the expression of each protein according to genotype, and the lack of significant differences in EAAT1, EAAT2 or glutamine synthetase levels when treated with glutamate or when an 'A1' phenotype was induced, is shown in Figure 5.2D.

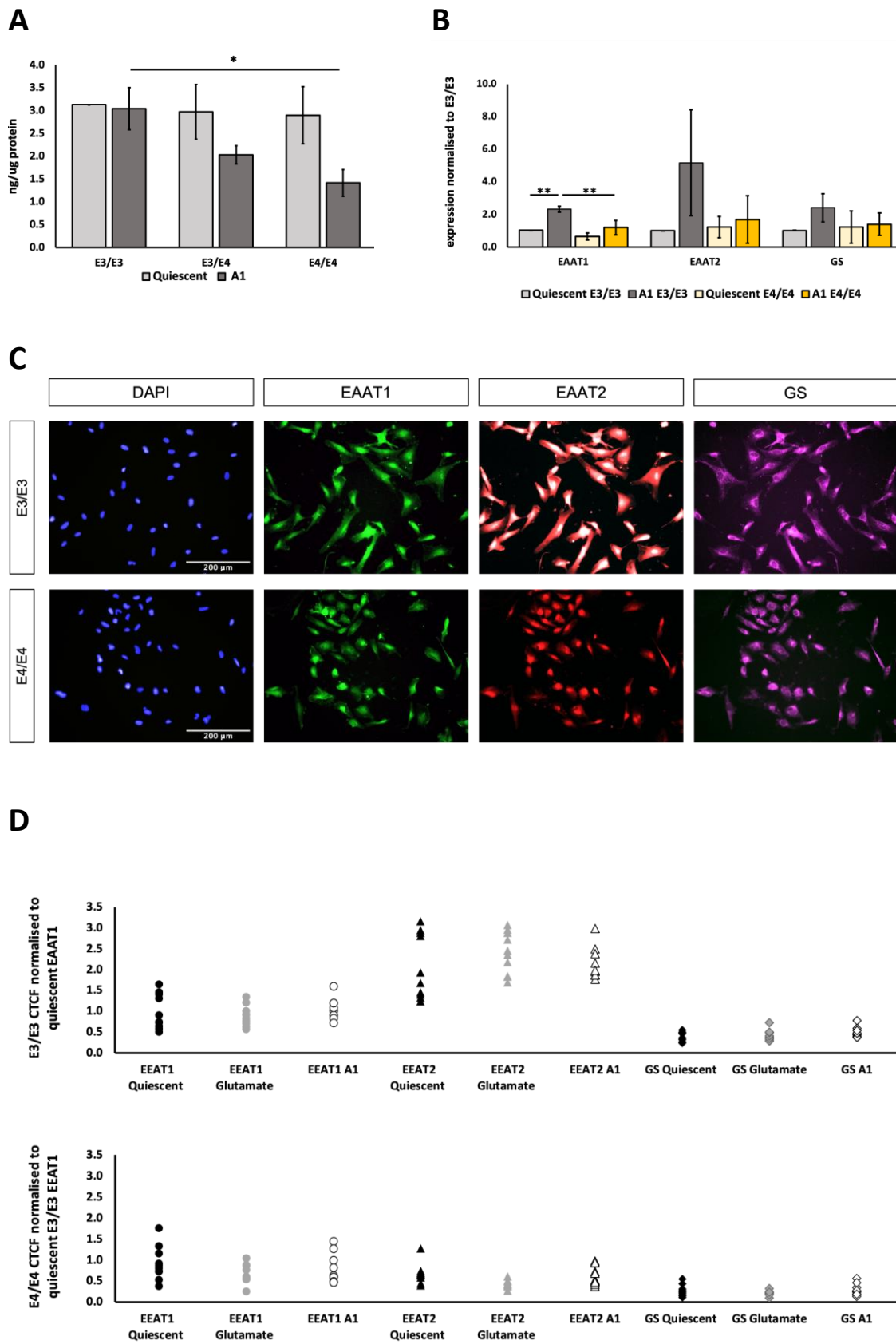
Figure 5.2E illustrates the effects of genotype on CTCF levels of EAAT1, EAAT2 and GS for each of the three treatment conditions. Despite there being a significant main

effect for genotype for EAAT1 [ $F(1, 55)=5.708$ ,  $P=0.020$ ] Tukey's post hoc tests did not show any significant differences in EAAT1 CTCF between E3/E3 and E4/E4 astrocytes for any of the three treatment conditions tested.

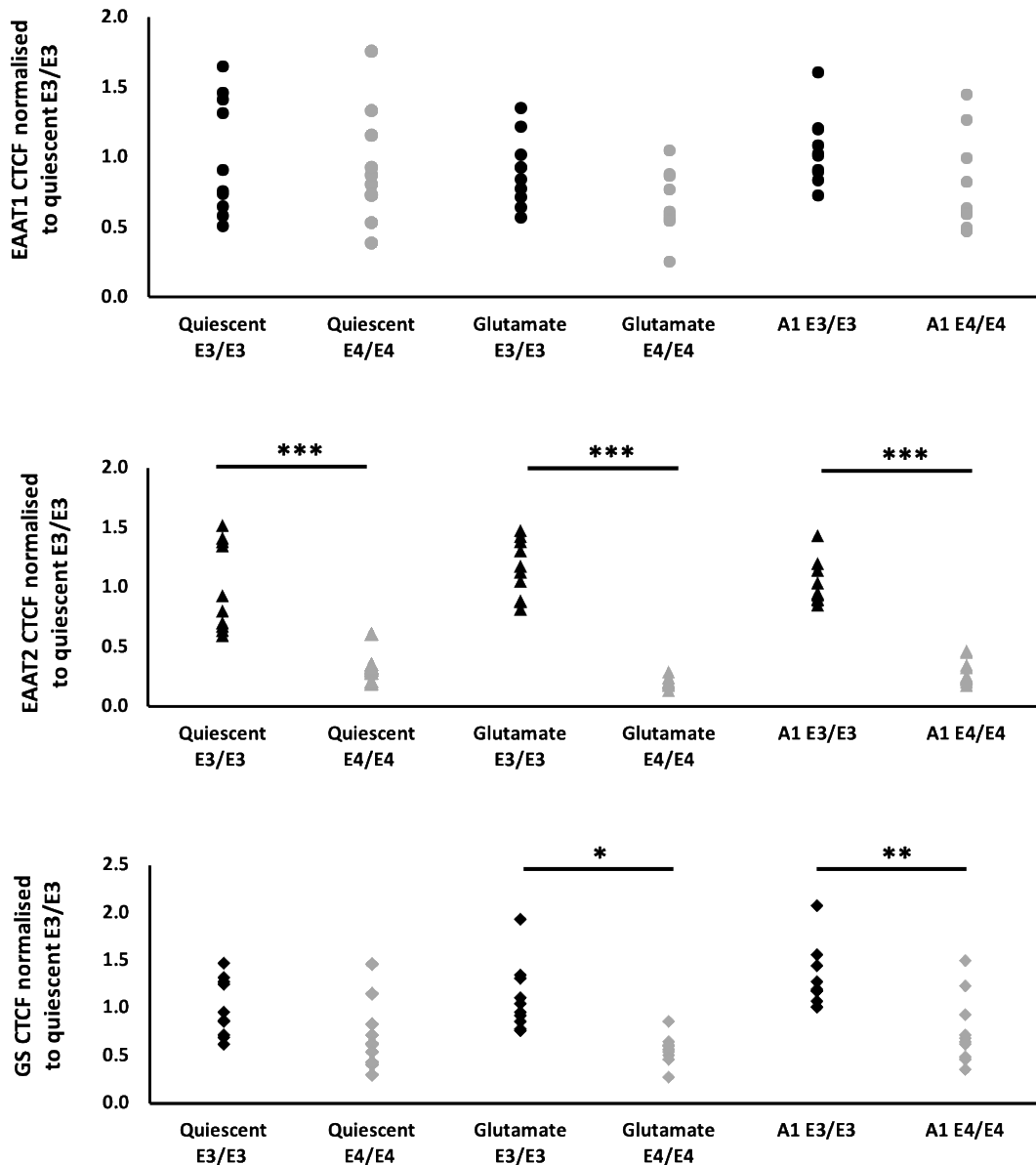
For EAAT2 there was a statistically significant main effect for genotype [ $F(1, 55)=225.043$ ,  $P<0.001$ ]. Tukey's post hoc tests showed significant differences in EAAT2 CTCF between E3/E3 and E4/E4 astrocytes for all three treatment conditions; quiescent (E3/E3 =  $6.40 \times 10^5$ , E4/E4  $2.10 \times 10^5$ ,  $P<0.001$ ), activated 'A1' (E3/E3 =  $6.57 \times 10^5$ , E4/E4 =  $1.89 \times 10^5$ ,  $P<0.001$ ) and glutamate treated (E3/E3 =  $6.83 \times 10^5$ , E4/E4 =  $1.34 \times 10^5$ ,  $P<0.001$ ).

For GS there was also a statistically significant main effect for genotype [ $F(1, 55)=32.676$ ,  $P<0.001$ ]. Tukey's post hoc tests did not show any significant difference by genotype in GS CTCF in quiescent astrocytes (E3/E3 =  $1.16 \times 10^5$ , E4/E4 =  $0.82 \times 10^5$ ,  $P=0.348$ ) but there were significant differences in activated 'A1' astrocytes (E3/E3 =  $1.50 \times 10^5$ , E4/E4 =  $0.85 \times 10^5$ ,  $P=0.006$ ) and glutamate treated astrocytes (E3/E3 =  $1.27 \times 10^5$ , E4/E4 =  $0.65 \times 10^5$ ,  $P=0.016$ ).

Figures 5.2A-E: results of glutamate experiments.



E



For all figures, data are presented as the mean  $\pm$  SD using two-way ANOVA with post-hoc Tukey's test. Blank = not significant, \*p < 0.05, \*\*p < 0.01, \*\*\*p < 0.001.

**A.** A two-way ANOVA was carried out on glutamate uptake by *APOE* genotypes and astrocyte treatments (quiescent vs activated 'A1'). There were statistically significant main effects of both genotype [F(2, 6)=5.324, p = 0.047] and treatment [F(1, 6)=12.598, p = 0.012] but no statistically significant interaction [F(1, 6)=3.081, p = 0.123]. Tukey's post hoc tests for glutamate uptake showed a significant difference between activated 'A1' E3/E3 and activated 'A1' E4/E4 P=0.048 but not between any other groups.

**B.** RT-qPCR data showing expression of EAAT1, EAAT2 and GS in E3/E3 and E4/E4 cells. Two-way ANOVAs were carried out for expression of EAAT1, EAAT2 and GS. For EAAT2 and GS there were no statistically significant main effects for genotype, treatment or interaction. For EAAT1, there were statistically significant effects for all three: genotype F(1, 8)=24.506 p = 0.001, treatment F(1, 8)=37.119, P<0.001, interaction F(1, 8)=6.086, p = 0.039. Tukey's post hoc tests between groups for

EAAT1 showed some significant differences: quiescent E3/E3 and activated E3/E3  $P=0.001$ , activated 'A1' E3/E3 and activated 'A1' E4/E4  $P=0.003$  but none between quiescent E3/E3 and quiescent E4/E4  $P=0.358$  or quiescent E4/E4 and activated 'A1' E4/E4  $P=0.123$ ).

**C.** Representative immunofluorescent images showing EAAT1, EAAT2 and GS expression in E3/E3 and E4/E4 cells.

**D and E.** Corrected cell total fluorescence values for EAAT1, EAAT2 and GS by D) genotype in order to highlight differences in treatment conditions and E) by treatment conditions to highlight differences between genotypes. For **D&E** each data point represents a single field containing an average of 40 astrocytes. Two-way ANOVAs were carried out for expression of CTCF levels of EAAT1, EAAT2 and GS.

- For EAAT1 there was a statistically significant main effect for genotype [ $F(1, 55)=5.708$ ,  $P=0.020$ ] but none for treatment or interaction. However, Tukey's post hoc tests did not show any significant differences in EAAT1 CTCF between E3/E3 and E4/E4 astrocytes for any of the three treatment conditions tested.
- For EAAT2 there was a statistically significant main effect for genotype [ $F(1, 55)=225.043$ ,  $P<0.001$ ], but none for treatment or interaction. Tukey's post hoc tests showed significant differences in EAAT2 CTCF between E3/E3 and E4/E4 astrocytes for all three treatment conditions; quiescent ( $P<0.001$ ), activated 'A1' ( $P<0.001$ ) and glutamate treated ( $P<0.001$ ).
- For GS there was a statistically significant main effect for genotype [ $F(1, 55)=32.676$ ,  $P<0.001$ ], but none for treatment or interaction. Tukey's post hoc tests showed a significant differences in GS CTCF between E3/E3 and E4/E4 astrocytes ( $P=.0016$ ) for two of the three treatment conditions; quiescent ( $P=0.348$ ), activated 'A1' ( $P=0.006$ ) and glutamate treated ( $P=0.016$ ).

### 5.3 Phagocytosis

The innate immune response is regarded as the body's first line of defence against pathological processes; phagocytosis is one of its fundamental elements. Although microglia have long been considered the primary phagocytic cell in the CNS, there is increasing appreciation of astrocytes' role in this key biological function<sup>385,386</sup>.

Both microglia and astrocytes have vital phagocytic roles including the removal of cell debris, toxic proteins and apoptotic cells as well as the engulfment of synapses. It has been speculated that perturbations of phagocytosis may play a role in both AD and neurodegenerative disease more widely. There is also evidence to suggest that astrocytes and microglia communicate with each other, in particular, microglia appear to have a key role in inducing the potentially damaging 'A1' astrocytic phenotype<sup>309</sup> which is characterised by, amongst other things, impaired phagocytosis<sup>253</sup>.

Two recent studies using iPSC-derived astrocytes from isogenic ApoE lines demonstrated that APOE4 astrocytes show impaired A $\beta$  uptake compared with APOE3 astrocytes<sup>202,260</sup>. However, to our knowledge, the effect of *APOE* genotype on the 'A1' astrocytic phenotype has not previously been investigated in any human *APOE* models.

Phagocytosis was assessed in quiescent astrocytes and those with the 'A1' phenotype which was induced by exposing astrocytes to C1q, IL-1 $\alpha$  and TNF- $\alpha$  for a period of 24 hours. After 24 hours, the phagocytic capacity of cells was assessed using the method described in section 2.2.6; data are normalised to the levels seen in quiescent *APOE33* cells.

A two-way ANOVA was carried out on percentage phagocytosis by *APOE* genotypes and astrocyte treatments (quiescent vs activated 'A1'). There were statistically significant main effects of both genotype [F(2, 12)=16531.483, P <0.001] and treatment [F(1, 12)=3834.069, P=0.019] plus a statistically significant interaction [F(1, 12)=7809.903, p = 0.001].

Tukey's post hoc tests between groups revealed significant differences between quiescent E3/E3 and activated 'A1' E3/E3 ( $P=0.001$ ), activated 'A1' E3/E3 and activated 'A1' E3/E4 ( $P=0.001$ ), and activated 'A1' E3/E3 and activated 'A1' E4/E4 ( $P<0.001$ ).

### 5.3.1 Possible mechanisms of reduced phagocytosis in E4/E4 astrocytes

Phagocytic activity of astrocytes is mediated via two main pathways, MEGF10 and MERTK; in a murine model, knockout of either of these phagocytic receptors has been shown to block synaptic pruning<sup>385</sup>. MEGF10 binds C1q opsonised cells enabling astrocytic phagocytosis<sup>387,388</sup>; ABCA1 is also required in this pathway but its function is poorly understood. The second phagocytic pathway is the MERTK pathway which works with the integrin pathway to control rearrangement of the actin cytoskeleton upon phagocytosis<sup>389</sup>.

In order to investigate whether either of these pathways were implicated in the differences in phagocytosis found in 'A1' astrocytes, expression of MERTK and MEGF10 was calculated in quiescent and 'A1' astrocytes which had been differentiated for a total of 12 weeks using the methods previously outlined. Three separate differentiations were used with three biological replicates and three technical replicates for each condition. As previously described, expression was first normalised to  $\beta$ -actin then normalised to expression levels in quiescent *APOE33* astrocytes.

Two-way ANOVAs were carried out for expression of MEGF10 and MERTK. For MEGF10 there were no statistically significant main effects for genotype, treatment or interaction between them. For MERTK, there were statistically significant effects genotype  $F(1, 8)=11.684$ ,  $P=0.009$  but not treatment or interaction. Tukey's post hoc tests for MERTK showed a significant difference between activated 'A1' E3/E3 and activated 'A1' E4/E4  $P=0.033$  but not for any other groups (quiescent E3/E3 and activated E3/E3  $P=0.115$ , quiescent E3/E3 and quiescent E4/E4  $P=0.573$  or quiescent E4/E4 and activated E4/E4  $P=0.971$ ).

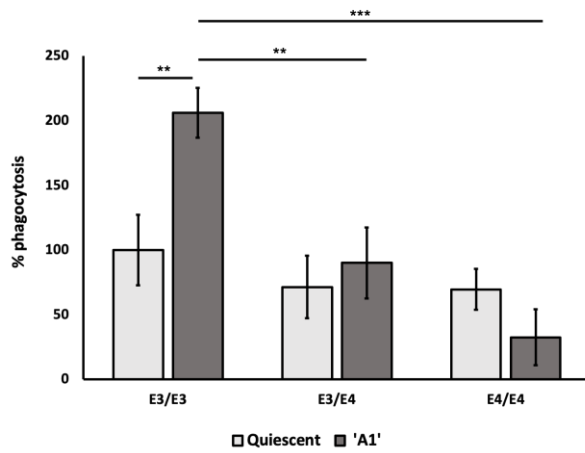
Although it is known that MERTK works with the integrin pathway to regulate rearrangement of the actin cytoskeleton upon phagocytosis the precise details of this process are unknown<sup>389</sup>. In cell culture, the in vivo distribution of microtubules is analogously present in stellating astrocytes, where microtubules co-extend with intermediate filaments in forming the processes<sup>390</sup>. It would be expected, therefore, that expression of intermediate filaments (namely GFAP and vimentin) would increase in activated astrocytes to facilitate phagocytosis. This is indeed the case as it has been shown that intermediate filament proteins are increased in reactive astrocytes and, in murine models, the absence of intermediate filaments makes astrocytes less efficient in dealing with the acute stage of various CNS injuries<sup>211</sup>.

The gene and protein expression of GFAP in quiescent and 'A1' astrocytes was investigated using RT-qPCR (methods identical to those used for MEGF10 and MERTK) and ICC respectively. Gene expression of vimentin was also measured but ICC was not performed due to the lack of a suitable antibody at the time of the initial differentiations.

No statistically significant differences in gene expression of GFAP or vimentin was found (Figures 5.3D&E) but GFAP expression using calculation of corrected total cell fluorescence (CTCF) was found to be significantly different; methods described in Chapter 2.2.2. A two-way ANOVA was carried out on GFAP CTCF levels by *APOE* genotype and astrocyte treatments (quiescent vs activated 'A1'). There were statistically significant main effects of both genotype [ $F(1, 37)=5.767, P=0.021$ ] and treatment [ $F(1, 37)=40.334, P<0.001$ ] plus a statistically significant interaction [ $F(1, 37)=8.679, p = 0.006$ ]. Tukey's post hoc tests showed that in the quiescent state, GFAP CTCF in E4/E4 cells was 1.41-times greater than that of E3/E3 cells with the result approaching significance ( $P=0.089$ ). When activated, GFAP CTCF was significantly different in E4/E4 cells (quiescent E4/E4 1.41 to 2.07;  $P=0.005$ ) but stayed virtually the same in E3/E3 cells (1.00 and 0.93 respectively;  $P=0.976$ ). The difference between 'A1' E3/E3 and E4/E4 astrocytes was also significant (values 1.00 and 2.07 respectively,  $P<0.001$ ).

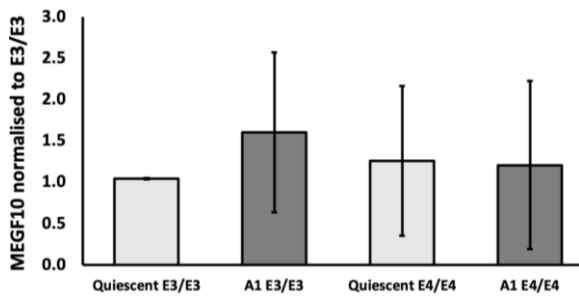
Figure 5.3A-F: results of phagocytosis experiments.

**A**

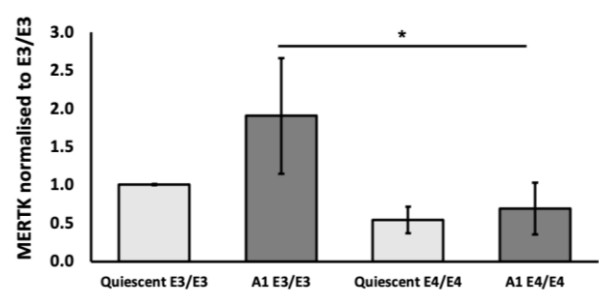


All data are presented as mean  $\pm$  SD using 2-way ANOVA (with Tukey multiple comparison test). For all figures, blank or ns = not significant, \*p<0.05, \*\*p<0.01, \*\*\*p < 0.001.

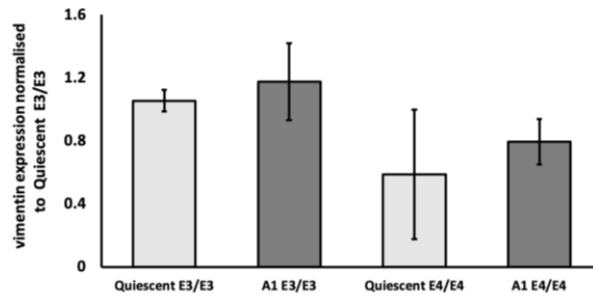
**B**



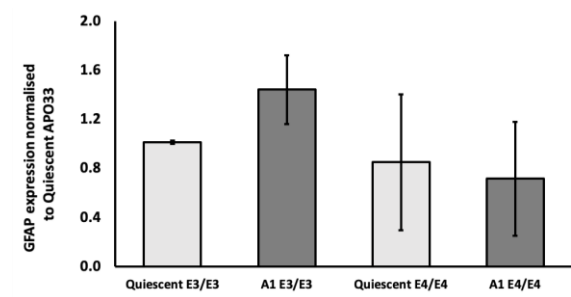
**C**



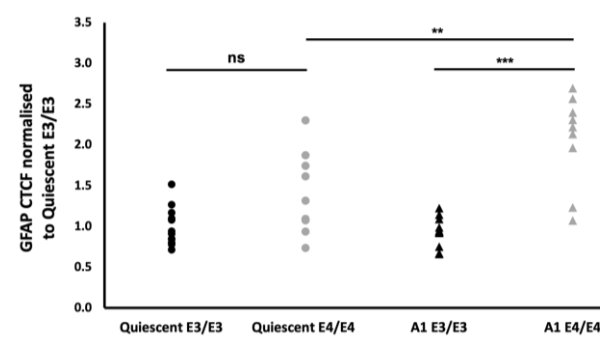
**D**



**E**



**F**



**A:** Represents data from 3 separate differentiations. Percentage phagocytosis is normalised to the result in Quiescent E3/E3 astrocytes (100%). A two-way ANOVA was carried out on percentage phagocytosis by APOE genotypes and astrocyte treatments (quiescent vs activated 'A1'). There were statistically significant main effects of both genotype [F(2, 12)=16531.483, P <0.001] and treatment [F(1, 12)=3834.069, P=0.019] plus a statistically significant interaction [F(1, 12)=7809.903, p = 0.001]. Tukey's post hoc tests between groups revealed significant differences between quiescent E3/E3 and activated 'A1' E3/E3 (P=0.001), activated 'A1' E3/E3 and activated 'A1' E3/E4 (P=0.001), and activated 'A1' E3/E3 and activated 'A1' E4/E4 (P<0.001).

**B & C:** are RT-qPCR data showing expression of MEGF10 and MERTK respectively from three separate differentiations; data are normalised to levels in Quiescent E3/E3 cells. Two-way ANOVAs were carried out for expression of MEGF10 and MERTK. For MEGF10 there were no statistically significant main effects for genotype, treatment or interaction between them. For MERTK, there were statistically significant effects genotype F(1, 8)=11.684, P=0.009 but not treatment or interaction. Tukey's post hoc tests for MERTK showed a significant difference between activated 'A1' E3/E3 and activated 'A1' E4/E4 P=0.033 but not for any other groups (quiescent E3/E3 and activated E3/E3 P= 0.115, quiescent E3/E3 and quiescent E4/E4 P=0.573 or quiescent E4/E4 and activated E4/E4 P=0.971).

**D. & E.** are RT-qPCR data showing expression of vimentin and GFAP from 3 separate differentiations; data are normalised to levels in Quiescent E3/E3 cells. Two-way ANOVAs were carried out for expression of the genes coding for the intermediate filaments GFAP and vimentin. For GFAP there were no statistically significant main effects for genotype or treatment nor any interaction between the two. For vimentin, genotype showed a statistically significant effect [F(1, 8)=8.552, p = 0.019] but no statistically significant effect of treatment or interaction effects; Tukey's post hoc tests between groups did not, however, reveal any significant differences (quiescent E3/E3 and quiescent E4/E4 P=0.183, activated 'A1' E3/E3 and activated 'A1' E4/E4 P=0.315, quiescent E3/E3 and activated E3/E3 P= 0.931 and quiescent E4/E4 and activated E4/E4 P=0.750).

**F.** shows the corrected total cell fluorescence (CTCF) for GFAP; the data represents 2 separate differentiations. Each data point represents a single field containing an average of 50 astrocytes. . A two-way ANOVA was carried out on GFAP CTCF levels by APOE genotype and astrocyte treatments (quiescent vs activated 'A1'). There were statistically significant main effects of both genotype [F(1, 37)=5.767, P=0.021] and treatment [F(1, 37)=40.334, P<0.001] plus a statistically significant interaction [F(1, 37)=8.679, p = 0.006]. Tukey's post hoc tests between groups revealed a significant difference between quiescent E4/E4 and activated 'A1' E4/E4 (1.41 and 2.07 respectively, P=0.005) however the result for quiescent E3/E3 and activated 'A1' E3/E3 was not significant (1.00 and 0.93 respectively, P=0.976). There was also a significant difference between activated 'A1' E3/E3 and activated 'A1' E4/E4 (0.93 and 2.07, P<0.001) but no such difference between E3/E3 and E4/E4 in their quiescent states (1.00 and 1.41, P=0.089).

## 5.4 Discussion

The findings above suggest that astrocytes with the *E4/E4* genotype are sub-functional rather than toxic with significant differences observed in two of their key physiological functions: glutamate uptake and phagocytosis.

### 5.4.1 Glutamate uptake

Our results demonstrated that glutamate uptake was not affected by *APOE* genotype in quiescent cells but that 'A1' astrocytes of *E4/E4* genotype demonstrated significantly impaired glutamate uptake compared to those with an *E3/E3* genotype. This is similar to the findings of Hyvarinen and colleagues who found that cytokine treatment (with IL-1 $\beta$  and TNF- $\alpha$ ) impaired the glutamate uptake capacity of astrocytes<sup>378</sup>.

Gene expression analysis of EAAT1, EAAT2 and GS was undertaken in quiescent and 'A1' astrocytes. For both *E3/E3* and *E4/E4* astrocytes there were significant increases from the quiescent to activated 'A1' state but no differences between genotypes. There were no such differences in the expression of EAAT2 and GS.

When protein expression of EAAT1, EAAT2 and GS was examined (using CTCF levels) EAAT2 was found to be significantly reduced in quiescent *E4/E4* cells compared to *E3/E3* and that this relationship remained when astrocytes were induced to the reactive 'A1' phenotype and in glutamate treated cells. For GS, there were statistically significant decreases in *E4/E4* astrocytes compared to *E3/E3* astrocytes in the activated 'A1' and glutamate treated states but not in quiescent cells. In contrast to gene expression, for EAAT1 there were no differences between *APOE* genotypes in any of the three treatment states.

As noted above, once taken up from the synaptic cleft by astrocytes, glutamate is metabolised into glutamine by GS. As well as reduction in EAAT2, lower levels of GS in *E4/E4* cells when compared to *E3/E3* cells was found; this was approaching significance

for quiescent cells but statistically significant for cells treated with glutamate and in 'A1' cells. Again, this is consistent with published literature which has shown an age-dependent decrease of GS in the hippocampus of triple-transgenic AD mice<sup>391</sup> plus reduced expression in the temporal cortex of patients with AD<sup>392</sup>.

Although the reduction of EAAT2 is a very interesting, and consistent, finding it does not appear to explain why glutamate uptake was largely unaffected in quiescent cells (although there was a trend towards a reduction in glutamate uptake) and the difference only manifested in 'A1' cells. It would have been interesting to see if the differences in EAAT2 levels in glutamate treated cells were potentiated in glutamate treated 'A1' cells however this experiment was not undertaken.

The literature shows, however, that dysfunction of glial glutamate transporters may represent a phenomenon common to many neurodegenerative conditions including ALS, HD and AD<sup>225,393</sup>. Decreased glutamate transporter activity in the midfrontal cortex of autptic AD brain samples has been found in association with a reduction in key synaptic proteins such as synaptophysin<sup>394</sup>. In a transgenic mouse model of AD, glutamate transporter levels were lower than in wild-type littermates<sup>395</sup>.

It is also interesting that in this model, EAAT2 was the protein most markedly affected by *APOE* genotype. While both EAAT1 and EAAT2 are predominantly localised in peri-synaptic astrocytes, EAAT2 performs 90% of glutamate uptake in the mammalian CNS<sup>396</sup>. Furthermore, while EAAT2 protein expression is found throughout the brain, it predominates across the forebrain particularly in the hippocampus<sup>397-399</sup>. EAAT1 on the other hand is most highly expressed in the cerebellum, an area relatively spared in AD<sup>400</sup>.

Given the key role of EAAT2 in regulating extracellular glutamate concentrations, it is unsurprising that its expression and activity have profound effects on neuroprotection and neuropathology. Multiple neurodegenerative diseases have been associated with reduced EAAT2 expression and function including ALS<sup>401</sup>, Parkinson's disease<sup>402</sup> and AD<sup>402,403</sup>. Furthermore, cortical neuron cultures are significantly less vulnerable to

glutamate when cultured in an astrocyte-rich environment suggesting that the sensitivity of neurons to glutamate toxicity may be dependent upon astrocyte, and specifically EAAT2, function<sup>404</sup>.

In common with our results, previous studies have found that, although protein expression of EAAT2 is decreased, mRNA levels have tended to be unaffected suggesting that post-transcriptional modifications are involved<sup>395</sup>. There are several possible reasons for this: in protein lysates from the inferior parietal lobe of AD brains and A $\beta$ -treated synaptosomes, EAAT2 was found to exist in a sub-optimal oxidised form<sup>405</sup>. Another study of autaptic AD brains found that while wild type EAAT2 showed a global reduction in expression, brain regions susceptible to neuronal loss demonstrated greater expression of splice variants that reduced glutamate transport in an in vitro assay<sup>406</sup> while another found an abnormal detergent-insoluble EAAT2 in vulnerable brain regions of AD patients<sup>407</sup>. Finally, in brain slices, A $\beta$  treatment results in the internalisation of EAAT2, which reduces glutamate clearance by astrocytes<sup>408</sup>. Therefore, transcriptional, post-transcriptional and post-translational mechanisms may account for the dysregulation of EAAT2 in AD. It has already been demonstrated that ApoE4 acts as a transcription factor binding to the promoter region of around 1700 genes involved in a range of physiological processes<sup>409–411</sup>. It seems plausible therefore that ApoE4 is having an effect on the transcription of EAAT2 especially as studies examining the role of ApoE4 on transcription have largely found repressive effects<sup>410</sup>.

Another potential mechanism of interest is the effect of the NF- $\kappa$ B signalling pathway on EAAT2 expression. As will be discussed in the next chapter, TNF- $\alpha$  is probably the most well-studied and well-known activator of NF- $\kappa$ B<sup>412</sup> but it also acts as its receptor as a gene target of NF- $\kappa$ B<sup>413</sup>. It has been shown that NF- $\kappa$ B can intrinsically activate EAAT2 but that EAAT2 gene expression is negatively regulated by TNF- $\alpha$  via a NF- $\kappa$ B-dependent mechanism in H4 astrogloma cells<sup>414</sup>. This pathway is also of relevance to our findings in the next section on phagocytosis.

#### 5.4.2 Phagocytosis

The results above show that, while phagocytosis in quiescent astrocytes is unaffected by *APOE* genotype, dose-dependent differences are apparent in activated 'A1' astrocytes with E4/E4 astrocytes exhibiting significantly impaired phagocytosis.

The existing literature suggests that the effect of the 'A1' phenotype on phagocytosis in astrocytes is not straightforward. A recent study which where TNF- $\alpha$  was applied to astrocytes differentiated from human iPSCs noted that phagocytic activity was enhanced (while glutamate uptake was suppressed)<sup>415</sup>. These findings contrast with those of the original Liddelow paper where decreased synaptosome phagocytosis was reported in 'A1' astrocytes<sup>309</sup>. Our results presented here suggest that the phagocytic response in 'A1' astrocytes might be influenced by *APOE* genotype and this might explain the different results seen in these two papers however the *APOE* genotype of the iPSC used in the Zhou study is not mentioned while the effects in the Liddelow paper were seen in *Aldh1l1*-eGFP transgenic mice.

*APOE* genotype has been shown to differentially control the rate of astrocyte-mediated phagocytosis in murine models, such that *APOE2* potentiates and *APOE4* prevents efficient synapse elimination by astrocytes *in vitro* and *in vivo*<sup>416</sup>. *APOE4* genotype has also been shown to impair astrocytic autophagy, the process by which cells induce degradation of major cellular constituents including dysfunctional organelles and protein aggregates<sup>261</sup>.

It might appear counterintuitive that loss of phagocytic capacity is the phenotype associated with the risky E4/E4 genotype however studies in both human and mouse models consistently show that the loss of reactive astrocytes during the early phases of injury results in exacerbation of clinical signs, scar disorganisation, persistence of inflammatory cells, BBB alterations and neuronal death although, by contrast astrocyte depletion during the chronic phase of disease ameliorates disease expression and reduces leukocyte infiltration into the CNS (reviewed in Colombo and Farina, 2016).

It has been speculated that a decrease in the overall phagocytic capacity of astrocytes may lead to the accumulation of senescent synapses and their debris, which may be at least partially responsible for the enhanced vulnerability of the brain to AD<sup>416</sup>.

The results above demonstrate that the differences in phagocytosis in 'A1' astrocytes might be attributable to the MERTK pathway. Although it is known that MERTK works with the integrin pathway to regulate rearrangement of the actin cytoskeleton upon phagocytosis<sup>389</sup>, the precise details of this process are unknown. In cell culture, the *in vivo* distribution of microtubules is analogously present in stellating astrocytes, where microtubules co-extend with intermediate filaments in forming the processes<sup>390</sup>. It might be expected, therefore, that expression of intermediate filaments (namely GFAP and vimentin) would increase in activated astrocytes to facilitate phagocytosis. In fact, it has been shown that when astrocytes undergo astrogliosis they exhibit increased expression of the intermediate filament proteins including GFAP, vimentin and nestin<sup>417</sup> and, in a murine model, the absence of intermediate filaments makes astrocytes less efficient in dealing with the acute stage of various CNS injuries<sup>211</sup>.

One would expect, therefore, that E4/E4 genotype might be associated with a reduction in the expression of intermediate filament proteins thus attenuating their phagocytic capacity. However, our results suggest that opposite, that GFAP expression is increased in 'A1' astrocytes. Although this appears inconsistent with the finding that MERTK expression is increased in E3/E3 'A1' astrocytes but not in E4/E4 'A1' astrocytes, an increase in GFAP in E4/E4 astrocytes is more consistent with findings of clinico-pathological studies.

After activation, astrocytes express an enhanced level of GFAP which is considered marker of astrogliosis<sup>418,419</sup> and increased GFAP expression corresponds to the severity of astroglial activation<sup>418</sup>. GFAP-positive activated astrocytes are reported in association with neuritic plaques in AD<sup>420</sup> and in human post-mortem studies the number of GFAP-positive astrocytes in layer I/II of the entorhinal cortex was higher in those with pathologically confirmed AD than controls and was associated with degree

of cognitive decline<sup>421</sup>. Furthermore, an early post-mortem study using brain tissue from 73 AD cases found that GFAP expression was significantly increased in patients carrying the *APOE4* allele compared to those without it<sup>250</sup>.

In the recent study by Hyvarinen and colleagues, using iPSC-derived astrocytes, they found downregulation of GFAP at both the gene and total protein levels upon cytokine treatment (IL-1 $\beta$  and TNF- $\alpha$ ) after 7 days (interestingly, vimentin levels remained stable). The measurements described above were taken after only 24 hours of cytokine treatment but there was a slight, non-significant decrease in CTCF levels in the *APOE33* astrocytes. It could, therefore, be that the 'physiological' response to cytokine treatment is a reduction in GFAP.

Like EAAT2, it has also been noted that GFAP expression is linked to NF- $\kappa$ B signalling. Activated NF- $\kappa$ B is detected in reactive astrogliosis<sup>422</sup> and is activated by a range of extrinsic GFAP-regulatory factors including bFGF, CNTF, IL-1, IL-6, TGF- $\beta$ 1, and, most notably, TNF- $\alpha$ . In a model using human glioblastoma A172 cells and primary human brain astrocyte cells both aspirin (an inhibitor of NF- $\kappa$ B activity) and cells transfected with an expression vector encoding a super-repressor I $\kappa$ B $\alpha$  protein to specifically inhibit NF- $\kappa$ B activity demonstrated reduced the levels of GFAP mRNA and protein<sup>423</sup>.

So, although the increase in GFAP seen in cytokine activated E4/E4 cells is consistent with the phenotype seen in AD and other neurodegenerative diseases it does not fit neatly with the proposed mechanism of control by MERTK and the mechanism by which astrocytic expression of GFAP is increased in the neurodegenerative CNS remains unclear. It seems that impairment of phagocytosis linked to changes in expression of intermediate filament proteins is too simple an explanation and that other changes in gene and cytokine expression may underlie the differences seen. Exploration of this possibility forms the basis of the next chapter.

## 5.5 Conclusions

In this chapter the method described by Ben Barres' group to induce cells with the potentially damaging 'A1' phenotype has been utilised successfully to explore two key astrocytic functions, glutamate uptake and phagocytosis. Although there are no *APOE*-dependent differences in quiescent cells, changes occur when cells are stressed.

Impaired glutamate uptake by E4/E4 astrocytes may be linked to decreased EEAT2 expression. Although defects in glutamate transport and EEAT2 have been linked to AD (and other neurodegenerative diseases) for several years this is, to our knowledge, the first study to show that this phenotype is associated with the E4/E4 genotype. The findings described above also suggest that impairment of phagocytosis may be linked to *APOE* genotype-dependent differences in the MERTK pathway and GFAP expression but that the relationship is not straightforward. It is also intriguing that both EEAT2 and GFAP expression are linked to NF- $\kappa$ B signalling which will be discussed in greater depth in the next chapter.

As noted in the previous chapter, a key limitation of this study is that, despite efforts to mature astrocytes they still display a relatively immature genetic signature at 12 weeks. Although this period of differentiation is in line other published studies<sup>350</sup>, ideally, it would be useful to conduct experiments with more mature astrocytes to see whether differences remain or are indeed accentuated.

Another issue is that, although we were able to show changes in EEAT2 and GFAP expression via immunocytochemistry, we were unable to complete Western Blotting because of changes to working practices in the wake of the COVID-19 pandemic. Protein samples have been taken, however, and it is hoped these experiments can be undertaken when full access to the laboratory resumes.

Despite these shortcomings, this model has proved to be effective in elucidating two key *APOE*-associated phenotypes which may be contributing to the pathogenesis of AD.

## 6 Effect of *APOE* genotype on microglial to astrocyte signalling

Microglial/astrocyte cross-talk is currently one of the most investigated areas in neurodegeneration. Recent work has made it clear that signalling between these two CNS sentinels is a key part of the inflammatory cascade now considered to be central to AD pathogenesis. This isogenic model provides a way to explore the effect of the *APOE* genotype on this process.

When astrocytes undergo astrogliosis, proliferation and release of factors such as cytokines, chemokines (chemotactic cytokines) and growth factors is enhanced<sup>424</sup>. Chemokines are classically defined by their role in inducing directional migration and activation of leukocyte subsets into inflammatory sites<sup>425</sup>. They also play a key role in cellular communication between astrocytes, infiltrating leukocytes and other cells thus regulating CNS inflammation, neuroendocrine responses and even behaviour<sup>426</sup>.

In mammals, the chemokine group comprises approximately 50 endogenous peptides, released by immune cells, and 20 receptors<sup>427</sup>. They have a highly conserved tertiary structure and are subdivided into four groups (CC, CXC, CX3C and C) based on the relative positions of two conserved cysteine residues near their N-terminus<sup>428</sup>. Many chemokines share a common receptor and most bind to more than one<sup>429</sup>.

### 6.1 Results

#### 6.1.1 Results in quiescent astrocytes

A Human Cytokine Antibody Array (Abcam #ab133997) was used to test for differences in the production of 42 cytokines in quiescent astrocytes and 'A1' astrocytes of E3/E3 and E4/E4 genotypes in two separate differentiations; full methods are described in Chapter 2.2.7.

Inspection of the membranes showed that 20 of the 42 targets were visibly present in quiescent samples in both experiments and whose levels of intensity remained positive when background levels were subtracted; ENA-78, GRO, GRO- $\alpha$ , IL-1 $\beta$ , IL3, IL-5, IL-8, IL-1 $\beta$ , MCP-1, MCP-2, MCSF, RANTES, SDF-1, TARC, TNF- $\alpha$ , TNF- $\beta$ , EGF, IGF-1, Oncostatin M and PDGF.

The most abundantly expressed molecules were IL-8 (CXCL8), MCP-1 (CCL2), GRO (which measures all GRO isoforms –  $\alpha$ ,  $\beta$  and  $\gamma$ ), and GRO $\alpha$  (CXCL1); results are depicted in Figures 6.1A. Outside of the 4 most highly expressed cytokines (see Figure 6.1B), all others were detected at much lower levels; approximately 10-times lower in most cases and many showed considerable variation between differentiations. Although there was a general trend towards higher expression of most cytokines in E4/E4 astrocytes, no statistically significant differences in cytokine levels in quiescent cells were found between *APOE* genotypes.

#### 6.1.2 Results in activated 'A1' astrocytes

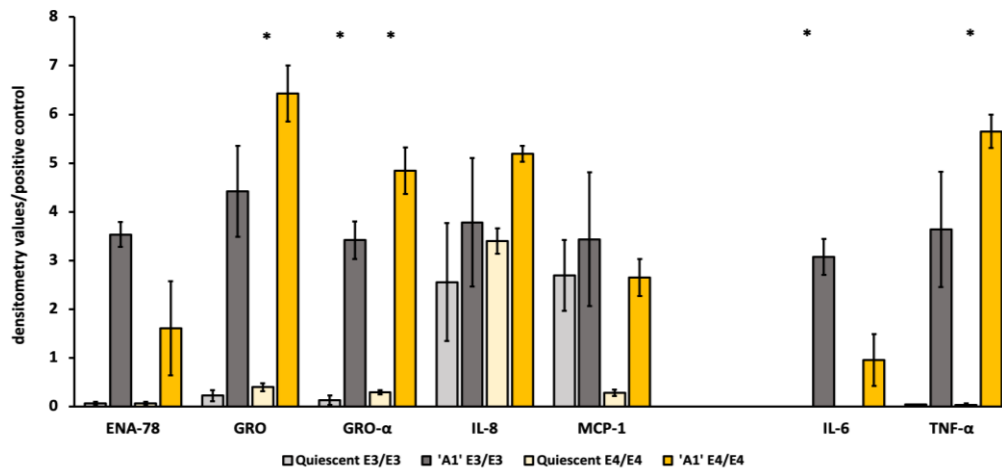
After induction of the 'A1' phenotype, several cytokines/chemokines showed a clear increase including IL-6 and TNF- $\alpha$  which were not detected in quiescent samples and ENA-78 (CXCL5) which was found in quiescent cells but at very low levels. GRO, GRO- $\alpha$  and TNF- $\alpha$  demonstrated significant differences between pre and post treatment levels in both E3/E3 and E4/E4 genotypes. For ENA-78 and IL-6 there was a statistically significant increase in levels post treatment in E3/E3 cells but not in E4/E4 cells. The situation was reversed for IL-8, MCP-1 and RANTES where there was a statistically significant increase in levels post treatment in E3/E3 cells but not in E4/E4 cells. The table below shows these results plus p-values which have not been corrected for multiple testing; the asterisks denote values that remain significant after application of the Benjamini-Hochberg test).

**Table 6.1: summary of significant cytokine array results.**

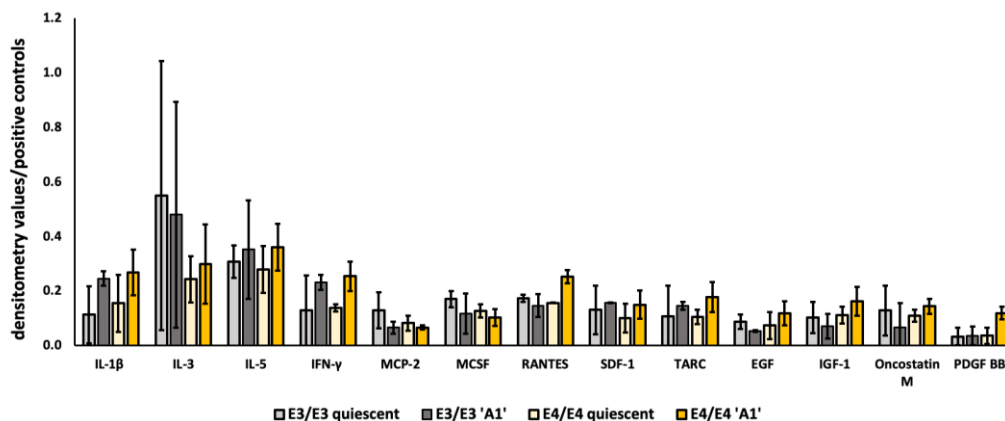
Chemokine	Genotype	Pre and post treatment values	P-value
ENA-78	E3/E3	0.07-3.54	0.003
IL-6	E3/E3	0.04-3.64	0.007
GRO- $\alpha$	E3/E3	0.14-3.42	0.007*
GRO	E3/E3	0.23-4.42	0.024
TNF- $\alpha$	E3/E3	0.04-3.64	0.050
TNF- $\alpha$	E4/E4	0.03-5.65	0.002*
GRO	E4/E4	0.40-6.43	0.005*
GRO- $\alpha$	E4/E4	0.30-4.84	0.006*
MCP-1	E4/E4	0.28-2.65	0.013
IL-8	E4/E4	3.40-5.19	0.014
RANTES	E4/E4	0.16-0.25	0.029

In activated 'A1' astrocytes, the only significant difference (at the uncorrected  $p < 0.05$  level) between *APOE* genotypes was in IL-6 (E3/E3 = 3.64, E4/E4=0.96;  $p = 0.043$ ). GRO- $\alpha$  ( $p = 0.082$ ) and RANTES ( $p = 0.090$ ) were approaching significance but none remained significant after adjustment for multiple testing using the Benjamini-Hochberg method.

### 6.1A Highly expressed cytokines in Quiescent and 'A1' astrocytes by genotype.



### 6.1B Other cytokines expressed in Quiescent and 'A1' astrocytes by genotype.



## 6.2 Discussion

### 6.2.1 Cytokine expression in quiescent astrocytes

It has been shown previously by Choi and colleagues (using a protein microarray) that non-stimulated human astrocytes, in culture derived from fetal tissue, expressed eight cytokines including G-CSF, GM-CSF, GRO $\alpha$  (CXCL1), IL-6, IL-8 (CXCL8), MCP-1 (CCL2), MIF and Serpin E1<sup>430</sup>.

As noted in the results section, 20 of the 42 targets were present in quiescent samples identifying cytokines which have, hitherto, not been found to be expressed by astrocytes. There are two main explanations for the wider range of cytokines and growth factors detected in our samples; first that the population of astrocytes used for experiments was impure, however, as noted in Chapter 4 expression of neuronal markers was entirely absent. The other possibility is that the cytokine array format is more sensitive; for example, the manufacturers, Abcam, state that their membranes can detect as little as 4 pg/ml of MCP-1 in contrast to their similar MCP-1 ELISA assay which has a sensitivity of 40 pg/ml of MCP-1. Furthermore, the recent study using astrocytes derived from isogenic *APOE* lines measured with a Luminex multiplex immunoassay showed that 24 of 45 chemokines, cytokines and growth factors tested were differentially expressed by *APOE* genotype however the identity of all 24 were not listed<sup>263</sup>. This suggests that the secretory profile of astrocytes may be wider than previously thought. It should also be noted that a number of cytokines/chemokines that have been found to be expressed by astrocytes were not including in our assay, most notably IP-10 (CXCL10), but also others including MIF, Serpin E1, eotaxin (CCL11), LIF and the growth factors HGF, BMP-2A, BMP-3, neuromodulin (GAP43), BDNF and VEGF-D.

Two glycoproteins that have been found to be expressed by astrocytes previously but not detected by our assay were G-CSF and GM-CSF; these have been found in studies which have used astrocytes derived from fetal<sup>430</sup> and post-mortem tissue<sup>424</sup> but were

not mentioned in the study which used astrocytes derived from isogenic lines<sup>263</sup>. It is possible, therefore, that the differentiation process does not fully recapitulate the expression profile of resident astrocyte populations.

#### 6.2.2 *APOE* dependent differences in quiescent astrocytes

While the results presented here are in agreement with previous studies with respect to the most abundantly expressed molecules in quiescent astrocytes (IL-8 (CXCL8), MCP-1 (CCL2), GRO, and GRO $\alpha$  (CXCL1)), there were no significant differences in the expression of cytokines between quiescent E3/E3 and E4/E4 astrocytes.

In a study using astrocytes derived from isogenic *APOE* lines, 24 of 45 chemokines cytokines and growth factors measured with a Luminex multiplex immunoassay, were differentially expressed by *APOE* genotype however the identity of all 25 were not listed. When absolute protein levels were compared between E3/E3 and E4/E4 astrocytes, 10 proteins showed significantly higher levels in the media from E4/E4 glia including SDF-1a (CXCL12), MIP-1b (CCL4), Eotaxin (CCL11), IP-10 (CXCL10) and RANTES (CCL5), cytokines (IL-8, LIF and IL-6) and growth factors (HGF and VEGF-D)<sup>263</sup>. The difference between this study and ours is likely due to the greater number of replications performed in this study and it is possible that the Luminex method is more sensitive than the array used here. It should be noted, however, that the findings in the Luminex study contradict those of an earlier paper which observed significantly *reduced* constitutive secretion of the pro-inflammatory mediators IL-8 (CXCL8) and MCP-1 (CCL2) in astrocyte conditioned media from *APOE44* patients with sporadic AD compared to cells from controls<sup>256</sup>.

#### 6.2.3 Activated 'A1' astrocytes

A number of papers have examined the effects of stimulating astrocytes with TNF- $\alpha$  and IL-1 $\beta$  or combinations of the two although, to date, none have done so in astrocytes with different *APOE* genotypes. The paper referenced above by Choi and colleagues found that following stimulation with IL-1 $\beta$  and TNF- $\alpha$ , activated astrocytes

newly produced IL-1 $\beta$ , IL-1ra, TNF- $\alpha$ , IP-10 (CXCL10), MIP-1 $\alpha$  (CCL3) and RANTES (CCL5), in addition to the induction of sICAM-1 and complement component 5<sup>430</sup>. Another study looking at gene expression in astrocytes cultured from human adult post-mortem specimens found that treatment of astrocytes with either IL-1 $\beta$  and TNF- $\alpha$ , or both, led to induction of a similar set of astrocyte genes, including those encoding the chemokines CCL2 (MCP-1), CCL5 (RANTES), and CXCL8 (IL-8), growth factors including BMP-2A, BMP-3, neuromodulin (GAP43), BDNF, and G-CSF, and receptors such as the CRF receptor, the calcitonin receptor (CTR), and TKT<sup>424</sup>. A more recent paper by Hyvarinen and colleagues found that the most highly secreted proteins in response to IL-1 $\beta$  and TNF- $\alpha$  were chemokines IP-10 (CXCL10), ENA-78 (CXCL5), IL-8 (CXCL8), MCP-1 (CCL2), GRO- $\alpha$  (CXCL1) and RANTES (CCL5)<sup>378</sup>.

In activated astrocytes, our results were in almost total agreement with Hyvarinen and colleagues although IP-10 (CXCL10), which was also found to be highly expressed in their study, was, unfortunately, not part of our assay<sup>378</sup>. In addition, some cytokines/chemokines which were not detected, or found at very low levels, in quiescent samples were found to be highly expressed in activated 'A1' astrocytes, namely IL-6 and TNF- $\alpha$ . This agreement with previous studies suggests that our astrocytic differentiation was successful in producing cells with the expected secretory profile.

#### 6.2.4 Differences between APOE genotypes in 'A1' astrocytes

Although the overall secretory pattern of 'A1' astrocytes was in line with published data, there were some differences between *APOE* genotypes. Further elucidation of these patterns and their possible implications is discussed in the following sections.

##### 6.2.4.1 *GRO*, *GRO- $\alpha$* (CXCL1), *IL-8* (CXCL8) and *ENA-78* (CXCL5)

*GRO*, *GRO- $\alpha$*  (CXCL1), *IL-8* (CXCL8) and *ENA-78* (CXCL5) are grouped due to their convergence on the CXCR2 receptor and their common role in neutrophil transmigration.

The results presented here showed differences between levels of GRO (which included all GRO isoforms) and GRO- $\alpha$  in quiescent and 'A1' astrocytes for both E3/E3 and E4/E4 cells with result in E4/E4 astrocytes remaining significant after multiple testing correction. For ENA-78 the difference was only significant for E3/E3 cells. For IL-8, the situation was reversed with a significant increase in 'A1' E4/E4 cells but not in E3/E3 cells. In terms of differences between 'A1' astrocytes of E3/E3 and E4/E4 genotypes, only the difference in GRO- $\alpha$  was approaching significance ( $p=0.082$ ).

CXCL1 and CXCL8 have both been shown to first route neutrophils to the site of insult<sup>431-433</sup> then induce morphologic changes and degranulation activating the release of proteases and reactive oxygen species (ROS)<sup>433,434</sup>. CXCL5 was first characterised as an inducible factor following stimulation of cells with the inflammatory cytokines IL-1 $\beta$  and TNF- $\alpha$ <sup>435</sup> and using transcriptome analysis was found to be the most up-regulated gene in human spinal cord astrocytes treated with IL-1 $\beta$ . Like CXCL1 and CXCL8, CXCL5 is also a potent neutrophil attractant and activator<sup>436</sup>.

While the healthy brain is considered to be an immune-privileged site lacking extensive neutrophil immune-surveillance, massive neutrophil recruitment across the blood brain barrier (BBB) occurs in conditions such as bacterial meningitis<sup>437</sup>. Neutrophil infiltration has also been shown in a mouse model of AD where neutrophils adhered to the endothelial lining of the brain's blood vessels before migrating into the brain parenchyma. Neutrophil infiltration was associated with cognitive deficits and, interestingly, depletion of neutrophils restored cognitive function<sup>438</sup>.

Reported sources of the neutrophil-specific chemokines CXCL1, CXCL8 and CXCL5 include activated microglia and endothelial cells however astrocytes are thought to be the primary source<sup>439,440</sup>. Furthermore, the infiltrated neutrophils themselves are a major source of CXC chemokines, potentially amplifying leukocyte recruitment and the inflammatory response<sup>441</sup>.

Increased levels of all three chemokines have been found in the CSF and/or brain parenchyma of patients with AD. Higher CXCL8 levels were found in brain tissue lysates from AD patients when compared to those of age-matched controls<sup>442</sup> and it has been described as the most highly induced chemokine in the brain of AD patients<sup>443</sup>; it is also found in CSF samples from patients with both MCI and AD<sup>444</sup>. CXCL1 is increased in the CSF of patients with MCI, very mild and mild AD was found to be one of the best predictive biomarkers after A $\beta$ 42, tau and phosphorylated tau<sup>445</sup>. In hippocampal tissue from AD patients, reactive astrocytes near amyloid plaques were CXCL5-immunopositive and transcript levels of CXCL5 were found to be three- to fivefold higher AD, increasing with successive Braak stages<sup>440,446</sup>.

A common feature of the CXCL1, CXCL5 and CXCL8 chemokines is their convergence on CXCR2 which is the common receptor for all three although CXCL8 may also bind to CXCR1<sup>428,447</sup>. CXCR2 is strongly expressed on neurons and high levels have been reported in dystrophic neurites in hippocampal tissue from AD patients<sup>448</sup>. CXCR2 is also expressed by microglia and astrocytes<sup>449</sup> albeit at low levels in un-activated cells. Once stimulated by cytokines such as IL-1 $\beta$  and TNF $\alpha$ , or *in vivo* after traumatic brain injury or demyelination, CXCR2 expression is greatly upregulated<sup>450</sup>.

While CXCR2 has been shown to be the most important receptor for chemotaxis<sup>451</sup> it may also have a variety of other functions which may be relevant to the pathophysiology of AD; in the main they may be considered beneficial effects. CXCR2 has been found to have a role in removal and thus, regulation of chemokines in the CNS<sup>452</sup> and in neurotransmission via modulation of calcium channel excitability<sup>453</sup> or enhancing glutaminergic activity<sup>454</sup>. It may also increase the resistance of astrocytes and neurons to cell death *in vitro*<sup>455,456</sup> and also displays neurotrophic effects via interaction with its ligands CXCL8 and CXCL1<sup>450</sup>.

In conclusion, there is a great deal of evidence to suggest that CXCL1, CXCL8 and CXCL5 and their common receptor CXCR2 are implicated in the pathogenesis of AD. Our findings suggest that the increased levels seen may be attributable to the E4/E4 genotype.

#### 6.2.4.2 MCP-1 (CCL2)

CCL2, also known as Monocyte Chemoattractant Protein-1 (MCP-1) was the first human chemokine to be characterised and is able to attract and activate cells of the monocyte lineage including monocytes, macrophages and microglia<sup>457,458</sup>.

In the CNS, CCL2 is predominantly produced by astrocytes and resident microglia<sup>459,460</sup>. It has also been found to be produced by neurons in response to brain ischaemia<sup>461</sup>. During normal conditions, expression is consistently low but is subject to significant upregulation during an inflammatory response<sup>462</sup> or as a result of CNS insults<sup>463</sup>.

In common with other studies, CCL2 was found to be one of the five most highly-expressed chemokines. Oddly, CCL2 was highly expressed in quiescent E3/E3 samples but not E4/E4 samples; after activation, levels from E3/E3 and E4/E4 cells were not significantly different. Given that CCL2 is known to be highly induced by TNF- $\alpha$  it seems likely that the high levels in quiescent E3/E3 cells might be spurious.

MCP-1 and its receptor CCR2 are sometimes considered the canonical chemokines associated with AD. CCL2 appears to have a detrimental role in AD pathogenesis, as its overexpression has been found in the brain parenchyma<sup>464,465</sup>. Increased levels have also been found in CSF; one study found that CCL2 levels appear to peak early in the disease course at the MCI stage and, when combined with CSF Tau, P-tau and A $\beta$ 42 levels, could be used to predict both future conversion to AD and the rate of cognitive decline<sup>466</sup>. Another study, however, found that CCL2 levels increased with disease severity and was also associated with the degree of temporal lobe and grey matter atrophy<sup>467</sup>. Increased CCL2 has also been found in plasma where levels correlated with cognitive decline with AD patients having higher levels than MCI patients and controls, and severe AD patients exhibiting the highest levels<sup>468</sup>.

Although increased levels of parenchymal and CSF CCL2 are found in AD, *deficits* of CCR2 (the CCL2 receptor) are associated with the disease. In a transgenic mouse model of AD, CCR2 deficiency accelerates memory deficits and disease progression<sup>469</sup>. This is

thought to be secondary to impaired macrophage/microglial recruitment which seems to be CCR2 dependent, and at least in the early stages of AD, may be beneficial facilitating the clearance of A $\beta$  and other debris<sup>470</sup>.

However, robust experimental evidence suggests that elevated CCL2 and subsequent recruitment of macrophages into the brain is detrimental. So it seems while the initial phase of macrophage recruitment may be beneficial, over time, activated glia induce a cycle of inflammatory mediator release (including chemokines) which causes a pathological astrogliosis and microgliosis that contributes to neuronal dysfunction and cell death<sup>471</sup>.

It could be that the CCR2 receptor, like other chemokines and chemokine receptors is pleiotropic, and has beneficial properties beyond its role in microglial chemotaxis; one example is that, in a mouse model using hippocampal slices, it induced stem-cell migration into sites of damage<sup>472</sup>.

Another possibility is that chronic exposure to excessive amount of its main ligand CCL2 causes downregulation of CCR2. Conversely, the initiating event might be lower expression of CCR2 which induces upregulation of CCL2. What is clear, however, is that increased CCL2 is consistently associated with AD but the mechanism by which it induces pathological change requires further investigation.

#### 6.2.4.3 *RANTES (CCL5)*

CCL5 is also known as regulated upon activation, normal T cell expressed and secreted (RANTES). CCL5 and its receptors (CCR1, CCR3 and CCR5) are expressed on endothelial cells, glia, and neurons throughout the brain<sup>473</sup>. There was a statistically significant increase in levels of CCL5 in activated E4/E4 cells compared to quiescent E4/E4 cells however the difference did not withstand multiple testing. The difference between activated E3/E3 and E4/E4 astrocytes was approaching significance (E3/E3 =0.15, E4/E4 =0.25; p=0.09).

Like most of the chemokines already described, the expression of CCL5 in quiescent astrocytes is low but is upregulated upon incubation with TNF- $\alpha$  or IL-1 $\beta$ <sup>474</sup>. CCL5 has been implicated in neurodegenerative diseases and elevated expression of CCL5 has been found in the microcirculation of patients with AD<sup>475</sup>. The functional role of RANTES in AD is not completely clear and many contradictory effects have been described<sup>470</sup> however increases in CCL5 contribute to the recruitment of immune cells associated with increased neuronal death<sup>475</sup>; it also induces a pro-inflammatory microglial phenotype not provoked by other chemokines<sup>476</sup>.

Arguably the best described effect of CCL5, however, is its influence on glutamate exocytosis in human neurons via activation of the CCR1, CCR3 and CCR5 receptors<sup>477</sup>. CCL5-mediated facilitation of the spontaneous outflow of glutamate from both isolated nerve terminals and slices was prevented by a broad-spectrum antagonist of the CCR1, CCR3, and CCR5 subtypes, confirming the involvement of these receptors<sup>478</sup>. A further study found that glutamate exocytosis from cortical synaptosomes was prevented by the selective CCR1 antagonist BX513 and by the selective CCR5 antagonist DAPTA, compatible with the involvement of CCR1/CCR5 heterodimers in the process of glutamate exocytosis<sup>479</sup>. Furthermore, CCR5 deficiency results in enhanced long-term potentiation (LTP) and learning/memory performances, while neuronal CCR5 overexpression causes memory deficits<sup>480</sup>.

Like CCL5 itself, the CCR5 receptor is expressed at low levels under physiological conditions but is rapidly upregulated to abnormal pathological levels upon stimulation with TNF- $\alpha$  and IL-1 $\beta$  which may be acting in an autocrine (released by the astrocytes themselves) or paracrine fashion (released by neighbouring microglial cells). The net effect is a persistent adaptation leading to a significant increase in the expression the CCR proteins<sup>462</sup>. This cascade of events occurs during inflammation, so that the overexpression of the receptors targeted by CCL5 is an event intimately linked to pathological conditions<sup>477</sup>. Although the higher expression of CCL5 was a non-significant result the direction of the relationship and the findings described above suggest that this might be a real effect which warrants further exploration.

#### 6.2.4.4 *IL-6 and TNF- $\alpha$*

IL-6 and TNF- $\alpha$  (along with IL-1 $\beta$ ) are considered the three main pro-inflammatory cytokines. The general consensus is that IL-6 and TNF- $\alpha$  acting in concert lead to active gliosis, mediate inflammation and contribute to neuropathology and eventually neurodegeneration<sup>481,482</sup>.

To recap, there were significant differences in TNF- $\alpha$  levels pre and post treatment in both E3/E3 and E4/E4 genotypes however only the difference in E4/E4 remained significant after the Benjamini-Hochberg test was applied. However, the difference between 'A1' E3/E3 and E4/E4 astrocytes was not-significant (E3/E3 =3.64, E4/E4 5.65;  $p=0.148$ ). IL-6 demonstrated a significant increase post treatment in E3/E3 cells but not in E4/E4 cells which did not remain significant after the Benjamini-Hochberg test. In activated 'A1' astrocytes, IL-6 was the only cytokine to show a significant difference (at the uncorrected  $p<0.05$  level) between APOE genotypes (E3/E3 = 3.64, E4/E4=0.96;  $p=0.043$ ); unexpectedly, however, the levels were greater in E3/E3 cells than E4/E4 cells.

Under physiological conditions, levels of CNS IL-6 and TNF- $\alpha$  remain low however they increase in response to CNS injury and inflammation<sup>481,483</sup>. Several laboratories have reported elevated IL-6 expression at both the mRNA and protein levels in the brains of AD patients; it is also found in diffuse (rather than neuritic) plaques suggesting that the accumulation of IL-6 may be a relatively early event (reviewed in Zhao and Schwartz, 1998).

The results presented above showed expression of IL-6 was reduced in activated E4/E4 cells compared to E3/E3 cells which may appear spurious or contradictory however the role of IL-6 (and indeed TNF- $\alpha$ ) is more nuanced than being simply 'pro-inflammatory'. The pleiotropic nature of cytokines has been discussed several times in the preceding sections and beneficial roles for IL-6 within the CNS has been described. In a rat model of ischaemia induced by occlusion of the middle cerebral artery injection of IL-6 into the ischaemic region significantly reduced brain damage. IL-6 was also found to

promote survival of cultured basal forebrain cholinergic neurons<sup>485</sup>. It has also been shown to stimulate nerve growth factor (NGF) production in astrocytes in addition to acting as a neurotrophic itself and acting synergistically with NGF<sup>486,487</sup>. It has also been found to induce neuronal differentiation in pheochromocytoma PC12 cells<sup>488</sup>. There are plausible reasons, therefore, why IL-6 expression might be reduced in activated E4/E4 astrocytes when compared to their E3/E3 counterparts but repetition of these experiments would need to be undertaken to say for sure.

Murine and human studies have consistently shown increases in TNF- $\alpha$  levels in AD; in one study TNF- $\alpha$  in the CSF of patients with AD was, on average, 25-fold higher than controls, with levels related to cerebral neuronal damage, apoptosis, and to clinical variables of dementia<sup>489</sup>. Furthermore, a large body of evidence supports that ApoE4, either recombinantly applied or endogenously expressed, confers an increase in pro-inflammatory cytokine production across rodent and human species, in blood, brain, and microglia (reviewed in Fernandez, 2019<sup>264</sup>); the effects of *APOE* genotype on astrocytic production of TNF- $\alpha$  has been largely neglected. TNF- $\alpha$  inhibitors, which are widely used in a variety of inflammatory conditions, have shown some promise in treating AD and a recent review called for a large-scale trial to assess their effectiveness<sup>490</sup>.

#### 6.2.4.5 *Common pathways: NF- $\kappa$ B signalling and tau-phosphorylation*

While the pleiotropic nature of cytokines and their differential expression at various points in the neurodegenerative process makes it difficult to draw conclusions about the meaningfulness of some of our results, what does appear interesting is the convergence on common pathways. The convergence of the CXCL1, CXCL5 and CXCL8 chemokines on the CXCR2 receptor has already been discussed but there are two pathways that link the majority, if not all, of the most highly upregulated chemokines, namely their common effects on NF- $\kappa$ B signalling and tau-phosphorylation.

#### 6.2.4.6 *Tau-phosphorylation*

Neurofibrillary tangles (NFTs) containing phosphorylated tau are one of the pathological hallmarks of AD and, as described in Chapter 1, correlate with cognitive deficits more closely than A $\beta$  burden. The first common thread linking some of the chemokines and compounds upregulated in 'A1' astrocytes is their ability to cause tau hyperphosphorylation although the precise mechanisms by which they do so are different with several tau kinases, including cdk5/p25, GSK-3 $\beta$ , and p38-MAPK implicated.

Several studies have shown an increase in tau phosphorylation in response to TNF- $\alpha$ . Gene delivery of TNF- $\alpha$  into the CNS of triple transgenic AD mice induced microglial activation and enhanced intracellular levels of hyperphosphorylated tau<sup>491</sup>. Another study showed that either activated microglia producing TNF- $\alpha$  or the glia-derived cytokine TNF- $\alpha$  alone were able to induce the accumulation of tau preferentially in neurites<sup>492</sup>.

Administration of physiological doses of IL-6 to hippocampal neurons resulted in increased hyperphosphorylated tau which the authors attributed to an increased activity of CDK5/p35 complex as inhibition of CDK5 activity with butyrolactone-I prevented the appearance of hyperphosphorylated tau<sup>493</sup>.

The CXCR2 receptor ligands have also been shown to cause tau hyperphosphorylation. While the effects of CXCL5 and CXCL8 interaction with CXCR2 have not been investigated with respect to tau hyperphosphorylation, CXCL1 (GRO $\alpha$ ) interacting with CXCR2 is known to be a trigger for the ERK1/2 and PI-3 kinase pathways in murine primary cortical neurons<sup>494</sup> while in aged mice CXCL1-induced activation of GSK3 $\beta$  led to phosphorylation of tau<sup>495</sup>.

While experimental evidence of direct hyperphosphorylation of tau by CCL2 and CCL5 has not been observed in the literature, increased levels of CCL2 has been associated with increases in pathogenic tau<sup>496</sup>. A positive correlation between the levels of CCL2

and p-tau in CSF in AD patients has also been noted<sup>497</sup>. To date, there are no published reports describing the effects of CCL5 deficiency on tau pathology in a transgenic tau model but it has been noted that this is an important gap in current knowledge which would help clarify the role of CCR5 ligands in AD development<sup>498</sup>.

To conclude, microglial activation is known to induce tau phosphorylation and aggregation<sup>499</sup>. It is possible that at least some of this effect is mediated by the induction of the 'A1' astrocytic phenotype and its attendant upregulation of chemokine and cytokines. In turn, it appears that this pro-inflammatory phenotype may be potentiated by the E4/E4 genotype suggesting another way in which it may be contributing to the pathological process seen in AD.

#### 6.2.4.7 *NF-κB signalling*

The second, more robust, connection between the chemokines upregulated in 'A1' astrocytes is NF-κB signalling. Nuclear factor-kappa B (NF-κB) signalling is a key regulator of innate immunity via gene regulation. It is implicated in systemic aging, inflammation and apoptosis as well as the pathogenesis of several neurodegenerative diseases<sup>500,501</sup>.

TNF-α is known to be one of the key activators of the NF-κB family of transcription factors so it is unsurprising that the induction of the 'A1' phenotype by, amongst other things, TNF-α results in increased expression of cytokines whose genes are regulated by NF-κB. What is interesting, however, is that this pathway also links to EAAT2 and GFAP which are the two proteins that may underlie the differences seen in, respectively, glutamate uptake and phagocytosis. Furthermore, these effects appear to be influenced by *APOE* genotype.

The NF-κB family of transcription factors consists of five different subunits (c-Rel, p65/RelA, p50, RelB, and p52), which interact to form transcriptionally active homo and heterodimers<sup>502</sup>. Inactive NF-κB dimers are sequestered in the cytoplasm bound to the IκB inhibitory proteins. NF-κB-inducing stimuli activate the IκB kinase complex

resulting in sequential phosphorylation, ubiquitination, and degradation of I $\kappa$ B. Upon the detachment of the I $\kappa$ B, the exposure of DNA-binding domain and nuclear localisation sequence allows the NF- $\kappa$ B dimer to translocate to the nucleus to bind the target gene promoter regions<sup>503</sup>.

NF- $\kappa$ B is expressed in the CNS in neurons and glial cells existing mostly as p50/p65 heterodimers<sup>503</sup>. In glial cells, basal NF- $\kappa$ B activity is very low. Under certain conditions NF- $\kappa$ B-dependent gene expression in glial subtypes can have beneficial outcomes in maintaining brain health but chronic or excessive glial activation of NF- $\kappa$ B has been shown to be neurotoxic<sup>504</sup>.

TNF- $\alpha$  is probably the most well-studied activator of NF- $\kappa$ B<sup>412</sup>. TNF- $\alpha$  is exquisitely linked with NF- $\kappa$ B, serving as both an activator and its receptor as a gene target of NF- $\kappa$ B<sup>413</sup>. The interaction of IL-6 and NF- $\kappa$ B are similarly well known<sup>505</sup>. In addition, the five chemokines most strongly upregulated in our 'A1' astrocytes (CXCL1, CXCL5, CXCL8, CCL2 and CCL5) are also direct targets of NF- $\kappa$ B<sup>430</sup>. Post-mortem studies of the AD brain generally indicate increased expression and/or activation of NF- $\kappa$ B (specifically the p50 and p65 sub-units), particularly in regions preferentially affected in AD such as the hippocampus and entorhinal cortex; immunohistochemical analysis has also indicated co-localisation of p50 and pathological tau and upregulation of p50 in NFT-containing neurons (reviewed in Snow and Albeni, 2016).

The final reason for supposing a role for NF- $\kappa$ B in the pathogenesis of AD is its impact on the two most important risk genes; *APOE* and *TREM2*. Promoter analysis and functional studies link expression of each of these genes to regulation by NF- $\kappa$ B (reviewed in Dresselhaus and Meffert, 2019). Conversely, the RelA (v-rel avian reticuloendotheliosis viral oncogene homolog A/nuclear factor NF- $\kappa$ B p65 subunit) subunit of the NF $\kappa$ B complex has been found to immunoprecipitate with ApoE3, as well as ApoE4; however, only ApoE4 led to the translocation of RelA into the nucleus, suggesting the possibility that ApoE affects NF $\kappa$ B-mediated gene transcription, as well as being a target of NF $\kappa$ B itself<sup>410</sup>.

### 6.3 Conclusions

Although the lack of significant differences between *APOE* genotypes in reactive astrocytes was disappointing, the cytokine arrays did provide some useful information.

First, the results demonstrated that induction of the 'A1' astrocytic phenotypes leads to massive upregulation of several cytokines demonstrating the success of differentiating a quiescent, 'resting' phenotype. Second, when activated, the secretory profile of the astrocytes was highly congruent with published data giving further weight to the assertion that the differentiation described in this thesis produces prototypic astrocytes successfully.

The results also suggest that the E4/E4 genotype may be associated with a potentiated inflammatory response to microglial induction of the 'A1' astrocytic phenotype. The pattern of cytokine upregulation is not random with the most increased falling into particular groupings. Perhaps most intriguing, however, is the suggestion that *APOE* genotype might be affecting the expression of TNF- $\alpha$  which is at the very heart of the inflammatory process. Very little work has been undertaken looking at the specific relationship between *APOE* genotype and TNF- $\alpha$  production; should such an effect be proven, it would allow appropriate targeting of trials of anti-TNF- $\alpha$  treatments.

The main weakness of this work is the lack of repeat experiments; the data above are based on only two separate differentiations as the costs of the antibody membranes precluded further replications. Furthermore, although, having 42 cytokine targets provides a great deal of data it can be difficult to find significant effects once multiple testing is taken into account increasing the risk of Type II errors. In fact, it has suggested that multiple testing corrections should not be undertaken for such arrays leaving the reader to draw their own conclusions about the validity of the data.

The key strength of using such cytokine arrays, however, is that they suggest where future work might be best directed and, in particular, this work has highlighted NF- $\kappa$ B activity as a potential target. Further work is needed to determine the extent to which

NF- $\kappa$ B regulates ApoE4 and whether these signalling pathways are impacted in AD. However, the dual functions of NF- $\kappa$ B in the innate immune response and cognitive processes, its upregulation in ageing and neurodegenerative conditions, its intimate relationship with TNF- $\alpha$  plus its purported effects on *APOE* and *TREM2* regulation suggest that further investigation of this potential therapeutic target is warranted.

## 7 The effect of *APOE* genotype on cholesterol metabolism

One of the best known physiological functions of ApoE is its role in lipid metabolism, transporting cholesterol, mainly from astrocytes to neurons, where it is an essential component in processes that are vital to maintaining cognitive integrity including axonal growth, synaptic formation and remodelling<sup>170,171</sup>.

Lipid and cholesterol processing mechanisms have been consistently implicated in the pathogenesis of SAD by pathway analyses<sup>127,129,172</sup>. This molecular cascade involves, including *APOE*, 6 of the top 10 genetic risk factors for SAD identified by GWAS in the past 10 years<sup>507</sup>. These genes are clusterin (*CLU*, also known as ApoJ) which like ApoE acts as a cholesterol transporter; *PICALM* and *BIN1* which are both implicated in receptor mediated endocytosis (RME) involved in the internalisation and transport of lipids; *ABCA7* which promotes phospholipid (but not cholesterol) efflux; and *SORL1* which is a member of the LDL receptor family. A number of other genes involved in this pathway (*ACAT*, *LRP*, *LPL*, *LDLR*, *ABCA1*, *CETP*) have also been associated with SAD in small genetic and functional studies (reviewed in 7) however the results are contradictory and none have been found to have genome-wide significance.

Using the isogenic astrocyte model characterised in Chapters 3 and 4, this chapter describes phenotypic differences between E3/E3 and E4/E4 cells related to cholesterol pathways and attempts to explain the possible mechanisms at play.

### 7.1 Cholesterol homeostasis in the CNS

The brain is the most cholesterol-rich organ in the human body. Although it represents only 2% of the average body mass, it contains approximately 20% of the body's cholesterol<sup>509</sup>. After myelination, the bulk of cholesterol in the adult brain is maintained in myelin with minimal loss (half-life up to 5 years) but around 30% is metabolically active and found in the membranes of glial cells and neurons<sup>510</sup>. Maintenance of this large surface area plus the formation of new dendrites requires

the continuous addition of new membrane and thus cholesterol<sup>230</sup>. So while the overall turnover of cholesterol in the CNS is very low, it has been estimated that in individual neurons and astrocytes it may be up to 20% per day depending on the brain area and the precise cell type<sup>510</sup>.

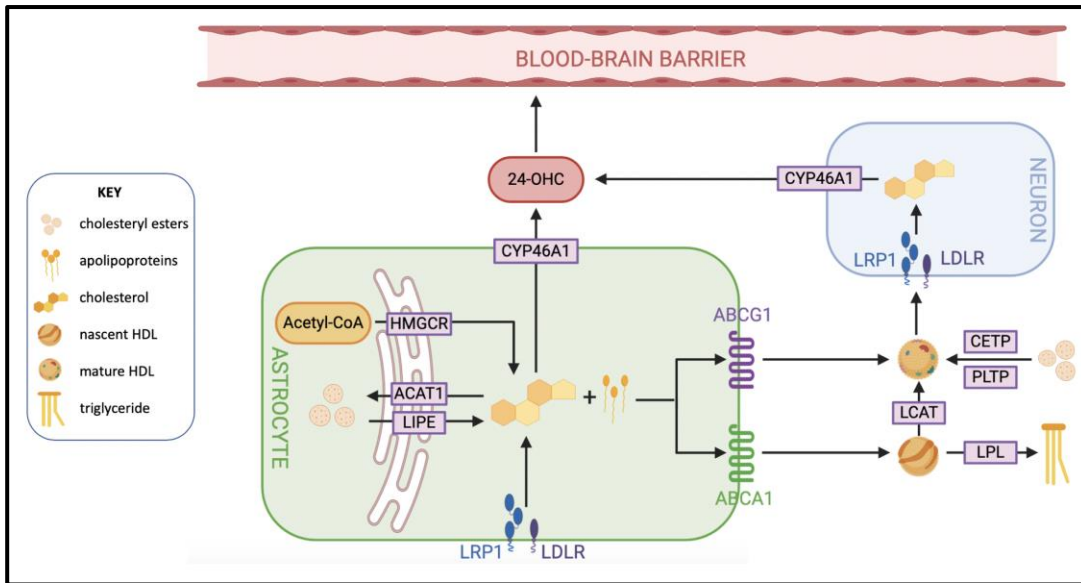
Perturbations in cholesterol homeostasis have been described in normal aging as well as a number of neurodegenerative conditions<sup>511</sup>. Post-mortem examination of human hippocampi reported an age-related decline of specific cholesterol precursors and concluded that cholesterol synthesis decreases with age<sup>512</sup>. In addition, brain cholesterol levels are substantially reduced in the hippocampus and cortical areas in AD brains compared to controls<sup>173,174</sup>. Defects in CNS cholesterol homeostasis are also causal in some CNS syndromes including Niemann-Pick type C disease, a fatal cholesterol storage disease caused by mutations in the NPC-1 or NPC-2 gene products, and Smith-Lemli-Opitz syndrome, a potentially fatal condition caused by a defect in the 7-dehydrocholesterol-7-reductase, causing cholesterol to be replaced with 7-dehydrocholesterol. Interestingly, Niemann-Pick C (NPC) shows Alzheimer-like tau pathology in youth or adolescence without the amyloid plaque deposition<sup>513</sup>.

#### 7.1.1 Cholesterol synthesis

When the blood-brain barrier (BBB) is intact, dietary and hepatic cholesterol cannot cross it therefore the brain requires *de novo* cholesterol synthesis which occurs primarily in astrocytes<sup>137,170</sup>. Although neurons are capable of producing cholesterol, this tends to be confined to early development. When synaptogenesis accelerates, and cholesterol requirements increase, the production is 'outsourced' to astrocytes where the process is more efficient<sup>171,231,232</sup>.

The regulation of CNS cholesterol metabolism has largely been extrapolated from the model characterised in the cardiovascular system and several aspects of CNS-specific cholesterol metabolism have not been fully elucidated. A simplified scheme demonstrating the key mechanisms and the genes involved is shown in Figure 7.1.

**Figure 7.1: cholesterol metabolism in the CNS.**



Cholesterol is derived from acetate in the endoplasmic reticulum (ER), with conversion of Acetyl-CoA via HMGCR the rate limiting step. Cholesterol bound to lipoproteins may also enter cells via the LDLR and LRP1 receptors. Excess cholesterol is converted to cholesteryl esters (CE) by ACAT1; hormone sensitive lipase (encoded by LIPE) performs the reverse function. Cholesterol and apolipoproteins combine to form lipoproteins which leave astrocytes via the concerted action of ABCA1 and ABCG1. These high density lipoproteins (HDL) particles then undergo maturation likely involving the activity of LCAT, CETP, PLTP and LPL which tend to add cholesteryl esters and remove triglyceride. Cholesterol may also leave the cell after being converted to 24S-hydroxycholesterol by CYP46A1 which can cross the blood brain barrier.

Cells sense their level of cholesterol through the membrane-bound sterol regulatory element-binding protein (SREBP) which acts to upregulate cholesterol synthesis<sup>514</sup>. Cellular cholesterol is synthesised primarily in the endoplasmic reticulum (ER) from acetate in a process that involves over 30 enzymatic steps. It is initiated by the conversion of acetyl-CoA to 3-hydroxy-3-methylglutaryl-CoA (HMG-CoA) and then irreversibly converted to mevalonate by the rate-limiting enzyme, HMG-CoA reductase (HMGR). This is followed by multi-step enzymatic reactions that sequentially convert mevalonate to cholesterol in a 19-step process, involving two pathways the Bloch and Kandutsch-Russel pathways which operate predominantly in astrocytes and neurons, respectively<sup>515</sup>.

### 7.1.2 Cholesterol efflux and transport

Apolipoproteins are proteins that bind lipids to form lipoproteins. Four major classes of lipids are found in lipoproteins: triacylglycerols (TGs), unesterified cholesterol, cholesteryl esters (CE) and phospholipids<sup>516</sup>. The various apolipoproteins tend to bind the four classes of lipid to different degrees. ApoE is one of a subset of plasma apolipoproteins that are also present in the CNS and is regarded to be the quantitatively most important<sup>511</sup>. Others include apolipoprotein J/clusterin (APOJ/CLU), apolipoprotein D (APOD) and Apolipoprotein A1 (APOA1). The main source of apolipoproteins in the CNS is astrocytes except for APOA1 which is synthesised in endothelial cells of brain capillaries and by the choroid plexus epithelium<sup>515</sup>. ApoE is also produced by microglia and neurons although at much lower levels than in astrocytes<sup>145</sup> however neuronal synthesis is upregulated with aging and under stress<sup>146–148</sup> which is thought to redistribute lipids and strengthen ApoE-mediated signalling for neuronal and synaptic repairs<sup>137</sup>.

Excess cholesterol is sensed by the nuclear Liver X Receptor (LXR), which upregulates a suite of genes that control expression of proteins that facilitate cholesterol efflux including ApoE, ABCA1 and ABCG1. Cholesterol efflux from astrocytes (and neurons) is enabled by two mechanisms. The first is passive diffusion, in which cholesterol is desorbed down the concentration gradient onto acceptor molecules. The second is an apolipoprotein-dependent pathway involving release via ATP-binding cassette proteins<sup>517</sup>.

The two key ATP-binding cassette proteins are ABCA1 and ABCG1 which coordinate the mobilisation of cholesterol from cytoplasmic pools to the cell surface membrane<sup>518</sup>. ABCA1 catalyses the initial transfer of lipids onto lipid-free apolipoproteins to form nascent particles. Nascent astrocyte particles contain little core lipid, are primarily discoidal in shape, contain ApoE and ApoJ<sup>519</sup> but do not contain cholesteryl esters<sup>520</sup>. In contrast, the mature lipoproteins found in CSF are the size and density of plasma HDL, are spherical, contain core lipid and up to 60% esterified cholesterol<sup>521</sup>. This difference between astrocyte-derived and CSF-derived

particles is explained by a maturation process; nascent particles act as acceptors for additional cholesterol removed from cells by a second phase of efflux mediated by ABCG1 which allows them to become fully-lipidated, mature high-density lipoproteins (HDL)<sup>522,523</sup>.

The final part of the maturation process is achieved by the addition of CEs to HDL. This is thought to occur via the action of three different enzymes and proteins: Lecithin-cholesterol acyltransferase (LCAT), cholesteryl ester transfer protein (CETP) and plasma phospholipid transfer protein (PLTP). The best elucidated of these is the action of LCAT which is an enzyme found in the interstitium and CSF<sup>524–526</sup>. It converts free cholesterol on the surface of HDL to CEs, which then enter the hydrophobic core of the HDL particle and allows for greater unesterified cholesterol efflux from cells to the surface of HDL<sup>527</sup>. This process relies upon ABCA1 and ApoE as deficiency of either results in lipid-poor HDL particles that are ineffective LCAT substrates (Hirsch-Reinshagen et al., 2009).

In contrast to LCAT, the action of CETP in the CNS is poorly understood and while some studies have detected it in CSF<sup>529</sup> others have not<sup>524</sup>. In plasma, CETP action results in the net transfer of CE from HDL to LDL (in exchange for triglycerides) which leads to smaller HDL particles enabling glomerular filtration, urinary excretion and thus lower plasma HDL levels; animals that lack CETP have very high HDL levels, very low LDL and thus decreased cardiovascular risk. In the CNS, sources suggest CETP matures HDL particles by transferring CEs to them<sup>528,530</sup> which would likely increase their size as the size of HDL particles corresponds to the layers of cholesteryl ester in the core<sup>531</sup>. This appears to be different to CETP's role in plasma but may be due to the lack of LDL within the CNS.

There may also be a third process involving plasma phospholipid transfer protein (PLTP). PLTP is one of the main factors regulating the size and composition of HDL in plasma and plays an important role in controlling peripheral HDL levels<sup>532</sup>. Although it is unclear whether it performs the same role in the CNS, it has been found in most

areas of the brain, predominantly in glial cells, at concentrations that suggest local synthesis<sup>533</sup>.

Another enzyme which appears to play an important part in this maturation process is lipoprotein lipase (LPL) however its precise function within the CNS is enigmatic.

In plasma, LPL, hydrolyses triglycerides in VLDL particles resulting in smaller, cholesterol-enriched intermediate-density lipoproteins and finally cholesterol-rich, triglyceride-poor LDLs<sup>516</sup>. However, as VLDL and LDL are not present in the CNS, it has been speculated that it may undertake a similar role on HDL particles, increasing the lipid content and size of lipoproteins by processing triglycerides in exchange for cholesterol<sup>516,534</sup>. Alongside CETP, PLTP and LCAT, LPL seems to be part of an important delipidation/esterification process which increases the cholesterol binding capacity of lipoproteins thus facilitating reverse cholesterol transport.

### 7.1.3 Cholesterol endocytosis

Cholesterol is taken up by cells (mainly neurons and astrocytes) through receptor-mediated endocytosis of ApoE by LDL receptors. There are around 10 members of this family but the two main receptors involved in cholesterol endocytosis are the low-density lipoprotein receptor LDLR and LRP1. LDLR is the prototypic member of the LDLR family. It is localised on the outer cellular membrane of several cells and its most important action is the internalisation of lipoproteins, removing cholesterol and cholesteryl esters from the circulation<sup>530</sup>. In fact, LDLR has no known ligand other than ApoE in the CNS<sup>535</sup> and LDLR knockout mice show memory and learning deficits<sup>156</sup>.

LRP1 is expressed highly in neurons and to a lesser degree in glia whereas the reverse is true for LDLR<sup>137</sup>. In murine models, LRP1 gene deletion leads to embryonic death. In cellular models LRP1 deletion leads to a reduction in cholesterol and triglyceride levels, synaptic and dendritic spine loss and neuronal cell degeneration<sup>536</sup>. ApoE-lipoprotein particles secreted by astrocytes have higher affinity for LDLR than for LRP1. In contrast, mature CSF-isolated HDL particles bind more avidly to LRP1 than to LDLR<sup>137</sup>.

Following receptor-mediated endocytosis, the ApoE-containing HDL-like particles are hydrolysed in the lysosome, and the remaining ApoE is either degraded intracellularly or re-lipidated in the secretory pathway or at the cell surface<sup>537</sup>. This releases cholesterol that can be used for synapse formation and dendritic proliferation.

#### 7.1.4 Cholesterol storage

Accumulation of free cholesterol is toxic for cells<sup>538</sup> so levels are strictly maintained by ensuring a balance between synthesis and removal. As described above, overall regulation of cholesterol metabolism is under the control of two main genes; SREBP activation increases the transcription of gene products that function to increase cellular cholesterol levels whereas Liver X Receptor (LXR) activation, encoded by the genes NR1H2 and NR1H3, facilitates processes leading to cholesterol removal from cells<sup>539</sup>.

Cholesterol may efflux from the cell (as described above) or be stored within it. About 1% of the total cholesterol content of the brain exists in its esterified form<sup>540</sup> also called lipid droplets. These cytosolic lipid droplets are formed by the esterification of cholesterol by acylcoenzyme A:cholesterol acyltransferase 1 (ACAT1, also known as SOAT1); in a murine model, genetic reduction of ACAT1 decreased the concentration of cholesterol esters in the brain by 86%<sup>541</sup>. Although ACAT1 is thought to be more active in neurons than in glial cells<sup>542</sup> it becomes active in astrocytes when exogenous cholesterol is overloaded or when ApoE is lacking<sup>543</sup>. CEs may also be converted back to cholesterol by the action of hormone sensitive lipase (also known as cholesterol ester hydrolase) encoded by the LIPE gene<sup>539</sup>.

Cholesterol may also undergo CYP46A1-dependent<sup>544</sup> conversion to the oxysterol 24S-hydroxycholesterol (24-OHC), which, unlike cholesterol itself can freely cross the blood-brain barrier (BBB) to enter the plasma where it is picked up by plasma lipoproteins, transported to the liver, metabolised to bile acids, and excreted<sup>511</sup>. Furthermore, as 24S-Hydroxycholesterol is a potent activator of the LXRs it may also indirectly stimulate efflux of cholesterol from astrocytes via a mechanism involving

ABCA1<sup>511,545</sup>. Although conventional wisdom suggests that CYP46A1 is only found in neurons, some CYP46 immunoreactivity in glial cells has also been reported in post-mortem samples from patients who had died with advanced SAD<sup>546</sup>.

## 7.2 Results

Astrocytes were differentiated from NPCs for 8 weeks using the methods described in Chapter 4. Each isogenic line was seeded at the same density 3 days before harvesting and fed with serum-free media. After 72 hours, cells and media were harvested for analysis; 100uL of media was retained to perform BCA for normalisation of results. The results below represent data from either two or three separate differentiations.

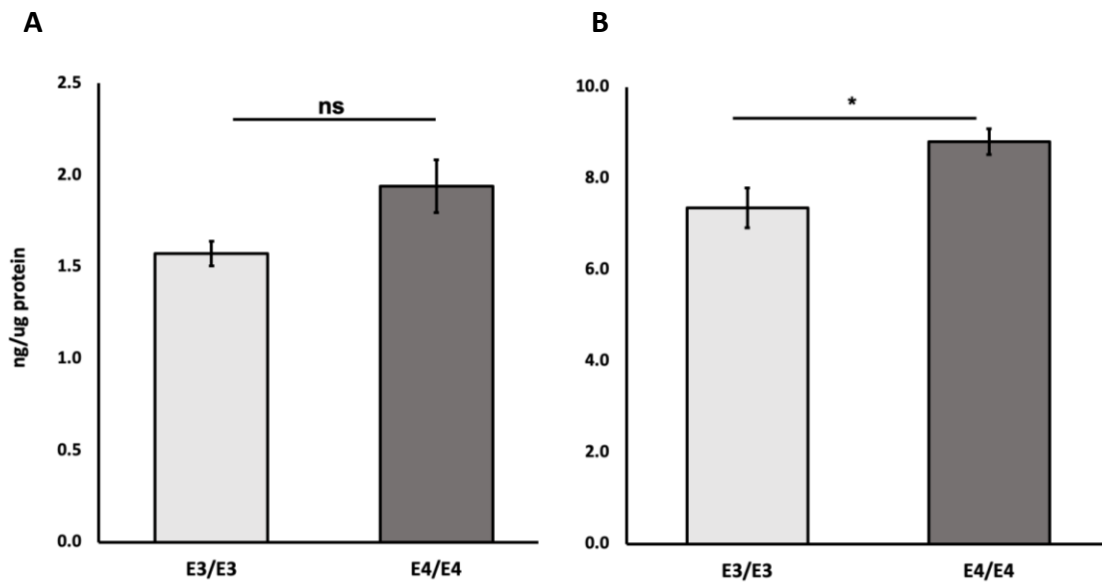
### 7.2.1 Cholesterol levels

Levels of cholesterol and cholesteryl esters in both astrocyte lysates and media were measured using High Performance Liquid Chromatography (HPLC) (full methods described in Chapter 2.2.8). Consistent with recently published data, levels of both free, intracellular and effluxed cholesterol were higher in the E4/E4 samples compared to the E3/E3 samples; approximately 20% higher in cell lysates ( $p=0.058$ ) and 23% higher in media ( $p=0.046$ ) – see Figure 7.2A&B. These results accord with other isogenic *APOE* studies which found a 20% increase in intracellular cholesterol<sup>263</sup> and 20-30% in effluxed cholesterol<sup>263,547</sup> in *E4/E4* astrocytes compared to *E3/E3*.

Free (ie unesterified) cholesterol levels in cells were also tested using filipin staining and corrected total cell fluorescence (CTCF) (see Section 2.2.2 for full methods) in untreated cells and those that had been subject to a cholesterol challenge of 10ug/ml 24 hours prior to staining. This concentration was chosen as it was the ‘physiological’ level found in the samples above and was also found to be efficacious in previous studies<sup>170,548</sup>. Results were normalised to those of untreated E3/E3 cells.

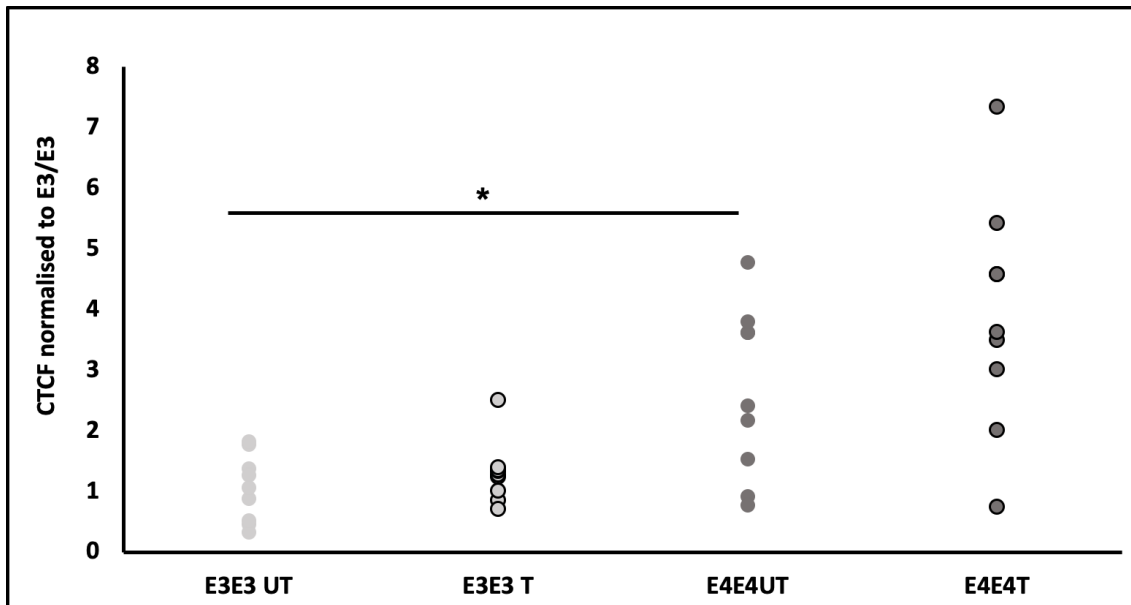
Average filipin fluorescence in untreated E4/E4 astrocytes was 2.64 times greater than in untreated E3/E3 astrocytes ( $p=0.02$ ). There was no significant difference in filipin levels in treated and untreated E3/E3 astrocytes ( $p=0.957$ ) whereas treated E4/E4 astrocytes had filipin levels almost 50% higher than in untreated E4/E4 astrocytes with the result approaching significance ( $p=0.085$ ); results are shown in Figure 7.3.

**Figure 7.2: cholesterol levels in A) astrocyte lysates and B) astrocyte media.**



Data show mean values +/- SD and are from 3 separate differentiations, with three biological replicates for each differentiation.

**Figure 7.3: filipin fluorescence in untreated and cholesterol treated astrocytes.**



Data shown are from 3 separate differentiations. Each dot represents a single field containing, on average, measurements from 18 astrocytes.

### 7.2.2 Cholesteryl ester levels

In addition to cholesterol levels, cholesteryl esters were measured in lysates and media using High Performance Liquid Chromatography (HPLC) (methods described in Chapter 2). Of the 12 cholesteryl esters tested, in cell lysates 9 were higher in E4/E4 astrocytes and 3 were higher in E3/E3 astrocytes (Figure 7.4). There was a general trend for higher levels of short-chain CEs in E4/E4 samples with the trend reversed for the three longest chain CEs tested (CE20:4, CE20:5 and CE22:6) where levels were higher in E3/E3 samples. However, none of these results reached significance.

In media, results were remarkably consistent with all species of CE, on average, 79% higher (range 72-85%) in E4/E4 samples than E3/E3 samples (8 of the 12 cholesteryl esters significantly so at the  $p < 0.05$  level after application of the Benjamini-Hochberg multiple comparison test); see Figure 7.5. When the ratio of cholesterol and cholesteryl esters in lysate and media for each genotype were compared, the lysate:media ratio of cholesterol itself was very similar in E3/E3 and E4/E4 samples (0.216 and 0.220 respectively). For CEs, however, the ratio was higher in E4/E4 samples in all but the shortest CE (Figure 7.6).

### 7.2.3 Gene expression in cholesterol metabolism pathways

In order to explain the increases in cholesterol and cholesteryl ester levels in E4/E4 samples, RNA was extracted from cells from the same differentiations used to measure cholesterol and cholesteryl esters and underwent RT-qPCR. The expression of several genes in cholesterol metabolism pathways were measured in E3/E3 and E4/E4 astrocytes (Figure 7.7). Means were compared using T-test and several genes, denoted by asterisks, were significantly different at the  $p < 0.05$  level after the Benjamini-Hochberg multiple comparison test was applied. The genes, their functions and the expression results are outlined in Table 7.1. A pictorial representation of these changes is found in Figure 7.8.

Figure 7.4: cholesteryl ester levels in astrocyte lysates.

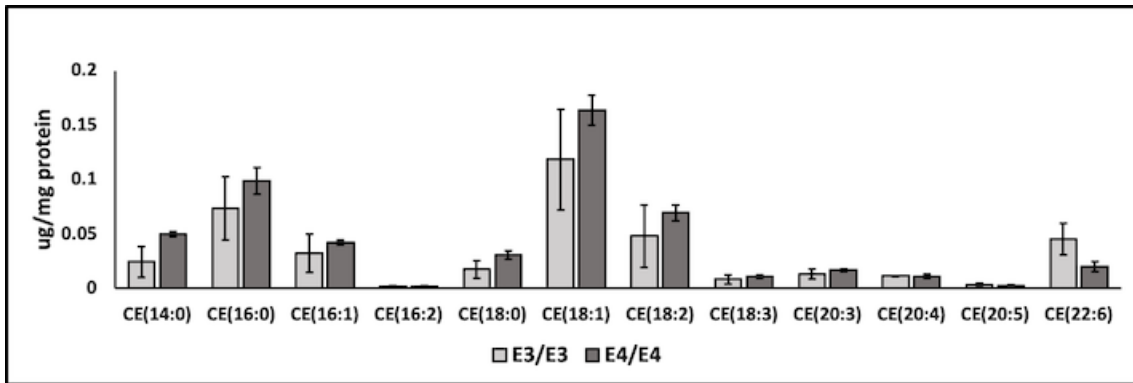


Figure 7.5: cholesteryl ester levels in astrocyte media.

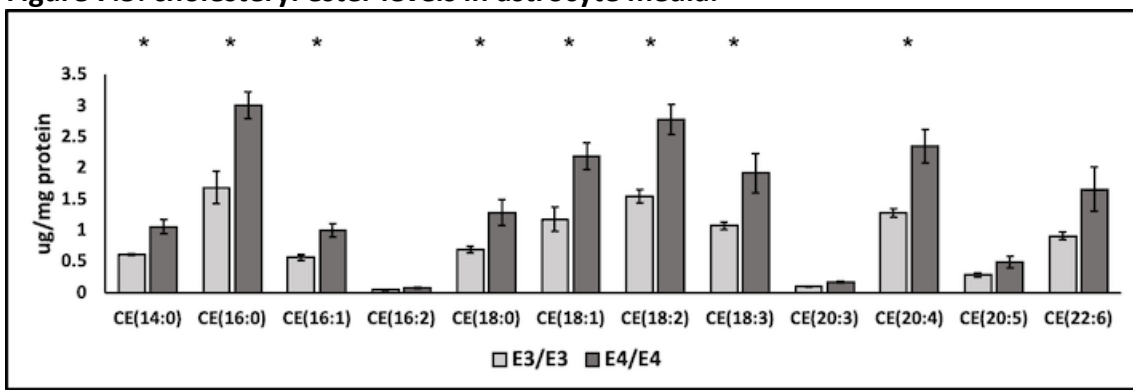


Figure 7.6: ratio of CE in media:lysate in E3/E3 and E4/E4 samples.

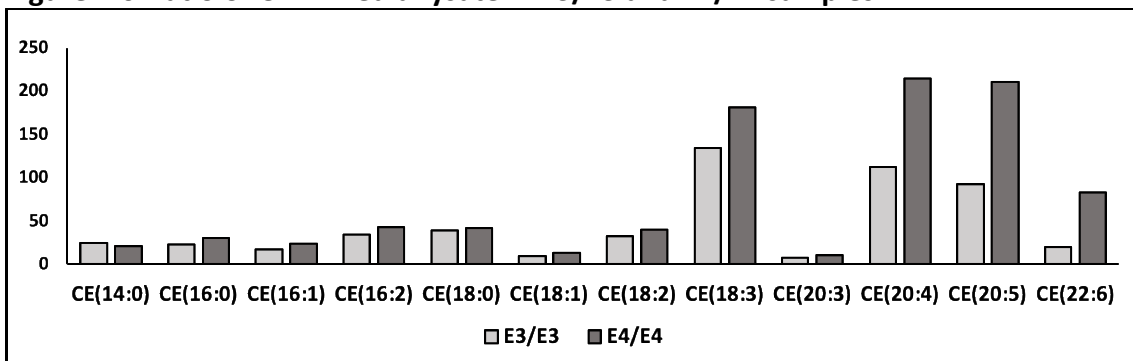
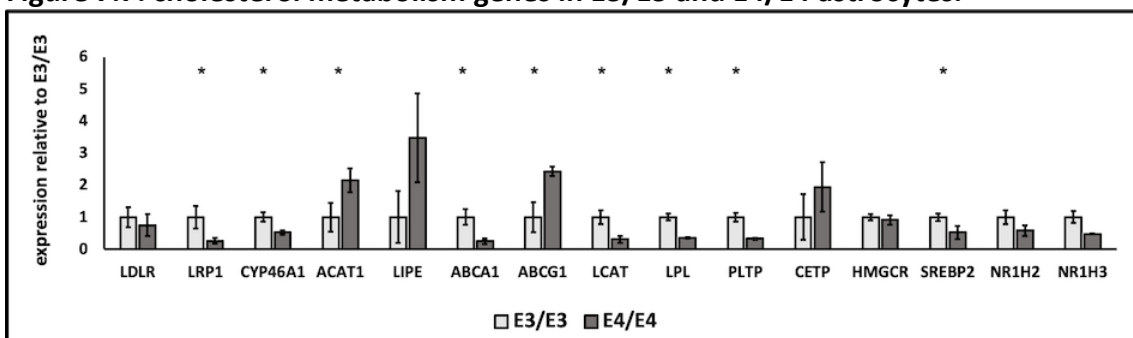


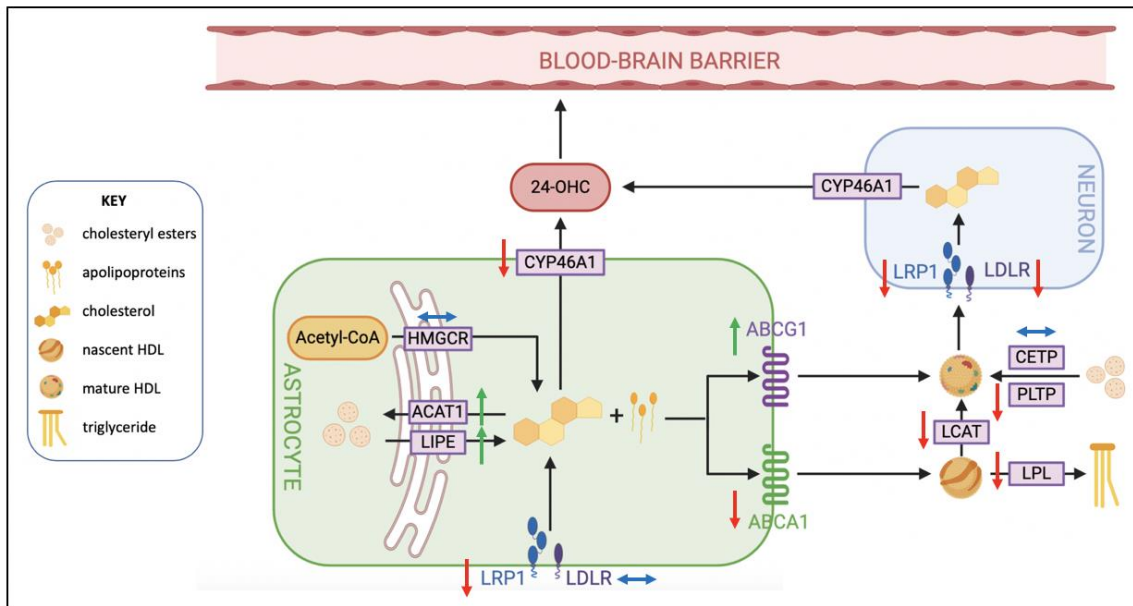
Figure 7.7: cholesterol metabolism genes in E3/E3 and E4/E4 astrocytes.



**Table 7.1: function & expression of cholesterol metabolism genes in E4/E4 cells.**

Gene	Function	Effect
SREBP	Senses intracellular cholesterol levels and upregulates cholesterol synthesis.	Decreased
LXR genes (NR1H2/3)	Upregulate a suite of genes that control expression of proteins that mediate cellular cholesterol release and uptake.	Decreased
HMGCR	Rate limiting step in cholesterol synthesis.	No change
ABCA1 & ABCG1	Coordinate the mobilisation of cholesterol from cytoplasmic pools to the cell surface membrane.	Decreased Increased
ACAT1	Intracellular conversion of cholesterol to CE.	Increased
LIPE	Intracellular conversion of CE to cholesterol.	Increased
LCAT	Conversion of free cholesterol on the HDL surface to CEs.	Decreased
CETP	Transfer of CEs to HDL particles.	No change
PLTP	Maturation of nascent to mature HDL particles (probable).	Decreased
LPL	Adds cholesterol to HDL particles in exchange for triglycerides.	Decreased
LDLR & LRP1	LDL receptor family members that endocytose lipoproteins.	No change Decreased
CYP46A1	Converts cholesterol to 24S-hydroxycholesterol.	Decreased

**Figure 7.8: expression of cholesterol metabolism genes in E4/E4 astrocytes**



## 7.3 Discussion

### 7.3.1 ApoE levels

The effect of *APOE* genotype on ApoE levels was described in Chapter 4 but is obviously highly relevant here. Lower levels of ApoE were found consistently in E4/E4 astrocytes, at both the gene and protein level. This accords with the vast majority of published literature.

It was suggested that the reason for lower levels of ApoE in E4/E4 cells was likely a combination of lower production, increased degradation and increased binding. Of particular relevance to this chapter, investigation of lipid particles generated by ApoE3 and ApoE4 expressing astrocytes has shown that ApoE3 has the ability to generate similarly sized ApoE lipid particles with fewer ApoE molecules than ApoE4. In fact, ApoE4-containing lipid particles may contain 2-fold numbers of ApoE molecules compared with an ApoE3- containing lipid particle<sup>179</sup> thus lowering free ApoE levels.

### 7.3.2 Cholesterol levels

Consistent with other studies, cholesterol levels in E4/E4 astrocytes were approximately 20% higher than in E3/E3 cells. While the increase in intracellular cholesterol might be explained, in the most simplistic terms, by either increased synthesis/influx or decreased efflux the concomitant increase of cholesterol in the media of E4/E4 astrocytes makes the explanation more complicated. The measurement of filipin fluorescence showed that, in the presence of a cholesterol challenge, E4/E4 astrocytes take up and accumulate more lipid than E3/E3 cells even though baseline levels of cholesterol are already higher. In tandem, these results suggest that cholesterol metabolism is dysregulated in E4/E4 astrocytes. The subsequent discussions explores how this dysregulation may be occurring.

### 7.3.2.1 *Intracellular cholesterol: synthesis and influx*

Cholesterol synthesis is under the control of SREBP2, the 'master gene' that increases the transcription of gene products that function to increase cellular cholesterol levels. SREBP2 was significantly lower in E4/E4 astrocytes than in E3/E3 cells (52.2% of E3/E3 value,  $p=0.024$ ) which is an appropriate and anticipated response to increased intracellular cholesterol and recapitulates the finding by Lin and colleagues in their isogenic *APOE* model<sup>202</sup>. However, the expression of HMG-CoA reductase (HMGCR), which catalyses the conversion of 3-hydroxy-3-methylglutaryl-CoA (HMG-CoA) to mevalonic acid, the rate limiting step in cholesterol synthesis was not significantly different between E3/E3 and E4/E4 astrocytes. Taken together, these results suggest that the increased levels of cholesterol in E4/E4 astrocytes are not due to increased synthesis but there may be some decoupling of the relationship between SREBP2 and HMGCR which means that the latter fails to respond as expected to increased intracellular cholesterol levels.

Cholesterol is not just synthesised within astrocytes but may also be taken up by them via the LDL receptors LDLR and LRP1. Although no significant difference was found in expression of LDLR in E4/E4 astrocytes, expression of LRP1 was significantly downregulated (26.5% of E3/E3 value,  $p=0.02$ ). While one of the key roles of LRP1 is to internalise ApoE-containing lipoproteins, it has others which make it difficult to draw inferences about the significance of this downregulation. However, such a downregulation would be an appropriate physiological response to increased intracellular cholesterol levels and may suggest that increased influx is unlikely to contribute to the raised cholesterol levels that are observed.

### 7.3.2.2 *Cholesterol efflux*

As described above, cholesterol efflux in astrocytes is achieved by the concerted action of ABCA1 and ABCG1; in neurons, the role of ABCG1 is replaced by ABCG4<sup>549</sup>. ABCA1 facilitates the initial cholesterol efflux to lipid-free ApoE and ApoJ to form nascent lipoproteins which are then further lipidated by ABCG1. Similar to cholesterol

synthesis, the whole process of cholesterol efflux is under the control of the ‘master’ LXR genes, NR1H2 and NR1H3, which encode LXR- $\beta$  and LXR- $\alpha$  respectively.

In murine cell culture models, ApoE4 has been found to be less efficient at cholesterol efflux than ApoE2 or ApoE3<sup>176,179,550</sup> which is thought to be due to the relative lipidation of different isoforms. In the mouse brain, ApoE4 was found to be hypolipidated relative to ApoE3<sup>551</sup>. The same effect has been observed in human CSF where ApoE complexes of *APOE4*-positive individuals were found to be smaller and hypolipidated compared to those from *APOE4*-negative individuals<sup>552,553</sup>. In a (non-isogenic) model of iPSC-derived astrocytes, cells with the *APOE44* genotype produced lipoprotein particles which were smaller and with less cholesterol than their *APOE33* counterparts<sup>372</sup>.

The results above suggest two main mechanisms that would cause hypolipidation of ApoE4 HDL (the second which relates to esterification of HDL is discussed in the next section). The first is related to ABCA1 gene expression which was significantly lower in E4/E4 astrocytes than in E3/E3 cells (24.7% of E3/E3 levels;  $p=0.007$ ). It has been suggested recently that this may be caused by ApoE4 trapping ABCA1 in late-endosomes impairing its recycling to the cell membrane<sup>554</sup>. For ABCG1 the result was reversed (243.0% of E3/E3 levels;  $p=0.008$ ). It has been suggested that such an increase in ABCG1 may be an attempt to compensate for the lack of ABCA1 in order to maintain ApoE–HDL lipidation<sup>509</sup>. However, as the expression of ABCG1 is much lower than that of ABCA1 this compensatory mechanism may not be entirely efficacious.

### 7.3.2.3 *Cholesterol movement across the blood brain barrier*

CYP46A1 is the enzyme responsible for the conversion of cholesterol to 24S-hydroxycholesterol (24-OHC), which, unlike cholesterol itself, can freely cross the blood-brain barrier (BBB). This is a major elimination pathway which is responsible for 40-50% of brain cholesterol turnover<sup>544</sup>. Although most of the literature suggests that CYP46A1 is not expressed in astrocytes, the results above suggest that it is, albeit at relatively low levels. Furthermore, the expression is significantly lower in E4/E4

astrocytes than E3/E3 astrocytes and – given the importance of this pathway for cholesterol elimination - may be another contributory factor to the accumulation of free cholesterol in E4/E4 astrocytes. While one explanation for this result is contamination with neuronal cells, the complete absence of *MAP2* expression in samples (as noted in Chapter 4) would suggest otherwise.

The other way in which cholesterol may be excreted from the CNS is as lipoproteins which can exit the brain through the CSF. Excess cholesterol is transferred to ApoE containing lipoproteins from the interstitial fluid to the perivascular fluid and from there to the brain surface, where it is removed with the bulk flow of the CSF<sup>145</sup>. It is estimated that this process may remove as much as 2mg of cholesterol per day given that CSF is turned over approximately three times per day. The lower levels of ApoE4, combined with its reduced cholesterol binding capacity, may well inhibit this process and be another contributor to the increased cholesterol levels seen in E4/E4 cells.

### 7.3.3 Changes in cholesteryl ester levels (CEs)

Excess cholesterol is toxic to cells so its accumulation is tightly controlled. One of the main mechanisms for maintaining cholesterol levels is its conversion to cholesteryl esters which constitute about 1% of the total cholesterol in the CNS exists<sup>543</sup>.

In this study, levels of cholesteryl esters were non-significantly increased within E4/E4 astrocytes but significantly increased in E4/E4 astrocyte media. This departs from findings in other recent studies using isogenic *APOE* lines; one found no significant differences in the levels of cholesteryl esters<sup>263</sup> (the other recent study did not measure them<sup>202</sup>).

Despite this, there is a significant body of work which implicates cholesteryl esters in AD (both sporadic and familial). An elevation of cholesteryl esters (chains 14:20) was observed in the CNS of SAD patients and in three transgenic FAD mouse models<sup>555</sup>. The observation was particularly marked in the entorhinal cortex of human subjects where

CEs were typically 1.7-fold higher than controls with the most notable differences in CE-16:1, CE-16:0, and CE-18:1.

A lipidomic study which used a battery of plasma metabolites to predict SAD patients from controls<sup>556</sup> found that a combination of 10 metabolites, 6 of which were long chain cholesteryl esters, could discriminate patients from controls (although plasma levels of the CEs were lower in cases than controls). While the study compared SAD cases and controls rather than *APOE* status, as one might expect, the presence of *APOE* alleles was far greater in the cases (percentage of control with at least one *APOE4* allele was 17.5% cf 58% of cases) so it is possible the phenotypes seen were attributable to *APOE* status.

Most recently, Van der Kant and colleagues tested a library of >1,600 compounds for their ability to inhibit phosphorylated Tau (pTau) accumulation (a key AD phenotype) in cultured FAD iPSC-derived neurons<sup>557</sup>. Their initial screen found that four statins (atorvastatin, simvastatin, fluvastatin, and rosuvastatin), which reduce cholesterol levels by inhibiting levels of HMGCR, also reduce levels of pTau. They went on to investigate a number of other compounds which inhibit specific steps of the cholesterol pathway and found mechanistically different cholesterol-lowering drugs all reduce pTau. They also found that, despite the effects on pTau levels, changes in free cholesterol levels were not detected for most compounds, however all compounds significantly reduced the levels of total cholesterol (free + esterified cholesterol) through a strong reduction of cholesteryl esters. The authors suggest that reductions in cholesteryl esters, not free cholesterol, mediate the effects of the different compounds on pTau levels and, as such, may play an important role in the phenotypes seen in AD.

#### 7.3.3.1 *Possible mechanisms of CE accumulation in E4/E4 astrocytes*

Given that cholesterol levels in E4/E4 astrocytes are increased, one would expect esterification mechanisms to be concomitantly upregulated. Intracellular conversion of cholesterol to CEs is performed by ACAT1. An increase in ACAT1 transcripts with age

has been described in rat models<sup>558</sup> and pharmacological inhibition and genetic ablation of ACAT1, lowers beta-amyloid production and rescues cognitive function in transgenic models of AD<sup>540,541,559</sup>. Furthermore, ACAT1 polymorphisms are linked to SAD although the data are inconsistent<sup>508</sup>.

Expression of ACAT1 was increased two-fold in E4/E4 astrocytes compared to E3/E3 astrocytes (214.9% of E4/E4 levels,  $p=0.032$ ). Interestingly, however, the expression of LIPE, the gene which encodes hormone-sensitive lipase which converts CEs back to cholesterol, was also upregulated 3.5-fold in E4/E4 astrocytes compared to E3/E3 astrocytes however this result was not significant owing to the large variation in LIPE values (347.7% of E3/E3,  $p=0.349$ ). In terms of relative expression of ACAT1 and LIPE, ACAT1 expression was approximately twice that of LIPE expression in both E3/E3 and E4/E4 cells suggesting that the balance between esterification and reverse esterification is unaffected by APOE genotype. Furthermore, the increase in CEs in E4/E4 lysates was proportional to the increase in cholesterol levels (both around 20%) which suggests that the increases seen in ACAT1 and LIPE might simply be appropriate physiological responses to the increases in intracellular cholesterol.

#### 7.3.4 Extracellular esterification mechanisms

As described above, there are 4 different proteins and enzymes which esterify cholesterol in HDL particles contributing to their increased cholesterol binding capacity and to their size: LCAT, LPL, CETP and PLTP.

As previously noted, a key driver of HDL particle size is the size of the cholesteryl ester core. The discoidal, nascent lipoproteins effluxed from astrocytes via ABCA1 are 'matured' by the addition of cholesteryl esters via the actions of LCAT which converts cholesterol within lipoproteins to CEs; CETP and PLTP may also contribute to this process however their mechanism of action within the CNS is unclear. LCAT expression in E4/E4 cells was significantly lower than in E3/E3 cells (30.7% of *APOE33* levels;  $p=0.006$ ). This accords with existing literature where, in CSF from SAD patients, LCAT activity was 50% lower than in CSF from controls<sup>524</sup>. ApoE4 is also less

efficient than ApoE3 in activating LCAT to form cholesteryl esters and in converting discoidal particles to spherical ApoE-containing lipoproteins<sup>560</sup>. Finally, downregulation of ABCA1 is also associated with the formation of smaller ApoE-containing lipoprotein particles<sup>509,561</sup> and with the accentuation of the ApoE4 phenotype<sup>562</sup>; this may be because ApoE and ABCA1 are required to form a suitable substrate on which LCAT may act.

PLTP expression was also significantly reduced in E4/E4 astrocytes compared to E3/E3 cells (32.6% of E3/E3 levels;  $p=0.001$ ). Although one initial study suggests that PLTP levels were increased in brain tissue homogenates from SAD patients<sup>533</sup>, all subsequent studies have shown that levels are reduced. The same authors found that PLTP levels are reduced in the CSF of SAD patients (and in neurological diseases more generally) and, interestingly, that CSF PLTP activity positively correlated with ApoE concentration in SAD<sup>563</sup>. PLTP deficiency has also been shown to impair cognitive function and increased amyloid deposition in murine models<sup>564,565</sup>. The best described role of PLTP is the transfer of lipids between various different classes of lipoproteins, in particular, in increasing the size of HDL particles<sup>566</sup>. However, it also significantly reduces levels of phosphorylated tau which may be another link between cholesterol metabolism and tau-phosphorylation<sup>567</sup>.

There is significant evidence to suggest a role for LPL in the pathogenesis of SAD. Interestingly, the highest expression of LPL in the CNS is in the hippocampus and polymorphisms have been associated with SAD although inconsistently so<sup>568</sup>. LPL gene expression in E4/E4 astrocytes was significantly lower than in E3/E3 cells (35.4% of E3/E3 levels;  $p<0.000$ ). While the precise role of LPL in the CNS is still disputed, it is known to have triglyceride hydrolase activity and contributes to receptor-mediated lipoprotein uptake<sup>508</sup>. LPL is also upregulated in response to CNS injury which may reflect its potential role in scavenging and recycling of cholesterol released from dying cells and degenerating terminals<sup>534</sup>. When astrocytes were treated with a cocktail of cytokines to induce the 'A1' phenotype seen in CNS injury, LPL was significantly increased in E3/E3 astrocytes (81.2% increase compared to quiescent E3/E3 cells;

p=0.022) whereas a significant decrease was observed in E4/E4 cells (28.9% decrease compared to quiescent E3/E3 cells; p=0.049).

#### 7.4 Conclusions

Decreased synapse number has long been recognised as the strongest quantitative neuropathological correlate of the cognitive changes seen in SAD. Cholesterol homeostasis is vital for synaptic formation and remodelling, and thus maintaining cognitive integrity, so any perturbations will have serious consequences.

The model system created here has recapitulated key findings of two recent papers that have also used isogenic *APOE* models, notably the decreased levels of ApoE and increased levels of cholesterol in E4/E4 astrocytes. However, it has also uncovered new data, importantly increases in both intracellular and extracellular cholesteryl ester levels in E4/E4 astrocytes.

A number of impairments in cholesterol metabolism in E4/E4 cells have been highlighted. To summarise:

- the cholesterol synthesis master-gene *SREBP2* is appropriately downregulated in response to the increased intracellular cholesterol in E4/E4 astrocytes, however, the *HMGCR* gene involved in the key rate limiting step of cholesterol formation is not. This suggests some form of decoupling of the relationship between *SREBP2* and *HMGCR*.
- Expression of *ABCA1* is inappropriately downregulated in E4/E4 cells suggesting an impairment of cholesterol efflux.
- *CYP46A1*, which converts cholesterol to 24S-hydroxycholesterol by enabling it to cross the blood-brain barrier, is downregulated in E4/E4 astrocytes which may also contribute to increased intracellular cholesterol levels.

Perhaps the most interesting findings pertain to esterification. Cholesteryl esters are increased in both astrocyte lysates and media (although this was only significant in

media). While the accumulation of intracellular esters appears to be a normal physiological response to the increased intracellular cholesterol, the increase in extracellular esters is difficult to explain. There is a dearth of literature explaining how cholesteryl esters leave cells and what happens to them extracellularly.

What is clear is that hypolipidation of ApoE4 HDL is a well described phenomenon and is likely to be a key contributor to the synaptic deficits associated with the E4/E4 genotype. Esterification is vital to the lipidation process, increasing the carriage of cholesterol by lipoproteins, and the presence of at least four different esterification mechanisms suggests it is of great biological importance. We have demonstrated that three of these four mechanisms may be impaired in E4/E4 astrocytes.

Although there are numerous studies investigating the effect of ageing, SAD and *APOE* status on the various constituent parts of the cholesterol metabolism, to our knowledge, this is the first study which looks at gene expression in the system as a whole enabling a more complete understanding of how the *APOE* genotype affects cholesterol metabolism.

While a great deal of further work is necessary to elucidate the precise mechanisms at play, including investigation of how gene expression maps to protein and enzyme levels, this study provides a solid foundation for that endeavour.

## 8 General discussion

### 8.1 Summary of key findings

Sporadic Alzheimer's disease is a multifactorial disease with age the key risk factor. While there are no causative genes in SAD, *APOE* remains the most important genetic risk factor with a lifetime risk for E4/E4 homozygotes of almost 70%<sup>569</sup>. To put this in perspective, this is similar to genes in Mendelian diseases, such as BRCA1 in breast cancer, rather than those of low-risk common alleles identified by GWAS in complex diseases. A sound understanding of the role of *APOE* in SAD is vital but, until recent years, it has been relatively neglected.

The aim of this thesis was to identify ways in which the *APOE* genotype contributes to the pathogenesis of sporadic Alzheimer's disease by:

- creating isogenic *APOE* cell lines;
- differentiating those isogenic stem cells into astrocytes; and
- identifying phenotypic differences between astrocytes with E3/E3 and E4/E4 genotypes in their quiescent and reactive states.

This thesis has reported a relatively efficient and reproducible method for producing isogenic *APOE* cell lines using CRISPR Cas-9 technology. While most sources have reported a maximum HDR editing efficiency of around 40%<sup>570</sup>, the method presented here resulted in the incorporation of the HDR template on one allele in approximately 50% of cells. However, because the most common editing event was a single nucleotide change on the other allele, or often in addition to the HDR template, the vast majority of clones were unusable. Screening of approximately 100 clones resulted in two useable clones with the HDR template on one allele and wild-type sequence on the other suggesting an overall efficiency of approximately 2%.

The method used to differentiate astrocytes used a combination of three different protocols<sup>347,350,354</sup> to produce a very pure population of astrocytes from NPCs. These

showed upregulation of key astrocytic markers via both qPCR and ICC plus the absence of the neuronal marker MAP2. The astrocyte differentiation protocol targeted production of astrocytes with a quiescent phenotype in order that it could be stressed to explore differences between astrocytes in resting and reactive ('A1') states; for this, the method described by Liddelow and colleagues was used whereby cells were treated with TNF $\alpha$ , Il-1 $\alpha$  and C1q<sup>309</sup>.

Astrocytes differentiated for 8 weeks from NPCs from the wild-type and isogenic lines were then used in a variety of experiments to explore the effects of *APOE* genotype on normal astrocyte physiology. The key findings were as follows:

- ApoE levels (protein and gene expression) were significantly lower in E4/E4 astrocytes than in E3/E3 cells.
- Reactive E4/E4 astrocytes demonstrated significantly reduced uptake of glutamate which appeared to be attributable to reduced expression of the EAAT2 glutamate receptor.
- Reactive E4/E4 astrocytes showed significantly reduced phagocytosis. MERTK gene expression (one of two regulators of phagocytosis) was significantly higher in 'A1' E3/E3 astrocytes than their E4/E4 counterparts. As MERTK works to regulate rearrangement of the actin cytoskeleton which co-extends with intermediate filaments to form astrocytic processes the key intermediate filaments, vimentin and GFAP, were measured. Perhaps counterintuitively, GFAP expression (measured with immunofluorescence) was significantly higher in both quiescent and reactive E4/E4 cells than in E3/E3 cells showing an inverse relationship with MERTK.
- Cytokine arrays demonstrated a more pro-inflammatory profile in reactive 'A1' E4/E4 astrocytes than their E3/E3 counterparts highlighting the central roles of TNF- $\alpha$  and NF- $\kappa$ B signalling.
- Levels of cholesterol, measured with GC-MS, were significantly higher in the media of E4/E4 astrocytes. When measured with filipin fluorescence, intracellular free cholesterol was significantly higher in E4/E4 than E3/E3 astrocytes.

- Measurements of filipin fluorescence also showed that cholesterol treated E4/E4 astrocytes take up and accumulate more cholesterol than E3/E3 cells even though baseline levels are already higher suggesting that cholesterol metabolism is dysregulated in E4/E4 astrocytes.
- Levels of both intracellular and extracellular cholesteryl ester levels were increased in E4/E4 astrocytes (the latter significantly so). Analysis of differences in key cholesterol metabolism genes showed several pathways that might be perturbed in E4/E4 astrocytes especially esterification mechanisms.

## 8.2 Central role of astrocytes in synaptic function in Alzheimer's disease

The original aim of this thesis was to examine the effect of *APOE* genotype on synaptic function as this is generally accepted to be the best neuropathological correlate of the cognitive changes in SAD. However, it became apparent at the outset that astrocytes perform a huge and varied range of functions to maintain CNS homeostasis so, before examining neuron-astrocyte interactions, a better understanding of how *APOE* affects normal astrocyte physiology was necessary. The isogenic model described here provided an excellent platform to explore this.

Astrocytes have long been the poor cousin within the CNS to the extent that they were once regarded as mere scaffolding. Now at a time when greater interest is being paid to them they are at risk, once again, of being overshadowed because of the burgeoning interest in microglia. While microglia undoubtedly have a key role in the pathogenesis of AD and other neurodegenerative diseases, I would argue strongly that astrocytes are at least as important. Bart de Strooper has commented that 'the astroglia population is strikingly under-investigated in AD-related studies'<sup>571</sup>. Despite the recent accumulation of genes which appear to be centred on microglia there are similar numbers that are solely or predominantly expressed by astrocytes, including *APOE*.

I would argue that the perturbations in normal astrocyte physiology, which largely converge on synaptic dysfunction, may represent initiating events that lie at the heart of AD pathogenesis, including:

- Failure of efflux and esterification mechanisms which ensure appropriate lipidation of ApoE particles leading to reduced carriage of cholesterol from astrocytes to neurons which in turn impairs the creation and repair of dendrites;
- Decreased uptake of glutamate causing damaging excitotoxicity; and
- Reduced astrocytic phagocytosis allowing the accumulation of damaged and senescent synapses.

While these processes occur throughout an individual's life-span, the brain's huge cognitive reserve is able to mask these effects for several years but clinical symptoms manifest when this is exhausted. The ongoing process of astrogliosis, which occurs throughout life in response to various CNS insults, may play a vital role in the rate at which cognitive reserve is depleted.

### 8.3 Astrogliosis: a potential therapeutic target

Although the scheme above puts astrocyte dysfunction at the heart of the disease process this is not to say that microglia are inconsequential. The majority of phenotypes described above were only unmasked in reactive 'A1' astrocytes. Induction of the 'A1' astrocytic phenotype is driven by microglia (which produce the TNF $\alpha$ , IL-1 $\alpha$  and C1q that stimulate the astrocytes); this is an important way in which astrocyte-microglial cross-talk may be contributing to the pathogenesis of AD.

As described previously, astrogliosis is the process by which astrocytes undergo changes in gene expression, cellular structure and function in response to various CNS insults<sup>375</sup>. It is a prominent feature in a wide range of CNS pathologies including AD where greater astrogliosis is seen in patients than in age-matched controls<sup>250</sup>. As noted

in Chapter 5, astrogliosis is not a simple stereotypic response but rather a finely tuned spectrum of changes that range from reversible alterations in gene expression and cellular hypertrophy to pronounced cell proliferation with permanent tissue rearrangement<sup>375</sup>. Although reactive astrocytes are a pathological substrate noted at the end-stage of disease, human PET studies using monoamine oxidase B (MaoB), a marker of astrocytic activity, have confirmed that astrogliosis is an early event seen before amyloid accumulation<sup>572</sup>.

Much work has been undertaken in recent years to elucidate the process of astrogliosis although the intricacies remain enigmatic. Better understanding of glial interactions is vital to our understanding of the AD disease process and, as others have suggested before, intervening in the process of astrogliosis may be a therapeutic target for neurodegenerative diseases<sup>573,574</sup>.

#### 8.4 A unifying theme? Nuclear factor-kappa B (NF-kB) signalling

Although the astrocytic phenotypes noted above are relatively diverse, those differences seen in 'A1' astrocytes converge on the NF-kB signalling pathway. Nuclear factor-kappa B (NF-kB) signalling is a key regulator of innate immunity via gene regulation and has been implicated in systemic aging, inflammation and synaptic dysfunction as well as the pathogenesis of several neurodegenerative diseases<sup>500,501</sup>.

It is perhaps obvious that NF-kB related pathways would be affected in 'A1' astrocytes given that the TNF- $\alpha$  used to induce them is known to be one of the key activators of the NF-kB family of transcription factors; what has been shown in this thesis, however, is that the effects of NF-kB may be altered by *APOE* genotype. A literature search found a single paper published in 2005 which showed that, following intracerebroventricular injection of LPS, expression of inflammation-related genes was significantly higher and more prolonged in ApoE4 than in ApoE3 transgenic mice with NF-kB gene clusters significantly enriched<sup>267</sup>. To our knowledge, however, this is the first time that this relationship has been found in a human model system.

In Chapter 4 it was noted that both protein and RNA levels of ApoE are decreased in E4/E4 astrocytes suggesting that ApoE4 may negatively impact its own transcription. In Chapter 6, it was suggested that ApoE4 may be acting more widely as a transcription factor: a study using chromatin immunoprecipitation and high-throughput DNA sequencing, found that ApoE4 undergoes nuclear translocation binding specifically and, with high affinity, to numerous DNA sites including the promoter regions of 1700 genes. Notably, many of these genes had cellular functions implicated in AD pathogenesis including trophic support, programmed cell death, synaptic function, insulin resistance and aging<sup>410</sup>.

It seems possible therefore that, as well as the direct functional effects of different ApoE isoforms, it may also be acting as a transcription factor for other genes including NF- $\kappa$ B. The precise nature of the interaction between *APOE* and NF- $\kappa$ B is not yet established but there is evidence to suggest a bi-directional relationship. Promoter analysis and functional studies have linked expression of *APOE* to regulation by NF- $\kappa$ B (reviewed in Dresselhaus and Meffert, 2019). Conversely, interaction of ApoE4 (but not ApoE3) and the RelA subunit of the NF $\kappa$ B complex led to nuclear translocation of RelA, suggesting the possibility that ApoE4 affects NF $\kappa$ B-mediated gene transcription<sup>410</sup>.

As discussed earlier in this thesis, new gene discovery and pathway analyses have highlighted the role of immunity, and specifically the innate immune system, in the pathogenesis of AD. The NF- $\kappa$ B pathway is a key part of the innate immune system and so it has been suggested as a potential therapeutic target, especially as there is good evidence to suggest that it plays a role in synaptic dysfunction<sup>506,575</sup>. Further experiments to check the levels of NF- $\kappa$ B expression (at the gene and protein level) according to *APOE* genotype, and whether they associate with the phenotypes described here, would verify this relationship. This would confirm NF- $\kappa$ B signalling as an area for further enquiry and would allow appropriate targeting of any future clinical trials of agents within this pathway according to *APOE* genotype.

There is also a way in which NF- $\kappa$ B may be related to the cholesterol pathways. The study undertaken by Rik van der Kant and colleagues was described in Chapter 7; it

showed that a variety of lipid lowering agents, including statins, lowered levels of phosphorylated tau in a human iPSC model. It was also noted that, while lipid lowering drugs did not affect levels of total cholesterol, they consistently lowered levels of cholesteryl esters. It has long been suspected that drugs such as statins are pleiotropic and one such additional effect may be attenuation of the NF- $\kappa$ B-mediated inflammatory response; one study showed that all statins tested inhibited LPS-induced NF- $\kappa$ B binding activity in monocytes in a dose-dependent manner<sup>576</sup>. Two other studies showed that these effects are not restricted to LPS or TNF- $\alpha$  induced inflammation; rosuvastatin was found to modulate neuronal cell death by inhibiting the overexpression of NF- $\kappa$ B in the CA1 region of hippocampus in response to a high cholesterol diet<sup>577</sup> while in a model of traumatic brain injury (TBI), simvastatin administration attenuated NF- $\kappa$ B-mediated inflammatory response in the injured rat brain<sup>578</sup>. The precise details of this, and in particular whether esterification mechanisms are affected by NF- $\kappa$ B signalling, would need to be investigated but does show that NF- $\kappa$ B may be affecting AD pathogenesis in ways unrelated to TNF- $\alpha$  induced responses.

## 8.5 The place of the astro-centric view alongside traditional neuropathological models

As described in Chapter 1, the traditional pathological substrates of SAD are beta-amyloid and phosphorylated tau. One of the aims of this thesis was to challenge the beta-amyloid centric view of Alzheimer's disease due to the repeated failure of amyloid based therapies and the existence of better clinicopathological correlates, namely synaptic function.

Beta-amyloid has traditionally been considered the driver of the disease process in SAD, partly due to the presence of amyloid deposits but also because of the key role of amyloid-related genes (APP, PSEN1 and PSEN2) in familial AD. I would argue, however, that accumulation of amyloid may actually be a by-product of the perturbations seen in other physiological processes. For example, as discussed in Chapter 7, ApoE4 tends

to be hypolipidated compared to ApoE3 causing less efficient carriage of cholesterol from astrocytes to neurons where it is needed for maintaining and forming new dendrites which are essential for synaptic function. Hypolipidated ApoE4 is also a poor ligand for the neuronal receptors LDLR and LRP1 which impacts on endocytosis of cholesterol into neurons. ApoE mediated elimination of beta-amyloid relies on the same LDLR/LRP1 dependent pathway<sup>579</sup> therefore hypolipidation of ApoE4 has a simultaneous effect on cholesterol and beta-amyloid homeostasis. Once present in the CNS, there is indisputable evidence to suggest that beta-amyloid accelerates the pathophysiological process (it has even been shown to promote astroglial NF- $\kappa$ B activation; Lian *et al.*, 2015) however the assertion that it is the first, and central, pathogenic change deserves further scrutiny.

The presence of phosphorylated tau correlates far better with the cognitive deficits seen in AD than beta-amyloid deposits and whether p-tau or synaptic measures are the best clinicopathological correlate in AD is a matter of conjecture. Unlike beta-amyloid, p-tau appears to be more intimately related to some of the aberrant E4/E4-dependent phenotypes described in this thesis. For example, the increase in cholesteryl esters is associated with an increase in p-tau and the use of statins and cholesterol lowering agents were found to simultaneously reduce levels of p-tau and cholesteryl esters. In Chapter 6 it was noted that several of the pro-inflammatory cytokines (especially the Pi3k pathway chemokines) upregulated in E4/E4 astrocytes also increase levels of p-tau. Furthermore, increased glutamate has been shown to increase tau phosphorylation<sup>421</sup>. One of the key aims of any future work will be to examine if, and how, the phenotypes described above relate to levels of tau phosphorylation in neurons.

## 8.6 Future work

The generation and characterisation of these cell lines represents a tool which can be used to examine the role of *APOE* genotype on phenotypes seen in various cell types. This thesis has described a method for producing astrocytes but the edited stem cells could be differentiated to any cell type of interest. Similarly, the CRISPR method could be used to produce other *APOE* isogenic lines or adapted to edit genes at other loci; the screening method developed as part of this thesis is a particular strength of this model.

The key shortcoming of this study is that, despite best efforts to differentiate astrocytes with typical morphology and expression, the 12-week astrocytes used for experimentation were still relatively immature; 26-week astrocytes showed greater upregulation of a panel of astrocytic genes and were more morphologically prototypic. Having now optimised a maturation method, any future work should be based on a longer differentiation protocol.

The other key issue is that this study examined astrocytes in isolation. While I believe this has been the right approach to uncover some of the astrocytic phenotypes described, it is becoming increasingly obvious that neuron-astrocyte and astrocyte-microglial interactions are of vital importance to neurodegenerative disease processes and co-culture models of varying degrees of sophistication are required. Of particular interest is the differential effects of ApoE depending on its cellular source<sup>149</sup>.

In terms of future work, the first stage will be to further investigate the role of the NF- $\kappa$ B signalling pathway. This will be done by examining the gene expression of various parts of the NF- $\kappa$ B network including IKK and the p50 and p65 sub-units. It is also hoped that stored samples might be used to quantify protein levels of these markers and, importantly, to verify their phosphorylation status.

It would also be helpful to re-capitulate the findings presented here in other model systems. For example, it would be relatively simple to verify them in human post-

mortem histopathological samples. After that, the next stage would be to investigate the effects of the phenotypes described above on synaptic health using a neuron-astrocyte co-culture model; at its most basic this could be neurons of different *APOE* genotypes cultured with astrocyte conditioned media through to more sophisticated physical co-culture systems. Some key neuronal/synaptic phenotypes would include ratios of p-tau/tau, a dendritic branching assay using the Opera Phenix High Content Screening System (exploratory work, not included in this thesis, was undertaken to optimise this) and the use of multi-electrode arrays (MEAs) to measure network connectivity in neuronal cultures, the use of which has already been optimised by our research group.

In conclusion, this thesis has described a model system which allows easy exploration of *APOE* genotype/phenotype interactions and uncovered a number of phenotypes which may be of relevance to the disease process. While there is undoubtedly a great deal of work to be done to replicate these findings and uncover further phenotypes this thesis provides a solid basis for future work and highlights areas of enquiry that are most likely to be fruitful.

## References

1. Brookmeyer, R., Johnson, E., Ziegler-Graham, K. & Arrighi, H. M. Forecasting the global burden of Alzheimer's disease. *Alzheimers. Dement.* **3**, 186–191 (2007).
2. Markowitsch, H. J. & Staniloiu, A. Amnesic disorders. *Lancet* **380**, 1429–1440 (2012).
3. Peters, F. *et al.* The neural correlates of verbal short-term memory in Alzheimer's disease: an fMRI study. *Brain* **132**, 1833–1846 (2009).
4. Johnson, J. W. & Kotermanski, S. E. Mechanism of action of memantine. *Curr. Opin. Pharmacol.* **6**, 61–67 (2006).
5. Selkoe, D. J. & Hardy, J. The amyloid hypothesis of Alzheimer's disease at 25 years. *EMBO Mol. Med.* **8**, 595–608 (2016).
6. Cummings, J., Lee, G., Ritter, A. & Zhong, K. Alzheimer's disease drug development pipeline: 2018. *Alzheimer's Dement. Transl. Res. Clin. Interv.* **4**, 195–214 (2018).
7. Cummings, J., Lee, G., Ritter, A., Sabbagh, M. & Zhong, K. Alzheimer's disease drug development pipeline: 2020. *Alzheimer's Dement. Transl. Res. Clin. Interv.* **6**, 1–29 (2020).
8. Verkhratsky, A., Olabarria, M., Noristani, H. N., Yeh, C. Y. & Rodriguez, J. J. Astrocytes in Alzheimer's Disease. *Neurotherapeutics* **7**, 399–412 (2010).
9. Chun, H. & Lee, C. J. Reactive astrocytes in Alzheimer's disease: A double-edged sword. *Neurosci. Res.* **126**, 44–52 (2018).
10. Weingarten, M. D., Lockwood, A. H., Hwo, S. Y. & Kirschner, M. W. A protein factor essential for microtubule assembly. *Proc. Natl. Acad. Sci. U. S. A.* **72**, 1858–1862 (1975).
11. de Calignon, A. *et al.* Propagation of tau pathology in a model of early Alzheimer's disease. *Neuron* **73**, 685–697 (2012).
12. Guo, T., Noble, W. & Hanger, D. P. Roles of tau protein in health and disease. *Acta Neuropathol.* **133**, 665–704 (2017).
13. Wisniewski, H. M., Narang, H. K. & Terry, R. D. Neurofibrillary tangles of paired helical filaments. *J. Neurol. Sci.* **27**, 173–181 (1976).
14. Braak, H. & Braak, E. Staging of alzheimer's disease-related neurofibrillary

- changes. *Neurobiol. Aging* **16**, 271–278 (1995).
15. Braak, F., Braak, H. & Mandelkow, E.-M. A sequence of cytoskeleton changes related to the formation of neurofibrillary tangles and neuropil threads. *Acta Neuropathol.* **87**, 554–567 (1994).
  16. Braak, H. & Braak, E. Neuropathological staging of Alzheimer-related changes. *Acta Neuropathol.* **82**, 239–259 (1991).
  17. Ulrike C. Muller and Hui Zheng. Physiological Functions of APP Family Proteins. *Cold Spring Harb. Perspect. Med.* **2**, 1–17 (2012).
  18. Ward, R. V *et al.* Fractionation and characterization of oligomeric, protofibrillar and fibrillar forms of beta-amyloid peptide. *Biochem. J.* **348 Pt 1**, 137–144 (2000).
  19. Jarrett, J. T., Berger, E. P. & Lansbury, P. T. J. The carboxy terminus of the beta amyloid protein is critical for the seeding of amyloid formation: implications for the pathogenesis of Alzheimer's disease. *Biochemistry* **32**, 4693–4697 (1993).
  20. Sumner, I. L., Edwards, R. A., Asuni, A. A. & Teeling, J. L. Antibody engineering for Optimized immunotherapy in Alzheimer's disease. *Front. Neurosci.* **12**, 1–12 (2018).
  21. Cummings, J. L., Vinters, H. V, Cole, G. M. & Khachaturian, Z. S. Alzheimer's disease: etiologies, pathophysiology, cognitive reserve, and treatment opportunities. *Neurology* **51**, S2-17; discussion S65-7 (1998).
  22. Serrano-Pozo, A., Frosch, M. P., Masliah, E. & Hyman, B. T. Neuropathological alterations in Alzheimer disease. *Cold Spring Harb. Perspect. Med.* **1**, a006189 (2011).
  23. Khachaturian, Z. S. Diagnosis of Alzheimer's disease. *Arch. Neurol.* **42**, 1097–1105 (1985).
  24. Mirra, S. S. *et al.* The Consortium to Establish a Registry for Alzheimer's Disease (CERAD). Part II. Standardization of the neuropathologic assessment of Alzheimer's disease. *Neurology* **41**, 479–486 (1991).
  25. Hyman, B. T. & Trojanowski, J. Q. Consensus recommendations for the postmortem diagnosis of Alzheimer disease from the National Institute on Aging and the Reagan Institute Working Group on diagnostic criteria for the neuropathological assessment of Alzheimer disease. *Journal of neuropathology*

- and experimental neurology* **56**, 1095–1097 (1997).
26. Thal, D. R., Rüb, U., Orantes, M. & Braak, H. Phases of A $\beta$ -deposition in the human brain and its relevance for the development of AD. *Neurology* **58**, 1791–1800 (2002).
  27. Montine, T. J. *et al.* National institute on aging-Alzheimer's association guidelines for the neuropathologic assessment of Alzheimer's disease: A practical approach. *Acta Neuropathol.* **123**, 1–11 (2012).
  28. Hyman, B. T. *et al.* National Institute on Aging-Alzheimer's Association guidelines for the neuropathologic assessment of Alzheimer's disease. *Alzheimer's Dement.* **8**, 1–13 (2012).
  29. Hardy, J. & Selkoe, D. J. The Amyloid Hypothesis of Alzheimer's Disease: Progress and Problems on the Road to Therapeutics. *Science (80-. )*. **297**, 353–356 (2002).
  30. Arriagada, P. V, Marzloff, K. & Hyman, B. T. Distribution of Alzheimer-type pathologic changes in nondemented elderly individuals matches the pattern in Alzheimer's disease. *Neurology* **42**, 1681–1688 (1992).
  31. Giannakopoulos, P. *et al.* Tangle and neuron numbers, but not amyloid load, predict cognitive status in Alzheimer's disease. *Neurology* **60**, 1495–1500 (2003).
  32. Rentz, D. M. *et al.* Cognition, reserve, and amyloid deposition in normal aging. *Ann. Neurol.* **67**, 353–364 (2010).
  33. Nelson, P. T. *et al.* Correlation of alzheimer disease neuropathologic changes with cognitive status: A review of the literature. *J. Neuropathol. Exp. Neurol.* **71**, 362–381 (2012).
  34. Bouras, C., Hof, P. R., Giannakopoulos, P., Michel, J. P. & Morrison, J. H. Regional distribution of neurofibrillary tangles and senile plaques in the cerebral cortex of elderly patients: a quantitative evaluation of a one-year autopsy population from a geriatric hospital. *Cereb. Cortex* **4**, 138–150 (1994).
  35. Knopman, D. *et al.* Neuropathology of cognitively normal elderly. *J. Neuropathol. Exp. Neurol.* **62**, 1087–1095 (2003).
  36. Gertz, H. J. *et al.* The relationship between clinical dementia and neuropathological staging (Braak) in a very elderly community sample. *Eur. Arch. Psychiatry Clin. Neurosci.* **246**, 132–136 (1996).

37. Leuzy, A. *et al.* Tau PET imaging in neurodegenerative tauopathies—still a challenge. *Mol. Psychiatry* 1112–1134 (2019). doi:10.1038/s41380-018-0342-8
38. Jin, M. *et al.* Soluble amyloid beta-protein dimers isolated from Alzheimer cortex directly induce Tau hyperphosphorylation and neuritic degeneration. *Proc. Natl. Acad. Sci. U. S. A.* **108**, 5819–5824 (2011).
39. Shankar, G. M. *et al.* Amyloid-beta protein dimers isolated directly from Alzheimer's brains impair synaptic plasticity and memory. *Nat. Med.* **14**, 837–842 (2008).
40. Jack, C. R. J. *et al.* NIA-AA Research Framework: Toward a biological definition of Alzheimer's disease. *Alzheimers. Dement.* **14**, 535–562 (2018).
41. Bateman, R. J. *et al.* Clinical and biomarker changes in dominantly inherited Alzheimer's disease. *N. Engl. J. Med.* **367**, 795–804 (2012).
42. Villemagne, V. L. *et al.* Amyloid beta deposition, neurodegeneration, and cognitive decline in sporadic Alzheimer's disease: a prospective cohort study. *Lancet. Neurol.* **12**, 357–367 (2013).
43. Jack, C. R. *et al.* NIA-AA Research Framework: Toward a biological definition of Alzheimer's disease. *Alzheimer's and Dementia* (2018). doi:10.1016/j.jalz.2018.02.018
44. Yankner, B. A. *et al.* Neurotoxicity of a fragment of the amyloid precursor associated with Alzheimer's disease. *Science* **245**, 417–420 (1989).
45. Walsh, D. M. & Selkoe, D. J. Deciphering the molecular basis of memory failure in Alzheimer's disease. *Neuron* **44**, 181–193 (2004).
46. Haass, C. & Selkoe, D. J. Soluble protein oligomers in neurodegeneration: lessons from the Alzheimer's amyloid beta-peptide. *Nat. Rev. Mol. Cell Biol.* **8**, 101–112 (2007).
47. Esparza, T. J. *et al.* Amyloid-beta oligomerization in Alzheimer dementia versus high-pathology controls. *Ann. Neurol.* **73**, 104–119 (2013).
48. Gandy, S. *et al.* Days to criterion as an indicator of toxicity associated with human Alzheimer amyloid-beta oligomers. *Ann. Neurol.* **68**, 220–230 (2010).
49. Lacor, P. N. *et al.* Synaptic targeting by Alzheimer's-related amyloid beta oligomers. *J. Neurosci.* **24**, 10191–10200 (2004).
50. Wang, H.-W. *et al.* Soluble oligomers of beta amyloid (1-42) inhibit long-term

- potentiation but not long-term depression in rat dentate gyrus. *Brain Res.* **924**, 133–140 (2002).
51. De Felice, F. G. *et al.* Alzheimer's disease-type neuronal tau hyperphosphorylation induced by A beta oligomers. *Neurobiol. Aging* **29**, 1334–1347 (2008).
  52. Terry, R. D. Do neuronal inclusions kill the cell? *J. Neural Transm. Suppl.* **59**, 91–93 (2000).
  53. Sahara, N., Maeda, S. & Takashima, A. Tau oligomerization: a role for tau aggregation intermediates linked to neurodegeneration. *Curr. Alzheimer Res.* **5**, 591–598 (2008).
  54. Lasagna-Reeves, C. A., Castillo-Carranza, D. L., Jackson, G. R. & Kaye, R. Tau oligomers as potential targets for immunotherapy for Alzheimer's disease and tauopathies. *Curr. Alzheimer Res.* **8**, 659–665 (2011).
  55. Himmelstein, D. S., Ward, S. M., Lancia, J. K., Patterson, K. R. & Binder, L. I. Tau as a therapeutic target in neurodegenerative disease. *Pharmacol. Ther.* **136**, 8–22 (2012).
  56. Lasagna-Reeves, C. A. *et al.* Tau oligomers impair memory and induce synaptic and mitochondrial dysfunction in wild-type mice. *Mol. Neurodegener.* **6**, 39 (2011).
  57. Zempel, H. & Mandelkow, E. Lost after translation: missorting of Tau protein and consequences for Alzheimer disease. *Trends Neurosci.* **37**, 721–732 (2014).
  58. Kimura, T., Ishiguro, K. & Hisanaga, S.-I. Physiological and pathological phosphorylation of tau by Cdk5. *Front. Mol. Neurosci.* **7**, 65 (2014).
  59. Terry, R. D. *et al.* Physical Basis of Cognitive Alterations in Alzheimer's Disease: Synapse loss Is the Major Correlate of Cognitive Impairment. *Ann. Neurol.* **30**, 572–580 (1991).
  60. DeKosky, S. T. & Scheff, S. W. Synapse loss in frontal cortex biopsies in Alzheimer's disease: correlation with cognitive severity. *Ann. Neurol.* **27**, 457–64 (1990).
  61. Selkoe, D. J. Alzheimer's Disease Is a Synaptic Failure. *Science (80-. )*. **298**, 789–792 (2002).
  62. Sudhof, T. C. Review The Presynaptic Active Zone. *Neuron* **75**, 11–25 (2012).

63. Südhof, T. C. Neuroligins and neurexins link synaptic function to cognitive disease. *Nature* **455**, 903 (2008).
64. Sheng, M. & Kim, E. The postsynaptic organization of synapses. *Cold Spring Harb. Perspect. Biol.* **3**, a005678 (2011).
65. Azevedo, F. A. C. *et al.* Equal numbers of neuronal and nonneuronal cells make the human brain an isometrically scaled-up primate brain. *J. Comp. Neurol.* **513**, 532–541 (2009).
66. Korade, Z. & Mirnics, K. Programmed to be human? *Neuron* **81**, 224–226 (2014).
67. Spires-jones, T. L. & Hyman, B. T. The Intersection of Amyloid Beta and Tau at Synapses in Alzheimer's Disease. *Neuron* **82**, 756–771 (2014).
68. Bliss, T. V & Gardner-Medwin, A. R. Long-lasting potentiation of synaptic transmission in the dentate area of the unanaesthetized rabbit following stimulation of the perforant path. *J. Physiol.* **232**, 357–374 (1973).
69. Spires-Jones, T. L. & Hyman, B. T. Review The Intersection of Amyloid Beta and Tau at Synapses in Alzheimer ' s Disease. *Neuron* **82**, 756–771 (2014).
70. Redondo, R. L. & Morris, R. G. M. Making memories last: the synaptic tagging and capture hypothesis. *Nat. Rev. Neurosci.* **12**, 17–30 (2011).
71. Collingridge, G. L., Peineau, S., Howland, J. G. & Wang, Y. T. Long-term depression in the CNS. *Nat. Rev. Neurosci.* **11**, 459–473 (2010).
72. Tavosanis, G. Dendritic structural plasticity. *Dev. Neurobiol.* **72**, 73–86 (2012).
73. Christof Koch and Anthony Zador. The Function of Dendritic Spines : Devices Rather Than Electrical Compartmentalization Subservicing Biochemical. *J. Neurosci.* **13**, 413–422 (1993).
74. Alvarez, V. A. & Sabatini, B. L. Anatomical and physiological plasticity of dendritic spines. *Annu. Rev. Neurosci.* **30**, 79–97 (2007).
75. Bosch, M. & Hayashi, Y. Structural plasticity of dendritic spines. *Curr. Opin. Neurobiol.* **22**, 383–388 (2012).
76. Urbanska, M., Blazejczyk, M. & Jaworski, J. Molecular basis of dendritic arborization. *Acta Neurobiol. Exp. (Wars).* **68**, 264–288 (2008).
77. Gonatas, N. K., Anderson, W. & Evangelista, I. The contribution of altered synapses in the senile plaque: an electron microscopic study in Alzheimer's dementia. *J. Neuropathol. Exp. Neurol.* **26**, 25–39 (1967).

78. Scheff, S. W. & Price, D. A. Synapse loss in the temporal lobe in Alzheimer's disease. *Ann. Neurol.* **33**, 190–9 (1993).
79. Scheff, S. W., DeKosky, S. T. & Price, D. A. Quantitative assessment of cortical synaptic density in Alzheimer's disease. *Neurobiol. Aging* **11**, 29–37
80. Moolman, D. L., Vitolo, O. V, Vonsattel, J.-P. G. & Shelanski, M. L. Dendrite and dendritic spine alterations in Alzheimer models. *J. Neurocytol.* **33**, 377–387 (2004).
81. Lanz, T. A., Carter, D. B. & Merchant, K. M. Dendritic spine loss in the hippocampus of young PDAPP and Tg2576 mice and its prevention by the ApoE2 genotype. *Neurobiol. Dis.* **13**, 246–253 (2003).
82. Games, D. *et al.* Alzheimer-type neuropathology in transgenic mice overexpressing V717F beta-amyloid precursor protein. *Nature* **373**, 523–527 (1995).
83. Spires, T. L. *et al.* Dendritic spine abnormalities in amyloid precursor protein transgenic mice demonstrated by gene transfer and intravital multiphoton microscopy. *J. Neurosci.* **25**, 7278–7287 (2005).
84. Mucke, L. *et al.* High-level neuronal expression of abeta 1-42 in wild-type human amyloid protein precursor transgenic mice: synaptotoxicity without plaque formation. *J. Neurosci.* **20**, 4050–4058 (2000).
85. Hartley, D. M. *et al.* Protofibrillar intermediates of amyloid beta-protein induce acute electrophysiological changes and progressive neurotoxicity in cortical neurons. *J. Neurosci.* **19**, 8876–8884 (1999).
86. Li, X., Alafuzoff, I., Soininen, H., Winblad, B. & Pei, J.-J. Levels of mTOR and its downstream targets 4E-BP1, eEF2, and eEF2 kinase in relationships with tau in Alzheimer's disease brain. *FEBS J.* **272**, 4211–4220 (2005).
87. Rocher, A. B., Kinson, M. S. & Luebke, J. I. Significant structural but not physiological changes in cortical neurons of 12-month-old Tg2576 mice. *Neurobiol. Dis.* **32**, 309–318 (2008).
88. Dickstein, D. L., Brautigam, H., Stockton, S. D. J., Schmeidler, J. & Hof, P. R. Changes in dendritic complexity and spine morphology in transgenic mice expressing human wild-type tau. *Brain Struct. Funct.* **214**, 161–179 (2010).
89. Wattmo, C. & Wallin, Å. K. Early- versus late-onset Alzheimer's disease in clinical

- practice: cognitive and global outcomes over 3 years. *Alzheimers. Res. Ther.* **9**, 70 (2017).
90. Palasí, A. *et al.* Differentiated clinical presentation of early and late-onset Alzheimer's disease: is 65 years of age providing a reliable threshold? *J. Neurol.* **262**, 1238–1246 (2015).
  91. Koedam, E. L. G. E. *et al.* Early-versus late-onset Alzheimer's disease: more than age alone. *J. Alzheimers. Dis.* **19**, 1401–1408 (2010).
  92. Cacace, R., Sleegers, K. & Van Broeckhoven, C. Molecular genetics of early-onset Alzheimer's disease revisited. *Alzheimer's Dement.* **12**, 733–748 (2016).
  93. Chaudhury, S. *et al.* Polygenic risk score in postmortem diagnosed sporadic early-onset Alzheimer's disease. *Neurobiol. Aging* **62**, 244.e1-244.e8 (2018).
  94. Kunkle, B. W. *et al.* Early-onset Alzheimer disease and candidate risk genes involved in endolysosomal transport. *JAMA Neurol.* **74**, 1113–1122 (2017).
  95. Tang, M. *et al.* Neurological Manifestations of Autosomal Dominant Alzheimer's Disease from the DIAN cohort and a meta-analysis HHS Public Access. *Lancet Neurol* **15**, 1317–1325 (2016).
  96. Campion, D. *et al.* Early-Onset Autosomal Dominant Alzheimer Disease: Prevalence, Genetic Heterogeneity, and Mutation Spectrum. *Am. J. Hum. Genet.* **65**, 664–670 (2002).
  97. Janssen, J. C. *et al.* Early onset familial Alzheimer's disease. *Neurology* **60**, 235 LP – 239 (2003).
  98. Tanzi, R. E. *et al.* Amyloid beta protein gene: cDNA, mRNA distribution, and genetic linkage near the Alzheimer locus. *Science* **235**, 880–884 (1987).
  99. Van Broeckhoven, C. *et al.* Failure of familial Alzheimer's disease to segregate with the A4-amyloid gene in several European families. *Nature* **329**, 153–155 (1987).
  100. Prasher, V. P. *et al.* Molecular mapping of Alzheimer-type dementia in Down's syndrome. *Ann. Neurol.* **43**, 380–383 (1998).
  101. Rovelet-Lecrux, A. *et al.* APP locus duplication causes autosomal dominant early-onset Alzheimer disease with cerebral amyloid angiopathy. *Nat. Genet.* **38**, 24–26 (2006).
  102. Holmes, C. Genotype and phenotype in Alzheimer's disease. *Br. J. Psychiatry*

- 180**, 131–134 (2002).
103. Sherrington, R. *et al.* Cloning of a gene bearing missense mutations in early-onset familial Alzheimer's disease. *Nature* **375**, 754–760 (1995).
  104. Theuns, J. *et al.* Genetic variability in the regulatory region of presenilin 1 associated with risk for Alzheimer's disease and variable expression. *Hum. Mol. Genet.* **9**, 325–331 (2000).
  105. Levy-Lahad, E. *et al.* Candidate gene for the chromosome 1 familial Alzheimer's disease locus. *Science* **269**, 973–977 (1995).
  106. Bird, T. D. *et al.* Wide range in age of onset for chromosome 1--related familial Alzheimer's disease. *Ann. Neurol.* **40**, 932–936 (1996).
  107. Selkoe, D. & Kopan, R. Notch and Presenilin: regulated intramembrane proteolysis links development and degeneration. *Annu. Rev. Neurosci.* **26**, 565–597 (2003).
  108. van der Flier, W. M., Pijnenburg, Y. A. L., Fox, N. C. & Scheltens, P. Early-onset versus late-onset Alzheimer's disease: The case of the missing APOE  $\epsilon$ 4 allele. *Lancet Neurol.* **10**, 280–288 (2011).
  109. Bigio, E. H., Hynan, L. S., Sontag, E., Satumtira, S. & White, C. L. Synapse loss is greater in presenile than senile onset Alzheimer disease: implications for the cognitive reserve hypothesis. *Neuropathol. Appl. Neurobiol.* **28**, 218–227 (2002).
  110. Pottier, C. *et al.* High frequency of potentially pathogenic SORL1 mutations in autosomal dominant early-onset Alzheimer disease. *Mol. Psychiatry* **17**, 875–879 (2012).
  111. Slattery, C. F. *et al.* R47H TREM2 variant increases risk of typical early-onset Alzheimer's disease but not of prion or frontotemporal dementia. *Alzheimers. Dement.* **10**, 602-608.e4 (2014).
  112. Pottier, C. *et al.* TREM2 R47H variant as a risk factor for early-onset Alzheimer's disease. *J. Alzheimers. Dis.* **35**, 45–49 (2013).
  113. Gatz, M. *et al.* Role of genes and environments for explaining Alzheimer disease. *Arch. Gen. Psychiatry* **63**, 168–74 (2006).
  114. Silverman, J. M., Li, G., Mohs, R. C. & Davis, K. L. Patterns of risk in first-degree relatives of patients with Alzheimer's disease. *Arch. Gen. Psychiatry* **51**, 577–86 (1994).

115. Harold, D. *et al.* Genome-wide association study identifies variants at CLU and PICALM associated with Alzheimer's disease. *Nat. Genet.* **41**, 1088–93 (2009).
116. Lambert, J.-C. *et al.* Genome-wide association study identifies variants at CLU and CR1 associated with Alzheimer's disease. *Nat. Genet.* **41**, 1094–9 (2009).
117. Seshadri, S. *et al.* Genome-wide analysis of genetic loci associated with Alzheimer disease. *JAMA* **303**, 1832–1840 (2010).
118. Hollingworth, P. *et al.* Common variants at ABCA7, MS4A6A/MS4A4E, EPHA1, CD33 and CD2AP are associated with Alzheimer's disease. *Nat. Genet.* **43**, 429–435 (2011).
119. Naj, A. C. *et al.* Common variants at MS4A4/MS4A6E, CD2AP, CD33 and EPHA1 are associated with late-onset Alzheimer's disease. *Nat. Genet.* **43**, 436–441 (2011).
120. Lambert, J. C. *et al.* Meta-analysis of 74,046 individuals identifies 11 new susceptibility loci for Alzheimer's disease. *Nat. Genet.* **45**, 1452–8 (2013).
121. Sims, R., Hill, M. & Williams, J. The multiplex model of the genetics of Alzheimer's disease. *Nat. Neurosci.* **23**, 311–322 (2020).
122. Ridge, P. G., Mukherjee, S., Crane, P. K. & Kauwe, J. S. K. Alzheimer's disease: analyzing the missing heritability. *PLoS One* **8**, e79771 (2013).
123. Jonsson, T. *et al.* Variant of TREM2 associated with the risk of Alzheimer's disease. *N. Engl. J. Med.* **368**, 107–116 (2013).
124. Guerreiro, R. *et al.* TREM2 variants in Alzheimer's disease. *N. Engl. J. Med.* **368**, 117–127 (2013).
125. Sims, R. *et al.* Rare coding variants in PLCG2, ABI3, and TREM2 implicate microglial-mediated innate immunity in Alzheimer's disease. *Nat. Genet.* **49**, 1373–1384 (2017).
126. Jones, L. *et al.* Genetic evidence implicates the immune system and cholesterol metabolism in the aetiology of Alzheimer's disease. *PLoS One* **5**, e13950 (2010).
127. Lambert, J., Grenier-Boley, B., Chouraki, V. & Heath, S. Implication of the Immune System in Alzheimer's Disease : Evidence from Genome-Wide Pathway Analysis. **20**, 1107–1118 (2010).
128. Jones, L. Convergent genetic and expression data implicate immunity in Alzheimer's disease. *Alzheimers Dement* **11**, 1–14 (2014).

129. Kunkle, B. W. *et al.* Genetic meta-analysis of diagnosed Alzheimer's disease identifies new risk loci and implicates A $\beta$ , tau, immunity and lipid processing. *Nat. Genet.* **51**, 414–430 (2019).
130. Pericak-Vance, M. a *et al.* Linkage studies in familial Alzheimer disease: evidence for chromosome 19 linkage. *Am. J. Hum. Genet.* **48**, 1034–1050 (1991).
131. Strittmatter, W. J. *et al.* Apolipoprotein E: high-avidity binding to beta-amyloid and increased frequency of type 4 allele in late-onset familial Alzheimer disease. *Proc. Natl. Acad. Sci. U. S. A.* **90**, 1977–1981 (1993).
132. Bertram, L. Alzheimer's disease genetics current status and future perspectives. *Int. Rev. Neurobiol.* **84**, 167–84 (2009).
133. Corder, E. H. *et al.* Protective effect of apolipoprotein E type 2 allele for late onset Alzheimer disease. *Nat. Genet.* **7**, 180–184 (1994).
134. Bertram, L., Lill, C. M. & Tanzi, R. E. The genetics of alzheimer disease: Back to the future. *Neuron* **68**, 270–281 (2010).
135. Liu, C., Kanekiyo, T., Xu, H. & Bu, G. Apolipoprotein E and Alzheimer disease: risk, mechanisms and therapy. *Nat. Rev. Neurol.* **9**, 106–118 (2013).
136. Mahley, R. W., Huang, Y. & Rall, S. C. J. Pathogenesis of type III hyperlipoproteinemia (dysbetalipoproteinemia). Questions, quandaries, and paradoxes. *J. Lipid Res.* **40**, 1933–1949 (1999).
137. Bu, G. Apolipoprotein E and its receptors in Alzheimer's disease: pathways, pathogenesis and therapy. *Nat. Rev. Neurosci.* **10**, 333–344 (2009).
138. Hatters, D. M., Peters-Libeu, C. A. & Weisgraber, K. H. Apolipoprotein E structure: insights into function. *Trends Biochem. Sci.* **31**, 445–454 (2006).
139. Weisgraber, K. H. Apolipoprotein E: structure-function relationships. *Adv. Protein Chem.* **45**, 249–302 (1994).
140. Dong, L. M. *et al.* Human apolipoprotein E. Role of arginine 61 in mediating the lipoprotein preferences of the E3 and E4 isoforms. *J. Biol. Chem.* **269**, 22358–22365 (1994).
141. Morrow, J. A. *et al.* Effect of arginine 172 on the binding of apolipoprotein E to the low density lipoprotein receptor. *J. Biol. Chem.* **275**, 2576–2580 (2000).
142. Morrow, J. A. *et al.* Differences in stability among the human apolipoprotein E isoforms determined by the amino-terminal domain. *Biochemistry* **39**, 11657–

- 11666 (2000).
143. Dong, L. M. & Weisgraber, K. H. Human apolipoprotein E4 domain interaction. Arginine 61 and glutamic acid 255 interact to direct the preference for very low density lipoproteins. *J. Biol. Chem.* **271**, 19053–19057 (1996).
  144. Mahley, R., Nathan, B. & Pitas, R. Apolipoprotein E: Structure, Function, and Possible Roles in Alzheimer's Disease. *Ann. New York Acad. Sci.* **777**, 139–145 (1996).
  145. Pitas, R. E., Boyles, J. K., Lee, S. H., Foss, D. & Mahley, R. W. Astrocytes synthesize apolipoprotein E and metabolize apolipoprotein E-containing lipoproteins. *Biochim. Biophys. Acta (BBA)/Lipids Lipid Metab.* **917**, 148–161 (1987).
  146. Xu, P. T. *et al.* Human apolipoprotein E2, E3, and E4 isoform-specific transgenic mice: human-like pattern of glial and neuronal immunoreactivity in central nervous system not observed in wild-type mice. *Neurobiol. Dis.* **3**, 229–245 (1996).
  147. Xu, Q. *et al.* Profile and regulation of apolipoprotein E (ApoE) expression in the CNS in mice with targeting of green fluorescent protein gene to the ApoE locus. *J. Neurosci.* **26**, 4985–4994 (2006).
  148. Boschert, U., Merlo-Pich, E., Higgins, G., Roses, A. D. & Catsicas, S. Apolipoprotein E expression by neurons surviving excitotoxic stress. *Neurobiol. Dis.* **6**, 508–514 (1999).
  149. Buttini, M. *et al.* Cellular source of apolipoprotein E4 determines neuronal susceptibility to excitotoxic injury in transgenic mice. *Am. J. Pathol.* **177**, 563–569 (2010).
  150. Reiman, E. M. *et al.* Fibrillar amyloid-beta burden in cognitively normal people at 3 levels of genetic risk for Alzheimer's disease. *Proc. Natl. Acad. Sci. U. S. A.* **106**, 6820–6825 (2009).
  151. Holtzman, D. M. *et al.* Apolipoprotein E isoform-dependent amyloid deposition and neuritic degeneration in a mouse model of Alzheimer's disease. *Proc. Natl. Acad. Sci. U. S. A.* **97**, 2892–2897 (2000).
  152. De Strooper, B. & Karran, E. The Cellular Phase of Alzheimer's Disease. *Cell* **164**, 603–615 (2016).

153. Ye, S. *et al.* Apolipoprotein (apo) E4 enhances amyloid beta peptide production in cultured neuronal cells: apoE structure as a potential therapeutic target. *Proc. Natl. Acad. Sci. U. S. A.* **102**, 18700–18705 (2005).
154. He, X., Cooley, K., Chung, C. H. Y., Dashti, N. & Tang, J. Apolipoprotein receptor 2 and X11 alpha/beta mediate apolipoprotein E-induced endocytosis of amyloid-beta precursor protein and beta-secretase, leading to amyloid-beta production. *J. Neurosci.* **27**, 4052–4060 (2007).
155. Osenkowski, P., Ye, W., Wang, R., Wolfe, M. S. & Selkoe, D. J. Direct and potent regulation of gamma-secretase by its lipid microenvironment. *J. Biol. Chem.* **283**, 22529–22540 (2008).
156. Castellano, J. M. *et al.* Human apoE isoforms differentially regulate brain amyloid-beta peptide clearance. *Sci. Transl. Med.* **3**, 89ra57 (2011).
157. Wildsmith, K. R., Holley, M., Savage, J. C., Skerrett, R. & Landreth, G. E. Evidence for impaired amyloid beta clearance in Alzheimer's disease. *Alzheimers. Res. Ther.* **5**, 33 (2013).
158. LaDu, M. J. *et al.* Isoform-specific binding of apolipoprotein E to beta-amyloid. *J. Biol. Chem.* **269**, 23403–23406 (1994).
159. Deane, R. *et al.* apoE isoform-specific disruption of amyloid beta peptide clearance from mouse brain. *J. Clin. Invest.* **118**, 4002–4013 (2008).
160. Verghese, P. B. *et al.* ApoE influences amyloid-beta (Abeta) clearance despite minimal apoE/Abeta association in physiological conditions. *Proc. Natl. Acad. Sci. U. S. A.* **110**, E1807-16 (2013).
161. Jiang, Q. *et al.* ApoE promotes the proteolytic degradation of Abeta. *Neuron* **58**, 681–693 (2008).
162. Kobayashi, M., Ishiguro, K., Katoh-Fukui, Y., Yokoyama, M. & Fujita, S. C. Phosphorylation state of tau in the hippocampus of apolipoprotein E4 and E3 knock-in mice. *Neuroreport* **14**, 699–702 (2003).
163. Tesseur, I. *et al.* Expression of human apolipoprotein E4 in neurons causes hyperphosphorylation of protein tau in the brains of transgenic mice. *Am. J. Pathol.* **156**, 951–964 (2000).
164. Brecht, W. J. *et al.* Neuron-specific apolipoprotein e4 proteolysis is associated with increased tau phosphorylation in brains of transgenic mice. *J. Neurosci.* **24**,

- 2527–2534 (2004).
165. Wang, C. *et al.* Gain of toxic apolipoprotein E4 effects in human iPSC-derived neurons is ameliorated by a small-molecule structure corrector. *Nat. Med.* **24**, 1–11 (2018).
  166. Huang, Y. *et al.* Apolipoprotein E fragments present in Alzheimer’s disease brains induce neurofibrillary tangle-like intracellular inclusions in neurons. *Proc. Natl. Acad. Sci. U. S. A.* **98**, 8838–8843 (2001).
  167. Harris, F. M. *et al.* Carboxyl-terminal-truncated apolipoprotein E4 causes Alzheimer’s disease-like neurodegeneration and behavioral deficits in transgenic mice. *Proc. Natl. Acad. Sci. U. S. A.* **100**, 10966–10971 (2003).
  168. D’Arcangelo, G. *et al.* Reelin is a ligand for lipoprotein receptors. *Neuron* **24**, 471–479 (1999).
  169. Hoe, H., Harris, D. C. & Rebeck, G. W. Multiple pathways of apolipoprotein E signaling in primary neurons. 145–155 (2005). doi:10.1111/j.1471-4159.2004.03007.x
  170. Mauch, D. H. *et al.* CNS synaptogenesis promoted by glia-derived cholesterol. *Science* **294**, 1354–7 (2001).
  171. Pfrieger, F. W. Outsourcing in the brain: Do neurons depend on cholesterol delivery by astrocytes? *BioEssays* **25**, 72–78 (2003).
  172. Jones, L., Harold, D. & Williams, J. Genetic evidence for the involvement of lipid metabolism in Alzheimer’s disease. *Biochim. Biophys. Acta* **1801**, 754–761 (2010).
  173. Ledesma, M. D. *et al.* Raft disorganization leads to reduced plasmin activity in Alzheimer’s disease brains. *EMBO Rep.* **4**, 1190–1196 (2003).
  174. Svennerholm, L. & Gottfries, C. G. Membrane lipids, selectively diminished in Alzheimer brains, suggest synapse loss as a primary event in early-onset form (type I) and demyelination in late-onset form (type II). *J. Neurochem.* **62**, 1039–1047 (1994).
  175. Hamanaka, H. *et al.* Altered cholesterol metabolism in human apolipoprotein E4 knock-in mice. *Hum. Mol. Genet.* **9**, 353–361 (2000).
  176. Michikawa, M., Fan, Q. W., Isobe, I. & Yanagisawa, K. Apolipoprotein E exhibits isoform-specific promotion of lipid efflux from astrocytes and neurons in

- culture. *J. Neurochem.* **74**, 1008–1016 (2000).
177. Riddell, D. R. *et al.* Impact of apolipoprotein E (ApoE) polymorphism on brain ApoE levels. *J. Neurosci.* **28**, 11445–11453 (2008).
  178. Rapp, A., Gmeiner, B. & Hutterer, M. Implication of apoE isoforms in cholesterol metabolism by primary rat hippocampal neurons and astrocytes. *Biochimie* **88**, 473–483 (2006).
  179. Gong, J.-S. *et al.* Apolipoprotein E (ApoE) isoform-dependent lipid release from astrocytes prepared from human ApoE3 and ApoE4 knock-in mice. *J. Biol. Chem.* **277**, 29919–29926 (2002).
  180. Mahley, R. W., Weisgraber, K. H. & Huang, Y. Apolipoprotein E: structure determines function, from atherosclerosis to Alzheimer's disease to AIDS. *J. Lipid Res.* **50 Suppl**, S183-8 (2009).
  181. Masliah, E., Mallory, M., Veinbergs, I., Miller, A. & Samuel, W. Alterations in apolipoprotein E expression during aging and neurodegeneration. *Prog. Neurobiol.* **50**, 493–503 (1996).
  182. Nathan, B. P. *et al.* The inhibitory effect of apolipoprotein E4 on neurite outgrowth is associated with microtubule depolymerization. *J. Biol. Chem.* **270**, 19791–19799 (1995).
  183. Holtzman, D. M. *et al.* Low density lipoprotein receptor-related protein mediates apolipoprotein E-dependent neurite outgrowth in a central nervous system-derived neuronal cell line. *Proc. Natl. Acad. Sci. U. S. A.* **92**, 9480–9484 (1995).
  184. Sun, Y. *et al.* Glial fibrillary acidic protein-apolipoprotein E (apoE) transgenic mice: astrocyte-specific expression and differing biological effects of astrocyte-secreted apoE3 and apoE4 lipoproteins. *J. Neurosci.* **18**, 3261–3272 (1998).
  185. Brodbeck, J. *et al.* Rosiglitazone increases dendritic spine density and rescues spine loss caused by apolipoprotein E4 in primary cortical neurons. *Proc. Natl. Acad. Sci. U. S. A.* **105**, 1343–1346 (2008).
  186. Dumanis, S. B. *et al.* ApoE4 decreases spine density and dendritic complexity in cortical neurons in vivo. *J. Neurosci.* **29**, 15317–15322 (2009).
  187. Jain, S., Yoon, S. Y., Leung, L., Knoferle, J. & Huang, Y. Cellular source-specific effects of apolipoprotein (apo) E4 on dendrite arborization and dendritic spine

- development. *PLoS One* **8**, e59478 (2013).
188. Ji, Y. *et al.* Apolipoprotein E isoform-specific regulation of dendritic spine morphology in apolipoprotein E transgenic mice and Alzheimer's disease patients. *Neuroscience* **122**, 305–315 (2003).
  189. Sun, G.-Z. *et al.* Hippocampal synaptic and neural network deficits in young mice carrying the human APOE4 gene. *CNS Neurosci. Ther.* **23**, 748–758 (2017).
  190. Mahley, R. W. & Huang, Y. Apolipoprotein e sets the stage: response to injury triggers neuropathology. *Neuron* **76**, 871–885 (2012).
  191. Arendt, T. *et al.* Plastic Neuronal Remodeling Is Impaired in Patients with Alzheimer's Disease Carrying Apolipoprotein E 4 Allele. *J. Neurosci.* **17**, 516–529 (1997).
  192. Li, G. *et al.* GABAergic interneuron dysfunction impairs hippocampal neurogenesis in adult apolipoprotein E4 knockin mice. *Cell Stem Cell* **5**, 634–645 (2009).
  193. Levi, O. & Michaelson, D. M. Environmental enrichment stimulates neurogenesis in apolipoprotein E3 and neuronal apoptosis in apolipoprotein E4 transgenic mice. *J. Neurochem.* **100**, 202–210 (2007).
  194. Yun, S. H. *et al.* Estradiol enhances long term potentiation in hippocampal slices from aged apoE4-TR mice. *Hippocampus* **17**, 1153–1157 (2007).
  195. Qiao, F., Gao, X.-P., Yuan, L., Cai, H.-Y. & Qi, J.-S. Apolipoprotein E4 impairs in vivo hippocampal long-term synaptic plasticity by reducing the phosphorylation of CaMKIIalpha and CREB. *J. Alzheimers. Dis.* **41**, 1165–1176 (2014).
  196. Trommer, B. L. *et al.* ApoE isoform affects LTP in human targeted replacement mice. *Neuroreport* **15**, 2655–2658 (2004).
  197. Kitamura, H. W. *et al.* Age-dependent enhancement of hippocampal long-term potentiation in knock-in mice expressing human apolipoprotein E4 instead of mouse apolipoprotein E. *Neurosci. Lett.* **369**, 173–178 (2004).
  198. Chen, Y., Durakoglugil, M. S., Xian, X. & Herz, J. ApoE4 reduces glutamate receptor function and synaptic plasticity by selectively impairing ApoE receptor recycling. *Proc. Natl. Acad. Sci. U. S. A.* **107**, 12011–6 (2010).
  199. Butovsky, O. *et al.* Identification of a unique TGF-beta-dependent molecular and functional signature in microglia. *Nat. Neurosci.* **17**, 131–143 (2014).

200. Krasemann, S. *et al.* The TREM2-APOE Pathway Drives the Transcriptional Phenotype of Dysfunctional Microglia in Neurodegenerative Diseases Article The TREM2-APOE Pathway Drives the Transcriptional Phenotype of Dysfunctional Microglia in Neurodegenerative Diseases. *Immunity* **47**, 566-581.e9 (2017).
201. Zhang, B. *et al.* Integrated systems approach identifies genetic nodes and networks in late-onset Alzheimer's disease. *Cell* **153**, 707–720 (2013).
202. Lin, Y. T. *et al.* APOE4 Causes Widespread Molecular and Cellular Alterations Associated with Alzheimer's Disease Phenotypes in Human iPSC-Derived Brain Cell Types. *Neuron* **98**, 1141-1154.e7 (2018).
203. Yang, Y. *et al.* APOE3, but not APOE4, bone marrow transplantation mitigates behavioral and pathological changes in a mouse model of Alzheimer disease. *Am. J. Pathol.* **183**, 905–917 (2013).
204. Muth, C., Hartmann, A., Sepulveda-Falla, D., Glatzel, M. & Krasemann, S. Phagocytosis of Apoptotic Cells Is Specifically Upregulated in ApoE4 Expressing Microglia in vitro. *Front. Cell. Neurosci.* **13**, 181 (2019).
205. Cudaback, E., Li, X., Montine, K. S., Montine, T. J. & Keene, C. D. Apolipoprotein E isoform-dependent microglia migration. *FASEB J. Off. Publ. Fed. Am. Soc. Exp. Biol.* **25**, 2082–2091 (2011).
206. Guo, L., LaDu, M. J. & Van Eldik, L. J. A dual role for apolipoprotein e in neuroinflammation: anti- and pro-inflammatory activity. *J. Mol. Neurosci.* **23**, 205–212 (2004).
207. Gale, S. C. *et al.* APOepsilon4 is associated with enhanced in vivo innate immune responses in human subjects. *J. Allergy Clin. Immunol.* **134**, 127–134 (2014).
208. Allen, N. J. & Barres, B. A. Glia - more than just brain glue. *Nature* **457**, 675–677 (2009).
209. Khakh, B. S. & Sofroniew, M. V. Diversity of astrocyte functions and phenotypes in neural circuits. *Nat. Neurosci.* **18**, 942–952 (2015).
210. Bushong, E. A., Martone, M. E., Jones, Y. Z. & Ellisman, M. H. Protoplasmic astrocytes in CA1 stratum radiatum occupy separate anatomical domains. *J. Neurosci.* **22**, 183–192 (2002).
211. Pekny, M. & Pekna, M. Astrocyte intermediate filaments in CNS pathologies and regeneration. 428–437 (2004). doi:10.1002/path.1645

212. Arranz, A. M. & De Strooper, B. The role of astroglia in Alzheimer's disease: pathophysiology and clinical implications. *Lancet Neurol.* **18**, 406–414 (2019).
213. Medeiros, R. & LaFerla, F. M. Astrocytes: conductors of the Alzheimer disease neuroinflammatory symphony. *Exp. Neurol.* **239**, 133–8 (2013).
214. Verkhratsky, A., Parpura, V., Pekna, M., Pekny, M. & Sofroniew, M. Glia in the pathogenesis of neurodegenerative diseases. *Biochem. Soc. Trans.* **42**, 1291–1301 (2014).
215. Hsu, E. T. *et al.* Astrocytic degeneration in chronic traumatic encephalopathy. *Acta Neuropathol.* **136**, 955–972 (2018).
216. Yoshida, M. Astrocytic inclusions in progressive supranuclear palsy and corticobasal degeneration. *Neuropathology* **34**, 555–570 (2014).
217. Verkhratsky, A. & Nedergaard, M. Physiology of astroglia. *Physiol Rev* **98**, 239–389 (2018).
218. Sofroniew, M. V. & Vinters, H. V. Astrocytes: Biology and pathology. *Acta Neuropathol.* **119**, 7–35 (2010).
219. Nedergaard, M., Ransom, B. & Goldman, S. A. New roles for astrocytes: redefining the functional architecture of the brain. *Trends Neurosci.* **26**, 523–530 (2003).
220. Charles, A. C., Merrill, J. E., Dirksen, E. R. & Sanderson, M. J. Intercellular signaling in glial cells: calcium waves and oscillations in response to mechanical stimulation and glutamate. *Neuron* **6**, 983–992 (1991).
221. Perea, G., Navarrete, M. & Araque, A. Tripartite synapses: astrocytes process and control synaptic information. *Trends Neurosci.* **32**, 421–31 (2009).
222. Shigetomi, E., Bowser, D. N., Sofroniew, M. V & Khakh, B. S. Two forms of astrocyte calcium excitability have distinct effects on NMDA receptor-mediated slow inward currents in pyramidal neurons. *J. Neurosci.* **28**, 6659–6663 (2008).
223. Allen, N. J. Astrocyte Regulation of Synaptic Behavior. *Annu. Rev. Cell Dev. Biol.* **30**, 439–63 (2014).
224. Obara, M., Szeliga, M. & Albrecht, J. Regulation of pH in the mammalian central nervous system under normal and pathological conditions: facts and hypotheses. *Neurochem. Int.* **52**, 905–919 (2008).
225. Seifert, G., Schilling, K. & Steinhäuser, C. Astrocyte dysfunction in neurological

- disorders: a molecular perspective. *Nat. Rev. Neurosci.* **7**, 194–206 (2006).
226. Kofuji, P. & Newman, E. A. Potassium buffering in the central nervous system. *Neuroscience* **129**, 1045–1056 (2004).
227. Poopalasundaram, S. *et al.* Glial heterogeneity in expression of the inwardly rectifying K(+) channel, Kir4.1, in adult rat CNS. *Glia* **30**, 362–372 (2000).
228. Vasile, F., Dossi, E. & Rouach, N. Human astrocytes: structure and functions in the healthy brain. *Brain Struct. Funct.* **222**, 2017–2029 (2017).
229. Delaney, C. L., Brenner, M. & Messing, A. Conditional ablation of cerebellar astrocytes in postnatal transgenic mice. *J. Neurosci.* **16**, 6908–6918 (1996).
230. Goritz, C., Mauch, D. H. & Pfrieder, F. W. Multiple mechanisms mediate cholesterol-induced synaptogenesis in a CNS neuron. *Mol. Cell. Neurosci.* **29**, 190–201 (2005).
231. Nieweg, K., Schaller, H. & Pfrieder, F. W. Marked differences in cholesterol synthesis between neurons and glial cells from postnatal rats. *J. Neurochem.* **109**, 125–134 (2009).
232. Saito, M., Benson, E. P., Saito, M. & Rosenberg, A. Metabolism of cholesterol and triacylglycerol in cultured chick neuronal cells, glial cells, and fibroblasts: accumulation of esterified cholesterol in serum-free culture. *J. Neurosci. Res.* **18**, 319–25 (1987).
233. Pitas, R. E., Boyles, J. K., Lee, S. H., Foss, D. & Mahley, R. W. Astrocytes synthesize apolipoprotein E and metabolize apolipoprotein E-containing lipoproteins. *Biochim. Biophys. Acta* **917**, 148–61 (1987).
234. Boyles, J. K., Pitas, R. E., Wilson, E., Mahley, R. W. & Taylor, J. M. Apolipoprotein E associated with astrocytic glia of the central nervous system and with nonmyelinating glia of the peripheral nervous system. *J. Clin. Invest.* **76**, 1501–13 (1985).
235. Correa-Gillieron, E. M. & Cavalcante, L. A. Synaptogenesis in retino-receptive layers of the superior colliculus of the opossum *Didelphis marsupialis*. *Brain. Behav. Evol.* **54**, 71–84 (1999).
236. Steinmetz, C. C., Buard, I., Claudepierre, T., Nägler, K. & Pfrieder, F. W. Regional variations in the glial influence on synapse development in the mouse CNS. *J. Physiol.* **577**, 249–261 (2006).

237. Ullian, E. M., Christopherson, K. S. & Barres, B. A. Role for glia in synaptogenesis. *Glia* **47**, 209–16 (2004).
238. Pfrieger, F. W. & Barres, B. A. Synaptic efficacy enhanced by glial cells in vitro. *Science* **277**, 1684–7 (1997).
239. Nägler, K., Mauch, D. H. & Pfrieger, F. W. Glia-derived signals induce synapse formation in neurones of the rat central nervous system. *J. Physiol.* **533**, 665–79 (2001).
240. Ullian, E. M., Sapperstein, S. K., Christopherson, K. S. & Barres, B. A. Control of synapse number by glia. *Science* **291**, 657–61 (2001).
241. Stellwagen, D. & Malenka, R. C. Synaptic scaling mediated by glial TNF- $\alpha$ . *Nature* **440**, 1054–1059 (2006).
242. Hennekinne, L., Colasse, S., Triller, A. & Renner, M. Differential control of thrombospondin over synaptic glycine and AMPA receptors in spinal cord neurons. *J. Neurosci.* **33**, 11432–11439 (2013).
243. Weiss, N., Miller, F., Cazaubon, S. & Couraud, P.-O. The blood-brain barrier in brain homeostasis and neurological diseases. *Biochim. Biophys. Acta - Biomembr.* **1788**, 842–857 (2009).
244. Oksanen, M., Lehtonen, S., Jaronen, M., Goldsteins, G. & Hämäläinen, R. H. Astrocyte alterations in neurodegenerative pathologies and their modeling in human induced pluripotent stem cell platforms. *Cell. Mol. Life Sci.* **76**, 2739–2760 (2019).
245. Birch, A. M. The contribution of astrocytes to Alzheimer’s disease. *Biochem. Soc. Trans.* **42**, 1316–1320 (2014).
246. Haseloff, R. F., Blasig, I. E., Bauer, H. C. & Bauer, H. In search of the astrocytic factor(s) modulating blood-brain barrier functions in brain capillary endothelial cells in vitro. *Cell. Mol. Neurobiol.* **25**, 25–39 (2005).
247. Alvarez, J. I., Katayama, T. & Prat, A. Glial influence on the blood brain barrier. *Glia* **61**, 1939–1958 (2013).
248. Bazargani, N. & Attwell, D. Astrocyte calcium signaling: the third wave. *Nat. Neurosci.* **19**, 182–189 (2016).
249. Heneka, M. T. *et al.* Neuroinflammation in Alzheimer’s disease. *Lancet Neurol.* **14**, 388–405 (2015).

250. Overmyer, M. *et al.* Astrogliosis and the ApoE genotype. an immunohistochemical study of postmortem human brain tissue. *Dement. Geriatr. Cogn. Disord.* **10**, 252–257 (1999).
251. Cahoy, J. D. *et al.* A transcriptome database for astrocytes, neurons, and oligodendrocytes: a new resource for understanding brain development and function. *J. Neurosci.* **28**, 264–78 (2008).
252. Sofroniew, M. V. Multiple Roles for Astrocytes as Effectors of Cytokines and Inflammatory Mediators. *Neurosci.* **20**, 160–172 (2014).
253. Zamanian, J. L. *et al.* Genomic analysis of reactive astrogliosis. *J. Neurosci.* **32**, 6391–410 (2012).
254. Orre, M. *et al.* Acute isolation and transcriptome characterization of cortical astrocytes and microglia from young and aged mice. *Neurobiol. Aging* **35**, 1–14 (2014).
255. Colombo, E. & Farina, C. Astrocytes: Key Regulators of Neuroinflammation. *Trends Immunol.* **37**, 608–620 (2016).
256. Jones, V. C., Atkinson-Dell, R., Verkhatsky, A. & Mohamet, L. Aberrant iPSC-derived human astrocytes in Alzheimer’s disease. *Cell Death Dis.* **8**, e2696 (2017).
257. Bell, R. D. *et al.* Apolipoprotein E controls cerebrovascular integrity via cyclophilin A. *Nature* **485**, 512 (2012).
258. Halliday, M. R. *et al.* Accelerated pericyte degeneration and blood-brain barrier breakdown in apolipoprotein E4 carriers with Alzheimer’s disease. *J. Cereb. Blood Flow Metab.* **36**, 216–227 (2016).
259. Koistinaho, M. *et al.* Apolipoprotein E promotes astrocyte colocalization and degradation of deposited amyloid-beta peptides. *Nat. Med.* **10**, 719–726 (2004).
260. Zhao, J. *et al.* APOE  $\epsilon 4/\epsilon 4$  diminishes neurotrophic function of human iPSC-derived astrocytes. *Hum. Mol. Genet.* **26**, 2690–2700 (2017).
261. Simonovitch, S. *et al.* Impaired Autophagy in APOE4 Astrocytes. *J. Alzheimers. Dis.* **51**, 915–927 (2016).
262. Boisvert, M. M., Erikson, G. A., Shokhirev, M. N. & Allen, N. J. The Aging Astrocyte Transcriptome from Multiple Regions of the Mouse Brain. *Cell Rep.* **22**, 269–285 (2018).

263. Tcw, J. *et al.* Cholesterol and matrisome pathways dysregulated in human APOE ̳4 glia. **4**, (2019).
264. Fernandez, C. G., Hamby, M. E., McReynolds, M. L. & Ray, W. J. The Role of APOE4 in Disrupting the Homeostatic Functions of Astrocytes and Microglia in Aging and Alzheimer’s Disease. *Front. Aging Neurosci.* **11**, 1–18 (2019).
265. Chung, W.-S. *et al.* Novel allele-dependent role for APOE in controlling the rate of synapse pruning by astrocytes. *Proc. Natl. Acad. Sci.* **113**, 10186–10191 (2016).
266. Tzioras, M. Invited Review: APOE at the interface of inflammation , neurodegeneration and pathological protein spread in Alzheimer’s disease. *Neuropathol. Appl. Neurobiol.* **45**, 327–346 (2019).
267. Ophir, G. *et al.* Apolipoprotein E4 enhances brain inflammation by modulation of the NF-κB signaling cascade. *Neurobiol. Dis.* **20**, 709–718 (2005).
268. Lynch, J. R. *et al.* APOE genotype and an ApoE-mimetic peptide modify the systemic and central nervous system inflammatory response. *J. Biol. Chem.* **278**, 48529–48533 (2003).
269. Maezawa, I., Maeda, N., Montine, T. J. & Montine, K. S. Apolipoprotein E-specific innate immune response in astrocytes from targeted replacement mice. *J. Neuroinflammation* **3**, 1–6 (2006).
270. Prindull, G., Prindull, B. & Meulen, N. Haematopoietic stem cells (CFUc) in human cord blood. *Acta Paediatr. Scand.* **67**, 413–416 (1978).
271. Evans, M. J. & Kaufman, M. H. Establishment in culture of pluripotential cells from mouse embryos. *Nature* **292**, 154–156 (1981).
272. Thomson, J. A. *et al.* Embryonic stem cell lines derived from human blastocysts. *Science* **282**, 1145–1147 (1998).
273. Takahashi, K. *et al.* Induction of Pluripotent Stem Cells from Adult Human Fibroblasts by Defined Factors. *Cell* **131**, 861–872 (2007).
274. Pan, G., Li, J., Zhou, Y., Zheng, H. & Pei, D. A negative feedback loop of transcription factors that controls stem cell pluripotency and self-renewal. *FASEB J. Off. Publ. Fed. Am. Soc. Exp. Biol.* **20**, 1730–1732 (2006).
275. Aasen, T. *et al.* Efficient and rapid generation of induced pluripotent stem cells from human keratinocytes. *Nat. Biotechnol.* **26**, 1276–1284 (2008).

276. Loh, Y.-H. *et al.* Generation of induced pluripotent stem cells from human blood. *Blood* **113**, 5476–5479 (2009).
277. Chen, W., Huang, J., Yu, X., Lin, X. & Dai, Y. Generation of induced pluripotent stem cells from renal tubular cells of a patient with Alport syndrome. *Int. J. Nephrol. Renovasc. Dis.* **8**, 101–109 (2015).
278. Tamaoki, N. *et al.* Dental pulp cells for induced pluripotent stem cell banking. *J. Dent. Res.* **89**, 773–778 (2010).
279. McNeely, T., Leone, M., Yanai, H. & Beerman, I. DNA damage in aging, the stem cell perspective. *Hum. Genet.* (2019). doi:10.1007/s00439-019-02047-z
280. Weissman, I. L. Stem cells: units of development, units of regeneration, and units in evolution. *Cell* **100**, 157–168 (2000).
281. Altman, J. & Das, G. D. Autoradiographic and histological evidence of postnatal hippocampal neurogenesis in rats. *J. Comp. Neurol.* **124**, 319–335 (1965).
282. Gage, F. H., Ray, J. & Fisher, L. J. Isolation, characterization, and use of stem cells from the CNS. *Annu. Rev. Neurosci.* **18**, 159–192 (1995).
283. Alvarez-Buylla, A., Seri, B. & Doetsch, F. Identification of neural stem cells in the adult vertebrate brain. *Brain Res. Bull.* **57**, 751–758 (2002).
284. Kirschen, G. W. *et al.* Young at heart: Insights into hippocampal neurogenesis in the aged brain. *Behav. Brain Res.* **369**, 111934 (2019).
285. Reubinoff, B. E., Pera, M. F., Fong, C. Y., Trounson, A. & Bongso, A. Embryonic stem cell lines from human blastocysts: somatic differentiation in vitro. *Nat. Biotechnol.* **18**, 399–404 (2000).
286. Penney, J., Ralvenius, W. T. & Tsai, L.-H. Modeling Alzheimer’s disease with iPSC-derived brain cells. *Mol. Psychiatry* (2019). doi:10.1038/s41380-019-0468-3
287. Pre, D. *et al.* A time course analysis of the electrophysiological properties of neurons differentiated from human induced pluripotent stem cells (iPSCs). *PLoS One* **9**, e103418 (2014).
288. Odawara, A., Katoh, H., Matsuda, N. & Suzuki, I. Physiological maturation and drug responses of human induced pluripotent stem cell-derived cortical neuronal networks in long-term culture. *Sci. Rep.* **6**, 26181 (2016).
289. Robbins, J. P. *et al.* Clusterin Is Required for  $\beta$ -Amyloid Toxicity in Human iPSC-Derived Neurons. *Front. Neurosci.* **12**, 1–13 (2018).

290. Camp, J. G. *et al.* Human cerebral organoids recapitulate gene expression programs of fetal neocortex development. *Proc. Natl. Acad. Sci. U. S. A.* **112**, 15672–15677 (2015).
291. Gore, A. *et al.* Somatic coding mutations in human induced pluripotent stem cells. *Nature* **471**, 63–67 (2011).
292. Kilpinen, H. *et al.* Common genetic variation drives molecular heterogeneity in human iPSCs. *Nature* **546**, 370–375 (2017).
293. Gupta, R. M. & Musunuru, K. Expanding the genetic editing tool kit: ZFNs, TALENs and CRISPR-Cas9. *J. Clin. Investig. Investig.* **124**, 4154–4161 (2014).
294. Rouet, P., Smih, F. & Jasin, M. Expression of a site-specific endonuclease stimulates homologous recombination in mammalian cells. *Proc. Natl. Acad. Sci. U. S. A.* **91**, 6064–6068 (1994).
295. Chen, F. *et al.* High-frequency genome editing using ssDNA oligonucleotides with zinc-finger nucleases. *Nat. Methods* **8**, 753–755 (2011).
296. Streubel, J., Blucher, C., Landgraf, A. & Boch, J. TAL effector RVD specificities and efficiencies. *Nature biotechnology* **30**, 593–595 (2012).
297. Bogdanove, A. J. & Voytas, D. F. TAL effectors: customizable proteins for DNA targeting. *Science* **333**, 1843–1846 (2011).
298. Miller, J. C. *et al.* A TALE nuclease architecture for efficient genome editing. *Nat. Biotechnol.* **29**, 143–148 (2011).
299. Gasiunas, G., Barrangou, R., Horvath, P. & Siksnys, V. Cas9-crRNA ribonucleoprotein complex mediates specific DNA cleavage for adaptive immunity in bacteria. *Proc. Natl. Acad. Sci. U. S. A.* **109**, E2579-86 (2012).
300. Jinek, M. *et al.* A programmable dual-RNA-guided DNA endonuclease in adaptive bacterial immunity. *Science* **337**, 816–821 (2012).
301. Ran, F. A. *et al.* Double nicking by RNA-guided CRISPR cas9 for enhanced genome editing specificity. *Cell* **154**, 1380–1389 (2013).
302. DeWitt, M. A. *et al.* Selection-free genome editing of the sickle mutation in human adult hematopoietic stem/progenitor cells. *Sci. Transl. Med.* **8**, 360ra134 (2016).
303. Amoasii, L. *et al.* Gene editing restores dystrophin expression in a canine model of Duchenne muscular dystrophy. *Science (80-. ).* **362**, 86 LP – 91 (2018).

304. Ramaswamy, S. *et al.* Autologous and Heterologous Cell Therapy for Hemophilia B toward Functional Restoration of Factor IX. *Cell Rep.* **23**, 1565–1580 (2018).
305. De Silva, S. R. *et al.* Long-term restoration of visual function in end-stage retinal degeneration using subretinal human melanopsin gene therapy. *Proc. Natl. Acad. Sci. U. S. A.* **114**, 11211–11216 (2017).
306. Gaj, T. *et al.* In vivo genome editing improves motor function and extends survival in a mouse model of ALS. *Sci. Adv.* **3**, eaar3952 (2017).
307. Makarova, K. S. *et al.* Evolution and classification of the CRISPR-Cas systems. *Nature reviews. Microbiology* **9**, 467–477 (2011).
308. Byun, J. *et al.* Automated tool for the detection of cell nuclei in digital microscopic images: application to retinal images. *Mol. Vis.* **12**, 949–960 (2006).
309. Liddelw, S. A. *et al.* Neurotoxic reactive astrocytes are induced by activated microglia. *Nature* (2017). doi:10.1038/nature21029
310. Morizawa, Y. M. *et al.* Reactive astrocytes function as phagocytes after brain ischemia via ABCA1-mediated pathway. *Nat. Commun.* **8**, 1–14 (2017).
311. Livak, K. J. & Schmittgen, T. D. Analysis of relative gene expression data using real-time quantitative PCR and the 2<sup>(-Delta Delta C(T))</sup> Method. *Methods* **25**, 402–408 (2001).
312. Pfaffl, M. W. A new mathematical model for relative quantification in real-time RT-PCR. *Nucleic Acids Res.* **29**, e45 (2001).
313. Ran, F., Hsu, P., Wright, J. & Agarwala, V. Genome engineering using the CRISPR-Cas9 system. *Nat. Protoc.* **8**, 2281–308 (2013).
314. Jacobi, A. M. *et al.* Simplified CRISPR tools for efficient genome editing and streamlined protocols for their delivery into mammalian cells and mouse zygotes. *Methods* **121–122**, 16–28 (2017).
315. Doench, J. G. *et al.* Optimized sgRNA design to maximize activity and minimize off-target effects of CRISPR-Cas9. *Nat. Biotechnol.* 1–12 (2016). doi:10.1038/nbt.3437
316. Yang, L. *et al.* Optimization of scarless human stem cell genome editing. *Nucleic Acids Res.* **41**, 9049–9061 (2013).
317. Richardson, C. D., Ray, G. J., DeWitt, M. A., Curie, G. L. & Corn, J. E. Enhancing homology-directed genome editing by catalytically active and inactive CRISPR-

- Cas9 using asymmetric donor DNA. *Nat. Biotechnol.* 1–7 (2016).  
doi:10.1038/nbt.3481
318. Liang, X., Potter, J., Kumar, S., Ravinder, N. & Chesnut, J. D. Enhanced CRISPR/Cas9-mediated precise genome editing by improved design and delivery of gRNA, Cas9 nuclease, and donor DNA. *J. Biotechnol.* **241**, 136–146 (2016).
  319. Yonglun Luo. *CRISPR Gene Editing*. (2019).
  320. Listgarten, J. *et al.* Prediction of off-target activities for the end-to-end design of CRISPR guide RNAs. *Nat. Biomed. Eng.* **2**, 38–47 (2018).
  321. Scholer, H. R., Hatzopoulos, A. K., Balling, R., Suzuki, N. & Gruss, P. A family of octamer-specific proteins present during mouse embryogenesis: evidence for germline-specific expression of an Oct factor. *EMBO J.* **8**, 2543–2550 (1989).
  322. Shi, G. & Jin, Y. Role of Oct4 in maintaining and regaining stem cell pluripotency. *Stem Cell Res. Ther.* **1**, 39 (2010).
  323. Choi, S. M. *et al.* Reprogramming of EBV-immortalized B-lymphocyte cell lines into induced pluripotent stem cells. *Blood* **118**, 1801–1805 (2011).
  324. Dahlstrand, J., Lardelli, M. & Lendahl, U. Nestin mRNA expression correlates with the central nervous system progenitor cell state in many, but not all, regions of developing central nervous system. *Brain Res. Dev. Brain Res.* **84**, 109–129 (1995).
  325. Greig, L. C., Woodworth, M. B., Galazo, M. J., Padmanabhan, H. & Macklis, J. D. Molecular logic of neocortical projection neuron specification, development and diversity. *Nat. Rev. Neurosci.* **14**, 755–769 (2013).
  326. Stewart, M. J. *et al.* Clonal isolation of hESCs reveals heterogeneity within the pluripotent stem cell compartment. *Nat. Methods* **3**, 807–815 (2006).
  327. Sun, C. *et al.* Transcriptome variations among human embryonic stem cell lines are associated with their differentiation propensity. *PLoS One* **13**, 1–19 (2018).
  328. Tsai, S. Q. *et al.* GUIDE-seq enables genome-wide profiling of off-target cleavage by CRISPR-Cas nucleases. *Nat. Biotechnol.* **33**, 187–198 (2015).
  329. Cameron, P. *et al.* Mapping the genomic landscape of CRISPR-Cas9 cleavage. *Nat. Methods* **14**, 600–606 (2017).
  330. Yan, W. X. *et al.* BLISS is a versatile and quantitative method for genome-wide profiling of DNA double-strand breaks. *Nat. Commun.* **8**, 15058 (2017).

331. Zhang, S. *et al.* OCT4 and PAX6 determine the dual function of SOX2 in human ESCs as a key pluripotent or neural factor. **7**, 1–14 (2019).
332. Ellis, P. *et al.* SOX2, a persistent marker for multipotential neural stem cells derived from embryonic stem cells, the embryo or the adult. *Dev. Neurosci.* **26**, 148–165 (2004).
333. Graham, V., Khudyakov, J., Ellis, P. & Pevny, L. SOX2 functions to maintain neural progenitor identity. *Neuron* **39**, 749–765 (2003).
334. Matyash, V. & Kettenmann, H. Heterogeneity in astrocyte morphology and physiology. *Brain Res. Rev.* **63**, 2–10 (2010).
335. Oberheim, N. A. *et al.* Uniquely hominid features of adult human astrocytes. *J. Neurosci.* **29**, 3276–3287 (2009).
336. Zhang, Y. *et al.* Purification and Characterization of Progenitor and Mature Human Astrocytes Reveals Transcriptional and Functional Differences with Mouse. *Neuron* **89**, 37–53 (2016).
337. Tyzack, G., Lakatos, A. & Patani, R. Human Stem Cell-Derived Astrocytes: Specification and Relevance for Neurological Disorders. *Curr. Stem Cell Reports* **2**, 236–247 (2016).
338. Kageyama, R., Ohtsuka, T., Hatakeyama, J. & Ohsawa, R. Roles of bHLH genes in neural stem cell differentiation. *Exp. Cell Res.* **306**, 343–348 (2005).
339. Morrison, S. J. *et al.* Transient Notch activation initiates an irreversible switch from neurogenesis to gliogenesis by neural crest stem cells. *Cell* **101**, 499–510 (2000).
340. Bonni, A. *et al.* Regulation of gliogenesis in the central nervous system by the JAK-STAT signaling pathway. *Science (80-. ).* **278**, 477–483 (1997).
341. Urayama, S. *et al.* Chromatin accessibility at a STAT3 target site is altered prior to astrocyte differentiation. *Cell Struct. Funct.* **38**, 55–66 (2013).
342. Sloan, S. A. & Barres, B. A. Mechanisms of astrocyte development and their contributions to neurodevelopmental disorders. *Curr. Opin. Neurobiol.* **27**, 75–81 (2014).
343. Nakashima, K., Yanagisawa, M., Arakawa, H. & Taga, T. Astrocyte differentiation mediated by LIF in cooperation with BMP2. *FEBS Lett.* **457**, 43–46 (1999).
344. Takizawa, T. *et al.* DNA methylation is a critical cell-intrinsic determinant of

- astrocyte differentiation in the fetal brain. *Dev. Cell* **1**, 749–758 (2001).
345. Hutnick, L. K. *et al.* DNA hypomethylation restricted to the murine forebrain induces cortical degeneration and impairs postnatal neuronal maturation. *Hum. Mol. Genet.* **18**, 2875–2888 (2009).
346. Bonaguidi, M. A. *et al.* LIF and BMP signaling generate separate and discrete types of GFAP-expressing cells. *Development* **132**, 5503 LP – 5514 (2005).
347. Serio, A. *et al.* Astrocyte pathology and the absence of non-cell autonomy in an induced pluripotent stem cell model of TDP-43 proteinopathy. *Proc. Natl. Acad. Sci. U. S. A.* **110**, 4697–702 (2013).
348. Asano, H. *et al.* Astrocyte differentiation of neural precursor cells is enhanced by retinoic acid through a change in epigenetic modification. *Stem Cells* **27**, 2744–2752 (2009).
349. Chandrasekaran, A., Avci, H. X., Leist, M., Kobolák, J. & Dinnyés, A. Astrocyte Differentiation of Human Pluripotent Stem Cells: New Tools for Neurological Disorder Research. *Front. Cell. Neurosci.* **10**, (2016).
350. TCW, J. *et al.* An Efficient Platform for Astrocyte Differentiation from Human Induced Pluripotent Stem Cells. *Stem Cell Reports* **9**, 600–614 (2017).
351. Heni, M. *et al.* Insulin Promotes Glycogen Storage and Cell Proliferation in Primary Human Astrocytes. *PLoS One* **6**, e21594 (2011).
352. Krencik, R. & Zhang, S. C. S.-C. Directed differentiation of functional astroglial subtypes from human pluripotent stem cells. *Nat. Protoc.* **6**, 1710–1717 (2011).
353. Shaltouki, A., Peng, J., Liu, Q., Rao, M. S. & Zeng, X. Efficient generation of astrocytes from human pluripotent stem cells in defined conditions. *Stem Cells* **31**, 941–52 (2013).
354. Magistri, M. *et al.* A comparative transcriptomic analysis of astrocytes differentiation from human neural progenitor cells. *Eur. J. Neurosci.* **44**, 2858–2870 (2016).
355. Zhang, Z. *et al.* The Appropriate Marker for Astrocytes: Comparing the Distribution and Expression of Three Astrocytic Markers in Different Mouse Cerebral Regions. *Biomed Res. Int.* **2019**, 9605265 (2019).
356. Shaltouki, A., Peng, J., Liu, Q., Rao, M. S. & Zeng, X. Efficient generation of astrocytes from human pluripotent stem cells in defined conditions. *Stem Cells*

- 31**, 941–952 (2013).
357. Eng, L. F., Ghirnikar, R. S. & Lee, Y. L. Glial Fibrillary Acidic Protein : GFAP-Thirty-One Years (1969-2000). *Neurochem. Res.* **25**, 1439–1451 (2000).
358. Ogata, K. & Kosaka, T. Structural and quantitative analysis of astrocytes in the mouse hippocampus. *Neuroscience* **113**, 221–233 (2002).
359. Donato, R. *et al.* Functions of S100 proteins. *Curr. Mol. Med.* **13**, 24–57 (2013).
360. Raponi, E. *et al.* S100B expression defines a state in which GFAP-expressing cells lose their neural stem cell potential and acquire a more mature developmental stage. *Glia* **55**, 165–177 (2007).
361. Kim, K. *et al.* Role of Excitatory Amino Acid Transporter-2 (EAAT2) and glutamate in neurodegeneration: Opportunities for developing novel therapeutics. *J. Cell. Physiol.* **226**, 2484–2493 (2011).
362. Ramaswamy, G., Xu, Q., Huang, Y. & Weisgraber, K. H. Effect of Domain Interaction on Apolipoprotein E Levels in Mouse Brain. *J. Neurosci.* **25**, 10658 LP – 10663 (2005).
363. Rezeli, M. *et al.* Quantification of total apolipoprotein E and its specific isoforms in cerebrospinal fluid and blood in Alzheimer’s disease and other neurodegenerative diseases. *EuPA Open Proteomics* **8**, 137–143 (2015).
364. Bekris, L. M. *et al.* Multiple SNPs within and surrounding the apolipoprotein E gene influence cerebrospinal fluid apolipoprotein E protein levels. *J. Alzheimers. Dis.* **13**, 255–266 (2008).
365. Talwar, P. *et al.* Meta-analysis of apolipoprotein E levels in the cerebrospinal fluid of patients with Alzheimer’s disease. *J. Neurol. Sci.* **360**, 179–187 (2016).
366. Cruchaga, C. *et al.* Cerebrospinal fluid APOE levels: an endophenotype for genetic studies for Alzheimer’s disease. *Hum. Mol. Genet.* **21**, 4558–4571 (2012).
367. Toledo, J. B. *et al.* CSF Apo-E levels associate with cognitive decline and MRI changes. *Acta Neuropathol.* **127**, 621–632 (2014).
368. Beffert, U. *et al.* The neurobiology of apolipoproteins and their receptors in the CNS and Alzheimer’s disease. *Brain Res. Rev.* **27**, 119–142 (1998).
369. Bertrand, P., Poirier, J., Oda, T., Finch, C. E. & Pasinetti, G. M. Association of apolipoprotein E genotype with brain levels of apolipoprotein E and apolipoprotein J (clusterin) in Alzheimer disease. *Brain Res. Mol. Brain Res.* **33**,

- 174–178 (1995).
370. Glockner, F., Meske, V. & Ohm, T. G. Genotype-related differences of hippocampal apolipoprotein E levels only in early stages of neuropathological changes in Alzheimer's disease. *Neuroscience* **114**, 1103–1114 (2002).
371. Conejero-Goldberg, C. *et al.* Molecular signatures in post-mortem brain tissue of younger individuals at high risk for Alzheimer's disease as based on APOE genotype. *Mol. Psychiatry* **16**, 836–847 (2011).
372. Zhao, J. *et al.* APOE  $\epsilon 4/\epsilon 4$  diminishes neurotrophic function of human iPSC-derived astrocytes. *Hum. Mol. Genet.* **26**, 2690–2700 (2017).
373. Innerarity, T. L., Friedlander, E. J., Rall Jr., S. C., Weisgraber, K. H. & Mahley, R. W. The receptor-binding domain of human apolipoprotein E. Binding of apolipoprotein E fragments. *J. Biol. Chem.* **258**, 12341–12347 (1983).
374. Yamamoto, T., Choi, H. W. & Ryan, R. O. Apolipoprotein E isoform-specific binding to the low-density lipoprotein receptor. *Anal. Biochem.* **372**, 222–226 (2008).
375. Sofroniew, M. V. Astrogliosis. *Cold Spring Harb. Perspect. Biol.* **7**, 1–16 (2014).
376. Liu, C., Cui, G., Zhu, M., Kang, X. & Guo, H. Neuroinflammation in Alzheimer's disease: Chemokines produced by astrocytes and chemokine receptors. *Int. J. Clin. Exp. Pathol.* **7**, 8342–8355 (2014).
377. Trindade, P. *et al.* Short and long TNF-alpha exposure recapitulates canonical astrogliosis events in human-induced pluripotent stem cells-derived astrocytes. *Glia* 1–14 (2020). doi:10.1002/glia.23786
378. Hyvärinen, T. *et al.* Co-stimulation with IL-1 $\beta$  and TNF- $\alpha$  induces an inflammatory reactive astrocyte phenotype with neurosupportive characteristics in a human pluripotent stem cell model system. *Sci. Rep.* **9**, 1–15 (2019).
379. Nicholls, D. & Attwell, D. The release and uptake of excitatory amino acids. *Trends Pharmacol. Sci.* **11**, 462–468 (1990).
380. Lipton, S. A. & Rosenberg, P. A. Excitatory amino acids as a final common pathway for neurologic disorders. *N. Engl. J. Med.* **330**, 613–622 (1994).
381. Choi, D. W. Glutamate neurotoxicity and diseases of the nervous system. *Neuron* **1**, 623–634 (1988).

382. Doble, A. The role of excitotoxicity in neurodegenerative disease: implications for therapy. *Pharmacol. Ther.* **81**, 163–221 (1999).
383. Martinez-Hernandez, A., Bell, K. P. & Norenberg, M. D. Glutamine synthetase: glial localization in brain. *Science* **195**, 1356–1358 (1977).
384. Yu, A. C., Schousboe, A. & Hertz, L. Metabolic fate of <sup>14</sup>C-labeled glutamate in astrocytes in primary cultures. *J. Neurochem.* **39**, 954–960 (1982).
385. Chung, W.-S. *et al.* Astrocytes mediate synapse elimination through MEGF10 and MERTK pathways. *Nature* **504**, 394–400 (2013).
386. Bellesi, M. *et al.* Sleep Loss Promotes Astrocytic Phagocytosis and Microglial Activation in Mouse Cerebral Cortex. *J. Neurosci.* **37**, 5263–5273 (2017).
387. Vilalta, A. & Brown, G. C. Neurophagy, the phagocytosis of live neurons and synapses by glia, contributes to brain development and disease. *FEBS J.* **285**, 3566–3575 (2018).
388. Iram, T. *et al.* Megf10 Is a receptor for C1Q that mediates clearance of apoptotic cells by astrocytes. *J. Neurosci.* **36**, 5185–5192 (2016).
389. Jung, Y. J. & Chung, W. S. Phagocytic roles of glial cells in healthy and diseased brains. *Biomol. Ther.* **26**, 350–357 (2018).
390. Schiweck, J., Eickholt, B. J. & Murk, K. Important Shapeshifter : Mechanisms Allowing Astrocytes to Respond to the Changing Nervous System During Development , Injury and Disease. *Front. Cell. Neurosci.* **12**, 1–17 (2018).
391. Olabarria, M., Noristani, H. N., Verkhratsky, A. & Rodríguez, J. J. Age-dependent decrease in glutamine synthetase expression in the hippocampal astroglia of the triple transgenic Alzheimer’s disease mouse model: mechanism for deficient glutamatergic transmission? *Mol. Neurodegener.* **6**, 55 (2011).
392. Le Prince, G. *et al.* Glutamine synthetase (GS) expression is reduced in senile dementia of the Alzheimer type. *Neurochem. Res.* **20**, 859–862 (1995).
393. Maragakis, N. J. & Rothstein, J. D. Mechanisms of Disease: astrocytes in neurodegenerative disease. *Nat. Clin. Pract. Neurol.* **2**, 679–689 (2006).
394. Masliah, E., Alford, M., DeTeresa, R., Mallory, M. & Hansen, L. Deficient glutamate transport is associated with neurodegeneration in Alzheimer’s disease. *Ann. Neurol.* **40**, 759–766 (1996).
395. Masliah, E. *et al.* Abnormal glutamate transport function in mutant amyloid

- precursor protein transgenic mice. *Exp. Neurol.* **163**, 381–387 (2000).
396. Tanaka, K. *et al.* Epilepsy and exacerbation of brain injury in mice lacking the glutamate transporter GLT-1. *Science* **276**, 1699–1702 (1997).
397. Rothstein, J. D. *et al.* Localization of neuronal and glial glutamate transporters. *Neuron* **13**, 713–725 (1994).
398. Sutherland, M. L., Delaney, T. A. & Noebels, J. L. Glutamate transporter mRNA expression in proliferative zones of the developing and adult murine CNS. *J. Neurosci.* **16**, 2191–2207 (1996).
399. Lehre, K. P. & Danbolt, N. C. The number of glutamate transporter subtype molecules at glutamatergic synapses: chemical and stereological quantification in young adult rat brain. *J. Neurosci.* **18**, 8751–8757 (1998).
400. Arriza, J. L. *et al.* Functional comparisons of three glutamate transporter subtypes cloned from human motor cortex. *J. Neurosci.* **14**, 5559–5569 (1994).
401. Guo, H. *et al.* Increased expression of the glial glutamate transporter EAAT2 modulates excitotoxicity and delays the onset but not the outcome of ALS in mice. *Hum. Mol. Genet.* **12**, 2519–2532 (2003).
402. Cross, A. J. *et al.* Sodium dependent D-[3H]aspartate binding in cerebral cortex in patients with Alzheimer's and Parkinson's diseases. *Neurosci. Lett.* **79**, 213–217 (1987).
403. Li, S., Mallory, M., Alford, M., Tanaka, S. & Masliah, E. Glutamate transporter alterations in Alzheimer disease are possibly associated with abnormal APP expression. *J. Neuropathol. Exp. Neurol.* **56**, 901–911 (1997).
404. Rosenberg, P. A. & Aizenman, E. Hundred-fold increase in neuronal vulnerability to glutamate toxicity in astrocyte-poor cultures of rat cerebral cortex. *Neurosci. Lett.* **103**, 162–168 (1989).
405. Lauderback, C. M. *et al.* The glial glutamate transporter, GLT-1, is oxidatively modified by 4-hydroxy-2-nonenal in the Alzheimer's disease brain: the role of Abeta1-42. *J. Neurochem.* **78**, 413–416 (2001).
406. Scott, H. A., Gebhardt, F. M., Mitrovic, A. D., Vandenberg, R. J. & Dodd, P. R. Glutamate transporter variants reduce glutamate uptake in Alzheimer's disease. *Neurobiol. Aging* **32**, 553.e1–11 (2011).
407. Woltjer, R. L. *et al.* Aberrant detergent-insoluble excitatory amino acid

- transporter 2 accumulates in alzheimer disease. *J. Neuropathol. Exp. Neurol.* **69**, 667–676 (2010).
408. Scimemi, A. *et al.* Amyloid- $\beta$ 1-42 slows clearance of synaptically released glutamate by mislocalizing astrocytic GLT-1. *J. Neurosci.* **33**, 5312–5318 (2013).
409. Theendakara, V., Peters-Libeu, C. A., Bredesen, D. E. & Rao, R. V. Transcriptional Effects of ApoE4: Relevance to Alzheimer's Disease. *Mol. Neurobiol.* **55**, 5243–5254 (2018).
410. Theendakara, V. *et al.* Direct transcriptional effects of Apolipoprotein E. *J. Neurosci.* **36**, 685–700 (2016).
411. Simpson, J. E. *et al.* Microarray analysis of the astrocyte transcriptome in the aging brain: Relationship to Alzheimer's pathology and APOE genotype. *Neurobiol. Aging* **32**, 1795–1807 (2011).
412. Collart, M. A., Baeuerle, P. & Vassalli, P. Regulation of tumor necrosis factor alpha transcription in macrophages: involvement of four kappa B-like motifs and of constitutive and inducible forms of NF-kappa B. *Mol. Cell. Biol.* **10**, 1498–1506 (1990).
413. Santee, S. M. & Owen-Schaub, L. B. Human tumor necrosis factor receptor p75/80 (CD120b) gene structure and promoter characterization. *J. Biol. Chem.* **271**, 21151–21159 (1996).
414. Sitcheran, R., Gupta, P., Fisher, P. B. & Baldwin, A. S. Positive and negative regulation of EAAT2 by NF- $\kappa$ B: A role for N-myc in TNF $\alpha$ -controlled repression. *EMBO J.* **24**, 510–520 (2005).
415. Zhou, Q. *et al.* Neuroinflammatory astrocytes generated from cord blood-derived human induced pluripotent stem cells. *J. Neuroinflammation* **16**, 1–12 (2019).
416. Chung, W.-S. *et al.* Novel allele-dependent role for APOE in controlling the rate of synapse pruning by astrocytes. *Proc. Natl. Acad. Sci. U. S. A.* **113**, 10186–10191 (2016).
417. Ridet, J. L., Malhotra, S. K., Privat, A. & Gage, F. H. Reactive astrocytes: cellular and molecular cues to biological function. *Trends Neurosci.* **20**, 570–577 (1997).
418. Eng, L. F. & Ghirnikar, R. S. GFAP and Astrogliosis. *Brain Pathol.* **4**, 229–237 (1994).

419. Liddelw, S. A. & Barres, B. A. Reactive Astrocytes : Production, Function, and Therapeutic Potential. *Immunity* **46**, 957–967 (2017).
420. Nagele, R. G., Andrea, M. R. D., Lee, H., Venkataraman, V. & Wang, H. Astrocytes accumulate A $\beta$  42 and give rise to astrocytic amyloid plaques in Alzheimer disease brains. *Neuron* **37**, 197–209 (2003).
421. Kobayashi, E. *et al.* Activated forms of astrocytes with higher GLT-1 expression are associated with cognitive normal subjects with Alzheimer pathology in human brain. *Sci. Rep.* **8**, 2–13 (2018).
422. Zhang, W. *et al.* Neuronal activation of NF- $\kappa$ B contributes to cell death in cerebral ischemia. *J. Cereb. blood flow Metab. Off. J. Int. Soc. Cereb. Blood Flow Metab.* **25**, 30–40 (2005).
423. Bae, M. K. *et al.* Aspirin-induced blockade of NF- $\kappa$ B activity restrains up-regulation of glial fibrillary acidic protein in human astroglial cells. *Biochim. Biophys. Acta - Mol. Cell Res.* **1763**, 282–289 (2006).
424. Meeuwssen, S., Persoon-Deen, C., Bsibsi, M., Ravid, R. & Van Noort, J. M. Cytokine, chemokine and growth factor gene profiling of cultured human astrocytes after exposure to proinflammatory stimuli. *Glia* **43**, 243–253 (2003).
425. Luster, A. D. Chemokines--chemotactic cytokines that mediate inflammation. *N. Engl. J. Med.* **338**, 436–445 (1998).
426. Sternberg, E. M. Neural-immune interactions in health and disease. *Immunol. Rev.* **160**, 264–277 (1997). Find the latest version : Perspectives Series : Cytokines and the Brain. **100**, 2641–2647 (1997).
427. Charo, I. F. & Ransohoff, R. M. Mechanisms of disease: The many roles of chemokines and chemokine receptors in inflammation. *N. Engl. J. Med.* **354**, 610–621 (2006).
428. Bajetto, A., Bonavia, R., Barbero, S. & Schettini, G. Characterization of chemokines and their receptors in the central nervous system: Physiopathological implications. *J. Neurochem.* **82**, 1311–1329 (2002).
429. Devora Rossi, A. Z. The biology of chemokines and their receptors. *Annu. Rev. Immunol.* **18**, 217–242 (2000).
430. Choi, S. S., Lee, H. J., Lim, I., Satoh, J. I. & Kim, S. U. Human astrocytes: Secretome profiles of cytokines and chemokines. *PLoS One* **9**, (2014).

431. Bell, M. D., Taub, D. D. & Perry, V. H. Overriding the brain's intrinsic resistance to leukocyte recruitment with intraparenchymal injections of recombinant chemokines. *Neuroscience* **74**, 283–292 (1996).
432. Huber, A. R., Kunkel, S. L., Todd, R. F. 3rd & Weiss, S. J. Regulation of transendothelial neutrophil migration by endogenous interleukin-8. *Science* **254**, 99–102 (1991).
433. Cummings, C. J. *et al.* Expression and Function of the Chemokine Receptors CXCR1 and CXCR2 in Sepsis. *J. Immunol.* **162**, 2341 LP – 2346 (1999).
434. Baggiolini, M., Walz, A. & Kunkel, S. L. Neutrophil-activating peptide-1/interleukin 8, a novel cytokine that activates neutrophils. *J. Clin. Invest.* **84**, 1045–1049 (1989).
435. Chang, M. S., McNinch, J., Basu, R. & Simonet, S. Cloning and characterization of the human neutrophil-activating peptide (ENA-78) gene. *J. Biol. Chem.* **269**, 25277–25282 (1994).
436. Zaremba, J., Skrobański, P. & Losy, J. The level of chemokine CXCL5 in the cerebrospinal fluid is increased during the first 24 hours of ischaemic stroke and correlates with the size of early brain damage. *Folia Morphol. (Warsz).* **65**, 1–5 (2006).
437. Tunkel, A. R. *et al.* Practice Guidelines for the Management of Bacterial Meningitis. *Clin. Infect. Dis.* **39**, 1267–1284 (2004).
438. Zenaro, E. *et al.* Neutrophils promote Alzheimer's disease-like pathology and cognitive decline via LFA-1 integrin. *Nat. Med.* **21**, 880–886 (2015).
439. Lu, W. *et al.* Neutrophil-specific chemokines are produced by astrocytic cells but not by neuronal cells. *Brain Res. Dev. Brain Res.* **155**, 127–134 (2005).
440. Kamphuis, W. *et al.* GFAP and vimentin deficiency alters gene expression in astrocytes and microglia in wild-type mice and changes the transcriptional response of reactive glia in mouse model for Alzheimer's disease. *Glia* **63**, 1036–1056 (2015).
441. Vallès, A., Grijpink-Ongering, L., de Bree, F. M., Tuinstra, T. & Ronken, E. Differential regulation of the CXCR2 chemokine network in rat brain trauma: implications for neuroimmune interactions and neuronal survival. *Neurobiol. Dis.* **22**, 312–322 (2006).

442. Ashutosh *et al.* CXCL8 protects human neurons from amyloid- $\beta$ -induced neurotoxicity: Relevance to Alzheimer's disease. *Biochem. Biophys. Res. Commun.* **412**, 565–571 (2011).
443. Walker, D. G., Lue, L. F. & Beach, T. G. Gene expression profiling of amyloid beta peptide-stimulated human post-mortem brain microglia. *Neurobiol. Aging* **22**, 957–966 (2001).
444. Galimberti, D. *et al.* Intrathecal chemokine synthesis in mild cognitive impairment and Alzheimer disease. *Arch. Neurol.* **63**, 538–543 (2006).
445. Craig-Schapiro, R. *et al.* Multiplexed immunoassay panel identifies novel CSF biomarkers for alzheimer's disease diagnosis and prognosis. *PLoS One* **6**, (2011).
446. Kamphuis, W. *et al.* Glial fibrillary acidic protein isoform expression in plaque related astrogliosis in Alzheimer's disease. *Neurobiol. Aging* **35**, 492–510 (2014).
447. Persson, T. *et al.* Expression of the neutrophil-activating CXC chemokine ENA-78/CXCL5 by human eosinophils. *Clin. Exp. Allergy* **33**, 531–537 (2003).
448. Xia, M., Qin, S., McNamara, M., Mackay, C. & Hyman, B. T. Interleukin-8 receptor B immunoreactivity in brain and neuritic plaques of Alzheimer's disease. *Am. J. Pathol.* **150**, 1267–1274 (1997).
449. Flynn, G., Maru, S., Loughlin, J., Romero, I. A. & Male, D. Regulation of chemokine receptor expression in human microglia and astrocytes. *J. Neuroimmunol.* **136**, 84–93 (2003).
450. Semple, B. D., Kossmann, T. & Morganti-Kossmann, M. C. Role of chemokines in CNS health and pathology: A focus on the CCL2/CCR2 and CXCL8/CXCR2 networks. *J. Cereb. Blood Flow Metab.* **30**, 459–473 (2010).
451. Rose, J. J., Foley, J. F., Murphy, P. M. & Venkatesan, S. On the mechanism and significance of ligand-induced internalization of human neutrophil chemokine receptors CXCR1 and CXCR2. *J. Biol. Chem.* **279**, 24372–24386 (2004).
452. Cardona, A. E. *et al.* Scavenging roles of chemokine receptors: chemokine receptor deficiency is associated with increased levels of ligand in circulation and tissues. *Blood* **112**, 256–263 (2008).
453. Puma, C., Danik, M., Quirion, R., Ramon, F. & Williams, S. The chemokine interleukin-8 acutely reduces Ca(2+) currents in identified cholinergic septal neurons expressing CXCR1 and CXCR2 receptor mRNAs. *J. Neurochem.* **78**, 960–

- 971 (2001).
454. Lax, P. *et al.* Chemokine receptor CXCR2 regulates the functional properties of AMPA-type glutamate receptor GluR1 in HEK cells. *J. Neuroimmunol.* **129**, 66–73 (2002).
455. Saas, P. *et al.* A self-defence mechanism of astrocytes against Fas-mediated death involving interleukin-8 and CXCR2. *Neuroreport* **13**, 1921–1924 (2002).
456. Limatola, C., Ciotti, M. T., Mercanti, D., Santoni, A. & Eusebi, F. Signaling pathways activated by chemokine receptor CXCR2 and AMPA-type glutamate receptors and involvement in granule cells survival. *J. Neuroimmunol.* **123**, 9–17 (2002).
457. Rollins, B. J. Monocyte chemoattractant protein 1: a potential regulator of monocyte recruitment in inflammatory disease. *Mol. Med. Today* **2**, 198–204 (1996).
458. Yoshimura, T. *et al.* Purification and amino acid analysis of two human glioma-derived monocyte chemoattractants. *J. Exp. Med.* **169**, 1449–1459 (1989).
459. Barna, B. P. *et al.* Regulation of monocyte chemoattractant protein-1 expression in adult human non-neoplastic astrocytes is sensitive to tumor necrosis factor (TNF) or antibody to the 55-kDa TNF receptor. *J. Neuroimmunol.* **50**, 101–107 (1994).
460. Hanisch, U.-K. Microglia as a source and target of cytokines. *Glia* **40**, 140–155 (2002).
461. Che, X., Ye, W., Panga, L., Wu, D. C. & Yang, G. Y. Monocyte chemoattractant protein-1 expressed in neurons and astrocytes during focal ischemia in mice. *Brain Res.* **902**, 171–177 (2001).
462. Croitoru-Lamoury, J. *et al.* Expression of chemokines and their receptors in human and simian astrocytes: evidence for a central role of TNF alpha and IFN gamma in CXCR4 and CCR5 modulation. *Glia* **41**, 354–370 (2003).
463. Gourmal, N. G., Buttini, M., Limonta, S., Sauter, A. & Boddeke, H. W. Differential and time-dependent expression of monocyte chemoattractant protein-1 mRNA by astrocytes and macrophages in rat brain: effects of ischemia and peripheral lipopolysaccharide administration. *J. Neuroimmunol.* **74**, 35–44 (1997).

464. Sokolova, A. *et al.* Monocyte chemoattractant protein-1 plays a dominant role in the chronic inflammation observed in Alzheimer's disease. *Brain Pathol.* **19**, 392–398 (2009).
465. Vukic, V. *et al.* Expression of inflammatory genes induced by beta-amyloid peptides in human brain endothelial cells and in Alzheimer's brain is mediated by the JNK-AP1 signaling pathway. *Neurobiol. Dis.* **34**, 95–106 (2009).
466. Westin, K. *et al.* CCL2 is associated with a faster rate of cognitive decline during early stages of Alzheimer's disease. *PLoS One* **7**, e30525 (2012).
467. Kimura, A., Yoshikura, N., Hayashi, Y. & Inuzuka, T. Cerebrospinal Fluid C-C Motif Chemokine Ligand 2 Correlates with Brain Atrophy and Cognitive Impairment in Alzheimer's Disease. *J. Alzheimer's Dis.* **61**, 581–588 (2018).
468. Lee, W. J. *et al.* Plasma MCP-1 and cognitive decline in patients with Alzheimer's disease and mild cognitive impairment: A two-year follow-up study. *Sci. Rep.* **8**, 4–11 (2018).
469. El Khoury, J. & Luster, A. D. Mechanisms of microglia accumulation in Alzheimer's disease: therapeutic implications. *Trends Pharmacol. Sci.* **29**, 626–632 (2008).
470. Zuenka, A. R., Casolini, P., Lattanzi, R. & Maftai, D. Chemokines in Alzheimer's disease: New insights into prokineticins, chemokine-like proteins. *Front. Pharmacol.* **10**, 1–8 (2019).
471. Perry, V. H., Nicoll, J. A. R. & Holmes, C. Microglia in neurodegenerative disease. *Nat. Rev. Neurol.* **6**, 193–201 (2010).
472. Belmadani, A., Tran, P. B., Ren, D. & Miller, R. J. Chemokines regulate the migration of neural progenitors to sites of neuroinflammation. *J. Neurosci.* **26**, 3182–3191 (2006).
473. Azizi, G., Khannazer, N. & Mirshafiey, A. The potential role of chemokines in Alzheimer's disease pathogenesis. *Am. J. Alzheimers. Dis. Other Demen.* **29**, 415–425 (2014).
474. Barnes, D. A. *et al.* Induction of RANTES expression by astrocytes and astrocytoma cell lines. *J. Neuroimmunol.* **71**, 207–214 (1996).
475. Tripathy, D., Thirumangalakudi, L. & Grammas, P. RANTES upregulation in the Alzheimer's disease brain: a possible neuroprotective role. *Neurobiol. Aging* **31**,

- 8–16 (2010).
476. Skuljec, J. *et al.* CCL5 induces a pro-inflammatory profile in microglia in vitro. *Cell. Immunol.* **270**, 164–171 (2011).
477. Pittaluga, A. CCL5-glutamate cross-talk in astrocyte-neuron communication in multiple sclerosis. *Front. Immunol.* **8**, 1–13 (2017).
478. Musante, V. *et al.* RANTES modulates the release of glutamate in human neocortex. *J. Neurosci.* **28**, 12231–12240 (2008).
479. Di Prisco, S., Summa, M., Chellakudam, V., Rossi, P. I. A. & Pittaluga, A. RANTES-mediated control of excitatory amino acid release in mouse spinal cord. *J. Neurochem.* **121**, 428–437 (2012).
480. Zhou, M. *et al.* CCR5 is a suppressor for cortical plasticity and hippocampal learning and memory. *Elife* **5**, (2016).
481. Benveniste, E. N., Tang, L. P. & Law, R. M. Differential regulation of astrocyte TNF-alpha expression by the cytokines TGF-beta, IL-6 and IL-10. *Int. J. Dev. Neurosci. Off. J. Int. Soc. Dev. Neurosci.* **13**, 341–349 (1995).
482. Campbell, I. L. *et al.* Neurologic disease induced in transgenic mice by cerebral overexpression of interleukin 6. *Proc. Natl. Acad. Sci.* **90**, 10061–10065 (1993).
483. Gruol, D. L. & Nelson, T. E. Physiological and pathological roles of interleukin-6 in the central nervous system. *Mol. Neurobiol.* **15**, 307–339 (1997).
484. Zhao, B. & Schwartz, J. P. Involvement of cytokines in normal CNS development and neurological diseases: Recent progress and perspectives. *J. Neurosci. Res.* **52**, 7–16 (1998).
485. Hama, T., Miyamoto, M., Tsukui, H., Nishio, C. & Hatanaka, H. Interleukin-6 as a neurotrophic factor for promoting the survival of cultured basal forebrain cholinergic neurons from postnatal rats. *Neurosci. Lett.* **104**, 340–344 (1989).
486. Frei, K. *et al.* On the cellular source and function of interleukin 6 produced in the central nervous system in viral diseases. *Eur. J. Immunol.* **19**, 689–694 (1989).
487. März, P. *et al.* Sympathetic neurons can produce and respond to interleukin 6. *Proc. Natl. Acad. Sci.* **95**, 3251 LP – 3256 (1998).
488. Satoh, T. *et al.* Induction of neuronal differentiation in PC12 cells by B-cell stimulatory factor 2/interleukin 6. *Mol. Cell. Biol.* **8**, 3546–3549 (1988).
489. Tarkowski, E. *et al.* Cerebral pattern of pro- and anti-inflammatory cytokines in

- dementias. *Brain Res. Bull.* **61**, 255–260 (2003).
490. Ekert, J. O., Gould, R. L., Reynolds, G. & Howard, R. J. TNF alpha inhibitors in Alzheimer's disease: A systematic review. *Int. J. Geriatr. Psychiatry* **33**, 688–694 (2018).
491. Janelins, M. C. *et al.* Chronic neuron-specific tumor necrosis factor-alpha expression enhances the local inflammatory environment ultimately leading to neuronal death in 3xTg-AD mice. *Am. J. Pathol.* **173**, 1768–1782 (2008).
492. Gorlovoy, P., Larionov, S., Pham, T. T. H. & Neumann, H. Accumulation of tau induced in neurites by microglial proinflammatory mediators. *FASEB J. Off. Publ. Fed. Am. Soc. Exp. Biol.* **23**, 2502–2513 (2009).
493. Quintanilla, R. A., Orellana, D. I., González-Billault, C. & Maccioni, R. B. Interleukin-6 induces Alzheimer-type phosphorylation of tau protein by deregulating the cdk5/p35 pathway. *Exp. Cell Res.* **295**, 245–257 (2004).
494. Xia, M. & Hyman, B. T. GROalpha/KC, a chemokine receptor CXCR2 ligand, can be a potent trigger for neuronal ERK1/2 and PI-3 kinase pathways and for tau hyperphosphorylation—a role in Alzheimer's disease? *J. Neuroimmunol.* **122**, 55–64 (2002).
495. Zhang, X. F. *et al.* CXCL1 triggers caspase-3 dependent tau cleavage in long-term neuronal cultures and in the hippocampus of aged mice: Implications in Alzheimer's disease. *J. Alzheimer's Dis.* **48**, 89–104 (2015).
496. Joly-Amado, A. *et al.* CCL2 Overexpression in the Brain Promotes Glial Activation and Accelerates Tau Pathology in a Mouse Model of Tauopathy. *Front. Immunol.* **11**, 997 (2020).
497. Corrêa, J. D., Starling, D., Teixeira, A. L., Caramelli, P. & Silva, T. A. Chemokines in CSF of Alzheimer's disease patients. *Arq. Neuropsiquiatr.* **69**, 455–459 (2011).
498. Guedes, J. R., Lao, T., Cardoso, A. L. & El Khoury, J. Roles of microglial and monocyte chemokines and their receptors in regulating Alzheimer's disease-associated amyloid- $\beta$  and tau pathologies. *Front. Neurol.* **9**, 1–8 (2018).
499. Bhaskar, K. *et al.* Regulation of tau pathology by the microglial fractalkine receptor. *Neuron* **68**, 19–31 (2010).
500. Chen, C. H. *et al.* Increased NF- $\kappa$ B signalling up-regulates BACE1 expression and its therapeutic potential in Alzheimer's disease. *Int. J. Neuropsychopharmacol.*

- 15**, 77–90 (2012).
501. Bellucci, A. *et al.* Nuclear Factor- $\kappa$ B Dysregulation and  $\alpha$ -Synuclein Pathology: Critical Interplay in the Pathogenesis of Parkinson's Disease. *Front. Aging Neurosci.* **12**, 1–13 (2020).
  502. Perkins, N. D. Achieving transcriptional specificity with nf- $\kappa$ b. *Int. J. Biochem. Cell Biol.* **29**, 1433–1448 (1997).
  503. Meffert, M. K. & Baltimore, D. Physiological functions for brain NF-kappaB. *Trends Neurosci.* **28**, 37–43 (2005).
  504. Dresselhaus, E. C. & Meffert, M. K. Cellular specificity of NF- $\kappa$ B function in the nervous system. *Front. Immunol.* **10**, (2019).
  505. Atkinson, G. P., Nozell, S. E. & Benveniste, E. T. N. NF-kappaB and STAT3 signaling in glioma: targets for future therapies. *Expert Rev. Neurother.* **10**, 575–586 (2010).
  506. Snow, W. M. & Albeni, B. C. Neuronal gene targets of NF- $\kappa$ B and their dysregulation in alzheimer's disease. *Front. Mol. Neurosci.* **9**, 1–19 (2016).
  507. Poirier, J. *et al.* Apolipoprotein E and lipid homeostasis in the etiology and treatment of sporadic Alzheimer's disease. *Neurobiol. Aging* **35**, S3–S10 (2014).
  508. Wollmer, M. A. Cholesterol-related genes in Alzheimer's disease. *Biochim. Biophys. Acta - Mol. Cell Biol. Lipids* **1801**, 762–773 (2010).
  509. Robert W Mahley. Central Nervous System Lipoproteins: ApoE and Regulation of Cholesterol Metabolism. *Arter. Thromb Vasc Biol* **37**, 1305–1315 (2016).
  510. Dietschy, J. M. & Turley, S. D. *Thematic review series: Brain Lipids*. Cholesterol metabolism in the central nervous system during early development and in the mature animal. *J. Lipid Res.* **45**, 1375–1397 (2004).
  511. Bjorkhem, I. & Meaney, S. Brain cholesterol: long secret life behind a barrier. *Arterioscler. Thromb. Vasc. Biol.* **24**, 806–815 (2004).
  512. Thelen, K. M., Falkai, P., Bayer, T. A. & Lütjohann, D. Cholesterol synthesis rate in human hippocampus declines with aging. *Neurosci. Lett.* **403**, 15–19 (2006).
  513. Leduc, V., Jasmin-Bélanger, S. & Poirier, J. APOE and cholesterol homeostasis in Alzheimer's disease. *Trends Mol. Med.* **16**, 469–477 (2010).
  514. Brown, M. S. & Goldstein, J. L. The SREBP pathway: regulation of cholesterol metabolism by proteolysis of a membrane-bound transcription factor. *Cell* **89**,

- 331–340 (1997).
515. Pfrieger, F. W. & Ungerer, N. Cholesterol metabolism in neurons and astrocytes. *Prog. Lipid Res.* **50**, 357–371 (2011).
516. Wang, H. & Eckel, R. H. What are lipoproteins doing in the brain? *Trends Endocrinol. Metab.* **25**, 8–14 (2014).
517. Fielding, C. J. & Fielding, P. E. Cellular cholesterol efflux. *Biochim. Biophys. Acta - Mol. Cell Biol. Lipids* **1533**, 175–189 (2001).
518. Hirsch-Reinshagen, V. *et al.* The absence of ABCA1 decreases soluble ApoE levels but does not diminish amyloid deposition in two murine models of Alzheimer disease. *J. Biol. Chem.* **280**, 43243–43256 (2005).
519. LaDu, M. J. *et al.* Nascent astrocyte particles differ from lipoproteins in CSF. *J. Neurochem.* **70**, 2070–2081 (1998).
520. DeMattos, R. B. *et al.* Purification and characterization of astrocyte-secreted apolipoprotein E and J-containing lipoproteins from wild-type and human apoE transgenic mice. *Neurochem. Int.* **39**, 415–425 (2001).
521. Hirsch-Reinshagen, V. *et al.* LCAT synthesized by primary astrocytes esterifies cholesterol on glia-derived lipoproteins. *J. Lipid Res.* **50**, 885–893 (2009).
522. Gelissen, I. C. *et al.* ABCA1 and ABCG1 synergize to mediate cholesterol export to apoA-I. *Arterioscler. Thromb. Vasc. Biol.* **26**, 534–540 (2006).
523. Vaughan, A. M. & Oram, J. F. ABCA1 and ABCG1 or ABCG4 act sequentially to remove cellular cholesterol and generate cholesterol-rich HDL. *J. Lipid Res.* **47**, 2433–2443 (2006).
524. Demeester, N. *et al.* Characterization and functional studies of lipoproteins, lipid transfer proteins, and lecithin:cholesterol acyltransferase in CSF of normal individuals and patients with Alzheimer's disease. *J. Lipid Res.* **41**, 963–974 (2000).
525. Illingworth, D. R. & Glover, J. Lecithin: cholesterol acyl transferase activity in human cerebrospinal fluid. *Biochim. Biophys. Acta* **220**, 610–613 (1970).
526. Johnson, R. C. & Shah, S. N. Cholesterol Ester Metabolizing Enzymes in Human Brain: Properties, Subcellular Distribution and Relative Levels in Various Diseased Conditions. *J. Neurochem.* **31**, 895–902 (1978).
527. Oliveira, H. C. F. & De Faria, E. C. Cholesteryl ester transfer protein: The

- controversial relation to atherosclerosis and emerging new biological roles. *IUBMB Life* **63**, 248–257 (2011).
528. Fagan, A. M. & Holtzman, D. M. Astrocyte lipoproteins, effects of apoE on neuronal function, and role of apoE in amyloid- $\beta$  deposition in vivo. *Microsc. Res. Tech.* **50**, 297–304 (2000).
529. Albers, J. J., Tollefson, J. H., Wolfbauer, G. & Albright, R. E. J. Cholesteryl ester transfer protein in human brain. *Int. J. Clin. Lab. Res.* **21**, 264–266 (1992).
530. Vitali, C., Wellington, C. L. & Calabresi, L. HDL and cholesterol handling in the brain. *Cardiovasc. Res.* **103**, 405–413 (2014).
531. Atkinson, D., Tall, A. R., Small, D. M. & Mahley, R. W. Structural organization of the lipoprotein HDLc from atherosclerotic swine. Structural features relating the particle surface and core. *Biochemistry* **17**, 3930–3933 (1978).
532. Huuskonen, J., Olkkonen, V. M., Jauhiainen, M. & Ehnholm, C. The impact of phospholipid transfer protein (PLTP) on HDL metabolism. *Atherosclerosis* **155**, 269–281 (2001).
533. Vuletic, S. *et al.* Widespread distribution of PLTP in human CNS: Evidence for PLTP synthesis by glia and neurons, and increased levels in Alzheimer's disease. *J. Lipid Res.* **44**, 1113–1123 (2003).
534. Blain, J.-F. *et al.* A role for lipoprotein lipase during synaptic remodeling in the adult mouse brain. *Neurobiol. Dis.* **15**, 510–519 (2004).
535. Holtzman, D. M., Herz, J. & Bu, G. Apolipoprotein E and apolipoprotein E receptors: normal biology and roles in Alzheimer disease. *Cold Spring Harb. Perspect. Med.* **2**, 1–23 (2012).
536. Liu, Q. *et al.* Neuronal LRP1 knockout in adult mice leads to impaired brain lipid metabolism and progressive, age-dependent synapse loss and neurodegeneration. *J. Neurosci.* **30**, 17068–17078 (2010).
537. Tambini, M. D. *et al.* ApoE4 upregulates the activity of mitochondria-associated ER membranes. *EMBO Rep.* **17**, 27–36 (2016).
538. Tabas, I. Consequences of cellular cholesterol accumulation: basic concepts and physiological implications. *J. Clin. Invest.* **110**, 905–911 (2002).
539. Ikonen, E. Cellular cholesterol trafficking and compartmentalization. *Nat. Rev. Mol. Cell Biol.* **9**, 125–138 (2008).

540. Bryleva, E. Y. *et al.* ACAT1 gene ablation increases 24(S)-hydroxycholesterol content in the brain and ameliorates amyloid pathology in mice with AD. *Proc. Natl. Acad. Sci. U. S. A.* **107**, 3081–3086 (2010).
541. Hutter-Paier, B. *et al.* The ACAT inhibitor CP-113,818 markedly reduces amyloid pathology in a mouse model of Alzheimer's disease. *Neuron* **44**, 227–238 (2004).
542. Sakashita, N. *et al.* Localization of human acyl-coenzyme A: cholesterol acyltransferase-1 (ACAT-1) in macrophages and in various tissues. *Am. J. Pathol.* **156**, 227–236 (2000).
543. Karten, B., Campenot, R. B., Vance, D. E. & Vance, J. E. Expression of ABCG1, but not ABCA1, correlates with cholesterol release by cerebellar astroglia. *J. Biol. Chem.* **281**, 4049–4057 (2006).
544. Lund, E. G. *et al.* Knockout of the cholesterol 24-hydroxylase gene in mice reveals a brain-specific mechanism of cholesterol turnover. *J. Biol. Chem.* **278**, 22980–22988 (2003).
545. Abildayeva, K. *et al.* 24(S)-hydroxycholesterol participates in a liver X receptor-controlled pathway in astrocytes that regulates apolipoprotein E-mediated cholesterol efflux. *J. Biol. Chem.* **281**, 12799–12808 (2006).
546. Bogdanovic, N. *et al.* On the turnover of brain cholesterol in patients with Alzheimer's disease. Abnormal induction of the cholesterol-catabolic enzyme CYP46 in glial cells. *Neurosci. Lett.* **314**, 45–48 (2001).
547. Lin, Y. T. *et al.* APOE4 Causes Widespread Molecular and Cellular Alterations Associated with Alzheimer's Disease Phenotypes in Human iPSC-Derived Brain Cell Types. *Neuron* (2018). doi:10.1016/j.neuron.2018.05.008
548. Marullo, M. *et al.* Pitfalls in the detection of cholesterol in Huntington's disease models. *PLoS Curr.* **4**, e505886e9a1968 (2012).
549. Chen, J., Zhang, X., Kusumo, H., Costa, L. G. & Guizzetti, M. Cholesterol efflux is differentially regulated in neurons and astrocytes: Implications for brain cholesterol homeostasis. *Biochim. Biophys. Acta - Mol. Cell Biol. Lipids* **1831**, 263–275 (2013).
550. Minagawa, H. *et al.* Mechanism underlying apolipoprotein E (ApoE) isoform-dependent lipid efflux from neural cells in culture. *J. Neurosci. Res.* **87**, 2498–2508 (2009).

551. Hu, J. *et al.* Opposing effects of viral mediated brain expression of apolipoprotein E2 (apoE2) and apoE4 on apoE lipidation and A $\beta$  metabolism in apoE4-targeted replacement mice. *Mol. Neurodegener.* **10**, 1–11 (2015).
552. Heinsinger, N. M., Gachechiladze, M. A. & Rebeck, G. W. Apolipoprotein e genotype affects size of ApoE complexes in cerebrospinal fluid. *J. Neuropathol. Exp. Neurol.* **75**, 918–924 (2016).
553. Yassine, H. N. *et al.* The effect of APOE genotype on the delivery of DHA to cerebrospinal fluid in Alzheimer's disease. *Alzheimers. Res. Ther.* **8**, 25 (2016).
554. Rawat, V. *et al.* ApoE4 Alters ABCA1 Membrane Trafficking in Astrocytes. *J. Neurosci.* **39**, 1400–19 (2019).
555. Chan, R. B. *et al.* Comparative lipidomic analysis of mouse and human brain with Alzheimer disease. *J. Biol. Chem.* **287**, 2678–2688 (2012).
556. Proitsi, P. *et al.* Plasma lipidomics analysis finds long chain cholesteryl esters to be associated with Alzheimer's disease. *Transl. Psychiatry* **5**, (2015).
557. van der Kant, R. *et al.* Cholesterol Metabolism Is a Druggable Axis that Independently Regulates Tau and Amyloid- $\beta$  in iPSC-Derived Alzheimer's Disease Neurons. *Cell Stem Cell* **24**, 363-375.e9 (2019).
558. Mulas, M. F. *et al.* Dietary restriction counteracts age-related changes in cholesterol metabolism in the rat. *Mech. Ageing Dev.* **126**, 648–654 (2005).
559. Bhattacharyya, R. & Kovacs, D. M. ACAT inhibition and amyloid beta reduction. *Biochim. Biophys. Acta* **1801**, 960–965 (2010).
560. Chen, C. H. & Albers, J. J. Activation of lecithin: cholesterol acyltransferase by apolipoproteins E-2, E-3, and A-IV isolated from human plasma. *Biochim. Biophys. Acta* **836**, 279–285 (1985).
561. Wahrle, S. E. *et al.* ABCA1 is required for normal central nervous system ApoE levels and for lipidation of astrocyte-secreted apoE. *J. Biol. Chem.* **279**, 40987–40993 (2004).
562. Fitz, N. F. *et al.* Abca1 deficiency affects Alzheimer's disease-like phenotype in human ApoE4 but not in ApoE3-targeted replacement mice. *J. Neurosci.* **32**, 13125–13136 (2012).
563. Vuletic, S. *et al.* Reduced CSF PLTP activity in Alzheimer's disease and other neurologic diseases; PLTP induces ApoE secretion in primary human astrocytes

- in vitro. *J. Neurosci. Res.* **80**, 406–413 (2005).
564. Wang, H. *et al.* PLTP deficiency impairs learning and memory capabilities partially due to alteration of amyloid-beta metabolism in old mice. *J. Alzheimers. Dis.* **39**, 79–88 (2014).
565. Tong, Y. *et al.* Phospholipid transfer protein (PLTP) deficiency accelerates memory dysfunction through altering amyloid precursor protein (APP) processing in a mouse model of Alzheimer's disease. *Hum. Mol. Genet.* **24**, 5388–5403 (2015).
566. Tu, A. Y., Nishida, H. I. & Nishida, T. High density lipoprotein conversion mediated by human plasma phospholipid transfer protein. *J. Biol. Chem.* **268**, 23098–23105 (1993).
567. Dong, W., Albers, J. J. & Vuletic, S. Phospholipid transfer protein reduces phosphorylation of tau in human neuronal cells. *J. Neurosci. Res.* **87**, 3176–3185 (2009).
568. Wang, H. & Eckel, R. H. Lipoprotein Lipase in the Brain and Nervous System. *Annu. Rev. Nutr.* **32**, 147–160 (2012).
569. Genin, E. *et al.* APOE and Alzheimer disease: a major gene with semi-dominant inheritance. *Mol. Psychiatry* **16**, 903–907 (2011).
570. Dewitt, M. A., Corn, J. E. & Carroll, D. Genome editing via delivery of Cas9 ribonucleoprotein. *Methods* **121–122**, 9–15 (2017).
571. Strooper, B. De & Karran, E. Review The Cellular Phase of Alzheimer ' s Disease. *Cell* **164**, 603–615 (2016).
572. Carter, S. F. *et al.* Evidence for astrocytosis in prodromal alzheimer disease provided by 11C-deuterium-L-deprenyl: A multitracer PET paradigm combining 11C-Pittsburgh compound B and 18F-FDG. *J. Nucl. Med.* **53**, 37–46 (2012).
573. Colangelo, A. M., Alberghina, L. & Papa, M. Astroglisis as a therapeutic target for neurodegenerative diseases. *Neurosci. Lett.* **565**, 59–64 (2014).
574. Assefa, B. T., Gebre, A. K. & Altaye, B. M. Reactive Astrocytes as Drug Target in Alzheimer's Disease. *Biomed Res. Int.* **2018**, (2018).
575. Jones, S. V. & Kounatidis, I. Nuclear factor-kappa B and Alzheimer disease, unifying genetic and environmental risk factors from cell to humans. *Front. Immunol.* **8**, (2017).

576. Hilgendorff, A. *et al.* Statins differ in their ability to block NF-kappaB activation in human blood monocytes. *Int. J. Clin. Pharmacol. Ther.* **41**, 397–401 (2003).
577. Husain, I. *et al.* Rosuvastatin Attenuates High-Salt and Cholesterol Diet Induced Neuroinflammation and Cognitive Impairment via Preventing Nuclear Factor KappaB Pathway. *Neurochem. Res.* **42**, 2404–2416 (2017).
578. Chen, G. *et al.* Simvastatin reduces secondary brain injury caused by cortical contusion in rats: possible involvement of TLR4/NF-kappaB pathway. *Exp. Neurol.* **216**, 398–406 (2009).
579. Ruiz, J. *et al.* The apoE isoform binding properties of the VLDL receptor reveal marked differences from LRP and the LDL receptor. *J. Lipid Res.* **46**, 1721–1731 (2005).
580. Lian, H. *et al.* NFkB-Activated Astroglial Release of Complement C3 Compromises Neuronal Morphology and Function Associated with Alzheimer's Disease. *Neuron* **85**, 101–115 (2015).